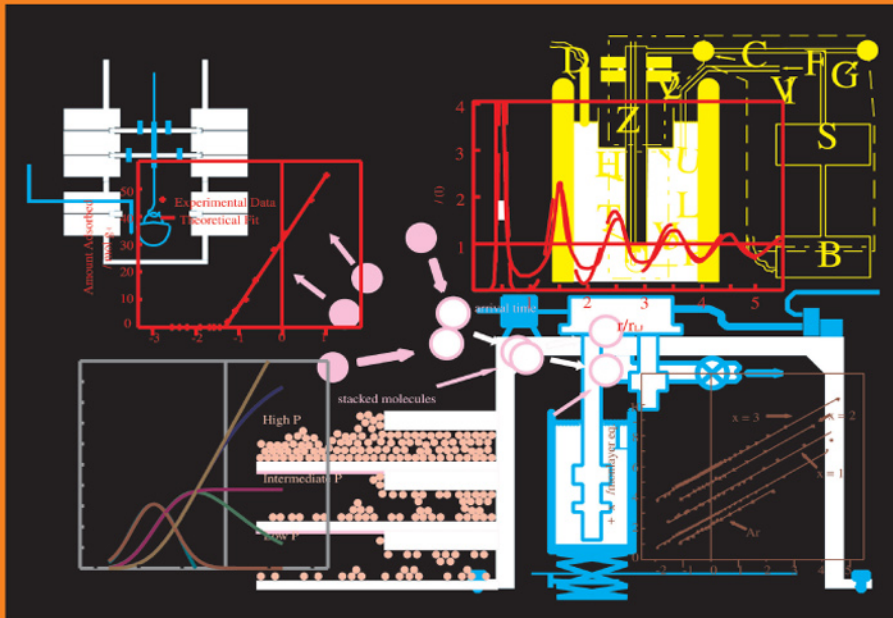# Surface Area and Porosity Determinations by Physisorption

Measurements and Theory

James B. Condon

Surface Area and Porosity Determinations by Physisorption

Measurements and Theory

This page intentionally left blank

Surface Area and Porosity Determinations by Physisorption

Measurements and Theory

James B. Condon

Professor of Chemistry
Roane State Community College
Harriman, TN 37748-5011
USA

Table of Contents

CHAPTER 2 : MEASURING THE PHYSISORPTION ISOTHERM

CHAPTER 3 : INTERPRETING THE PHYSISORPTION ISOTHERM

CHAPTER 5 : COMPARISON OF THE CHI EQUATION TO
            MEASUREMENTS

CHAPTER 7 : DENSITY FUNCTIONAL THEORY

Foreword

The objective of this book is to present the practice of measuring and interpreting physical adsorption. It is intended to be a practical guide and not an extensive review of either the literature or the theories involved with physical adsorption. Extensive reviews are available and the book by Gregg and Sing [1], though about 20 years old, is still highly recommended. A couple of more recent theoretical aspects are not covered in the book by Gregg and Sing. These are density functional theory (DFT) and chi (χ) theory for which there are no comprehensive reviews. A review by Evans [2] and additional article by Tarazona et al. [3, 4], would be a good start for DFT. χ theory [5, 6] is rather simple and will be explained in one of the chapters.

As with all scientific writing there are various levels that can be presented. For example, infrared spectroscopy could be used on simply the pattern recognition level or at the more sophisticated level of quantum mechanics. So it is with physical adsorption. One can use the data from physical adsorption measurements as a simple control device, i.e. "Does this powder have the right adsorption isotherm to meet production requirements?", or on a different level "What is the meaning of the isotherm in terms of surface and pore structure and chemical attractions?" For most applications, the level of sophistication is somewhat intermediate.

In this book, the simple interpretations of the physisorption experiments are presented in Chapter 1. Chapter 2 presents the important details on how to make the measurements usually associated with physical adsorption. If one already has a commercial instrument, this chapter may be irrelevant. Chapter 3 is designed to present step-by-step analysis of the isotherms by a few methods and to present other isotherm interpretations. It is generally not a good idea to rely upon manufacturers software supplied with the instruments. Although the programers are quite knowledgeable about physisorption, it is still best to examine the data carefully. Chapter 4

presents extensive derivations of some theories of adsorption starting with the disjoining pressure approach. The derivations of most isotherms have been extensively reviewed in other books (for example, see Gregg and Sing). After all, most have been used for more than 50 years. However, the more recent χ theory and DFT have not been reviewed. Therefore, more detailed descriptions of χ theory and DFT are presented along with some results. The analysis of one of the more promising techniques for studying adsorption, that is calorimetry, is not presented. A variety of others that are useful for porosity measurements such as X-ray, NM, FTIR, etc., are also not presented. There is a vast body of literature on these latter subjects which have been used extensively especially for the zeolites.

For most practical applications using commercial instruments, and given that one is accustomed to analysis that physical chemists use, Chapter 1 could suffice. The results of the theories formulated will be used in a "cook book" fashion in Chapter 1 with little explanation. The caveat to the simplified treatments is that occasionally a simple explanation for the behavior of the adsorption is not appropriate. Hopefully, by recognizing patterns in the original or transformed isotherms most misinterpretations can be avoided. The pattern recognition utilizes the set of isotherm "types" as originally presented by deBoer and modified by Brunauer [7] and later expanded by Sing [8] and by χ plot features. Recognition of the possibilities of the complicating features beyond the simple isotherm is important for physical adsorption to be of value. Such features may be interpreted in terms of multiple surface areas, pore sizes and volume, energies of adsorption and the distribution of pore sizes or of adsorption energies. The isotherms are generally interpreted in terms of these features and these features have physical quantities associated with them that in many cases would be useful to know.

Unfortunately, the physical quantities associated with the physical features listed above must be extracted using some theoretical assumptions and the associated mathematical manipulations. It is not at all certain at this time that any generalized theory is capable of this. The theories available yield quite different values for these quantities and at the moment there has not been any resolution as to which interpretation, if any, is correct. Most theories of adsorption do not even yield values for these physical quantities and some that claim to do so in reality do not. For example, the only theories that have a theoretical basis for calculating surface area of unknown samples are the Brunauer, Emmitt and Teller (BET) [9] and the χ theory. Both of these will be explained in the theoretical portions of this book. The BET is unquestionably the most widely used theory to calculate the surface area but it has some very serious

flaws. χ theory is a recent development that has not been thoroughly tested. Another possibility is the continuing development of DFT, which has so far not been successful in calculating the surface area independent of the BET results or from assumed equations of state. There are numerous theories and methods for determining (meso) pore volume; however, to determine the pore radius most rely upon BET. Furthermore, the BET is used as a correction in these methods as well. Most theories yield approximately the same answer, within a factor of 10, due to an obvious feature in the isotherm that would allow an educated guess to be correct.

There is hope that in the future some of these questions will be resolved, but for the moment there is a need for some answer even if only approximate. It is unlikely that any theory will yield answers with the precision which chemists or physicists are used to, say better than 1%, due not just to the uncertainties of the theories and the associated calculations, but also due to the defining questions regarding the physical quantities. For example, what is the pore size for pores in the range of 2 nm diameters? Where is the inner boundary for these pores? Atomic sizes begin to have meaning in this range. How does one account for surface roughness on a nearly atomic scale? Again, the same uncertainity in definition. Luckily, these questions may not be of practical importance in many applications. If a pore is large enough to allow, say, methanol to adsorb but not ethanol, there is a parameter that one could possibly extract to yield the distinction. If a catalyst's activity is proportional to the surface area, whatever that means, there is probably a parameter that is proportional to the surface area to make a relative distinction. So, in spite of the theoretical uncertainties, the measurement of physical adsorption is a very useful tool and promises to be more so in the future.

REFERENCES

[1] S.J. Gregg and K.S.W. Sing, Adsorption, Surface Area and Porosity, Academic Press, London and New York, ISBN 0-12-300956-1, 1982.

[2] R. Evans, in "Fundamentals of Inhomogeneous Fluids" (D. Henderson, ed.), p.85, Marcel Dekker, New York, 1992.

[3] P. Tarazona, Phys. Rev. A, 31 (1985) 2672, Phys. Rev. A, 32 (1985) 3148.

[4] P. Tarazona, U.M.B. Marconi and R. Evans, Mol. Phys., 60 (1987) 573.

[5] E.L. Fuller, Jr., J.B. Condon, Colloid Surf., 37 (1989) 171.

[6] J.B. Condon, Microporous Mesoporous Mat., 38 (2000) 359–383.

[7] S. Brunaur, L.S. Deming, W.S. Deming and E. Teller, J. Am. Chem. Soc., 62 (1940) 1723.

[8] S. Brunaur, P.H. Emmett and E.J. Teller, J. Am. Chem. Soc., 60 (1938) 309.

This page intentionally left blank

Acknowledgments

This page intentionally left blank

Symbol List

α = a constant relating A_w to A_{ex}, $0<\alpha<1$

α = surface coverage in the localized layer

$\beta = -kT$

γ = the surface tension of the liquid adsorptive

Γ = coverage or surface excess

Γ_1 = a monolayer surface excess

γ_{gl} = the surface tension between the gas and liquid phase

Γ_m = the value of Γ at which Φ is a minimum

δ = a distance parameter for correcting γ_{gl}

$\delta()$ = Dirac delta function

$\Delta\varepsilon = \varepsilon_{12} + \varepsilon_{21} - \varepsilon_{11} - \varepsilon_{22}$

$\Delta\mu = \mu_{ad} - \mu_{liquid}$

$\Delta\chi = \chi - \chi_c$

$\Delta\chi_p = \chi_p - \chi_c$

$\Delta\psi$ = the excess Helmholtz free energy functional derivative, normally from Carnahan–Starling

ΔE = a group of energy terms (=zero if the two molar volumes are the same) in binary adsorption

ΔH = enthalpy evolved

$\Delta \mathbf{H_v}$ = molar enthalpy of vaporization

$\varepsilon_{i,j}$ = energy of interaction between molecules i and j

$\zeta = Na_{ex}/A_s$

$\zeta_i = \zeta$ for the ith adsorbate

η_j = a probe value for the fit to the isotherm data

θ = the amount on the surface per unit area

$\theta_i = \theta$ in the ith "layer"

λ = the perturbation parameter

λ = "characteristic length" in disjoining pressure formulation

λ_f = the mean free path of the gas

μ_{ad} = the chemical potential of the adsorbate

μ_c = the chemical potential of the condensed phase flat

μ_g = the chemical potential of the adsorbent

μ_l = chemical potential of pure liquid phase at the saturation pressure

μ_{liq} = chemical potentials of the liquid

v = factor set for the sensitivity of the convergent of σ for mesoporosity

Ξ = the grand canonical ensemble

π = spreading pressure of adsorbate $\pi = \gamma_o - \gamma$

Π = the disjoining pressure

Π_0 = the disjoining pressure at $t = 0$

ρ = liquid density

$\rho(\mathbf{r})$ = number density function

$\rho(\mathbf{r})$ = a smoothed density function

$\rho\{r_1..r_M\}$ = number density of particle 1 at $\mathbf{r}_1$ … particle M at $\mathbf{r}_M$

ρ_0 = number density of homogeneous fluid

σ = the standard deviation in the pore size distribution

φ = an energy functional

Φ = the excess surface energy

$\chi = -\ln(-\ln(P/P_s))$

χ_p = the value of χ at which the capillary filling takes place, the mean is $\langle \chi_p \rangle$

a = the cross-sectional area of the adsorbate molecule

A = molar Helmholtz free energy

a_{ex} = $a/(1.84$–$1.92)$

A_{ex} = high-pressure area from slope (pore analysis) includes A_w and A_o

A_{excess} = an excess free-energy functional term to the Helmholtz free energy

$a_{ex,i}$ = a_{ex} for the ith adsorbate

$A_{external}$ = the external field contribution to the Helmholtz free energy

A_{gl} = the area of the adsorbate layer–gas interface

a_i = molecular diameter of ith molecule (used in DFT chapter)

A_I = the ideal gas contribution to the Helmholtz free energy

A_m = the molar area for an adsorbate

A_o = area of the pore openings

A_p = surface area inside the pores

A_{ref} = reference Helmholtz free energy

A_s = the surface area

$A_{s,i}$ = the surface areas for ith segment or plane in χ theory

A_w = edge-on walls or the non-porous area of the outer surface

b = pore fractal factor

b = buoyance correction coefficient

B = constant in the simplified Polanyi formulation

C = combinations used in deriving certain equations

C = the BET constant

$C^{(1)}$ = the singlet direct correlation function

$C^{(2)}$ = the direct correlation function

C_i = the KFG coefficients

$C_{p,ad}$ = heat capacity (constant pressure) of adsorbate

$C_{p,l}$ = the heat capacity at constant pressure for the liquid phase of adsorptive

d = distance

D = tube diameter

$\mathbf{D}_1$ = a distribution function which gets doubly integrated

$\mathbf{D}_2$ = a distribution function which gets both doubly and singly integrated

d_p = pore diameter (cylindrical) or distance between the slit pore sides

$E(\theta)$ = energy function for the Polanyi formulation

E_1 = energy of adsorption for the localized layer

E_a = energy of adsorption for the first adsorbate molecule

$E_{a,i}$ = E_a of coadsorbate i

$E_{a,i}$ = energy of adsorption for the first adsorbate molecule on the ith plane in χ theory

E_{LJ} = the Lennard–Jones 6–12 potential

f = a value is between 1.82 and 1.92 for χ theory

$\mathbf{f}(T)$ = portion of Ξ due to internal molecular modes, vibrational, etc.

$\mathbf{F}(x, T)$ = standard isotherm function

G = a parameter in mesopore fit (for χ it = A_s/fA_m)

G = gibbs' free energy

$g(\mathbf{r}_1, \mathbf{r}_2)$ = (two body) correlation function for position

h = a constant depending upon the pore geometry

H = the total of the classical potential and kinetic energy (Hamiltonian)

H = a parameter in mesopore fit (for χ it = pG)

I_{BET} = the intercept of the transformed BET plot

I_{hi} = the high-pressure intercept in the χ plot for porosity calculations

I_{lo} = the low-pressure intercept in the χ plot for porosity calculations

J = a parameter in mesopore fit (for χ it = V_p/V_m)

k = Boltzmann constant

K = simply an equilibrium constant

k' = a constant which includes k_{FHH} and n_m

k_{FHH} = an empirical constant in the Frenkel–Halsey–Hill isotherm

k_P = constant in the simplified Polanyi formulation

l = the total length of all the pores

$\langle l \rangle$ = average length per pore

l_p = the pore length

M = number of adsorbate molecules in localized first layer

M = the molar mass

M_{ad} = the molar mass of the adsorbate

m_b = "mass gain" from buoyancy

$m_{mf}(P)$ = correction for molecular flow (a function of pressure)

m_p = mass recording of the trial for mass flow correction

M_p = the molar mass of the buoyancy probe gas

N = number of adsorbate molecules

N = being the number of allowed layers in BDDT equation

n_1 = the number of moles adsorbed in the localized layer

N_A = Avogadro's number (6.022×10^{23} mol^{-1})

n_{ad} = amount of adsorbate

$n_{ad,i}$ = amount of adsorbate for ith adsorbate

n_i = incremental number of moles adsorbed for one data point.

N_i = number of adsorbate molecules of species i

n_m = the number of moles of adsorbate in a monolayer

n_p = the moles of adsorbate needed to fill the pores

N_p = the number of pore openings per gram

P = adsorptive pressure

P = one-dimensional pressure (not italicized to distinguish it from probability)

$\mathbf{P}(\chi)$ = probability normal mass function with χ as independent variable

$P\{\}$ = probability of whatever is in {} usually a particle position and/or velocity

P_1 = equilibrium pressure for a reading of a data point

P_{cr} = the critical adsorptive pressure in the BdB theory

P_f = final pressure reading for determining "dead space" or final reading for a data point

P_i = first pressure reading for determining "dead space" or initial reading for a data point

P_i = overpressure for the ith adsorbate

P_s = the saturated vapor pressure over the bulk liquid

$P_{s,i}$ = the saturated vapor pressure over the pure bulk liquid for ith adsorptive

Q = the integral energy of adsorption as defined by Hill

Q = the partition function

$\mathbf{Q}'$ = molar integral heat of adsorption as defined by Morrison, Los and Drain

Q' = integral heat of adsorption as defined by Morrison, Los and Drain

q_{la} = heat of the liquid-adsorbate transition

q_{st} = the isosteric heat

q_{st} = isosteric heat of adsorption

r = the distance between centers in the plane of the surface

R = the gas constant

r_c = the core radius

r_F = the Freundlich isotherm constant

r_{FHH} = an empirical constant in the Frenkel–Halsey–Hill isotherm ≈ 2 to 3

$\mathbf{r}_i$ = position of particle #i

r_m = the center-to-center distance between adsorbate molecules

r_p = pore radius (cylindrical)

r_p = the pore radius or half the distance across the pore

r_t = the radius of the immobile surface atom or ion

s = fraction of the excluded area compared to the hard-sphere ratio

S_{BET} = the slope of the transformed BET plot

S_{hi} = the high-pressure slope in the χ plot for porosity calculations

S_{lo} = the low-pressure slope in the χ plot for porosity calculations

t = the "film thickness" (before the prefilling starts)

t = time

T = temperature

T_1 = temperature of volume designated with V_1

T_2 = temperature of volume designated with V_2

T_3 = temperature of volume designated with V_3

t_{cr} = the critical thickness in the BdB theory

t_{mono} = a monolayer thickness

$t_{1/2}$ = the "half life" constant for pressure decay

u = potential energy

$\mathbf{U}$ = the unit step function

u_{ex} = the potential energy due to external force

u_{in} = potential energy due to inter-particle forces

V = the volume of gas adsorbed at STP

V = molar volume

V_1 = a calibrated volume

V_2 = manifold volume excluding the calibrated volume

V_3 = the volume at the sample temperature

V_d = the "dead space"

$\mathbf{v}_i$ = velocity of particle #i

V_m = the liquid adsorptive molar volume
V_{mon} = the volume of gas at STP that is required for a monolayer
V_p = total pore volume
V_s = the volume of the sample
$\mathbf{w}_i$ = Tarazona weighting functions
$x = P/P_s$
$z = \pi a^3 \rho/6$ where a is the diameter of the hard sphere
Z_N = the configuration partition function for N particles

Chapter 1

An Overview of Physisorption

INTRODUCTION SCOPE AND TERMINOLOGY

The term "physical adsorption" or "physisorption" refers to the phenomenon of gas molecules adhering to a surface at a pressure less than the vapor pressure. The attractions between the molecules being adsorbed and the surface are relatively weak and definitely not covalent or ionic. In Table 1 definitions used in this book and in most of the literature on physisorption are given [1].

For most adsorption experiments the temperature at which the measurements are made is less than the triple point of the gas being used but above its freezing point. This being the case, one would normally expect that the adsorbate characteristics resemble the liquid phase rather than the solid phase of the adsorptive. This is the normal assumption used for most adsorption theories. The principle measurement performed as an adsorption experiment is the measurement of the adsorption isotherm. The adsorption isotherm is the measurement of amount adsorbed versus adsorptive pressure at constant temperature. This is the easiest measurement to make. Another type of measurement is calorimetry. One form of calorimetry measures the amount of heat evolved as the adsorptive is adsorbed. Another form measures the heat capacity of the adsorbate. There are various forms of calorimetry but the most accurate methods are very difficult to perform and only a few examples are available in the literature. Another form of calorimetry, which is easier to perform, is scanning calorimetry. This calorimetry form is a good tool to determine qualitative features of the adsorption and to yield a fair indication of the physical quantities.

GENERAL DESCRIPTION OF PHYSISORPTION

For purpose of this book distinctions will be made between physical adsorption for the liquid-like state and in the solid-like state. Figs. 1 and 2 illustrate

Table 1
Some definitions needed to comprehend the first part of this book

Term	Definition
Adsorbate	The molecules adsorbed on the surface of the solid material
Adsorbent	The solid material upon which the adsorbate is adsorbed
Adsorption	Addition of adsorbate to the adsorbent by increasing the adsorptive pressure
Adsorptive	The gas in equilibrium with the adsorbate
Chemisorption	Enhancement of the amount of gas molecules on the surface of a solid caused by covalent or ionic bonding
Chi (χ) plot	A plot of amount adsorbed versus $-\ln(-\ln(P/P_s))$
Desorption	Removal of adsorbate from the adsorbent by decreasing the adsorptive pressure or increasing the temperature
Hysteresis	The phenomenon of the desorption isotherm being different from the adsorption isotherm. (The amount of adsorbate is greater for desorption.)
Macropores	Pores with diameters greater than 50 nm[a] (IUPAC definition [1])
Mesopores	Pores with diameters between 2 and 50 nm[a] (IUPAC definition [1])
Micropores	Pores with a diameter of less than 2 nm[a] (IUPAC definition [1])
Monolayer	A uniform liquid film of adsorbate one molecular layer thick
Monolayer equivalent	The amount of adsorbate that has the same number of molecules as the theoretical monolayer. Symbol for this is n_m
Physical adsorption	Enhancement of the amount of gas molecules on the surface of a solid caused by van der Waal forces (includes dipole–dipole, dipole-induced dipole, London forces and possibly hydrogen bonding.)
Physisorption	Same as physical adsorption
Standard plot	Refers to one of these: α–s plot, the t-thickness plot, the χ plot and others that may be specific to an adsorbate–adsorbent pair. A generalize standard plot function will be designated as $\mathbf{F}(P/P_s)$ in this book
2D	"2 Dimensional" refers to a cylindrical interface, i.e. cylindrical coordinates
3D	"3 Dimensional" refers to a spherical interface, i.e. spherical coordinates
Saturated vapor pressure (P_s)	the vapor pressure over the flat surface of the liquid adsorptive.

[a]The practical distinction between these depends upon conditions and especially the adsorbate. The above definition is based on nitrogen adsorbate and the IUPAC standard.
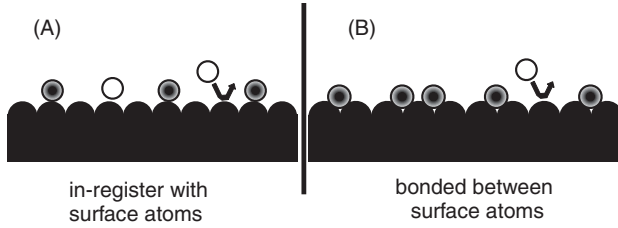
Fig. 1. A model of adsorption of the "in-register" type, e.g. chemisorption, epitaxy.
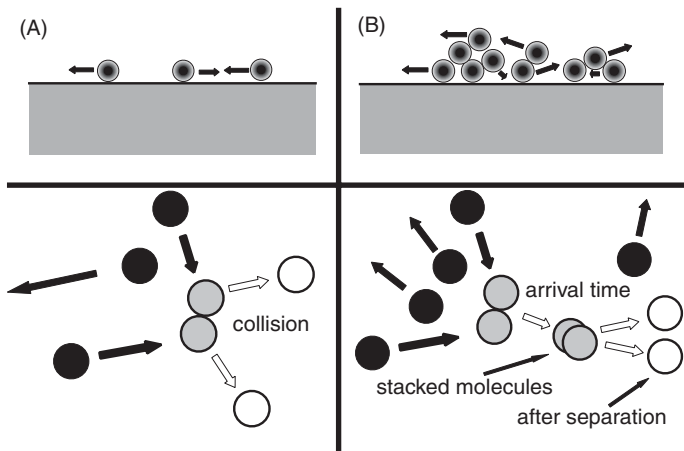
Fig. 2. Models of two types of physisorption. A, gas-like; B, liquid-like; ●, before encounter; ○, after encounter; hatched is during encounter.

the atomic scale difference between the two types of adsorption. For solid-like state of Fig. 1 the adsorbate molecules are located on definite sites in relation to the underlying atoms of the adsorbent. For example, they lie directly over one of the atoms or in between two or three atoms in a defined geometry. One could refer to this as an "in-register" adsorption or even "epitaxy". Chemisorption, where the attraction between the adsorbate and adsorbent is a covalent or ionic bond, would be an example of such adsorption. Adsorption well below the triple point in temperature would also be expected to follow this pattern. Additional adsorption above the first layer, might also be "in register".

The other mode of adsorption, which is the subject of this book, is illustrated in Fig. 2, of which two theoretical sub-possibilities exists. For this adsorption, referred to as physisorption, in adsorbent provides an

overall attraction for which no particular site has a strong enough attraction to localize the adsorbate. In other words, the adsorbate molecules are free to skate over the entire surface, at least for a fair distance, even though there might be bumpy spots. For this physisorption picture there can be further distinctions, one where the adsorbate is behaving as a gas and there is only adsorption on top of the adsorbate, or one where the adsorbate behaves like a liquid, where adsorbate molecules can roll over one another and an adsorptive molecule can adsorb upon an adsorbate molecule. Most adsorption isotherms are performed under conditions where the liquid-like condition is assumed to exist. Calculations of the gas-like state indicate that the amount that can be adsorbed in this fashion is very low for most practical experimental conditions. Nevertheless, one would expect some of this to exist even with the presence of the liquid-like adsorbate.

MEASURING THE SURFACE AREA BY PHYSISORPTION

There are two principal methods to measure the adsorption isotherm, volumetric and gravimetric. In both methods the adsorbent is held at a constant temperature, usually near or at the boiling point of the adsorptive. The adsorptive pressure is increased step-wise and held constant for a period of time to allow the adsorption to occur and the temperature of the adsorbent to re-equilibrate. The length of time required depends upon the physical arrangement and the system being studied. Since re-equilibration might take hours in some cases, it is best to monitor the progress of the adsorption to determine when equilibrium is achieved. The amount adsorbed is measure in the case of the volumetric system by measuring the pressure change and comparing this to the expected pressure change if the adsorbent were absent. In the case of the gravimetric measurement the amount adsorbed is indicated by the mass gain. In both cases, some corrections to the raw data must be performed to take into account the experimental set-up. Details of how this is done are presented in Chapter 2.

A typical isotherm then is a plot of the amount adsorbed versus the adsorptive pressure. Usually, the pressure is expressed as a ratio of the adsorptive pressure, P, to the saturated vapor pressure over the bulk liquid, P_s. The preferred unit for adsorbate amount is millimoles or micromoles adsorbate per gram of adsorbent (mmol g^{-1} or μmol g^{-1}). The literature has a variety of units for adsorbate with milliliters at STP ($T = 0°C$, P) preferred in most of the older literature.

Each of the methods of measuring the isotherm has advantages and disadvantages. Both isotherm measuring methods normally cool the sample to or below the boiling point of the adsorptive. The sample is then exposed to adsorptive gas while the gas pressure is measured. Since the temperature of the sample is known, usually by use of a gas–liquid thermometer, then the vapor pressure of the adsorptive over its liquid is known and thus the ratio P/P_s can be calculated. This is the most precisely measured physical quantity, although P_s could be significantly off if the temperature of the sample is not carefully checked. This measurement is common to all the techniques. The other measurement differs depending upon the technique.

The most common measurement of the isotherm is volumetric method. This method has the advantage that it is the simplest and relatively inexpensive. It has the disadvantage of a greater uncertainty in the results. In this technique the amount of gas adsorbed is determined by measuring how much gas is used from a reservoir. This sometimes referred to as a gas burette. There are several corrections that need to be checked, the principal one being what is referred to as the "dead volume". In this technique temperature measurements, both in the cooled zone and for the gas burette portion, are very important.

A low-cost alternative to the volumetric is the flow or carrier gas system. The disadvantage of this method is that the results are very uncertain and normally does not yield the isotherm.

Generally, the gravimetric method is more accurate and precise, however such instrumentation is more expensive and requires a little more skill and patience to operate. Normally one uses a balance that is referred to as a "microbalance". The balance should have *at least* a sensitivity of 10^{-6}. For example, if the normal load on the balance is about 1.0 g then it would normally be sensitive to 0.1 mg. For the most sensitive measurements one must make buoyancy corrections.

Calorimetric measurements are less common than the measurements mentioned above and yield a different physical quantity. To be effective, the calorimetric method needs to be combined with either the volumetric technique, which is normal, or with the gravimetric technique which is a little more difficult for high-quality work. Both methods are used. Calorimetry measures the temperature change as the adsorption occurs. This along with a heat capacity measurements of the resultant adsorbate–adsorbent combination yields the heat of adsorption as a function of pressure. Less precise calorimetric measurements measure only the heat evolved which gives

some idea of the various adsorption mechanism involved. Calorimetry is not widely used since accurate calorimetry is extremely difficult to perform and requires a great amount of time and effort.

PRELIMINARY ANALYSIS

The Adsorption Isotherm Types

Some of the forms of the isotherm are shown in Figs. 3–8. These types are labeled I through VI according to the classification developed by deBoer, codified by Brunauer et al. [2] and supplemented by Gregg and Sing [3]. These classifications are widely used in the literature on physisorption and normally have the interpretations listed in Table 2.

In type VI, an initial adsorption step may be observed if a chemisorption occurs along with physisorption, however the chemisorption portion should be somewhat irreversible and subsequent isotherms will differ from the first measured isotherm. The units on the abscissa in these figures are arbitrary. Today they are usually in mmol g^{-1}.

The first step in analysis of the isotherm is to determine to which classification the isotherm belongs. A further recommendation is to determine the classification of the isotherm according to the standard curve representation or the χ plot representation. This used to be more difficult than present since
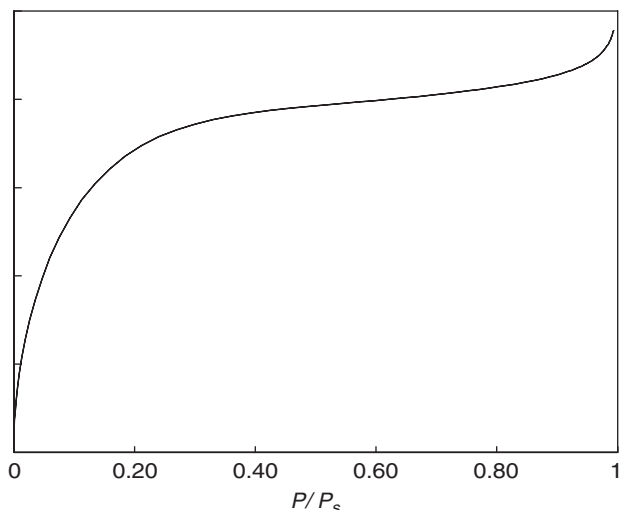
Fig. 3. Type I isotherm.
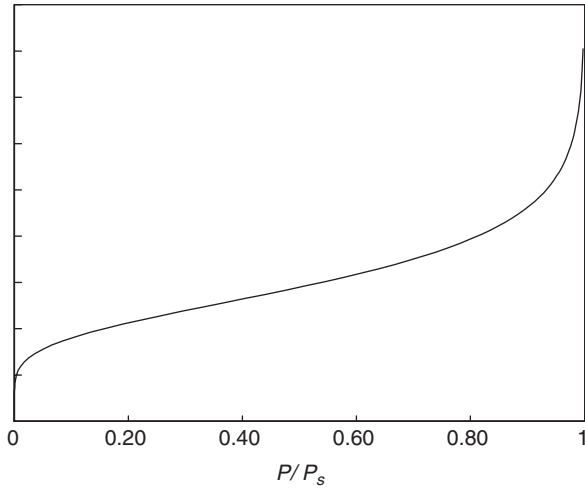
Fig. 4. Type II isotherm.
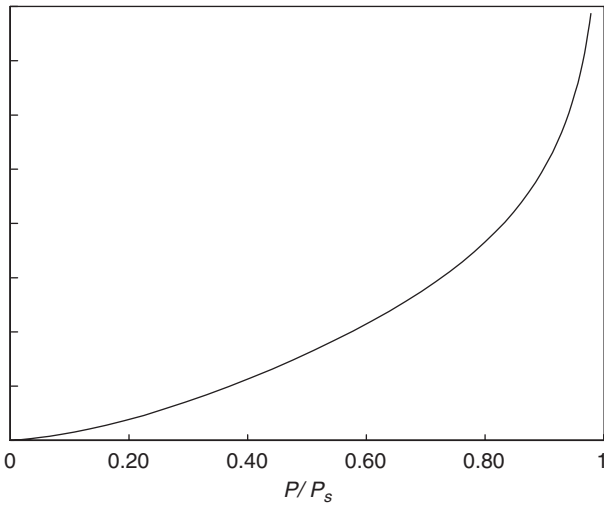
Fig. 5. Type III isotherm.

each adsorbent–adsorbate combination had its own standard curve that was numerically obtained. There is now a universal representation [4] of the standard curve based upon a quantum mechanical theory of adsorption. This representation is referred to as the chi, χ, representation. A χ plot is a plot of
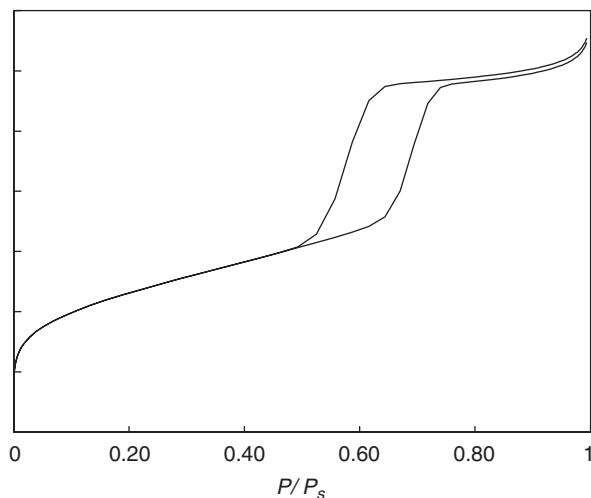
Fig. 6. Type IV isotherm.
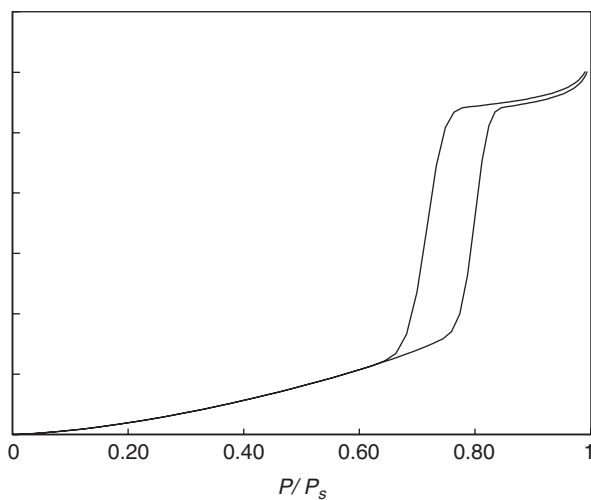
Fig. 7. Type V isotherm.

amount adsorbed versus the quantity $-\ln(-\ln(P/P_s))$. The explanation for this will be presented more fully in Chapter 4. In general the χ plot of a non-porous adsorbent for which there is only one energy of adsorption for a particular adsorbent–adsorbate combination is a straight line. Thus, deviations
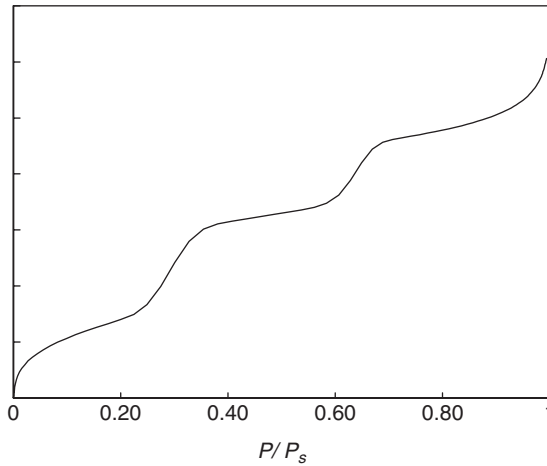
Fig. 8. Type VI isotherm.

Table 2
Classifications of physical adsorption isotherms

Type	Interpretation
I	This is characteristic of either a chemisorption isotherm (in which case the final upswing at high pressures may not be present) or physisorption on a material that has extremely fine pores (micropores)
II	This is characteristic of a material, which is not porous, or possibly macroporous, and has a high energy of adsorption
III	This is characteristic of a material, which is not porous, or possibly macroporous, and has a low energy of adsorption
IV	This is characteristic of a material, which contains mesoporosity and has a high energy of adsorption. These often contain hysteresis attributed to the mesoporosity
V	This is characteristic of a material, which contains mesoporosity and has a low energy of adsorption. These often contain hysteresis attributed to the mesoporosity
VI	This type of isotherm is attributed to several possibilities the most likely being, if the temperature is below the adsorptive triple point, that the adsorbate is more like a solid forming a structured layer, i.e. epitaxial growth. Other possible explanations include multiple pore sizes. If the steps are at the low-pressure portion of the isotherm, then the steps may be due to two or more distinct energies of adsorption. If the steps are at the high pressure part of the isotherm, then the steps might be due to sharp steps on the adsorbate surface

from this straight line in either the positive or negative direction indicates deviations from this simple case. Table 3 shows a summary of the possible features that the χ plot can have in addition to a straight line.

At the end of this chapter are the χ plots that correspond to the types I–VI isotherms given in Figs. 3–8. In addition a second type VI plot is presented that differs from the one presented in Fig. 8, which has the χ plot feature 5. When transformed, types II and III are identical and so are types IV and V. Thus, the χ representation cuts down on the number of isotherms to consider and specifies exactly the physical feature that each χ plot feature corresponds to. One of the possible type VI isotherms that shows feature 5 in Table 3 above can be distinguished from the pore-filling feature 3 in the χ plot, whereas in the isotherm this discernment is not possible.

It has been a general practice to determine where a monolayer of material is adsorbed by the following method. First, one inspects the isotherm, most of which have the appearance of type I or II. In the low-pressure end of the isotherm, there is a portion that has a negative curvature. In the middle of this curvature is the point called the "B" point. There are prescriptions as how to unbiasedly determine this point. There are two problems with this approach. First, the knee bend is somewhat gradual and, second, the point of sharpest bend is dependent upon the scale used to view the isotherm. This is assuming that one has data that has little scatter. Thus there are other

Table 3
Non-linear features of the χ plot

Item	Feature	Interpretation
1.	Positive curvature at the lowest pressures	A distribution of adsorption energies
2.	Negative curvatures	Decrease in adsorption potential due to filling of pores
3.	Large positive curvature followed by negative curvature to yield a slope of the χ plot that is less than at lower pressures	Mesopore filling due to capillary action
4.	Hysteresis associated with item 3.	Several possibilities: a shift in adsorption energy, odd shaped pores, major and minor pores, distortion of the adsorbent
5.	A break in the straight line at moderately low pressures	Similar to item 1 except the distribution may be 2 or 3 distinct values

unbiased mathematical methods, or at least this is the hope, to determine the monolayer value. The most widely used is the Brunaver, Emmett and Teller (BET) equation but there are other methods as well including standard plots and other theories. Unfortunately, most of the other methods, excepting the χ method, rely in some way on the BET to get started. (For example, for both α–s or t-plots, which are standard plots, the relationship to monolayers adsorbed depends upon the BET determination.) In the next chapter, a more detailed discussion of the "B" point is given. It seems, however, that this method is no better than a factor of 5. Even this is questionable with a type I isotherm where other interpretations of the negative curvature are operative.

Characterization of Hysteresis Loops

Hysteresis loops are classified into four types. These types were given the designation of H1–H4 by an IUPAC committee [5]. Figs. 9–12 are schematic representations of these four types.

The characteristics and conventional interpretation of these hysteresis loops are given in Table 4. However, there is much work still being performed to understand these forms. (See, for example, the recent publication by Roja et al. [6]. They interpret, with modeling to back up their conclusions, that the loop shapes, at least type H1 and H2, depend upon two factors: (1) the size difference between spherical chambers and connecting passages and (2) the number of passages versus chambers. Neimark and Ravikovitch [7], on the
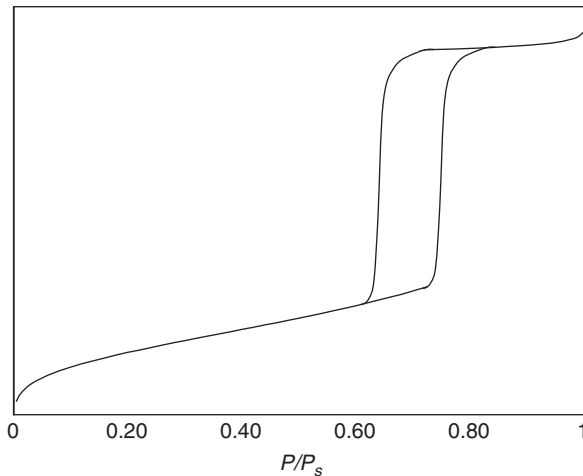
Fig. 9. Type H1 hysteresis loop.
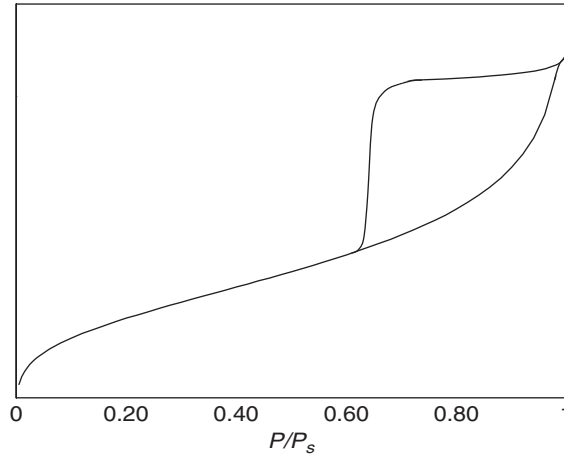
Fig. 10. Type H2 hysteresis loop.
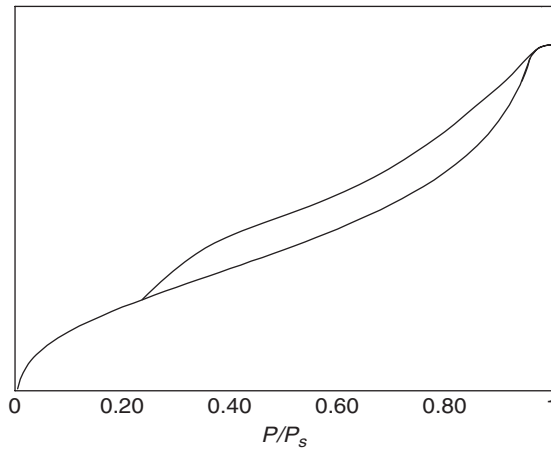
Fig. 11. Type H3 hysteresis loop.

other hand, have modeled adsorption in MCM-41-type zeolite with NLDFT methods. Their conclusion is that the adsorption branch corresponds to the spinodal condensation, i.e. metastable situation, and the desorption branch corresponds to the equilibrium capillary condensation/evaporation situation. Kowalczyk et al. [8], have calculated the hysteresis using a lattice density functional theory. The basis of their work stems from similar simulations by
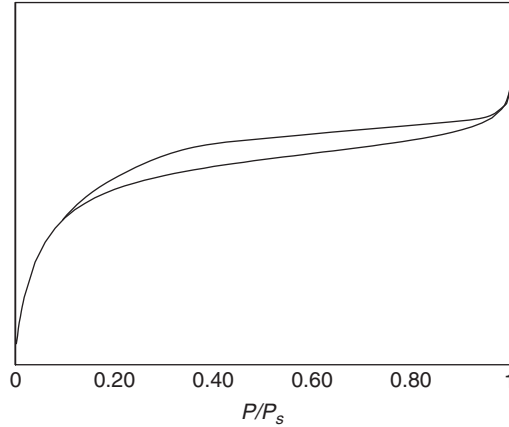
Fig. 12. Type H4 hysteresis loop.

Table 4
Characteristics and interpretation of hysteresis loop types

Type	Characteristics	Usual interpretation
H1	Nearly vertical and parallel adsorption and desorption branches	Regular even pores without interconnecting channels
H2	Sloping adsorption branch and nearly vertical desorption branch	Pores with narrow and wide sections and possible interconnecting channels
H3	Sloping adsorption and desorption branches covering a large range of P/P_s with underlying type II isotherm	Slit-like pores for which adsorbent–adsorbate pair which would yield a type II isotherm without pores
H4	Underlying type I isotherm with large range for the hysteresis loop	Slit-like pore for the type I adsorbent–adsorbate pair

Arnovitch and Donohue [9]. Their calculations demonstrate the H1-type hysteresis loop due to the curved moving meniscus. (This latter publication gives an extensive review of previous work.) Although some interpretations are given in Table 4, there is probably not any consensus at this time.

There appears to be a relative pressure (P/P_s) below which hysteresis does not occur. According to Harris [10], the value for this is 0.42 for nitrogen adsorption. Even for samples which demonstrate hysteresis above this value, if the loop extends to this value, then a sudden cut-off will occur.

Trens et al. [11], have correlated the intersection of the desorption branch with the adsorption branch at the low pressure (referred to as the "reversible pore filling" or "rpf") with thermodynamic properties. Specifically, it seems to follow the Clausius–Clapeyron equation and follows that relationship expected from corresponding states relationship. This indicates that the rpf is characteristic of a first-order gas–liquid transition. The enthalpy of this transition is somewhat higher than the liquid–gas transition in the bulk, which should not be surprising since the interaction of the solid with the adsorbate should supply an extra energy.

Further complicating comparing the various modeling with experimental data is the possibility that the energy of adsorption might shift, and possibly in a reproducible manner, from the adsorption branch to the desorption branch. Although such a shift cannot explain all of hysteresis, especially the types other than H1, it creates problems in comparing modeled hysteresis with observed hysteresis.

MEASURING THE SURFACE AREA FROM THE ISOTHERM

As hinted at in the previous section, if one can determine the amount of material in one monolayer of adsorbate, then the surface area can be calculated from this. One simply needs to know what the average cross-sectional area of the adsorbate molecule. The calculation is then rather simple. If n_m is the number of moles of adsorbate in a monolayer and a the cross-sectional area of the adsorbate molecule, then the surface area, A_s, is given by

$$A_s = n_m N_A a \tag{1}$$

where N_A is Avogadro's number (6.022×10^{23} mol^{-1}). Two problems are involved with this. Firstly, "how does one arrive at n_m?" Secondly, "what is the value for a?" In the first instance some theory should yield n_m. The most widely used theory is the BET [12], which assumes that the adsorbate molecules settle on two types of specific local sites, either a site on the adsorbent surface or on top of another adsorbate molecule. The spaces of the sites are exactly that expected for the close packing of the adsorbent molecules. Thus, the adsorptive solid phase spacing in the close-packed arrangement is used for a. This formulation seems to work quite well with the following provisos:

1. The adsorption is a high-energy adsorption, such as on silica.
2. The range of fit for the BET equation is restricted to 0.05–0.35 for the value of P/P_s.

The latter condition must be adjusted depending upon the adsorbate–adsorbent combinations. The BET equation is

$$\frac{n_{ad}}{n_m} = \frac{CP}{(P_s - P)\left[1 + (C-1)(P/P_s)\right]}$$ (2)

where n_{ad} is the amount of the adsorbate and C the (so-called) BET constant. This is normally rearranged to

$$\frac{P}{n_{ad}(P_s - P)} = \frac{1}{n_m C} + \frac{C-1}{n_m C}\frac{P}{P_s}$$ (3)

By plotting the quantity on the left of this equation versus P/P_s one can add the slope and intercept of this plot to obtain C and thus substitute this into either the slope or intercept expression to obtain n_m. The plot should be taken over the 0.05–0.35 P/P_s range as mentioned above. Beyond these values the linearity of the plot breaks down. (The sequence to derive this is to invert both sides of Eq. (2) and then multiply both sides by P/P_s. One might wonder why the latter operation was performed.) The most common adsorptive used is nitrogen and the value used for a is 16.2×10^{-20} m^2.

Another method to determine the surface area comes from χ theory. The values obtained by this method (as analyzed by Condon [13]) seem to agree with some other methods, such as the "absolute method" of Harkins and Jura [14] and the conclusions by Kaganer [15, 16]. It also consistent with X-ray analysis for some porous samples. For a non-porous, single energy surface the following equation holds according to χ theory [17]:

$$\frac{n_{ad}fA_m}{A_s} = n_m(\chi - \chi_c)U(\chi - \chi_c)$$ (4)

where U is the unit step function (i.e. negative values of n_{ad} are meaningless),

$$\chi = -\ln\left(-\ln\left(\frac{P}{P_s}\right)\right) \quad \text{and} \quad \chi_c = -\ln\left(\frac{-E_a}{RT}\right)$$ (5)

The constant *f* has a value between 1.82 and 1.92 depending upon the relative sizes of the adsorbate and adsorbent molecules or ions. From the plot of *n* versus χ one can obtain $n_m f$ as the slope and E_a can be calculated from the *x*-axis intercept. Eq. (1) is used to obtain the surface area. The value of *a* is calculated from the liquid density by:

$$a = \left(\frac{M}{\rho}\right)^{2/3} (N_A)^{1/3} \tag{6}$$

where *M* is the molar mass (units: g mol^{-1}) and ρ the liquid density (units: gm^{-3} obtained by multiplying the density in g mL by the factor 1×10^6 mL m^{-3}).

At this time, all the other theories that yield the isotherm or parts of the isotherm depend upon the BET, either directly or indirectly through a standard curve, in order to obtain the surface area.

DETERMINING POROSITY BY PHYSICAL ADSORPTION

There have been several methods to determine porosity using physical adsorption. The first step is to determine if the porosity consists of micropores or mesopores. By definition, macropores are too large to show up as pores within the experimental data range. Type I isotherm is usually interpreted as an indication of micropores. Type IV, V and possibly VI are characteristic of mesopores. A far as the χ plot or the standard plots features are concerned, whenever the slope of the plot decreases, with or without an intervening positive increase, pores are present. The presence of the intervening positive increase is an indication (χ definition) of mesopores. In the Brunauer, Deming, Deming and Teller (BDDT) designation, a type II or III isotherm does not indicate porosity, however in the χ transform a type II or III appearing isotherm might indeed indicate porosity. If a mix of micropores and mesopores are present then typing might prove difficult but the χ plot might reveal these individual features. If more than one size of micropore is present, the χ plot has proven to be successful in determining this [18]. Although both micropores and mesopores can be handled simultaneously, for clarity they will be separated in this treatment.

Micropores

Classically, micropores have been treated using the Langmuir [19, 20] isotherm with the assumption that since the micropores were too small for

more than one molecular layer to adsorb, that the multilayer consideration (as assumed for the BET) was irrelevant. The Langmuir equation is

$$\frac{n_{ad}}{n_m} = \frac{KP}{1+KP} \tag{7}$$

which may be rearranged to a linear form so

$$\frac{x}{n_{ad}} = \frac{1}{Kn_m} + \frac{x}{n_m} \tag{8}$$

where $x = P/P_s$. From the plot of x/n versus x the slope and intercept can be obtained to yield K and n_m. K is simply an equilibrium constant. From an analysis of standard curves, this analysis for n_m will be off by as much as a factor of 4 for physical adsorption in micropores.

Another possibility in analyzing for micropores is to modify the BET equation to allow for only a certain number of monolayers to adsorb. This introduces another parameter, i.e. the number of allowed monolayers. This equation is not widely used and has not proven to be successful. With N being the number of allowed layers, the modified equation, called the BDDT [21], is

$$\frac{n_{ad}}{n_m} = \frac{cx}{1-cx} \frac{1-(N+1)x^N + Nx^{N+1}}{1+(c+1)x-cx^{N+1}} \tag{9}$$

The most reasonable method to analyze micropores is to use the standard curves. Fig. 13 illustrates the technique. Plotting the amount adsorbed versus the standard plot value listed in the figure as $\mathbf{F}(P/P_o)$ (or in the case of a χ plot the χ value) one should obtain two linear regions. The slope of the low linear region (labeled L) is proportional to the surface area, including the surfaces of the micropores. The slope of the upper linear region (labeled H) is proportional, with the same proportionality constant, to the area outside the pores plus the pore openings. The (n/n_m) intercept of this upper line is the amount of adsorbent that can fit into the micropores. This is therefore an indication of the pore volume. It has been speculated that the round-off between these curves is an indication of the geometry of the pore. That is, a sharp transition indicates slit-like pores, whereas a rounded transition indicates more cylindrical pores. This is not entirely clear at this time.
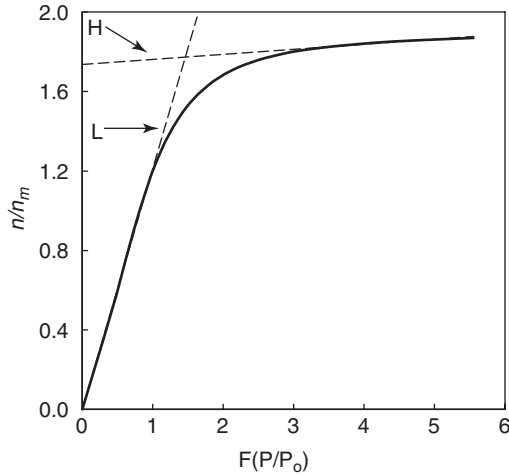
Fig. 13. A χ plot or standard plot of a type I isotherm.

Mesopores

Mesopores generate either a type IV or V isotherm. In types IV and V isotherms a similar strategy as that for micropores can be used as illustrated in Fig. 14. Notice, however in this case that the lower line, L, and the upper line, H, intersect at a higher value of χ than the commencement of the negative change in the slope. The analysis from these lines remains the same as for the micropore case (Fig. 13), but there is additional information. One could refer to such pores as "pre-filled" or "capillary filled" since it is normally attributed to capillary action. Notice that this particular part of the analysis an answer for the pore volume, total surface area and external surface area is independent of whether the adsorption or desorption branch of the isotherm is used.

The interpretation of the hysteresis loop is a matter of some current discussion. The primary explanation is based upon the Kelvin equation as modified by Cohan [22]. which is:

$$RT \ln\left(\frac{P}{P_s}\right) = \frac{h\gamma V_m}{r_p - t} \tag{10}$$

The following are the meanings of the new symbols, γ is the surface tension of the liquid adsorptive, V_m the liquid adsorptive molar volume, r_p the pore
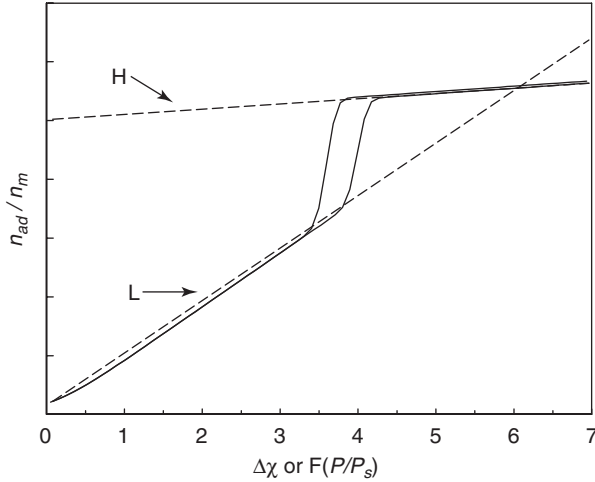
Fig. 14. A χ plot or a standard plot of either a type IV or V isotherm.

radius or half the distance across the pore, t the "film thickness" before the prefilling starts and h a constant depending upon the pore geometry. For h the following are used:

- $h = 1$ for slit-shaped pores
- $h = 2$ for cylindrical-shaped pores
- $1 < h < 2$ for oblate-shaped pores
- $h < 1$ for slits that have many concave sides.

Values above 2 would be an indication of some fractal arrangement. The t thickness is the thickness assumed given by the following equation:

$$t = \frac{r_{ad} V_m}{A_s} \tag{11}$$

Obtaining Pore Radius from the Two Slopes

The following then is the information that one would hope to extract from these plots. Assuming one can relate the slopes of L and H to areas either by comparison to non-porous standard or through the theoretical χ treatment, one has the areas A_s corresponding to the L slope and A_{ex} corresponding to the H slope. (χ treatment would use the analytical expressions of Eqs. (4) and (5).) These are related to the physical quantities of the total

surface, A_s, the area inside the pores, A_p, the total surface area of the pore openings, A_o, and the area of the edge-on walls or the non-porous area of the outer surface, A_w, by

$$A_s = A_p + A_w \tag{12}$$

$$A_{ex} = A_w + A_o \tag{13}$$

The total pore volume, V_p, should be well approximated by the intercept mentioned. At this point a geometry must be assumed to analyze further. If cylindrical pores are assumed then there will be an average length per pore, $\langle l \rangle$. Basing the following upon a fixed amount of adsorbent, conventionally exactly 1 g, one can construct the following equations:

$$V_p = \pi r_p^2 \langle l \rangle N_p \tag{14}$$

$$A_p = 2\pi r_p \langle l \rangle N_p \tag{15}$$

$$A_o = \pi r_p^2 N_p \tag{16}$$

where N_p is the number of pore openings per gram and r_p the pore radius. For microporous plots (Fig. 13), these equations present the problem that there are more physical quantities which need to be extracted than there is information available. For these cases, the assumption normally used is that $A_o \ll A_w$ thus making $A_{ex} = A_w$ and $A_p = A_s - A_{ex}$. Other assumptions could be made, for example if the wall thickness of the zeolite were about the same size as the pore radius, then $A_w \approx A_w$ and therefore $A_w \approx 0.5\ A_{ex}$. In general, one could insert a factor, $0 < \alpha < 1$ to relate A_w to A_{ex}. The r_p then would be

$$r_p = \frac{2V_p}{A_s - \alpha A_{ex}} \tag{17}$$

Eq. (17) is capable of yielding a range of values for the pore radius using the slopes and intercepts of the standard plots for both micropores and mesopores.

The Use of the Kelvin Equation Value of r_p for Mesopores

In the case of the analysis of mesopores (Fig. 14) a separate determination of r_p may be obtained using Eqs. (10) and (11). The pressure used in Eq. (10) is that at which a sudden increase is observed or the average value in the step. n_{ad} is for the purpose of calculating t extracted from the L portion of the standard plot or its extrapolation. Both of these assumptions are approximations. In general there is also a distribution of either pore sizes or of adsorption energies, which complicates this simplistic analysis. These complications can be overcome and are addressed in Chapter 6. The simple treatment however follows along these lines.

1. Using the value of r_p, which is obtained from Eqs.(10) and (11), determine the product $\langle l \rangle N_p$-from Eq. (14).
2. Substitute $r_p \langle l \rangle N_p$ into Eq. (15) to obtain A_p.
3. Obtain A_w by substituting A_p into Eq. (12).
4. Obtain A_o by substituting A_w into Eq. (13).
5. Obtain N_p by substituting A_p into Eq. (16).
6. $\langle l \rangle$ is then obtained by dividing out N_p from $\langle l \rangle N_p$.

Thus for an isotherm indicating mesoporosity one should be able to obtain all of the physical quantities unambiguously. This analysis requires very good data to yield results. Notice that in step 3, that A_p and A_s should be much larger than A_w. If this is not the case then there is a high uncertainty in A_w and obtaining a nonsense answer is possible.

Macropores

Almost by definition macropores cannot be observed in the isotherm, at least until now. This is because the pore filling would occur at pressures too close to the vapor pressure, P_s, to be reliably measured. This, however, may be changing. By using a differential technique and very good temperature control and handling methods Denoyel, Barrande and Beurroies [23] have been able to extend the reliable pressure range to 0.99985 of P_s and measured porosity up to 12 μm The analysis method should be identical to that used for mesopore (IUPAC).

STATISTICAL TREATMENT OF ISOTHERMS

The principal fact to keep in mind when analyzing an adsorption isotherm is that the pressure reading is invariably much more precise than the

measurement of the amount adsorbed. If a transform for P/P_s is used in the analysis, very little error (indeed usually insignificant error) is introduced in the statistical analysis. Whereas, if a transform is performed upon n_{ad} then a statistical error is introduced unless some compensating weighting factors are introduced.

For example, the linearized BET equation (Eq. (2)) transforms both P/P_s and n_{ad} but one need only be concerned with the error introduced by n_{ad}. There could be a significant error in the assumed value of P_s, however the recommendation is to use only values of P between 0.05 and 0.35 of P_s which eliminates most of this uncertainty. Since the function used in n_{ad} is $1/n_{ad}$ then the error is approximated by εn_{ad}^{-2}, where ε is the error or uncertainty expected in n_{ad}. The average uncertainty is often assumed to be constant regardless of the value of n_{ad}. Thus the lower the value of n_{ad}, the greater is the error in the transformed plot. In computing a linear least squares on the transformed plot a weighting factor of n_{ad}^2 should be used. Over the 0.05–0.35 P_s range this gives a variation in error of a factor of about 50. A more precise choice would be to use a non-linear least-squares routine for the untransformed equation (Eq. (14)) in which case the initial estimates of n_m and C could be obtained from the transformed plot.

The practical consequence of not using a weighted regression (least-squares) method is that under most practical conditions, the error is small when one uses the non-weighted regression. Simulations of adsorption on ceramic materials have indicated that a probable error of about 3–4% is introduced by the transform. The answer for the surface area from the non-weighted method is always less than the weighted value. Interpretation of the statistics from the transformed plot, however, is not straightforward. For example, what does the meaning of the statistical outputs such as R^2 and parameter deviations (σ_x and σ_y) indicate in the regression analysis?

The problems of interpretation of statistical parameters and error introduced by data transformation are not present in the standard isotherms, such as the α–s plot, t-plot or others, nor are they problems with the χ plot. In these cases, n remains untransformed and the error for the full range is approximately constant. A straight application of a simple linear regression is therefore appropriate. This makes the derived statistics, such as standard deviation, R^2, σ_x, σ_y, etc., easy and straightforward to interpret. These statistics then relate directly to the physical quantities that they are associated with.

ADSORPTION TYPES IN STANDARD ISOTHERM TRANSFORMATIONS

The type I–VI isotherms of Figs. 3–8, are shown in Figs. 15–20. In order for the type I to simulate a Langmuir isotherm as assumed one must include an energy of adsorption (that is E_a) as a distribution of energies. This, however is usually not observed experimentally since the very low pressure range is not normally measured. Type II and type III are basically identical except for the value for E_a. A distribution of E_a was added to the type III here for illustration
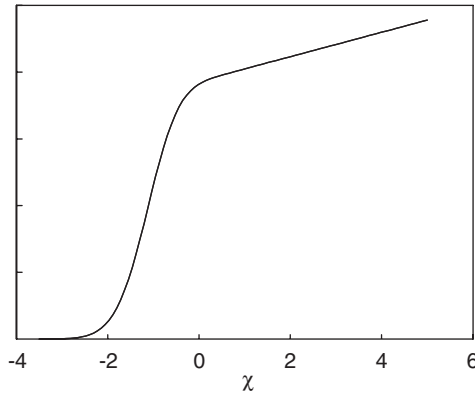
Fig. 15. Type I isotherm expressed as a standard plot or a χ plot. An energy distribution has been added to allow $n_{ad} \to 0$ simultaneous as $P \to 0$.
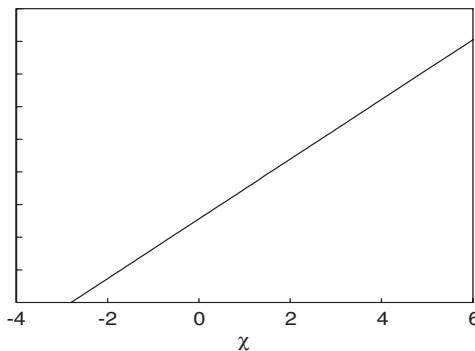
Fig. 16. Type II isotherm expressed as a standard plot of a χ plot. No energy distribution is assumed.
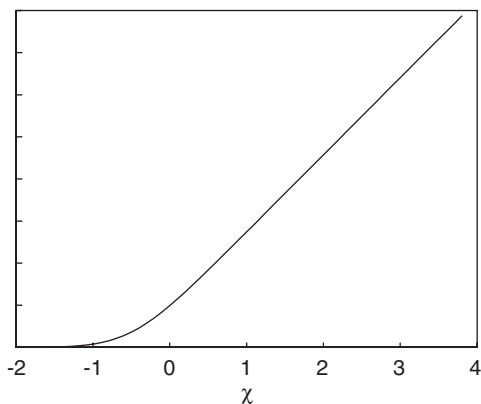
Fig. 17. Type III isotherm expressed as a standard plot or χ plot. An energy distribution has been added since low E_as usually include this.
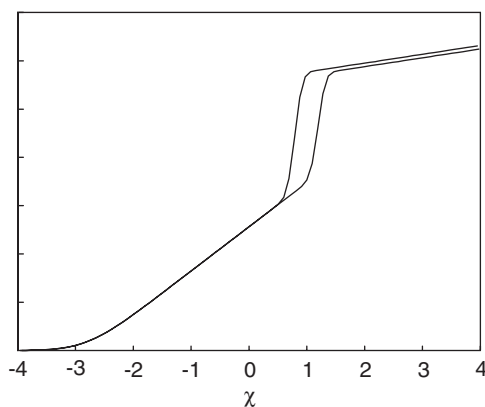
Fig. 18. Type IV isotherm expressed as a standard plot of χ plot.

purposes and is not a necessary feature. Types IV and V are also identical except for the differences in E_as.

There is a possibility of obtaining a false hysteresis loop if the energy of adsorption (E_a) shifts to a lower value for the desorption isotherm. This is very likely, so a plot of n_{ad} versus $\Delta\chi$ might be more appropriate. There is another plot that one can observe in the χ representation that might appear
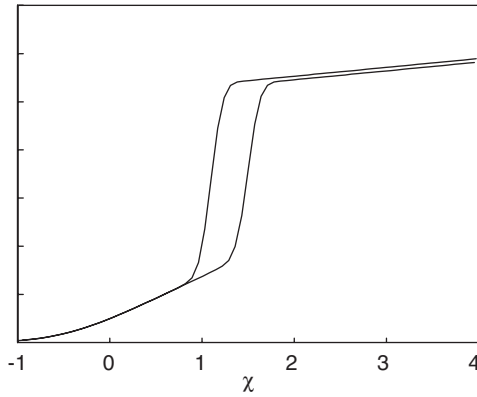
Fig. 19. Type V isotherm expressed as a standard plot or χ plot.
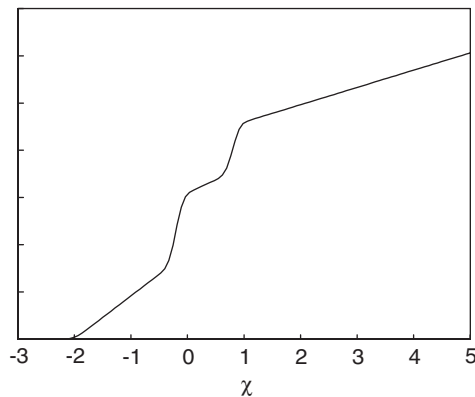
Fig. 20. Type VI isotherm expressed as a standard plot or χ plot.

as a type VI plot. This is characteristic of samples with two or more types of surface with differing energies (E_a) of adsorption. The feature, however, might be obscured in the normal isotherm representation. The standard or χ plot is represented by Fig. 21. Fig. 22 shows the normal isotherm one would obtain with the two different E_a values revealed in Fig. 21. This feature may not be obvious in the normal isotherm representation depending upon the various values but is very obvious in the standard or χ plot representation. This plot is very characteristic of carbon as an adsorbent.
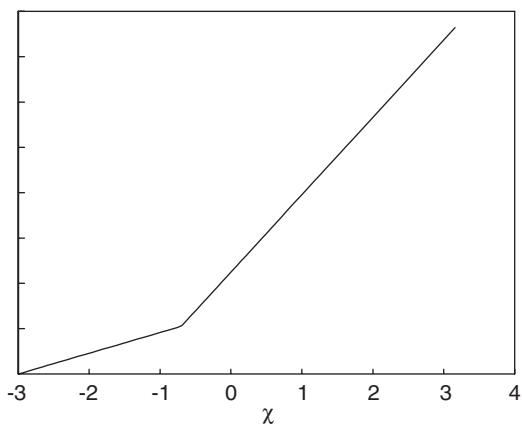
Fig. 21. A standard or χ plot of an alternate type VI isotherm (VIA). This is the result of two surfaces with differing E_as.
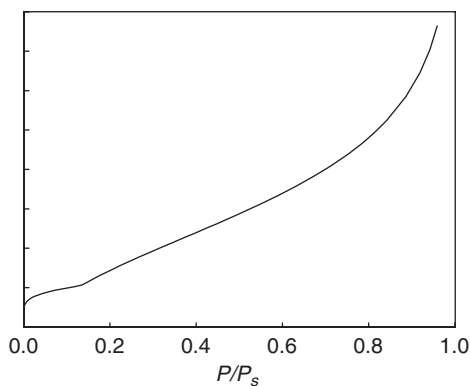
Fig. 22. The normal isotherm for the alternate type VI isotherm (VIA) where one can observe the steps due to different E_as.

REFERENCES

[1] D.H. Everett, IUPAC Mannual of Symbols and Terminology, Appendix 2, part 1, Colloid Surf. Sci., Pure Appl. Chem., 31 (1972) 578.
[2] S. Brunaur, L.S. Deming, W.S. Deming and E. Teller, J. Am. Chem. Soc., 62 (1940) 1723.
[3] S.J. Gregg and K.S.W. Sing, in Adsorption, Surface Area and Porosity, Academic Press, London, ISBN 0-12-300956-1, 1982.

[4] J.B. Condon, Langmuir, 17 (2001) 3423.

[5] K.S.W. Sing, D.H. Everett, R.A.W. Haul, L. Moscou, R. Pierotti, J. Rouquerol and T. Siemienwska, Pure Appl. Chem., 57 (1985) 603.

[6] F. Roja, K. Korhause, C. Felipe, J.M. Esparza, S. Cordero, A. Domingues and J. Il Riccardo, Phys. Chem. Chem. Phys., 4 (2002) 2346.

[7] A.V. Neimark and P.I. Ravikovitch, Micro. Mesporous Mat. 44–45 (2001) 697.

[8] P. Kowalczyk, K. Kaneko, L. Solarz, A.P. Terzyk, H. Tanaka and R. Holysk, Langmuir, 21 (2005) 6613.

[9] M.D. Donohue and G.L. Aranovich, J. Colloid Sci., 205 (1998) 121.

[10] M.R. Harris, Chem. Ind. (London), (1955) 288.

[11] P. Trens, N. Tanchoux, A. Galareau, D. Brunel, B. Fubini, E. Garrone, F. Fajula and F. DiRenzo, Langmuir, 21 (2005) 8560.

[12] S. Brunaur, P.H. Emmett and E.J. Teller, J. Am. Chem. Soc., 60 (1938) 309.

[13] J.B. Condon, Micropor. Mesoporous Mater., 53 (2002) 21.

[14] W.D. Harkins and G.J. Jura, J. Am. Chem. Soc., 66 (1944) 919.

[15] M.G. Kaganer, Dokl. Akad. Nauk SSSR, 122 (1959) 416.

[16] M.G. Kaganer, Zh. Fiz. Khim., 33 (1959) 2202.

[17] E.L. Fuller, Jr. and J.B. Condon, Colloids Surf. A, 37 (1989) 171.

[18] E.L. Fuller, Jr.,. "Morphology Of Carbons Deduced From Physisorption Isotherms: I. Nuclear Grade Graphite" and "Morphology Of Carbons Deduced From Physisorption Isotherms: II. Activated Carbon", 24th Conference on Carbon, Vol. 1, pp.14, 16, Jul 11–16, 1999.

[19] I. Langmuir, J. Am. Chem. Soc., 38 (1916) 2219.

[20] I. Langmuir, J. Am. Chem. Soc., 40 (1918) 1368.

[21] S. Brunauer, L.S. Deming, W.E. Deming and E. Teller, J. Am. Chem. Soc., 60 (1938) 309.

[22] L.H. Cohan, J. Am. Chem. Soc., 60 (1938) 433.

[23] B. Denoyel, M. Barrande and I. Beurroies, 7th International Conference on the Characterization of Porous Materials, 2005.

This page intentionally left blank

Measuring the Physisorption Isotherm

INTRODUCTION: EQUIPMENT REQUIREMENTS

There are principally two methods widely used to determine surface areas by physisorption. They are the volumetric method and the gravimetric method. The general object is the same for both. One wishes to measure the amount of a gas that adsorbs on the surface as a function of the pressure of this gas. One ends up with a series of paired data, the amount adsorbed versus pressure, from which some physical parameters are extracted. These parameters almost always include a number believed to be the surface area and a quantity related in some way to the strength of the forces holding the adsorbate to the adsorbent. Other parameters sometimes identified are the porosity in terms of pore size and volume. The volumetric technique uses one type of measurement to obtain both the data sets. This measurement is of the pressure. The gravimetric technique measures the pressure and the mass gain of the adsorbate with separate instrumentation, using some minor pressure corrections for the weight. Both techniques have their advantages and disadvantages, so it is important to be knowledgeable about both, especially if a decision is to be made as to which one to use or if a purchase is imminent.

The primary differences between the two are:

1. *Cost.* Usually, the gravimetric technique is costlier than the volumetric technique. The volumetric technique requires only high precision pressure transducers and high precision volume measurements. The gravimetric, however, requires a high precision vacuum balance and, perhaps, considerable set-up effort.
2. *Capability.* Usually, the gravimetric technique is more precise and accurate. It is a better research method than the volumetric technique. The volumetric technique is incapable of some measurements needed in research, but for most routine work, given some important caveats, it is sufficient.

The details which follow are required reading for a sound purchasing decision.

In both methods, the adsorption is performed in a temperature and pressure range just below the condensation point of the gas to liquid transition. Usually, the temperature is picked, for practical reasons, as the boiling point of the gas. For example, in measuring the adsorption of nitrogen, liquid nitrogen is used to control the temperature of the sample. This is a convenient coolant, which assures a known vapor pressure over the sample. Research work often gets away from this restriction in order to study the adsorption at other temperatures. This latter change could also increase the cost and complexity of the instrumentation. Liquids, however, which have a reasonable vapor pressure at room temperature and above are more easily handled. An example of a fairly well-characterized inert gas with a higher vapor pressure would be perfluoro-cyclohexane or sulfur hexafluoride. However, these are rarely used. Use of water, alkanes and alcohols are quite common and temperature control is only a minimal problem. There is always the question of interpretation with these gases, however.

For convenience, the following discussions will assume a nitrogen adsorbate and liquid nitrogen as the temperature controlling fluid. The sample will be referred to as a powder which is not a requirement. Contiguous, open porous samples are also characterized by the techniques.

THE VOLUMETRIC METHOD

Equipment Description

The basic volumetric method is shown schematically in Fig. 23. System parts are not to scale. This is an idealized system and some of the features may not be present on some of the commercial instruments. Furthermore, there may be features on some commercial instruments that are not shown here. An example is the matching tube system to automatically compensate for the "dead" volume. Sample chambers are usually constructed from Pyrex using metal vacuum flanges. Even though there are many systems that are all pyrex, an all-metal system is the best. The powdered sample (P) is contained in the sample tube (H). (*Note of caution* – if the powder sample is *produced in the tube*, such as hydriding a metal, one should be certain that enough room is available for expansion. A rule of thumb is at least a five fold expansion. Multiple chemical treatments are not recommended in this vertical arrangement due to packing and swelling. For that purpose, a horizontal tube with at least a 10-fold increase in effective
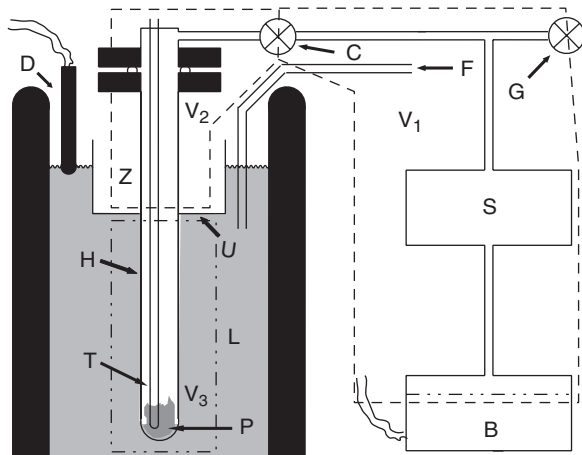
Fig. 23. Schematic of a volumetric system.

sample volume is recommended. In either case metal tubes are recommended.) This tube is immersed in a liquid nitrogen bath (L) for temperature control. Between the liquid nitrogen-cooled area and the rest of the equipment at room temperature (recommended to be thermostated to 0.1°C) is a transition zone (Z). This transition is indicated in the figure as the zone between the dashed lines in the upper (V_2) and lower (V_3) zone. It is recommended that this transition zone be controlled. One way to do this is to have a U-shaped cup (U) attached to the sample tube and control the liquid nitrogen such that the level is about halfway up this U-cup. Thus, one either has to watch the liquid nitrogen level carefully or use a level detector (D) to control the flow of liquid nitrogen (F) into the Dewar (large black object).

To admit gas, one opens the valve from the nitrogen supply (G) (nitrogen supply should have pressure controller, safety valves, etc.) with the valve to the sample area (C) closed. One then measures the pressure with a Bourdon or other membrane-type pressure transducer (B). With today's technology there is little reason to use the traditional manometers (and one very good reason not to). The volume between the two valves (S + tubing + valves + transducer) should be calibrated using PV methods and any competent standards laboratory can accomplish this. The valve C is opened when one wishes to adsorb the gas.

For temperature measurement, a thermometer well (T) is provided. In the case of liquid nitrogen temperatures, a gas ⇄ liquid equilibrium thermometer is recommended. This requires another pressure transducer and

additional tubing and valves, but yields the vapor pressure of N_2 directly. It is also very sensitive.

Determination Method

Note in Fig. 23 that there are three zones labeled indicating three volumes one must consider, V_1, V_2 and V_3. V_1 and V_2 are the "manifold". The volume of V_1, a calibrated volume, is already known at the beginning of the measurements. This calibration should have been performed either at a standard laboratory or against a secondary standard which is traceable. The first problem is to determine the volumes of V_2 and V_3.

What's the "dead space?"

Volumes V_2 and V_3 are at different temperatures, T_2 and T_3. Using the ideal gas equation, the total number of moles in the two volumes, assuming $P_2 = P_3 = P$ is

$$n = n_2 + n_3 = P/R \, (V_2/T_2 + V_3/T_3)$$

Imagine then that the entire region is a T_2 to yield an imaginary effective volume for the sum.

$$V_d = nRT_2/P$$

$$V_d = T_2(V_2/T_2 + V_3/T_3)$$

One could therefore think of the dead space (without sample) as a weighted average of V_2 and V_3 according to inverse temperature.

Normally V_2 is at a different temperature from V_3 so the total volume cannot be measured correctly. However, an effective volume called the *dead space*, V_d, can be measured. This quantity will then be used in subsequent calculations. To determine the dead space, one first does a calibration of the system without a sample with T_2 and T_3 (temperatures of V_2 and V_3) at the operating temperature anticipated. The adsorbing gas is admitted to the calibrated volume area V_1 (through valve G) with the valve to V_2 (C) closed. The pressure measurement, P_i, is taken. The valve C is then opened and a second pressure measurement, P_f, is taken. The dead space volume is given by

$$V_d = \frac{P_i V_1}{P_f} - V_1 \tag{18}$$

If the volume of the sample, V_s , is known, then a small correction can be made for its volume. This correction modifies Eq. (18) to

$$V_d = \frac{P_i V_1}{P_f} - V_1 - \frac{V_s T_3}{T_1} \tag{19}$$

The volume of the sample can be obtained if one knows both the open- and closed porosity of the sample and its theoretical density. The closed porosity of the sample should be included in V_s but the open porosity should not be included. These are subtle points which for many practical applications make little difference and can be ignored. At any rate, it is a good idea to attempt to subtract V_s even with crude data.

It is recommended that this dead space be measured over a range of pressures. A properly designed instrument will have little variation over a large pressure range. Problems concerning the location of the boundary between V_2 and V_3 can lead to errors. Furthermore, the transport properties of the gas can change with pressure, especially in the low-pressure range. In the next section, the errors due to uncertainty in the boundary between V_2 and V_3 and the error due to uncertainty in the gas transport properties is discussed further.

Once V_d is determined, one can apply this to the uptake of the adsorbate on the surface. After sealing the sample in the sample tube, with degassing and other preparation steps, the system is evacuated. The details of the degassing depend upon the sample. For careful scientific investigations degassing procedure, with for instance ceramics, would be to bake the entire system under an ultrahigh vacuum (better than 10^{-9} atm) at a temperature of $\geq 200°C$. Routine degassing is often much less vigorous. The interpretation of the data, however, is often dependent upon these steps. For the adsorption process one starts by first opening valve G and measuring the pressure (P_i). Then valve G is closed and valve C is opened and the pressure drop is followed until a new stable pressure is reached. This may take some time, and it is highly advised to have patience. During this step, it is also advised that the data be recorded and followed as a function of time. Usually, an exponential decay is observed, following a curve such as

$$P = P_f + (P_1 - P_f)\exp(0.692 t/t_{1/2}) \tag{20}$$

where $t_{1/2}$ is the "half life" constant for pressure decay, so that after a time, P_f is approached. The amount adsorbed for this single data point is given by

$$n_{ad} = \frac{P_i V_1 - P_f (V_d + V_1)}{RT} \tag{21}$$

After the first data point is taken, valve C is closed and the procedure is repeated. An additional amount is then adsorbed, again according to Eq. (21). One should keep a log of the values of P_i and P_f as the procedure advances. As one approaches the vapor pressure of the adsorbate in the bulk liquid state, P_s, the amount adsorbed per unit of pressure change becomes larger and larger. At some point, say $P = 0.95 - 0.99 P_s$, the measurements become impractical to perform and the procedure is terminated.

To obtain the total isotherm, the increments, i, of an amount, n_i, are added from n_1 to n_i for the total amount adsorbed at any particular P_f. This then yields the amount adsorbed as a function of gas pressure. For the analysis of this isotherm one should refer Chapter 1 or for a more advanced analysis Chapter 3.

Error Analysis for the Volumetric Method

In this section, potential errors for the volumetric technique are discussed. Also, relevant are the errors analyzed under *General Error Analysis* section.

Design Errors

Hopefully, none of these errors will be encountered. They are listed here so one can be aware of potential problems when constructing or buying equipment.

Uncertainty about the boundary between V_2 and V_3:

Most problematic with this design error is the sharpness and stability of the temperature transition from liquid N_2 (or other temperature control) to the room temperature region of V_2. The U-cup arrangement for liquid N_2 is recommended. Other temperatures or control methods will require similar thought. Some instruments come supplied with matching hang-down tubes to automatically compensate. If V_2 and V_3 vary during the measurements, thus varying V_d, then an unknown, unsystematic error is introduced.

Some instruments use a continuous correction to the dead volume by having a matched volume in the same temperature bath. With this arrangement it is not quite so necessary to make sure that the level of the bath is

constant. The temperature leveling cup "U" shown in Fig. 23 might not be necessary for precision work.

Poor Calibration of V_1

A poor calibration of V_1 is a systematic error and is additive across all n_i. This means that a 10% error in V_1 leads to a 10% error in the amount adsorbed. As errors go, this is not bad. Furthermore, a post calibration can correct all preceding errors directly. A 10% error in V_1 would also be unlikely, since even a crude measurement of volume should yield a number within 1%.

In determining the pore sizes using the modified Kelvin, a poor calibration of V_1 is not critical since the primary size determination is with the pressure measurement. It will directly affect the pore volume measurement.

Molecular Flow Versus Viscous Flow

This can be a large, usually unrecognized error. Proper tube design, that is, proper diameter tubing for the temperature and pressure ranges, is needed to avoid this problem. This is especially true in the low-pressure range. This error can be critical for the low-pressure work and can lead to incorrect conclusions, including the wrong values of surface area and porosity.

A discussion of the regions of the two realms can be found in most books on vacuum technology, for example the book by Roth [1]. The problem is that in the low-pressure range, P_3 is not equal to P_2 but is related to it by

$$\frac{P_2}{P_3} = \left(\frac{T_2}{T_3}\right)^{1/2} \tag{22}$$

At high pressures $P_2 = P_3$. The transition between these two regions is governed by the *Knudsen number*, which is the ratio of the tube diameter, D, to the mean free path of the gas, λ_f.

If $D/\lambda_f > 110$, then $P_2 = P_3$
If $D/\lambda_f < 1$, then (22) holds
If $1 < D/\lambda_f < 110$, something intermediate

The mean free path, λ_f, can be calculated from some gas equations of state, usually the van der Waal equation. Table 5 is a list of some typical values for λ_f which might be of importance. The λ_f is inversely proportional to the pressure, so the particular requirements of a system may be calculated from this table.

Table 5
Values for the mean free path, λ, and minimum sample tube diameters required for some gases are 25°C

Gas	λ_f at 10^{-3} atm (m)	λ_f at 10^{-4} atm (m)	λ_f at 10^{-5} atm (m)
H_2	1.2×10^{-4}	1.2×10^{-3}	1.2×10^{-2}
He	1.9×10^{-4}	1.9×10^{-3}	1.9×10^{-2}
N_2	6.6×10^{-5}	6.6×10^{-4}	6.6×10^{-3}
O_2	7.1×10^{-5}	7.1×10^{-4}	7.1×10^{-3}
Ar	7.0×10^{-5}	7.0×10^{-4}	7.0×10^{-3}
H_2O	4.5×10^{-5}	4.5×10^{-4}	4.5×10^{-3}
CO_2	4.3×10^{-5}	4.3×10^{-4}	4.3×10^{-3}
	Min. tube dia. /cm	Min. tube dia./cm	Min. tube dia./m
H_2	1.4	13.	1.35
He	2.1	21.	2.13
N_2	0.72	7.2	0.72
O_2	0.78	7.8	0.78
Ar	0.77	7.7	0.77
H_2O	0.49	4.9	0.49
CO_2	0.48	4.8	0.48

Note from the table that at low pressures (0.001 P_0 for the usual N_2 isotherm) the volumetric method breaks down. Although one can attempt corrections, the transition region is very hard to control and should be avoided.

One could argue that not much is adsorbed below 0.001 atm and therefore the error in the overall amount adsorbed is slight. Unfortunately, this is incorrect for some high-energy materials. For this adsorbent a monolayer equivalent is already adsorbed at this pressure. For analysis, with the use of Brunauer, Emmitt and Teller (BET) or other isotherms, this is critical and yields a large error. Notice that with this type of error, a systematic error is introduced in both the dependent and independent variable in the transformed BET equation. As will be seen later, however, this is not a serious error for the chi (χ) theory analysis if one is interested in only the surface area. (The caveat for this last statement is that for porous samples a much more complicated situation exists and thorough degassing and very low-pressure measurements may be required.) Besides note that the Knudsen correction is not necessary when one considers small size pores

since the immediately outside of the pores the temperature is the same as that inside the pores.

Equation of State Errors

The above discussion on how to calculate the amount of adsorbate was based on the ideal gas law. Whether this holds up or not can be easily checked. For N_2 using a liquid N_2 bath the error is slight. At full P_s the error is only about 0.03%. (In recent developments for measuring into the macropore range, a correction for this deviation may be necessary.) This might not be true for other adsorbates and other pressures and temperatures. The usual correction used for this is the Van der Waal equation, for which the constants may be found in many handbooks (e.g. the CRC Handbook [2]). A closer approximation would be the Carnahan–Starling [3] equation of state or an empirical virial equation.

Temperature Control of the Sample

A temperature error reading at the sample can affect the isotherm considerably in the upper pressure range. Such errors are usually attributed to radiative heating or inhomogeneous temperatures in the sample. Radiative heating is due to the infrared radiation originating in the V_2 section and traveling to the V_3 section. This is difficult to avoid. One possibility is to use baffles in the V_3 section to eliminate this radiation. Baffles, however, can complicate the molecular flow problem previously mentioned and should be carefully designed. Baffles are easier to use with the gravimetric technique. More about this error is presented in the "General Error Analysis" section.

Limit of Detection

Due to limitation of the pressure-sensing devices, the very low-pressure isotherms are almost never measured by the volumetric technique. The problem can be corrected by employing more than one sensor device to obtain values below 0.001 atm. Two problems are present for this technique. Firstly, the cross-calibration between the two pressure sensors must be very good to avoid large errors. Secondly, the problem of molecular flow becomes important as mentioned in a previous section. This leads to both an accounting problem and a problem in determining an important quantity for isotherm interpretation, the chemical potential of the adsorbate. Theoretically, these problems can be handled. Practically, it is easier and more certain not to use the volumetric method in this range.

Advantages and Disadvantages of the Volumetric Technique

One big advantage of the volumetric technique is that it is usually less costly. As one wishes to do more sophisticated work the cost naturally goes up.

The primary disadvantage of the technique is that it is not as suited for careful research work as the gravimetric technique. To use it in this mode, the cost advantage begins to disappear and the amount of effort required to do careful work becomes quite large, with many potential pitfalls. This is especially true for the low-pressure range of the isotherm, but it can also be true for the upper range where porosity measurements are extracted.

THE GRAVIMETRIC METHOD

Equipment Description

The principle of the gravimetric method is simpler than that of the volumetric method. For the gravimetric method, one simply brings in a pressure of the adsorbate and measures the mass gain of the sample. The isotherm is then simply mass gain (or reworked into preferred units such as moles) versus the pressure. In the engineering of the equipment, however, things are not so simple. The vacuum system is usually a conventional metal system but the balance is a very high-precision model. The method is usually confined to high-quality research work.

The instrumentation, which was used to determine the isotherms obtained in researching the χ theory cost around \$1 M (1970). Subsequently, five more instruments were built at a cost of less than \$500,000 each. Today the cost is considerably less. This is mentioned to indicate that the instrumentation is much more complex and sophisticated than at first appears. It is, however, true that the instrumentation was built for a purpose other than investigating physisorption and was more than required for physisorption measurements. A list of the system requirements for the high-quality work is below.

The system requirements are as follows [4]:

1. The balance should have at least a relative sensitivity of 1 μg per gram sample. This would be for argon or nitrogen adsorption on samples with a surface area of 1 $m^2\ g^{-1}$ or greater.
2. The system should be all ultrahigh vacuum, including the balance. High outgassing metals such as platinum should be avoided. Metals which react with hydrogen should also be avoided. The system should be capable of being baked to 400°C with hydrogen inside at a pressure of 10^{-2} atm.

3. The system should be fastened securely in a heavy table. A machine table is appropriate, but a table made from heavy metal is needed. This table should be fastened securely to a concrete floor, preferably a balance table floor with a foundation on bedrock. No attempt should be made to dampen vibrations to the table. This simply leads to intolerable drifting of the weight. The area where this is installed is hopefully free of excess vibrations through the earth. The area where the above-mentioned instruments were installed was susceptible to an occasional earthquake and to blasting in the distance. A few experiments had to be discarded due to these effects.
4. Some method for long-term data taking is required. The referred to balances were computer controlled and data taken automatically. Today, this should not be much of a challenge. Long-term data taking is required to determine the thermodynamically valid numbers.
5. Proper temperature baffling is a must.
   Fig. 24 shows baffles arrangement permanently in place using two copper gaskets on a two-side vacuum flange. To save space, the bottom matching flange had tapped holes for the flange bolts. A lower flange was used to access the hang-down pan. The upper matching flange for this flange also has tapped holes for the flange bolts. The holes in the copper gaskets, except for the holes for the
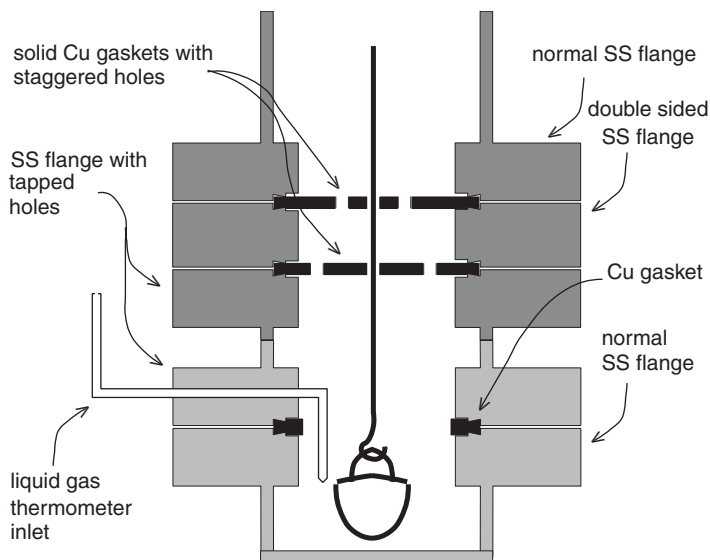
Fig. 24. A drawing of the gravimetric method sample area showing the baffle arrangement.

hang-down wire, were staggered both radially (not shown) and transversely as shown.

This arrangement allowed very little radiative heating and an assurance that the temperature read by the gas thermometer was very close to the sample temperature. It cannot be emphasized too strongly that an incorrect temperature reading is a serious, even invalidating, error. The temperature needs to be corrected to within 0.01°C, especially if one utilizes any part of the isotherm above $0.3P_s$.

6. Baking in hydrogen and sample admission with a counter flow of inert gas is often required. Therefore, provisions for this are needed. Additionally, it is recommended that a high quality, controlled and monitored glove box be available for the sample admission side of the balance, since the state of the surface is very sensitive to gas contamination.

7. Pressure gauges should range from 10 to 10^{-12} atm. A combination of Bourdon or diaphragm-type gauges and a Bayard–Alpert-type gauge would cover this. The diaphragm gauges are used for the pressure measurement for the isotherm. The sensitivity can be as low as 10^{-6} atm. The Bayard–Alpert gauges are needed for vacuum and degassing measurements.

Many of the requirements listed may be loosened, depending on the material being investigated and the quality of the work and pressure range needed.

Fig. 25 is an overall view of a typical gravimetric system. Provisions for the uniform operation of the cooling bath (L) utilizing a liquid nitrogen
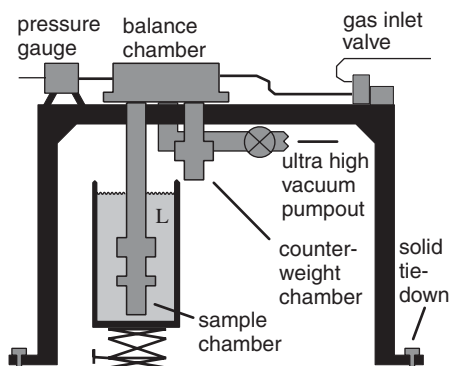
Fig. 25. An overview of the system used for the gravimetric method.

coolant are included here. The entire system is also temperature controlled with an air box. Temperature control is not quite as critical with the gravimetric system, excluding of course the sample temperature, since errors in the pressure measurement are not too great. For very precise measurement the use of a "U" cup about the hang-down tube would be advisable in order to minimize pressure variations. If the chamber area is minimized, as one might wish to do in order to measure two adsorbates simultaneously, this would probably be necessary. It may be advantageous to have the gas inlet valve, a controllable valve, which can be automatically controlled with a feedback loop from the pressure gauge. This can provide a fully automatic, computer-controlled system.

Determination Method

For careful work, the gravimetric method also needs to be pre-calibrated. This calibration is for some small corrections. Firstly, there is the *buoyancy* of the sample and the balance equipment. This correction is usually performed in one of two ways.

Method 1. A fully dense sample of equivalent volume as the anticipated sample is placed in the sample chamber. The system is then sealed and evacuated. All arrangements, such as the liquid nitrogen cooling bath, should be put in place just as if a sample were present. The adsorbate gas is admitted from very low pressures in increments up to nearly P_s. This should yield a very linear plot of "mass gain" or buoyancy, m_b versus pressure. The equation is

$$m_b = bP \tag{23}$$

where b can be either positive or negative. A least-squares routine should be used to determine b, so that the statistical information (R, σs, etc.) is available. For the isotherm, a quantity bP should therefore be subtracted from each isotherm data point.

Method 2. The second method is to determine the buoyancy with a non-adsorbing gas with the actual sample. For example, for a nitrogen adsorption isotherm, use of Ne or He as probe gases would be appropriate. The buoyancy, b, is calculated from the pressure of the probe gas, P_p, by

$$b = \frac{m_b M_{ad}}{P_p M_p} \tag{24}$$

where M_p is the molar mass of the probe gas and M_{ad} the molar mass of the adsorbate.

If the baffling or tubing is improperly designed or if one wishes to operate the instrument into and below the crossover from viscous to molecular flow, then a molecular flow correction must also be made. This means that Eq. (23) will not be linear in the very low-pressure range but will be approached at higher pressures. It is recommended that the first procedure be performed to yield b in the higher pressure range and make this subtraction from the full range of the calibration. The function left should be sample independent and repeatable for the particular instrument geometry. This should be an even smaller correction than buoyancy. If it is not, the use of different baffles or a longer hang-down tube should be considered. The equation relating the correction for molecular flow, $m_{mf}(P)$, in relation to the mass recording of the trial, m_p, is given by

$$m_{mf}(P) = m_p - bP \qquad (25)$$

Therefore, one can determine $m_{mf}(P)$ with a single calibration. The constant b, however, will change with the sample and needs to be determined for each type sample. For routine analysis of similar samples, that is, samples of the same theoretical density and closed porosity, one could initially determine b as a function of sample mass, thus saving some subsequent analysis time. If this is done, one must be sure to use the same counter weights on the other leg of the balance for a particular sample mass. One could also determine b as a function of sample mass and theoretical density, provided the samples contained no closed porosity.

For the actual measurement of the isotherm one simply admits the adsorbate to the system at the pressure desired and wait for the mass measurement to settle. This may take some time. For example, for low-pressure measurements several hours may be required for thermal equilibrium to be reached. Therefore, it is highly advised to have patience. See the comments before and after Eq. (20). For each mass data point, the buoyancy and molecular flow corrections are subtracted. For high-quality work the $T^{1/2}$ corrections are needed for pressure. Where this applies is indicated by the ratio of the function $m_{mf}(P)$ to P.

Error Analysis for the Gravimetric Technique

With the buoyancy correction and the molecular flow correction, the data obtained from the gravimetric technique should be very accurate. The limit of

detection is the limit imposed by the quality of the balance. Only small pressure corrections are needed in the low-pressure range. No pressure correction is required if the hang-down tube has been properly designed for the transition region and the pressures under consideration. However, this may not be possible if very low pressures are to be used as Table 5 would indicate.

(The diameter of the hang-down tube need not be restricted and in theory could be several meters wide. In the volumetric method this would create intolerable dead space problems. The room size could be the limit for the gravimetric method. This may not be as big a problem as at first appears, since the only problem with pressure is the question of what the pressure is in the sample area; that is, what is the true chemical potential? Thus, the pressure in the balance chamber area is irrelevant, albeit related. Molecular versus viscous flow is unimportant so long as $m_{mf}(P)$ is measured. An alternative pressure transducer method for only the sample area is possible by several arrangements.)

Advantages and Disadvantages of the Gravimetric Technique

The primary advantage of the gravimetric method is very high precision and accuracy. (A similar advantage is found in normal gravimetric analytical chemistry.) High-quality research work and pore analysis should be performed with this technique.

There are not many errors associated with the method. The calibration is relatively simple and for routine analysis, trivial. The gravimetric method is usually faster in routine mode than the volumetric method, due to the fact that fewer calibrations are needed.

Sample preparation, degassing, reacting and modifying are simpler and can be followed in a straightforward fashion in-situ using the mass changes. This is a very important advantage which is not generally or naturally available with the volumetric method. Switching over to production or preparation conditions and measurements under these conditions is very easy with no removal of the sample. Due to this, other investigations of the sample material can be combined with the surface analysis. Examples of this are the measurements of oxidation kinetics or catalytic activity.

The primary disadvantage is expense. In a gravimetric system it is expensive to purchase a good micro-balance. The sensitivity of the balance, and thus the quality of the work, is directly related to how much one spends. A second expense is the high-quality table and positioning. It was recommended that this table be tied directly to a concrete floor, preferably to a slab meant for a balance. This is an additional expense, but not absolutely

necessary. A third expense is the vacuum system and set-up expenses that rarely come with the balance.

A lot of near-by ground noise is also a problem. Earthquakes are not normally a problem since they are relatively rare, even in California, and some data might be lost for the normal surface analysis operation. For other, longer term studies, for which this system is suited, earthquakes and blasting within a range of several miles could be a problem. These latter studies, however, are not normally possible in a volumetric system anyway.

GENERAL ERROR ANALYSIS – COMMON TO BOTH VOLUMETRIC AND GRAVIMETRIC

In this section, errors that one should be aware of regardless of the technique are presented. There will be some duplication from the above discussion and potential errors due to theoretical interpretation are not covered. These will be addressed later. Most of these errors can be avoided with careful instrument design.

Pressure and Temperature Measurements

It is assumed here that the pressure and temperature measuring devices are properly calibrated. They should be traceable to the National Institute of Standards and Testing (for USA). The problem is to measure what one thinks is being measured. Here is a list of potential problems and their consequences.

1. Sample temperature problems can arise from inhomogeneous temperature of the sample.
   With respect to this problem, a highly exothermic adsorption can have a significant effect on sample temperature. (Significant in this case means 0.01°C or more.) The solution to this is to be patient in allowing the adsorption to settle down. Advice about this has already been given in both experimental sections.
2. Sample temperature problems can arise from radiative sample heating.
   With respect to this second problem, the gravimetric system would seem to suffer from this more than the volumetric. Proper baffling is therefore necessary. Another trick to play with the gravimetric method, in order to get the sample to temperature faster is to arrange a contact plate slightly below the sample pan. Being sure that the sample side is always a little heavier than the counter weight side, one can simply turn the balance off, allowing the sample pan to make contact with the

plate for thermal equilibration. Some manufacturers have some ingenious methods of decoupling the sample hang-down from the balance itself and provide such platforms as a part of the system. Alternatively, one can use patience. Volumetric analysis suffers from the problem that baffling is not advised due to pressure problems. However, direct contact with the thermostated walls is normal. It must be remembered, though, that many samples are quite insulating and thermal gradients are inevitable. For such samples, a new arrangement must be made to counter this, such as a horizontal bent tube.

The most likely error is that the sample temperature will be higher than measured or believed. Such an error leads to very large errors in P_s and essentially makes the high end of the isotherm useless. This is the range where porosity analysis is performed. To illustrate this problem, in Fig. 26 is a simulation of the effect of incorrect temperature control or measurement. For example, a temperature of only 0.5 K higher than assumed with liquid nitrogen yields an error of 8% in P_s. This translates to an adsorption error at $0.9P_0$ of a factor greater than 2. It could also create problems in analyzing for the surface area. If this error is known to exist then steps are possible with χ theory to overcome the problem.

3. Insufficient low-pressure pump-out and degassing can lead to false conclusions.
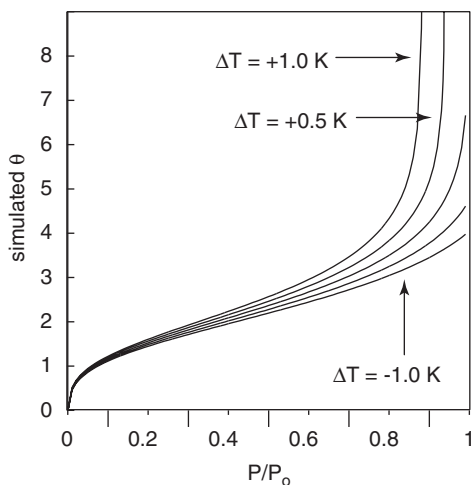
Fig. 26. Consequences of errors in temperature measurement/control in the isotherm.

For high-energy materials, such as ceramics, a monolayer can already exist on the surface of the sample at 10^{-6} atm (10^{-3} Torr) which is low vacuum. Although the surface area can be measured for most samples from this point, false conclusions can be drawn if one takes the data too seriously. A pump-out and degas should be performed to at least 10^{-9} atm and preferably lower. Most gravimetric systems are capable of this and 10^{-12} atm is not unusual.

Kinetic Problems

Between each increase or decrease in pressure, one should wait for the adsorption to settle. There are some instruments based on gravimetric methods which calculate how long this period should be. This computer decision is made on the adsorption behavior and the criteria can be set by the operator. In many cases a decision can be made as to how close to get to equilibrium, and stop the measurement at that point. Alternatively, the process can be speeded up somewhat by assuming that the approach to equilibrium is an exponential decay. Using this assumption, one can extrapolate to the equilibrium value. This has the potential danger of extrapolating too far from equilibrium for this assumption to be a good approximation. In either case, this obviously requires some type of pressure or mass recording. Automatic data taking is an ideal solution to this problem, allowing the instrument to work for 24 h. Many samples have very long settling times and without such a system there would be an enormous loss of time.

Sample Density Problems

The philosophical question sometimes comes up as to what to count as surface. Obviously, closed porosity is not counted in this method. If one has very small pores, they may or may not be counted. If poor degassing or low vacuum is used, then some small pores may already be filled before the measurement is made.

Another problem is what is referred to as *bed porosity*. This is the space between the particles. If porosity is the primary concern, then one needs to be concerned with bed porosity in the data interpretation. Bed porosity, however, is not normally a concern for most surface area analyses since it affects the higher portions of the isotherm and the values obtained at low pressure would suffice. Indeed if one were to use the traditional BET analysis, only relatively low-pressure data are used anyway.

CALORIMETRIC TECHNIQUES

Calorimetry is conceptually easy but in practice deceptively difficult.

Adiabatic Calorimetry

In Fig. 27 a schematic representation of a typical cryostat adiabatic calorimeter is shown. In this case liquid nitrogen is designated as the coolant. (The number of walls in the cryostat depends upon the temperature range selected. With helium temperatures, one needs an outer cryostat for liquid nitrogen and an inner cryostat for the liquid helium.) The various parts are as follows:

- G – gas inlet and vacuum pump-out port
- HL – heater leads
- I – insulating stand-offs
- C – copper adiabatic chamber
- H – heater coils for the adiabatic chamber
- CH – calibrating heater
- TS – temperature detector for the sample
- S – powder sample
- TC –adiabatic chamber temperature detector
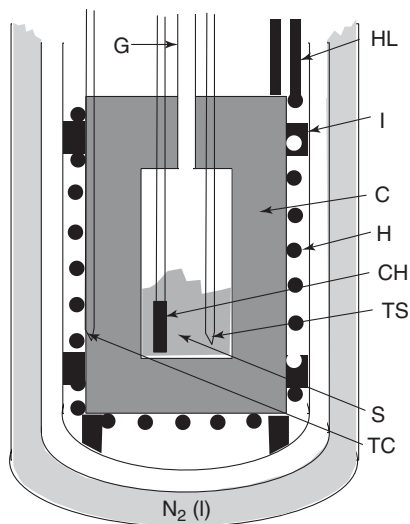
Fig. 27. A schematic of a liquid nitrogen-cooled adiabatic calorimeter.

The temperature sensors depend upon range and sensitivity requirements. They could include gas–liquid thermometers, platinum resistance thermometers, thermocouples or thermistors. It is advised to have more than one device in the sample and on the copper adiabatic shield. Very good computer adiabatic controllers are easy to construct. One must take into account in programming, the power required for various temperatures to match the heat capacity of the shield, that is, one needs to adjust the power and "damping" that the power supply puts out according to calorimeter and sample. This may take some preliminary runs to adjust it correctly.

Cooling in a vacuum could be a problem at low temperatures. It is traditional to do the preliminary cooling by back-filling both the sample chamber and the insulating spaces with helium. During the measurements, however, the cooling will need to be natural. The measurement of the isotherm is a necessary step in analyzing the data obtained from the calorimeter. The arrangement may be constructed so that the isotherm is obtained at the same time as the calorimetric data. Preliminary measurement of the calorimeter without a sample, in order to obtain the heat capacity of the calorimeter and of the powder, is highly recommended. By doing so, one can obtain the additional information of the heat capacity of the adsorbate.

The calculations required to obtain meaningful information are somewhat complex and tedious. These are described in the analysis section.

Measuring the Isosteric Heat of Adsorption

The isosteric heat, q_{st}, is the heat of adsorption at a constant adsorbate amount. In terms of thermodynamics it is related to the pressure and temperature by

$$q_{st} = \frac{RT\partial \ln P}{\partial (1/T)}\bigg|_{n_{ad}} \qquad (26)$$

Attempts have been made to determine this from the isotherms (for example see Joyner and Emmett [5]). To do this one measures two or more isotherms at different temperatures that are fairly close. One then fits the isotherms either manually, for example with a spline fit, or mathematically. Unfortunately, errors accumulate very heavily in this case and the choice of fit can greatly distort that answer. Use of the analytical form of the standard curves [6] may aid in this attempt and appears to be successful in some cases but porosity and multiple heats of adsorption make this unreliable as well.

The Thermal "Absolute" Method

Harkins and Jura [7] described a method of obtaining the surface area in an absolute way from a calorimetric measurement. They addressed many of the concerns regarding the method [8] but one must still qualify the method as being very limited. Porosity of any type would significantly alter the answer.

The apparatus is schematically represented in Fig. 28. The powdered sample, which is known to be non-porous, is allowed to equilibrate over liquid water. (In principle this should work for any liquid.) It is assumed that a film of water is adsorbed about the particles as envisioned in Fig. 29. The powder is then lowered into liquid water. In the process of doing this the outer film of the adsorbed water is destroyed thus releasing the surface energy of this film. Since the surface tension of water is known, then the surface area may be calculated from the heat evolved, ΔH, or by the simple equation,

$$\Delta H = \gamma_{gl} A_s \tag{27}$$

where γ_{gl} is the surface tension between the gas and liquid phase. Since the water vapor is nearly the saturation pressure they assumed that there were at least eight monolayers of water on the powder initially. This is believed to be sufficiently thick so that the component of the film energy due to the solid–liquid tension, γ_{sl} remains constant. (By more recent calculations the number of monolayer equivalents was closer to four monolayers. However, this is sufficient for the assumption to be approximately correct). In order to eliminate the possibility that there is additional heat of adsorption, they performed a series of experiments to measure the heat of immersion as a
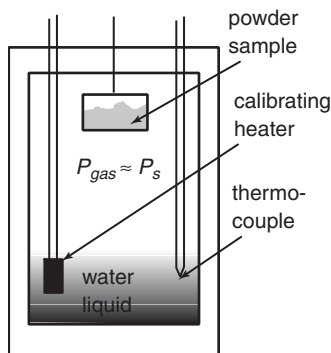
Fig. 28. A schematic of the Harkin and Jura calorimeter to measure the surface area of a powder.
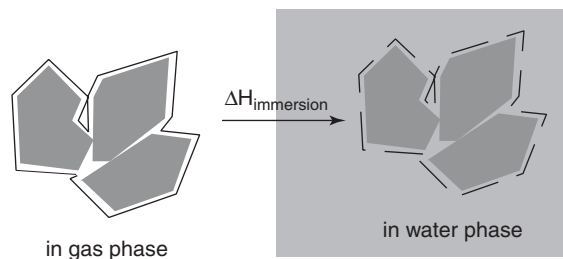
Fig. 29. A schematic of how the adsorbed film is destroyed when the powder is immersed in the liquid phase thus releasing its surface energy.

function of the exposure pressure [9]. Indeed, at the exposure pressure the value of the heat of immersion was leveling off.

There is not much work performed using this method. Possibly the reason for this is the uncertainty in the interpretation and the difficulty of controlling the experiment. Bed porosity should be a large problem, although one could find samples for experimentation that would minimize this problem. An example of these latter adsorbents would be the rare earth plasters. The measurement of the surface area in this case is at the very high-pressure region versus the BET, which is at the low-pressure region. Thus a comparison between the BET and this "absolute" method is somewhat questionable.

More importantly, for most researchers and engineers, this technique is very limited to special types of powders. With an unknown sample it does not seem to have much utility, as ingenious as it is.

Differential Scanning Calorimetry

Differential scanning calorimetry is often combined with thermogravimetric analysis of some type, which is thermal desorption or adsorption. The method yields fine details in the analysis. Adsorption experiments are performed by addition of the adsorbate at a rate that is

1. slow enough that the system is very close to equilibrium but
2. fast enough to obtain a temperature increase enough to measure in the differential mode.

The first criterion can be checked by doing some kinetic studies, either gravimetric or volumetric. The second criterion would probably be obvious during the calorimetry experiment. The calorimetry system has been described by Rouguerol et al. [10]. It provides details of the thermodynamics of

adsorption that gravimetric and volumetric methods may not be able to supply and is an excellent complimentary research tool. This is evident, for example, in the study of N_2 and Ar adsorption carbon (Sterling MT 1100) performed by Rouquerol et al. [11]. In this article there are clear peaks in the heat of adsorption in a region where the isotherm shows only a vague break. The difference between N_2, Ar and O_2 adsorptions are quite clear.

The differential scanning calorimeter has the advantage that the heat of adsorption or desorption is compared to a standard using a differential temperature measuring method, usually two thermopiles for which the voltage difference between them is measured. Fig. 30 is a schematic of the system that Rouquerol et al. employed. ("TCP" indicates the thermopile, "S" the sample chamber, "M" a matching reference chamber and "L" is a slow He leak.

FLOW METHOD OR CARRIER GAS METHOD

The flow technique or carrier gas technique is very similar to gas chromatography. A carrier gas, typically helium is used to carry adsorbate gas such as N_2. The sample is cooled down to the adsorption temperature (usually liquid N_2 temperature). During this cool-down, the adsorbate is adsorbed. A downstream detector, usually a heat conductivity detector, picks up the signal indicating that there is a decrease in the adsorbate. The
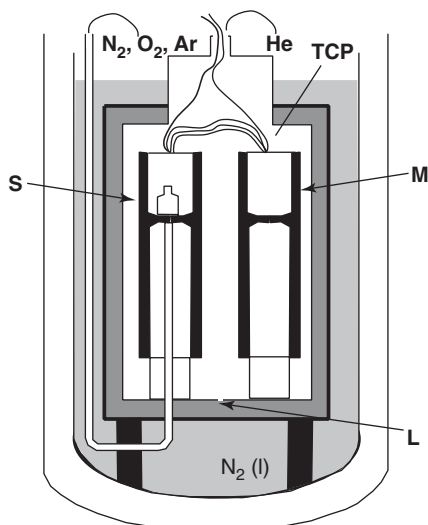
Fig. 30. Schematic of the differential calorimeter by Rouquerol et al.
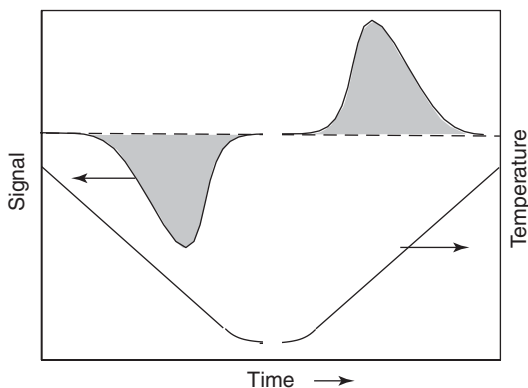
Fig. 31. Schematic of the signal observed for the flow system.

sample is allowed to cool long enough for the signal to return to the baseline. The coolant is then removed or the sample heated up by some method. A reverse signal is then detected indicating the desorption of the adsorbate. A schematic of the type of signal one observes is presented in Fig. 31. The detector is calibrated by the insertion of a shot of adsorbate gas without the coolant.

The primary advantages of this technique are:

1. the equipment is very inexpensive,
2. the throughput is very high.

The disadvantages of this technique are:

1. The precision and accuracy are poor;
2. Normally the isotherm is not obtained.

The technique is probably most useful for rapid throughput for quality assurance purposes, although this should not be the exclusive criterion since identical results can be obtained for very different samples.

In the appendix, a current listing of commercially available instruments for all the techniques and their manufacturer's specifications is given.

REFERENCES

[1] A. Roth, *Vacuum Technology*, North-Holland Publishing, Amsterdam, ISBN 0-444-10801-7, 1976.
[2] D.R. Lide, ed., "CRC in Handbook of Chemistry and Physics," 76th edition, pp.6–48, CRC Press, Boca Raton, FL, 1995 (or many other editions).

[3] N.F. Carnahan and K.E. Starling, J. Chem. Phys., 51 (1969) 635.

[4] K.A. Thompson, Microbeam. Anal., 22 (1987) 115.

[5] L.G. Joyner and P.H. Emmett, J. Amr. Chem. Soc., 70 (1948) 2353.

[6] J.B. Condon, Micropor. Mesopor. Mat., 53 (2002) 21.

[7] W.D. Harkins and G. Jura, J. Chem. Phys., 11 (1943) 430.

[8] W.D. Harkins and G. Jura, J. Chem. Phys., 13 (1945) 449.

[9] W.D. Harkins and G. Jura, J. Am. Chem. Soc.,71 (1944) 919.

[10] J. Rouquerol, R. Rouquerol, Y. Grillet and R.J. Ward, Characterization of Porous Solid, p. 67, IIUPAC Symposium, Elsevier Press, Amsterdam, 1988.

[11] J. Rouquerol, S. Partyka and F. Rouquerol, J. Chem. Soc., Faraday Trans. I, 73 (1977) 306.

This page intentionally left blank

Chapter 3

Interpreting the Physisorption Isotherm

OBJECTIVES IN INTERPRETING ISOTHERMS

It is normally conceded that an interpretation of the isotherm obtained is desirable. Intuitively, one would think that the interpretation of the isotherm would yield some measurement or estimate of the value for

- the surface area of the sample and
- some energy term related to the strength of the forces between the adsorbate and adsorbent.

These are the two basic parameters to be sought from adsorption isotherms. Other parameters include

- some measure of porosity, such as pore radius,
- the distribution of adsorption energies and
- the distribution of pore radii.

There are some isotherms which are most useful for finding the pore volume, but little else.

To be of practical use, the isotherm should be able to yield the parameters of surface area and adsorption energy for a surface of *unknown* composition. This point is often obscured in the literature with the development of various theories of adsorption. Theories that cannot yield the surface area and adsorption energy independently from some other method is of questionable value. Likewise, a theory of adsorption should also not be dependent upon the type of adsorbate or adsorbent. For example, a theory that requires a knowledge of the exact nature of the surface atoms and the interactions between these atoms and the adsorbate might yield some insight into the adsorption process but it has little practical predictive power. The reason for this is usually the exact nature of the adsorbent surface is unknown.

There are several isotherm interpretations available. The most widely used is the Brunauer, Emmett and Teller (BET) [1] and its various modifications including the Brunauer, Deming, Deming and Teller (BDDT) [2].

Another widely used isotherm, especially for porous material, is the Dubinin–Radushkevich (DR) [3],[4] isotherm. A modified theory of the latter, the DR–Kaganer (DRK) [5], applies to non-porous surfaces. Standard curves are more useful, especially if one is interested in porosity, although most depend upon calibration by some other interpretation, usually the BET. These standard curves include the α_s-curve (see Sing [6]), the *t*-curve (see deBoer et al. [7]), the Cranston and Inkley standard [8], the Karnavkhor, Fenelono and Gavrilov (KFG) [9] standard fit and others. The theories based upon density functional theory (DFT) and Monte Carlo simulations appear to be promising, but at the moment must be classified at best as a method of generating standard curves. Several theories have been developed but so far all require calibrations and are dependent upon the specifics of the adsorbate and adsorbent. Another isotherm, the chi (χ) curve, will be introduced here both theoretically and practically, as a analytical standard curve which does not require calibration with the BET.

It is first instructive to look at the general form of a typical isotherm. The general shape of the overall adsorption isotherm curve for the simplest (type I) cases of physisorption may be seen in the upper left graph of Fig. 32. The curves simulate three different isotherms. These simulations fit some standard isotherms. Historically, the monolayer was selected as being approximately at the position of the "knee" of the isotherm. This position is indicated roughly by the solid vertical line. This selection was in analogy to the Langmuir isotherm. Some judgement had to be made as to where this "knee" was, but it was roughly at about 0.03–0.1 of the vapor pressure. It turns out that for many materials studied at that time, this value gives the equivalent of a monolayer within about a factor of 4. The problem with this approach is that the shape of the curve in the low-pressure range is nearly invariant with scale. Thus if one uses a different scale, say the isotherm from 0–$0.1P_o$ instead of 0–$1P_o$, one gets a different position for the "knee." This is illustrated in Fig. 32 with the three different magnifications of these curves. To fix this problem, an non-bias analytical method was pursued. Several equations were constructed to describe these isotherms, some of which will be reviewed here.

The natural tendency was to seek an equation which could fit the obtained isotherms fairly well and yield an answer for the surface area. Several equations are available which fit many isotherms but do not yield the surface area or the energies involved. Until recently, the only known equation which could provide an answer was the BET equation. The following discussion is obviously not all-inclusive and the reader is referred to
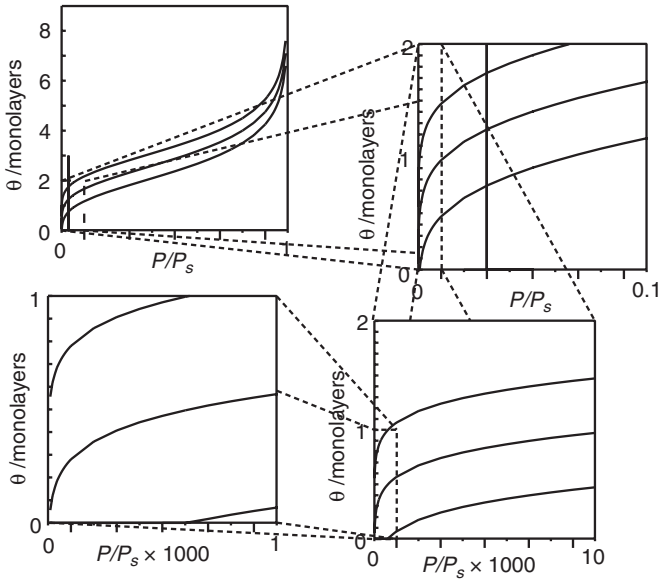
Fig. 32. Some typical adsoption isotherm for non-porous materials illustrating the problem of identifying the "knee" due to scaling.

other texts, such as that by Rudzinski and Everett [10], Adamson [11] or Hiemenz [12] for more information

It is hoped that within some of the isotherm equations there exist parameters which are identified with some physical quantity such as surface area or pore volume. To extract these parameters a least-squares routine of some sort may be used to determine the values. Some isotherm equations such as the BET, for surface area, and DR, for pore volume, restrict the range over which the fit is valid. This range is unfortunately a matter of judgement and phrase such as "over the linear range" is often used in the literature. In recent years there has been general agreement to use the saturation pressure range of 0.05–0.35, that is the pressure one would observe over the bulk liquid, P_s, for the BET equation. This works fine for some ceramic materials but unfortunately poorly for most organic materials. To make a judgement what the linear range is, one must plot a transformed set of equations. Figs. 33–35 show some examples of transformed plots, the BET and the DR. (or rather the DRK form where the moles of adsorbate in a monolayer is indicated by n_m. For the DR form this would be replaced by the moles of adsorbate needed to fill the pores, n_p.)
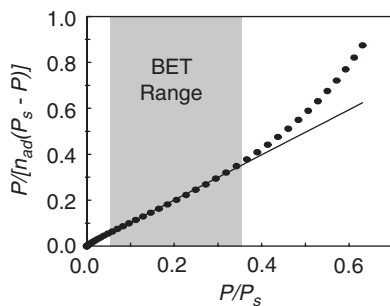
Fig. 33. The transformed BET plot to determine surface are typical of silica material. Linear range is assumed to be 0.05–0.35 of P_s.
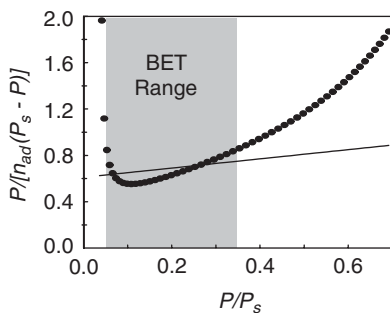
Fig. 34. The transformed BET plot for an organic material. The 0.05–0.35 range yields a very poor linear fit; thus a high range should be selected.
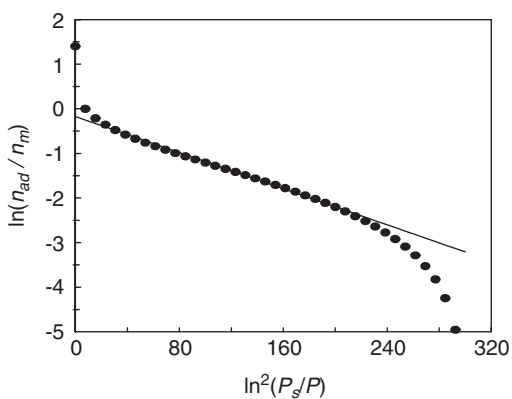
Fig. 35. A linear fit to the DRK representation of the adsorption isotherm for a non-porous surface. The fit covers about 2/3 of the $\ln^2$ range.

In the case of the BET, a linear portion of the curve for the high-energy surfaces such as silica and alumina is at about 0.05–0.35 of P_s. For lower energy surfaces this does not hold. The DRK transformed plot usually has a very long linear portion. The DR theory is useful for determining pore volumes. The intercept of the $\ln(n_{ad})$ axis should be a good indication of number of moles needed to fill the pore volume, n_p. For the DRK case it is an indication of the number of moles in a monolayer, n_m.

Almost all of the relative measurements, such as the "standard curves", refer back to the BET surface area measurement. One might say offhand, "What is the point of using the standard plots then when one could simply use the BET to begin with?" There are two principal reasons to use standard curves. First, one can use them when only a relative answer is needed, for example comparing two samples or for quality control. Second, it is generally agreed that the full isotherm contains other valuable information, particularly the mesoporosity and the microporosity. By a comparison with standard curves, which are (hopefully) characteristic of non-porous materials, one can deduce some measurements of porosity and possibly other properties.

From the above discussion, it is obvious that it is chancy to go on automatic when analyzing adsorption isotherms for the relevant physical quantities. In the following section, some more details are presented to enable one to extract some meaningful quantities from the isotherm.

The interpretation for the adsorption of more than one adsorbate has not been settled upon but the calculation made possible by χ theory is presented in the next chapter as an advanced subject. There are several equations and interpretations in the literature, all of which have either a weak foundation or are simply empirical for the materials at hand. This is fine and may be appropriate for organizing information for the moment, but should not be relied upon for predictions.

First, some analysis methods are presented which cover most of the practical applications for physisorption. The following, then, is a quick description of how to analyze the isotherm of the adsorption of one adsorbate.

DETERMINATION OF SURFACE AREA FROM ISOTHERMS

There are two methods of obtaining the surface area from the isotherm for adsorbent with unknown surface character: BET method and the χ theory method. Other theories either need the surface composition specified or use the BET as the basic equation to analyze the surface area. The BET is widely used and has been available since around 1938. Since this analysis is so

widely used, much of the information available for materials refer only to the BET surface area. The original data for the isotherms have been lost. Therefore, it is important to be able to use and interpret the isotherm in terms of the BET. The methodologies for both the BET and χ methods are presented here and the theories behind them are presented in a later chapter 4.

The BET Analysis

The original form for the BET equation is

$$\frac{V}{V_{mon}} = \frac{Cx}{(1-x)\left[1+(C-1)x\right]} \quad \text{where} \quad x = \frac{P}{P_s} \tag{28}$$

Here V indicates the volume of gas adsorbed at STP, V_{mon} the volume of gas that is required for a monolayer, P_s the vapor pressure of the bulk liquid at the same temperature, P the adsorptive pressure and C a constant. For analysis, the equation is rearranges into the transformed form:

$$\frac{x}{V(1-x)} = \frac{1}{CV_{mon}} + \frac{C-1}{CV_{mon}}x \tag{29}$$

The general approach to using transformed equations and the BET in particular is as follows:

1. Rework the data according to the transform required. In the case of the BET analysis, this means that the dependent variable (computer y) will be

$$y = \frac{x}{V(1-x)} \tag{30}$$

   The independent variable (computer x) is x $(=P/P_o)$.

2. Plot the x–y data and determine the slope and intercept over the region which appears as a straight line. (For repeated experiments, be sure to use the same region for consistency.) Many spread sheets have linear regression analysis built-in, but be sure to properly specify the range.

3. Equate the determined values of the slope, S_{BET}, and intercept, I_{BET}, with the expression for the slope and intercept in the transformed equation. Thus for the BET analysis,

$$S_{BET} = \frac{C-1}{CV_{mon}} \quad \text{and} \quad I_{BET} = \frac{1}{CV_{mon}} \tag{31}$$

4. Solve the parameters of interest from these slopes and intercepts. For the BET,

$$V_{mon} = \frac{1}{S_{BET} + I_{BET}}$$

(32)

and from V_{mon}, one can obtain

$$C = \frac{1}{V_{mon}I_{BET}}$$

(33)

5. Relate the parameters obtained to surface area or other physical quantities. For the BET, V_{mon} can be related to the number of moles of a monolayer. In the case of N_2 and Ar adsorption IUPAC has set a conversion factor. To convert this number into a surface area number, the IUPAC convention settled on a number of 16.2 Å^2 (0.162 nm^2) per nitrogen molecule as a standard. The origin of this number is from a recommendation by Emmett and Brunauer [13]. This recommendation used an equation relating the effective molecular cross-sectional area, a, to the liquid density, ρ, and the molar mass, M_{ad}:

$$a = 1.091 \left(\frac{M_{ad}}{N_A \rho} \right)$$

(34)

The constant 1.091 is referred to as the packing factor. Unfortunately, according to Pickering and Eckstrom [14], a depends upon the adsorbate and adsorbent. Furthermore, according to Emmett [15], it is also a function of C; very seldom is the parameter C reported.

In the above analysis it may be the number of moles, n_{ad}, adsorbed rather than volume being reported. What is reported may also be in terms of per gram of sample, which is the normal method of reporting. All the equations remain the same with number of moles, n_m, in a monolayer reported out. V_{mon} is usually reported in standard milliliter; so to convert in to moles:

$$n_m = \frac{V_{mon}}{22,400}$$

(35)

and to surface area in m^2 g^{-1}, with m as the sample mass in grams, is given as:

$$A_s = \frac{n_m a}{m} N_A$$

(36)

χ **Plot Analysis**

The basic equation for the χ theory is

$$\frac{nfA_m}{A_s} = -\ln\left[-\ln\left(P/P_s\right)\right] - \ln\left(-\frac{E_a}{RT}\right) \tag{37}$$

The equivalent steps in the analysis are:

1. The transformed equation is rather simple. Use $y = n_{ad}$ and $x = -\ln(-\ln(P/P_s))$.
2. Plot the transformed data. This may give more than one straight line segment. Refer to later sections for the meaning of these segments. At any rate if there is more than one straight line segment, analyze each separately.
3. Obtain the slope, S_i, and intercept, I_i, for each (i) segment. The slope yields the surface area according to

$$S_i = \frac{A_s}{fA_m} \quad \text{and} \quad I_i = S_i\left[-\ln\left(-\frac{E_a}{RT}\right)\right] \tag{38}$$

4. Obtain the surface area, using the value of 1.84 for f and determining the value of A_m (the molar area) from

$$A_m = (V_m)^{2/3}(N_A)^{1/3} \tag{39}$$

where V_m is the molar volume and N_A is Avogadro's number. The value of A_m for nitrogen is $8.97 \times 10^4 \, m^2 \, mol^{-1}$ and for argon is $7.90 \times 10^4 \, m^2 \, mol^{-1}$ at their normal boiling points. If there are several segments, the surface areas for each segment, $A_{s,i}$ is given by

$$A_{s,i} = 1.84A_m(S_i - S_{i-1}) \tag{40}$$

where $S_0 = 0$, i.e. there is no segment "0". The $E_{a,i}$ are given by

$$E_{a,i} = -RT \exp\left(-\frac{I_i}{S_i}\right) \tag{41}$$

Each $E_{a,i}$ is interpreted as the energy of adsorption for the ith type of surface. The *total area* upon which there is adsorption is the sum of surface areas starting with the lowest in value of χ ($= -\ln(-\ln(P/P_s))$) and summing

as the segments, $A_{s,i}$, appear, provided there is no negative curvature in the χ plot. If there is a sudden large increase followed by a sudden decrease to a slope of nearly zero, this is an indication of mesoporosity and needs special treatment.

The Method of Determining Surface Area by Dubinin et al.

It is questionable as to whether the various isotherms attributed to Dubinin and coworkers yield the surface area. They are definitely useful for finding the mesoporosity volume due to the clear linear extrapolation. According to Kaganer [16] the intercept of the DR equation is the monolayer amount. This seems to have been empirically based upon the BET formulation. The modified DR equation, referred to as the DRK equation, for a flat surface is

$$\ln\left(\frac{V}{V_{mon}}\right) = A \ln^2\left(\frac{P_s}{P}\right)$$

(42)

A plot of $\ln(V)$ versus $\ln^2(P/P_s)$ yields a plot which is linear over a fair range of values. A typical DRK plot has been presented in Fig. 35. It has been demonstrated [17], according to χ theory, that the value of V_{mon} is indeed proportional to the monolayer coverage. One of the problems with this formulation is that both porosity and surface area are dependent upon the intercept value. In other words, there is no way to separate the two physical quantities in this case. Therefore, if one has a sample that is porous and has a significant external area the separation of these two physical quantities is not possible.

The methodology for the DRK calculation is as follows:

1. Use $y=\ln V_{ad}$ or $y=\ln n_{ad}$ and use $x=(\ln(P/P_s))^2$
2. Plot y as function of χ and draw the best estimated fit for the portion that is the most linear. This would be roughly through point at the inflection point of the curve and should cover about 2/3 of the plot.
3. From the intercept ($y=0$) of the plot obtain $\ln V_{mon}$ or $\ln n_m$.
4. Convert to monolayer coverage or area as was done for the BET.

Tóth *T*-Equation Isotherm

Another theoretical treatment that matches the experimental results for many adsorbents is the Tóth [18] isotherms, referred to as the *T*-equation

[19]. The basic equation is

$$n_{ad} = \frac{n_m \left(1 + \dfrac{1}{K}\right)^{1/m} \dfrac{P}{P_s}}{\left[\dfrac{1}{K} + \left(\dfrac{P}{P_s}\right)^m\right]^{1/m} \left(1 - k\dfrac{P}{P_s} + kP_{r,e}\right)} \tag{43}$$

where n_m, K, m, k and $P_{r,e}$ are fitting parameters which were designated by the derivation. $P_{r,e}$ is a low relative pressure value and can be ignored with a small amount of distortion. This equation can be rearranged somewhat to yield a simpler looking equation, however, with five fitting parameters probably the best approach is to simply set up a minimum search routine.

It is not clear how useful this equation is although it is claimed that the parameter n_m yields the monolayer coverage value. The values obtained from this have been compared favorably with the BET values and, with some reservations, the same surface area value is obtained regardless of the adsorbent.

One of the basic assumptions for the theory behind the *T*-equation is the validity of Henry's law and the notion that the virial equation is a thermodynamic requirement. This latter assumption is approximately correct for many situations but is strictly incorrect.

The Harkins–Jura Absolute/Relative Method

Harkins and Jura [20] describe a method to obtain the absolute surface area of a solid by the following method. Firstly, the powder is exposed to a high vapor pressure of water. Indeed it is best to expose it in a high-sensitivity calorimeter over a reservoir of water. The powder is then allowed to fall into the reservoir and the amount of heat produced is measured. By doing so, one eliminates the outer surface of the adsorbed film releasing the energy associated with the liquid–gas interface surface tension. Since the liquid–gas surface tension energy is known one may then calculate from the amount of heat released the area of the powder (or at least the outer surface area of the adsorbed film before immersion).

The principal problem with this technique is the difficulties involved experimentally. Assuming that these are overcome, there are still the following questions: "Are the particles well dispersed after immersion?" and "Is there significant porosity or bed porosity in the sample that would lower the observed area due to capillary action?" Both of these questions were

addressed by Harkins and Jura [21]. One of the unforeseen problems is the variation in heats of adsorption with coverage. Thus, if the adsorbed film thickness is too thin then there will be an additional heat due to the additional adsorption. The can be accounted for by measuring the heat of adsorption as well.

This seems like a simple method and conceptually it is. However, those who have performed calorimetry, especially for physisorption, know fully well that such a method is experimentally very difficult and tricky, with many pitfalls and compensating calculations that are needed. This is definitely *not* recommended for the novice.

POROSITY DETERMINATIONS FROM THE ISOTHERM

There are three classifications of porosity. Officially the IUPAC has classified these according to pore diameter as follows:

- Below 2 nm – "micropores"
- Between 2 and 10 nm – "mesopores"
- Large than 10 nm – "macropores"

In this section a looser definition will be used. Micropores will be the smallest of the pore which do not cause any positive deviation from linearity in the standard plot or the χ plot. Micropore causes only negative curvatures in the standard plot. For mesopores there will exists a positive deviation due to pore filling, usually referred to as capillary filling, in the intermediate to high end of the standard or χ plot. This increase is then followed by a decrease in the slope to a value less than the slope before the capillary filling. Macropores are pores for which the capillary filling is at such a high pressure that it is not practical to observe it on the isotherm. The *official* definition might change as more sensitive instruments become available. The possibility of a change in the boundary between mesopores and macropores is very likely. Furthermore, the functional definitions presented here and the IUPAC definition may not always coordinate. Another point to remember is that the IUPAC definitions are geared to N_2 adsorption and there is no reason to presume that other adsorbates, for example, SF_6 which is much larger than N_2, should behave similarly.

How to exactly calculate porosity from the isotherms is a matter of much discussion at this time. The following is one method of interpreting the isotherm with respect to porosity. It is a more detailed and advanced method than presented in Chapter 6.

Micropore Analysis

Some typical data which indicate microporosity are in Fig. 36. The data used are from Goldman and Polanyi [22] for CS_2 adsorption on activated charcoal. Not much can be deduced from this isotherm as presented. A transformation of the plot (Fig. 37) using a standard isotherm begins the process.

1. Leave the *y*-axis as amount adsorbed, preferably in units of moles. Transform the P/P_s using a standard plot. Here the analytical [23] χ plot equation is being used for the standard plot.
2. Fit the high and low values to a straight line. These are labeled in the figure as S_{lo} and S_{hi}.
3. Extract the slopes from the high and low lines and the intercept from the high line.
4. The slopes, S_{lo} and S_{hi}, can be related to the surface areas of the pores and the external surface. This is an approximation for which one can find a minimum and a maximum surface area for pores. For the conversion, e.g. surface area, one must use either that listed for the standard isotherm, based on the BET, or use the χ theory conversion. Here, for illustration, the χ is being used.

Example. The slopes and the high intercept, I_{hi}, in Fig. 37 are

$S_{lo} = 4.53$ mmol g^{-1},
$S_{lo} = 0.257$ mmol g^{-1}
$I_{hi} = 8.54$ mmol g^{-1}
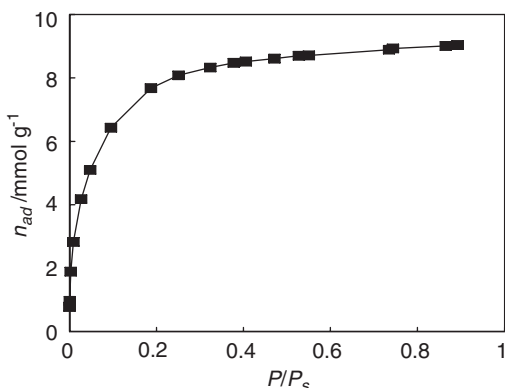
Fig. 36. A typical type I adsorption isotherm indicating microporosity.
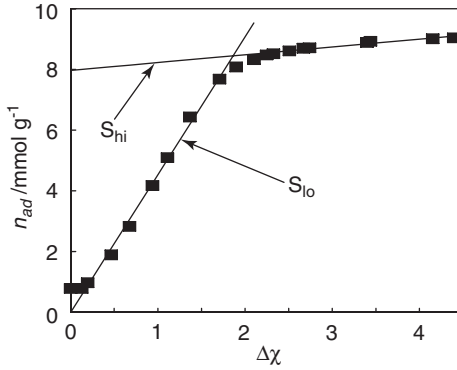
Fig. 37. The Transformed plot using a standard curve to change the x axis.

Using the conversion factor from Eq. (39) and the standard curve calibration (or for χ, Eqs. (4) and (5)) with the molar volume $V_m = 6.02 \times 10^{-5}$ m^3 mol^{-1} and therefore $A_m = 1.30 \times 10^5$ m^2 g^{-1} the following areas and volumes are obtained:

$A_p = 1082$ m^2 g^{-1}
$A_{ex} = 61.3$ m^2 g^{-1} d (A_{ex} includes both the wall edges and the pore openings.)
$V_p = 5.14 \times 10^{-7}$ m^3 g^{-1}

Use the following formulas for cylindrical and slit pores:

$$r_p = \frac{2V_p}{S_p} \quad \text{or} \quad d_p = \frac{4V_p}{S_p} \quad \text{for cylindrical pores}$$

$$d_p = \frac{2V_p}{S_p} \quad \text{for slit-like pores}$$

(44)

where r_p indicates pore radius or d_p indicates pore diameter or distance between the slit pore sides.

Thus the answer for the above example is $r_p = 9.5 \times 10^{-10}$ m ($d_p = 1.9 \times 10^{-9}$ m) for cylindrical pores and $d_p = 9.5 \times 10^{-10}$ m for slit-like pores.

A more sophisticated analysis has been presented in the literature [24] but the factor of 1.84 is missing. Using the method in the literature, which accounts for several other factors, the answer is $r_p = 9.7 \times 10^{-10}$ m, which might indicate that the additional effort is not worthwhile.

Mesoporosity Analysis

The following is the simple technique to calculate the mesoporosity. Again, a more sophisticated analysis exists but does not seem to be a great improvement.

Fig. 38 illustrates the parameters to be extracted from the χ plot (a plot of n adsorbed versus χ value). The analysis using the χ theory is similar to that used for standard curves such as the α–s[26, 27], except a standard from a similar non-porous material is not necessary. The following symbols are used in this analysis:

A_p = surface area inside pores
A_w = surface area of outside walls
A_o = area of pores openings
V_p = total pore volume
f = 1.84

Then

$$S_{lo} = \frac{(A_p + A_w)}{fA_m} \tag{45}$$
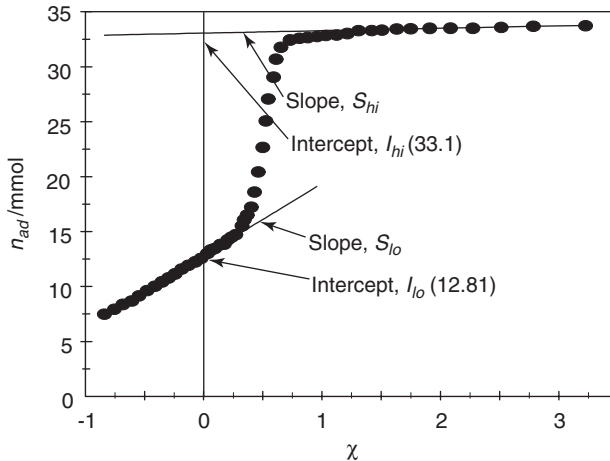
Fig. 38. Preliminary parameters obtained from the isotherm to analyze surface area and porosity. Data values were extracted from an article by Krug and Jaroniec [10].

and

$$S_{hi} = \frac{A_{ex}}{fA_m} = \frac{(A_o + A_w)}{fA_m} \tag{46}$$

The value of χ_c is required to make the subsequent calculations. χ_c is given by

$$\chi_c = -\frac{I_{lo}}{S_{lo}} \tag{47}$$

where I_{lo} is the intercept of the low-pressure linear portion. The pore volume is then

$$V_p = V_m(S_{hi}\chi_c + I_{hi}) \tag{48}$$

If $A_w << A_p$ then A_p can be obtained from Eq. (45) directly; otherwise it is true that

$$A_p \leq fA_m S_{lo} \tag{49}$$

These considerations may be used to make one of the estimates of the pore diameter, d_p. From the determined values,

$$d_p \geq \frac{2V_m(S_{hi}\chi_c + I_{hi})}{fA_m S_{lo}} \tag{50}$$

The other estimate, from the modified Kelvin equation, yields the diameter along with the pore size distribution. For the data analyzed here this distribution is assumed to be a normal distribution in χ. A more detailed analysis does not seem justified by the number of data points in the transition zone.

Obviously, if there is some microporosity present then unless it can be separated in the isotherm then the above answer may be far from correct. A better method of obtaining the mesoporosity is as follows using the modified Kelvin equation. The χ method is used here, but in principle any well-calibrated standard curve should work.

The capillary filling equation theory, that is the Kelvin equation as modified by Cohan [28], can be expressed for cylindrical pores as

$$-\ln\left(\frac{P}{P_s}\right) = \frac{2\gamma_{gl}}{RTr_c} \tag{51}$$

where γ_{gl} is the surface tension of the gas–liquid interface for the adsorption, r_c the core radius, and is equal to the pore radius, r_p, minus the "thickness" of the adsorbed layer, t. In light of χ theory this is modified to

$$e^{-\chi_p} = \frac{2\gamma_{gl}V_m}{RT(r_p - t)} \tag{52}$$

Here the χ_p is the value of χ at which the capillary filling takes place. (In the case of a distribution of pores it will be the mean value, $\langle\chi_p\rangle$.) The value of t is obtained by using the difference between χ_p and χ_c, or $\Delta\chi_p = \chi_p - \chi_c$, since this would be related to the overall thickness by

$$t = \frac{\Delta\chi_p V_m}{fA_m} \tag{53}$$

Thus,

$$r_p = \frac{2\gamma_{gl}V_m}{RT e^{-\chi_p}} + \frac{\Delta\chi_p V_m}{fA_m} \tag{54}$$

for $d_p = 2r_p$.

Eq. (51) along with the χ equations leads to a pore radius as given in Eq. (54). This equation is specifically dependent upon χ and therefore any positive deviation from the straight projected line in the χ plot can be interpreted as capillary filling. Initially, a probability normal mass function (PMF) in χ is assumed. To go beyond this assumption is, in principle, not difficult but for the data presented here it does not seem justified. The PMF, **P**, is

$$\mathbf{P}(\chi) = \frac{e^{-(\chi-\langle\chi_p\rangle)^2/2\sigma^2}}{\sqrt{2\pi\sigma^2}} \tag{55}$$

where σ is the standard deviation in the pore size distribution. A method of successive approximations is used to obtain $\langle \chi_p \rangle$ and σ. Using an initial estimate for $\langle \chi_p \rangle$ and setting σ to a very low value, a probe value for the fit to the isotherm data, η_j, is created from the equation

$$\eta_j = \mathbf{P}(\chi_j - \langle \chi_p \rangle)$$
$$+ \sum_{i=2}^{j} [(\chi_i - \chi_{i-1})(S_{lo} - S_{hi})(1 - \mathbf{P}(\chi_i - \langle \chi_p \rangle))] \tag{56}$$

where the subscript i indicates the ith data point between points k and l on either side of the pore filling. A new value of χ_p is calculated from a weighted average of χ using the square of the difference as the weighting factor, i.e.

$$\chi_p = \sum_{i=k}^{l} \chi_i (n_{ad,i} - \eta_i)^2 \bigg/ \sum_{i=k}^{l} (n_{ad,i} - \eta_i)^2 \tag{57}$$

Using this new χ_p, new estimates are made for η. This is repeated until convergence is satisfactory. If the fit on both sides of the transition had similar data scatter, the above method would work very well. However, there are different number of data points on two sides of the transition which weigh into the summations. To avoid this problem, it is best to select data points that are judged to be in the transition zone, along with roughly a few additional data points on either side of the transition. In other words, points k and l should be symmetrically located outside the transition zone.

The value of σ is obtained by a similar successive approximation method.

$$\sigma_{new} = \sigma_{previous} + v \sum_{i=k}^{1} \text{sign}(\chi_i - \chi_p)(n_{ad,i} - \eta_i) \tag{58}$$

where v is a factor set for the sensitivity of the convergent. It should be set small enough to avoid oscillations between approximations. (In place of the function behind the "Σ", one could use other functions to provide convergence such as "$(n_{ad,i} - \eta_i)^3$". However, this latter function seems to be considerably less stable.)

For the distribution, σ is in terms of χ and may be converted into distance by simply taking $\langle \chi_p \rangle + \sigma$ and determining its value to give $\langle r_p \rangle + \sigma$.

All of this seems rather involved but it gives the information that one needs, that is, the mean pore radius and the pore radius distribution. This

can easily be programmed into a simple spread sheet to ease the calculations, and more sophisticated programming is not necessary.

The above calculation should yield the correct answer under equilibrium conditions, which is often not obtained. Modifying the Kelvin equation (51) by eliminating the factor 2 for the adsorption branch has often been suggested. This assumes that the cylindrical adsorption does not collapse from the ends or from constrictions of the capillaries but rather from the sides. There are reasons to assume either one. Hysteresis is a big problem for mesopore measurements, and research by many groups on this subject is ongoing.

ISOTHERM FITS WHICH YIELD RELATIVE NUMBERS FOR THE SURFACE AREA

Langmuir Isotherm

The Langmuir isotherm is most appropriately suited for the description of chemisorption. The underlying assumption is that the adsorbate from the gas is in equilibrium with a bonded or tightly held species on the surface. A reaction such as

$$G + S \rightleftharpoons G - S$$
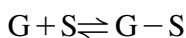
for the gas species, G, and the surface sites, S, is assumed. The site assumption is extremely important and restricts the use of this isotherm, as it does for any other isotherm based upon surface sites. The activity of the surface sites is assumed to be important and the activities are proportional to the number of moles, n_{ad}, on the surface. Therefore, by simple equilibrium calculation one gets

$$K = \frac{n_{ad}}{P_G(n_S - n_{ad})} \tag{59}$$

where n_S is the number of surface sites (here expressed in terms of moles) and P_G the pressure of the gas. This can be rearranged to

$$n_{ad} = n_S \left(\frac{P_G}{K' + P_G} \right) \tag{60}$$

where $K' = 1/K$. This isotherm has been widely used for chemisorption. For dissociative adsorption, consider an example of hydrogen chemisorption on

an active metal where a diatomic molecule will become monatomic on the surface or $H_2 + 2S \rightleftharpoons 2H-S$. Then eq. (60) is modified to

$$n_{ad} = n_S \left(\frac{P_{H_2}^{1/2}}{K' + P_{H_2}^{1/2}} \right) \tag{61}$$

The general shape of this curve is presented in Fig. 39 with different values of K. The value of n_S is set to 1 in this figure. The value of n_G approaches n_S as $P \rightarrow \infty$. For subsequent discussions one could say for this figure that estimating n_S by looking at where the "knee", at least on this scale, give a correct value within 50%. (This is deceptive due to the approximate invariance of the scaling.)

Using the Langmuir isotherm one cannot obtain a surface area number, unless one knows how the surface sites are distributed. If one knows that the approximate area required for one bonding location is 0.2 nm^{-2}, then one can conclude from a calculation of n_S what the area is. An assumption implied in this is that the activity of the surface site is proportional to the number of sites available divided by the original number, i.e. the mole fraction of species on the surface. In bulk calculations, this is referred to as the saturation limit. The assumption that full saturation is the same as the number of original sites may not be valid either in the bulk or on surfaces.
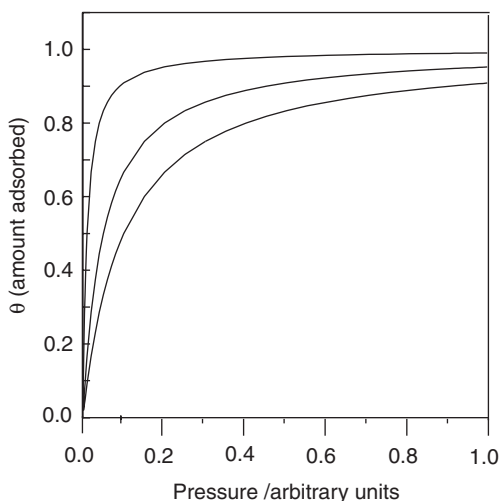
Fig. 39. Examples of Langmuir isotherms and the position of the "knee" as it varies with adsorption energy.

(Some readers may find this statement surprising. The effect where saturation is reached before the number of identical sites are used up has been observed in many solubility measurements with solids. The reasons are multiple, but one must remember that the solute modifies the solvent chemically, i.e. electronically.) This method of determining the surface area of a solid is often called titration, in analogy to solution chemistry.

As useful as the Langmuir isotherm is, due to the site assumption, it is impossible to use it for physisorption. There have been some derivations which assume that the sites do not exist; however, these derivations suffer from the unrealistic assumption of localized forces without localization. Implicit in chemical bonding is the assumption of directional, local bonds.

Freundlich Isotherm

The Freundlich isotherm was originally an empirical isotherm. There have been numerous theoretical justifications for it for many years up to the present. The equation for the isotherm is

$$n_{ad} = K_F P^{1/r_F} \tag{62}$$

where n_{ad} is the moles of the adsorbate on the surface and r_F is a constant, and will be referred to here as the Freundlich constant. A special case of $r_F = 1$ is referred to as "Henry's law," which *should not be confused with the solution equation of state called Henry's law*. The use of this latter name is confusing to some. The terminology probably should be avoided.

Of interest is the derivation of the Freundlich isotherm with $r_F = 1$ from the ideal two-dimensional surface gas. Assuming a surface equation of state similar to the ideal gas law, using π in place of P and A_s in place of V, one has

$$\pi A_s = n_{ad} RT \tag{63}$$

(Often the units for π are dyn m^{-2} to yield numbers that are simpler. This is not necessary, however. We prefers to leave all units in SI for simplicity. Today π is often reported in units of mJ m^{-2}) For most thermodynamic treatments (see Hiemenz [12]), the surface Gibbs-Duhem equation would be

$$-A_s d\gamma = n_{ad} d\mu \tag{64}$$

or since $\pi = \gamma_0 - \gamma$,

$$dy = \frac{n_{ad}RT}{A_s} d \ln P \tag{65}$$

Substituting in Eq. (63) and integrating and identifying $\gamma_0 - \gamma$ as π, one obtains the $\gamma_F = 1$ Freundlich isotherm with an arbitrary K. Reversing the process with any γ_F, will yield in place of Eq. (63),

$$\pi A_s = \frac{n_{ad}RT}{r_F} \tag{66}$$

which is difficult to justify (but has been and continues to be worked upon [29]).

The Freundlich isotherm equations do not have the surface area explicitly as a parameter in the equations. Therefore, the surface area cannot be determined using these equations.

Polanyi Formulations

Polanyi [30–32] basically stated that the free energy of the surface is a function of the coverage of the surface. Thus, the pressure is related to $E(\theta)$ as

$$f\left(RT \ln\left(\frac{P}{P_s}\right)\right) = E(\theta) \tag{67}$$

which is often simplified to

$$RT \ln P = E(\theta) \tag{68}$$

where θ is the amount on the surface per unit area. For convenience, θ will be used throughout as the amount on the surface relative to exactly one monolayer, or the *equivalent monolayer coverage*. One equivalent monolayer coverage is equal to the amount of material that, if it were all restricted to being in contact only with the solid surface, would exactly cover the entire surface. An especially successful isotherm of this form was found to be

$$RT \ln P = B e^{-k_p \theta} \tag{69}$$

where B and k_P are constants. This form of the equation was known for many years to be an excellent fit to most isotherms, indeed in the judgement of some [11] the best fit by far. This isotherm equation suffers from the same problem as the Freundlich isotherm equation. The surface area is not an explicit parameter in the equation, but is bound with a multiplicative constant, k_p.

Notice that using any formulation based on the Polanyi theory one cannot obtain the surface area without some additional assumption. This was the primary shortcoming of the approach.

deBoer–Zwikker Formulation

The deBoer–Zwikker [33] polarization theory is a special case of Eq. (69). Taking the ln of both sides of this equation and using relative pressures, i.e. compared to the vapor pressure of the liquid state of the adsorbate, one obtains

$$\ln \ln (P_s/P) = B - k_p \theta \tag{70}$$

deBoer–Zwikker derived a very similar equation from classical polarization theory, which was

$$\ln \ln (P_s/P) = \ln \left(\frac{\varepsilon_0}{RT} \right) - \left(\frac{aV_1}{v_0 A_s} \right) \tag{71}$$

from which the surface area could be derived. The problem with this formulation is that by using classical polarization theory one obtains numbers which are very far from correct. This theory was generally disregarded and deBoer pursued the standard curve route. Experimentally, however, this theory fits most adsorption data better than any of the other theories. Badmann et al. [34] used a similar function successfully in a much later publication.

The Frenkel, Halsey, Hill (FHH) Isotherm

The Frenkel–Halsey–Hill (FHH) isotherm has found much utilization due to the range specified for its application. It seems especially handy for porosity determinations. It seems to work well between relative pressures in the range 0.4–0.9. The equation is

$$\ln (P_s/P) = k_{FHH} \theta^{r_{FHH}} \tag{72}$$

where k_{FHH} is an empirical constant and r_{FHH} lies between 2 and 3. It is easier to transform this equation for plotting purposes; so

$$\ln \ln (P_s/P) = \ln k' + r_{FHH} \ln n_{ad} \tag{73}$$

where k' is a constant along with the monolayer coverage value. Obviously, this cannot be used to determine the monolayer coverage but may be used with caution to interpret data.

Analysis Using Standard Isotherms

Standard isotherm admittedly do not yield the surface area value by themselves. However, they are probably the most useful of the methods of analysis. The question as to why one would use an analysis that does not yield a value for the surface area may seem puzzling. First, there are times when all one really needs is a relative value. Second, the isotherms are useful for extrapolation and as input into various theories, such as porosity calculations. Most absolute numbers for surface area from these isotherms refer back to the BET equation for standardization. With a good standard, one can obtain values for surface area and porosity.

There are now several standard isotherms. However, the two most used are still the α–s standard isotherms and the t-thickness isotherm. The standard t-thickness isotherm on alumina may, however, be slightly inaccurate at higher pressures. There is a tendency today to construct a standard isotherm for the adsorbent–adsorbate pair being used. This is a bit tricky since these standard isotherms are usually used for porosity measurements, and to obtain a nearly flat surface that is energetically the same as the porous material seems unlikely. Nevertheless, it often seems to work.

The standard curve method follows these steps:

1. Measure an isotherm on a known material. In the case of silica and alumina and other materials mentioned later in this chapter, this has already been done.
2. Obtain the amount adsorbed as a function, **F**, of relative pressure, $x = P/P_s$ or

$$n_{ad} = A_s \mathbf{F}(x,T) \tag{74}$$

   Normally this curve is measured at only one temperature. If one knows the surface area of this standard, then the value of **F** is

scaled so that A_s in the above equation is the surface area value of the standard.

3. Plot n_{ad} of the unknown sample against the function **F**.

4. Calculate the surface area of the unknown as the slope times the known A_s.

Standard Isotherms

Isotherms measured on well-characterized material and are used for comparison with isotherms of unknowns are referred to as standard isotherms. Tables of a variety of standard isotherms that are described here are presented in this section.

The α_s-Curve Standard (see Sing, Everett and Ottewill [6])

The α_s-curve has an advantage that the original data have not been severely reworked. Originally, these plots were simple n-plots (i.e. number of moles adsorbed as a function of pressure.) The procedure for obtaining these curves was to obtain a multiplicity of adsorption isotherms on many powders of the same type of material. The surface area number, however, is based on the BET surface area. These curves are very useful for porosity determinations due to the high degree of confidence in the basic standard curve. The curve is averaged and smoothed for several similar silica samples. Generally, in the literature, it works quite well, even in the high-pressure range. Curves for both nitrogen and argon are available. The data in Table 6 are some starting data (from Bhambhani et al. [35] and the smoothed data as presented [36]. Table 7 presents some additional data by Payne et al. [37] for the same purpose. In Table 8 are the α–s curves normalized to P/P_s value of 0.4 [38].

The t-Curve

One of the earliest standard curves was the t-curve by Lippens, et al. [39], which was for the adsorption of N_2 on alumina. The data were reported in terms of film thickness in angstroms (unit designator Å and equal to 10^{-10} m). The data for both the smoothed curve and the original data are in Table 9. The conversion from volume adsorbed in mL g^{-1} is given by the equation

$$t = 3.54(V/V_m)\text{Å} \tag{75}$$

Table 6
α–s curves on silica for N_2

Smoothed curve				Original data	
P/P_s	µmol m^{-2}	P/P_s	µmol m^{-2}	P/P_s	Std. mL
0.001	4.0	0.340	14.5	0.008	44
0.005	5.4	0.360	14.8	0.025	52
0.010	6.2	0.380	15.1	0.034	57
0.020	7.7	0.400	15.5	0.067	61
0.030	8.5	0.420	15.6	0.075	64
0.040	9.0	0.440	16.1	0.083	65
0.050	9.3	0.460	16.4	0.142	70
0.060	9.4	0.500	17.0	0.183	77
0.070	9.7	0.550	17.8	0.208	78
0.080	10.0	0.600	18.9	0.275	85
0.090	10.2	0.650	19.9	0.333	90
0.100	10.5	0.700	21.3	0.375	96
0.120	10.8	0.750	22.7	0.425	100
0.140	11.3	0.800	25.0	0.505	109
0.160	11.6	0.850	28.0	0.558	117
0.180	11.9	0.900	37.0	0.592	122
0.200	12.4			0.633	130
0.220	12.7			0.692	148
0.240	13.0			0.733	165
0.260	13.3			0.775	194
0.280	13.6			0.792	204
0.300	13.9			0.825	248
0.320	14.2			0.850	296

From Ref. [26].

Table 7
Data for α–s curves

Ar data on SiO_2				N_2 data on SiO_2			
P/P_s	Std. mL	P/P_s	Std. mL	P/P_s	Std. mL	P/P_s	Std. mL
0.05	23.0	0.40	50.0	0.05	34.0	0.40	58.0
0.10	29.0	0.45	54.0	0.10	38.0	0.45	58.0
0.15	32.0	0.50	55.0	0.15	43.0	0.50	61.0
0.20	38.0	0.60	62.0	0.20	46.0	0.60	68.0
0.25	41.0	0.70	69.0	0.25	48.0	0.70	77.0
0.30	43.0	0.80	79.0	0.30	51.0	0.80	89.0
0.35	45.0	0.90	93.0	0.35	54.0	0.90	118.0

From Ref. [37].

Table 8
Smoothed α–s curve on silica normalized to $V_{0.4}$ as listed by Gregg and Sing

N$_2$				Ar			
P/P_s	$V/V_{0.4}$	P/P_s	$V/V_{0.4}$	P/P_s	$V/V_{0.4}$	P/P_s	$V/V_{0.4}$
0.001	0.26	0.280	0.88	0.01	0.243	0.32	0.900
0.005	0.35	0.300	0.90	0.02	0.324	0.34	0.923
0.010	0.40	0.320	0.92	0.03	0.373	0.36	0.948
0.020	0.50	0.340	0.94	0.04	0413	0.38	0.973
0.030	0.55	0.360	0.96	0.05	0.450	0.40	1.000
0.040	0.58	0.380	0.98	0.06	0.483	0.42	1.022
0.050	0.60	0.400	1.00	0.07	0.514	0.44	1.048
0.060	0.61	0.420	1.01	0.08	0.541	0.46	1.064
0.070	0.63	0.440	0.10	0.09	0.563	0.48	1.098
0.080	0.65	0.460	1.06	0.10	0.583	0.50	1.123
0.090	0.66	0.500	1.10	0.11	0.602	0.50	1.123
0.100	0.68	0.550	1.14	0.12	0.620	0.52	1.148
0.120	0.70	0.600	1.22	0.13	0.638	0.54	1.172
0.140	0.73	0.650	1.29	0.14	0.657	0.56	1.198
0.160	0.75	0.700	1.38	0.15	0.674	0.58	1.225
0.180	0.77	0.750	1.47	0.16	0.689	0.60	1.250
0.200	0.80	0.800	1.62	0.17	0.705	0.62	1.275
0.220	0.82	0.850	1.81	0.18	0.719	0.64	1.300
0.240	0.84	0.900	2.40	0.19	0.733	0.66	1.327
0.260	0.86			0.20	0.748	0.68	1.354
				0.22	0.773	0.70	1.387
				0.24	0.801	0.72	1.418
				0.26	0.826	0.74	1.451
				0.28	0.851	0.76	1486
				0.30	0.876	0.78	1.527

IUPAC Standards on Silica and Carbon

The original purpose of the IUPAC (compiled by Everett et al. [40]) round-robin investigation was to create some confidence in the methodology of adsorption isotherm measurements. Standard samples from the same production batches were used and various laboratories performed the same experiments. The results were not intended as standard curves but the agreement between the various laboratories was generally very good, within 2%. Therefore, these would be as good standards as one would be able to

Table 9
Data and smooth *t*-curve – N_2 adsorbed on alumina

t-Curve (smoothed data)				Original data	
P/P_s	t/Ä	P/P_s	t/Ä	P/P_s	t/Ä
0.08	3.51	0.80	10.57	0.083	3.54
0.10	3.68	0.82	11.17	0.101	3.72
0.12	3.83	0.84	11.89	0.119	3.82
0.14	3.97	0.86	12.75	0.137	3.97
0.16	4.10	0.88	13.82	0.159	4.10
0.18	4.23	0.90	14.94	0.181	4.22
0.20	4.36			0.200	4.38
0.22	4.49			0.227	4.45
0.24	4.62			0.242	4.61
0.26	4.75			0.260	4.72
0.28	4.88			0.285	4.86
0.30	5.01			0.300	5.01
0.32	5.14			0.321	5.14
0.34	5.27			0.339	5.24
0.36	5.41			0.365	5.42
0.38	5.56			0.386	5.55
0.40	5.71			0.408	5.67
0.42	5.86			0.422	5.85
0.44	6.02			0.440	5.98
0.46	6.18			0.458	6.13
0.48	6.34			0.480	6.31
0.50	6.50			0.499	6.44
0.52	6.66			0.520	6.62
0.54	6.82			0.542	6.79
0.56	6.99			0.560	6.97
0.58	7.17			0.579	7.15
0.60	7.36			0.599	7.30
0.62	7.56			0.617	7.51
0.64	7.77			0.635	7.71
0.66	8.02			0.661	7.92
0.68	8.26			0.679	8.22
0.70	8.57			0.700	8.52
0.72	8.91			0.718	8.88
0.74	9.27			0.744	9.24
0.76	9.65			0.758	9.59
0.78	10.07			0.780	10.03

From Ref. [39].

find. Apparently the archive for these standards no longer exists. The data presented below were extracted from the literature from laboratory "H". This seemed to be a typical data run. The isotherms determined were for Gisil silica, TK800 silica (silica in Table 10), Vulcan 3G carbon and Sterling FT carbon (carbons in Table 11).

RMBM Carbon Standard

A standard adsorption isotherm curve for activated carbon has been published by Rodriguez-Reinoso et al. (RMBM) [41]. The data and the *α-s* standard are presented in Table 12. The carbon studied was an activated carbon form and contained macropores and micropores [42]. The micropores were closed by heating to 2073 K [43]. The value for A_s was obtained from

Table 10
IUPAC silica isotherms

Gisil silica		TK800 silica			
P/P_s	V/std.mL g^{-1}	P/P_s	V/std.mL g^{-1}	P/P_s	V/std.mL g^{-1}
0.0076	44.1	0.0144	25.3	0.9151	123.5
0.0177	53.6	0.0217	28.2	0.9317	135.3
0.0412	55.9	0.0325	30.1	0.9476	147.4
0.0646	61.0	0.0433	32.5	0.9591	157.9
0.0773	63.4	0.0542	34.0	0.9678	165.7
0.0875	64.4	0.0664	35.4		
0.1394	71.2	0.0953	37.3		
0.1737	74.6	0.1358	40.4		
0.2028	78.0	0.1733	43.2		
0.2586	83.1	0.2167	46.3		
0.3144	88.1	0.3091	51.9		
0.3581	92.2	0.3553	54.8		
0.4202	97.6	0.3958	56.4		
0.4912	106.4	0.4694	61.2		
0.5400	114.6	0.5561	67.1		
0.5711	118.3	0.6406	73.5		
0.6116	127.5	0.7092	79.7		
0.6889	145.8	0.7042	82.6		
0.7276	162.7	0.7352	85.6		
0.7669	189.8	0.7887	94.3		
0.7840	199.3	0.8176	99.2		
0.8227	240.7	0.8486	105.6		
0.8461	288.1	0.8826	114.1		

Table 11
IUPAC carbon samples

Vulcan 3G				Sterling FT			
P/P_s	V^a	P/P_s	V^a	P/P_s	V^a	P/P_s	V^a
0.0006	2.13	0.2575	3.63	0.0006	11.7	0.2690	24.3
0.0123	2.50	0.3065	4.16	0.0077	15.1	0.3122	26.7
0.0300	2.56	0.3556	4.61	0.0242	16.1	0.3577	29.3
0.0460	2.62	0.4150	5.07	0.0432	16.5	0.4287	32.6
0.6190	2.66	0.4647	5.37	0.0585	17.1	0.4908	35.3
0.0766	2.72	0.5321	5.78	0.0857	17.9	0.5611	38.5
0.1318	2.89	0.6100	6.29	0.1390	19.5	0.6291	42.2
0.1747	3.09	0.7080	7.30	0.1821	20.7	0.7072	47.4
0.2084	3.24	0.7957	8.47	0.2129	22.0	0.7852	55.9
0.2354	3.50			0.2395	22.8		

^{a}Units for V: std mL g^{-1}

Table 12
Standard isotherm for activated charcoal

P/P_s	n/n_M	α–s	P/P_s	n/n_M	α–s	P/P_s	n/n_M	α–s
0.005	0.82	0.51	0.18	1.21	0.76	0.44	1.68	1.05
0.01	0.87	0.54	0.20	1.24	0.78	0.46	1.71	1.07
0.02	0.92	0.58	0.22	1.27	0.79	0.50	1.79	1.12
0.03	0.95	0.59	0.24	1.30	0.81	0.54	1.88	1.18
0.04	0.98	0.61	0.26	1.33	0.83	0.60	2.02	1.26
0.05	1.00	0.63	0.28	1.37	0.86	0.64	2.13	1.33
0.06	1.02	0.64	0.30	1.41	0.88	0.70	2.32	1.45
0.07	1.03	0.64	0.32	1.44	0.90	0.74	2.46	1.54
0.08	1.05	0.66	0.34	1.48	0.93	0.80	2.71	1.69
0.10	1.09	0.68	0.36	1.52	0.95	0.84	2.87	1.79
0.12	1.12	0.70	0.38	1.56	0.98	0.90	3.29	2.06
0.14	1.14	0.71	0.40	1.60	1.00	0.94	3.91	2.44
0.16	1.17	0.73	0.42	1.64	1.03			

From Ref. [41].

the BET surface area and was reported to be 4.3 – 4.4 m^2 g^{-1}. This curve is a smoothed curve and at the low-pressure range is very different from other standards. In the literature, there are several standards for carbon. There is probably an appropriate standard available for the carbon material of particular interest.

KFG Segmented Standard Carbon Curve

Karnaukhov et al. [9] have presented a standard curve with a segmented least-squares fit to the data of α versus P/P_s. The fit is for the equation

$$n_{ad} = \sum_{i=0}^{5} C_i \left[\ln\left(\frac{P_s}{P} \right) \right]^i \tag{76}$$

The coefficients, C_i, are listed in Table 13. n_{ad} is given here in units of μmol m^{-2} but the surface area per gram of sample is not listed. To use this in the usual fashion a α–s curve this is constructed from the coefficients presented in Table 14. This curve may be useful for determining mesoporosity. It does not extrapolate below 0.10 P/P_s.

Cranston and Inkley Standard for Pore Analysis

Cranston and Inkley [44] developed a general standard isotherm, which did a fair job for a variety of adsorbents including silica and alumina.

Table 13
KFG coefficients for a standard curve extracted from carbons

Range	Coefficients C_i					
	0	1	2	3	4	5
0.1–0.6	27.1667	23.449	16.75	6.5135	0.9971	0
0.55–0.92	46.5644	242.443	1120.65	2884.45	3729.22	1890.9
0.90–0.99	119.463	1983.14	130098	1.792×10^7	1.2438×10^7	3.4279×10^7

Table 14
α–s curve using coefficients form Table 13

P/P_s	$n/n_{0.4}$	P/P_s	$n/n_{0.4}$	P/P_s	$n/n_{0.4}$
0.1	0.680	0.6	1.219	0.9	1.969
0.2	0.800	0.65	1.287	0.92	2.117
0.3	0.903	0.7	1.374	0.94	2.328
04	1.000	0.75	1.471	0.96	2.694
0.5	1.103	0.8	1.582	0.98	3.827
0.6	1.215	0.85	1.734	0.99	5.236
0.55	1.153	0.9	1.977		

Basically, the data were averaged and smoothed to yield the standard curve. The data for this curve are not presented in their article but a graph of the averaged isotherm is given. It would be best for those who wish to use this curve to consult the original.

Thoria Standard Curves

Thoria has the interesting property that it can be fired to a high temperature without changing morphology. Thus, a degassing temperature to clean the surface at 1000°C does not change the surface area. It is therefore an interesting research tool as well as being used for a variety of commercial applications. In Table 15 is the standard nitrogen curves, obtained by Gammage et al. [45] for thoria out-gassed at 25°C are given. For higher out-gassing temperature the standard curve is the same at high values of χ (high relative pressure) but deviates with a χ plot break, at a low value of χ. This is due to the degassing of a higher energy plane. The original smoothed curve has been made into a α–s curve. The standard curve for water on thoria is in Table 16. A similar treatment has been used for the smoothed curve. The standard curve for argon adsorption is given in Table 17.

Table 15
Standard isotherms of low termperature out-gassed thoria

Original data				Smoothed α–s curve			
P/P_s	t (Ä)	P/P_s	t (Å)	P/P_s	$n/n_{0.4}$	P/P_s	$n/n_{0.4}$
0.016	1.43	0.602	6.93	0.010	0.221	0.300	0.865
0.027	1.72	0.660	7.38	0.020	0.303	0.350	0.933
0.036	2.30	0.701	7.86	0.030	0.351	0.400	1.000
0.078	2.84	0.758	8.38	0.040	0.394	0.450	1.063
0.104	3.17	0.802	9.06	0.050	0.428	0.500	1.135
0.138	3.42	0.848	9.93	0.060	0.457	0.550	1.202
0.205	3.92	0.898	11.22	0.070	0.486	0.600	1.279
0.248	4.39			0.080	0.510	0.650	1.361
0.358	5.07			0.090	0.534	0.700	1.452
0.402	5.36			0.100	0.558	0.750	1.558
0.462	5.72			0.150	0.649	0.800	1.678
0.501	6.13			0.200	0.726	0.850	1.832
0.558	6.42			0.250	0.798	0.900	2.038

Standard Curves for Lunar Soil

In Tables 17–21 the standard isotherms from lunar soil as supplied to NASA [46] are given. For these samples the standard curves have been converted here to α–s curves. The first three points were ignored for the

Table 16
Standard curve to water adsorption of thoria

Original data				Smoothed α–s curve			
P/P_s	t (Å)	P/P_s	t (Å)	P/P_s	$n/n_{0.4}$	P/P_s	$n/n_{0.4}$
0.010	0.92	0.535	5.32	0.010	0.169	0.100	0.526
0.048	1.65	0.555	5.62	0.015	0.216	0.150	0.625
0.068	2.48	0.595	6.18	0.020	0.253	0.200	0.710
0.115	2.82	0.655	6.42	0.025	0.283	0.250	0.787
0.152	3.15	0.711	6.85	0.030	0.309	0.300	0.859
0.205	3.34	0.758	7.35	0.035	0.332	0.350	0.930
0.260	3.68	0.795	8.46	0.040	0.353	0.400	1.000
0.321	4.11	0.850	9.32	0.045	0.372	0.450	1.071
0.355	4.85	0.900	10.42	0.050	0.390	0.500	1.144
0.465	5.08			0.055	0.407	0.550	1.220
				0.060	0.422	0.600	1.301
				0.065	0.437	0.650	1.389
				0.070	0.451	0.700	1.486
				0.075	0.465	0.750	1.596
				0.080	0.478	0.800	1.727
				0.085	0.490	0.850	1.891
				0.090	0.503	0.900	2.114

Table 17
Argon adsorption on 25°C out-gassed thoria

Original data				Smoothed α–s			
P/P_s	$t/(\text{Å})$	P/P_s	$t/(\text{Å})$	P/P_s	$t/(\text{Å})$	P/P_s	$t/(\text{Å})$
0.011	0.78	0.354	4.94	0.005	0.078	0.650	1.396
0.018	1.13	0.368	5.06	0.010	0.152	0.700	1.496
0.028	1.48	0.378	5.30	0.020	0.238	0.750	1.609
0.038	1.68	0.403	5.32	0.030	0.295	0.800	1.742
0.045	1.86	0.419	5.45	0.040	0.340	0.850	1.909
0.056	2.18	0.444	5.70	0.050	0.378	0.900	2.136
0.064	2.28	0.454	5.75	0.060	0.411		

Table 17 (continued)
Argon adsorption on 25°C out-gassed thoria

Original data				Smoothed α–s			
P/P_s	$t/(\text{Å})$	P/P_s	$t/(\text{Å})$	P/P_s	$t/(\text{Å})$	P/P_s	$t/(\text{Å})$
0.082	2.54	0.468	5.89	0.070	0.440		
0.103	2.81	0.484	5.96	0.080	0.467		
0.118	3.02	0.501	6.18	0.090	0.492		
0.135	3.22	0.520	6.32	0.100	0.516		
0.148	3.30	0.536	6.40	0.150	0.618		
0.158	3.45	0.555	6.52	0.200	0.704		
0.201	3.78	0.561	6.58	0.250	0.782		
0.228	3.94	0.577	6.82	0.300	0.857		
0.235	4.17	0.600	6.96	0.350	0.929		
0.258	4.30	0.652	7.47	0.400	1.000		
0.278	4.46	0.698	7.93	0.450	1.072		
0.302	4.66	0.748	8.55	0.500	1.147		
0.326	4.74	0.802	9.33	0.550	1.224		
0.347	4.88	0.818	9.58	0.600	1.307		

Table 18
N_2 adsorption of non-porous lunar soil

Original data		Smoothed α–s curve			
P/P_s	n_{ad} (μmol g^{-1})	P/P_s	$n/n_{0.4}$	P/P_s	$n/n_{0.4}$
0.00051	1.517	0.0005	0.238	0.070	0.616
0.0036	2.357	0.001	0.272	0.080	0.635
0.0069	2.815	0.002	0.310	0.090	0.652
0.013	3.318	0.003	0.335	0.100	0.668
0.027	3.941	0.004	0.353	0.150	0.738
0.054	4.505	0.005	0.368	0.200	0.797
0.106	5.390	0.010	0.418	0.250	0.851
0.159	5.968	0.015	0.451	0.300	0.902
0.211	6.374	0.020	0.477	0.350	0.951
0.267	6.734	0.025	0.498	0.400	1.000
0.319	7.387	0.030	0.516	0.450	1.050
0.382	7.470	0.035	0.533	0.500	1.101
0.419	7.395	0.040	0.547	0.550	1.154
0.464	7.770	0.050	0.573		
0.525	8.011	0.060	0.596		

Table 19
Argon adsorption on non-porous lunar soil

Original data				Smoothed α–s curve			
P/P_s	n_{ad} (μmol g^{-1})	P/P_s	n_{ad} (μmol g^{-1})	P/P_s	$n/n_{0.4}$	P/P_s	$n/n_{0.4}$
0.029	2.327	0.411	6.869	0.020	0.361	0.400	1.000
0.059	3.416	0.500	7.583	0.040	0.447	0.450	1.061
0.099	3.949	0.600	8.483	0.060	0.507	0.500	1.123
0.144	4.557	0.691	9.234	0.080	0.554	0.550	1.188
0.198	5.210	0.766	10.248	0.100	0.595	0.600	1.257
0.253	5.676			0.150	0.680	0.650	1.332
0.306	6.096			0.200	0.752	0.700	1.415
0.355	6.517			0.250	0.818	0.750	1.510
				0.300	0.880	0.800	1.621
				0.350	0.940		

Table 20
Adsorption of O_2 on non-porous lunar soil

Original data				Smoothed α–s curve			
P/P_s	n_{ad}(μmol g^{-1})	P/P_s	n_{ad}(μmol g^{-1})	P/P_s	$n/n_{0.4}$	P/P_s	$n/n_{0.4}$
0.0003	0.000	0.245	4.880	0.00380	0.000	0.100	0.490
0.0006	0.000	0.280	5.631	0.004	0.0051	0.150	0.597
0.0014	0.000	0.352	6.246	0.005	0.028	0.200	0.688
0.0033	0.038	0.397	6.682	0.010	0.106	0.250	0.771
0.0117	0.788	0.452	7.222	0.015	0.157	0.300	0.849
0.0335	1.567	0.523	7.770	0.020	0.196	0.350	0.925
0.065	2.477	0.575	8.281	0.025	0.229	0.400	1.000
0.099	3.078	0.644	8.926	0.030	0.257	0.450	1.076
0.132	3.491	0.713	9.857	0.035	0.282	0.500	1.155
0.161	3.911			0.040	0.304	0.550	1.237
				0.050	0.344	0.600	1.324
				0.060	0.379	0.650	1.418
				0.070	0.410	0.700	1.523
				0.080	0.438	0.750	1.642
				0.090	0.465		

α–s curve fit for oxygen adsorption. The reason for the zero values is discussed in the section Threshold phenomenon. Details about the lunar soils can be obtained in a US government report [47] and additional information is available from an article by Fuller [48].

Table 21
CO adsorption on non-porous lunar soil

Original data				Smoothed α–s curve			
P/P_s	n_{ad} (μmol g^{-1})	P/P_s	n_{ad} (μmol g^{-1})	P/P_s	$n/n_{0.4}$	P/P_s	$n/n_{0.4}$
0.0006	2.793	0.219	7.583	0.0005	0.304	0.050	0.610
0.0031	3.378	0.274	8.071	0.001	0.335	0.100	0.697
0.0114	4.204	0.324	8.521	0.002	0.370	0.150	0.760
0.0215	4.557	0.389	8.694	0.003	0.392	0.200	0.815
0.0460	5.541	0.425	9.047	0.004	0.409	0.250	0.864
0.0854	6.119	0.484	9.497	0.005	0.422	0.300	0.910
0.133	6.607	0.538	9.970	0.010	0.469	0.350	0.955
0.177	7.132			0.015	0.499	0.400	1.000
				0.020	0.522	0.450	1.045
				0.025	0.542	0.500	1.092
				0.030	0.558	0.550	1.141
				0.035	0.573	0.600	1.192
				0.040	0.586	0.650	1.248

REFERENCES

[1] S. Brunauer, P.H. Emmett and E.J. Teller, Am. Chem Soc., 60 (1938) 309.

[2] S. Brunauer, L.S. Deming, W.E. Deming and E. Teller, J. Am. Chem. Soc., 60, (1938) 309.

[3] M.M. Dubinin, E.D. Zaverina and L.V. Radushkevich, Zh. Fiz. Khim., 21 (1947) 1351.

[4] M.M. Dubinin, Chemistry and Physics of Carbon, Vol. 2, p. 51, Dekker, New York, 1966.

[5] M.G. Karganer, Zhur. Fiy. Khim., 33 (1959) 2202.

[6] K.S.W. Sing, in "Surface Area Determination" D. H. Everett and R. H. Ottewill (eds.), p. 25, Butterworths, London, 1970.

[7] J.H. deBoer, B.G. Linsen and Th. J. Osinga, J. Catal., 4 (1965) 643.

[8] R.W. Cranston and F.A. Inkley, Adv. Catal., 9 (1957) 143.

[9] A.P. Karnaukhov, V.B. Fenelonov and V.Yu. Gavrilov, Pure Appl. Chem., 61 (1989) 1913.

[10] W. Rudzinski and D.H. Everett, Adsorption of Gases on Heterogeneous Surfaces, Academic Press, New York, 1992.

[11] A.W. Adamson, Physical Chemistry of Surfaces, 2nd Ed., Wiley, New York, 1967.

[12] P.C. Hiemenz, Principles of Colloid and Surface Chemistry, 2nd Ed., Marcel Dekker, New York, ISBN 0-8247-7476-0, (1986).

[13] P.H. Emmett and S. Brunauer, J. Am. Chem. Soc., 59 (1937) 1553.

[14] H.L. Pickering and H.C. Eckstrom, J. Am. Chem. Soc., 71 (1952) 4775.

[15] P.H. Emmett, J. Am. Chem. Soc., 65 (1946) 1784.

[16] M.G. Kaganer, Zhur. Fiy. Khim., 33 (1959) 2202.

[17] J.B. Condon, Microporous Mesoporous Mat., 38 (1000) 359.

[18] J. Tóth, Adv. Colloid. Interf. Sci., 55 (1955) 1.

[19] J. Tóth, Colloid. Surface. 49 (1990) 57.

[20] D. Harkins and G. Jura, J. Chem. Phys., 11 (1943) 430.

[21] D. Harkins and G. Jura, J. Chem. Phys., 13 (1945) 449.

[22] F. Goldman and M. Polanyi, Physikal. Chem., 132 (1928) 321.

[23] J.B. Condon, Langmuir, 17 (2001) 3423.

[24] J.B. Condon, Microporous Mesoporous Mat., 55 (2002) 15.

[25] M. Krug and M. Jaroniec, Microporous Mesoporous Mater., 44–45 (2001) 723.

[26] M.R. Bhanbhani, R.A. Cutting, K.S.W. Sing and D.H. Turk, J. Colloid Inter. Sci., 82 (1981) 534.

[27] S. Gregg and K.S.W. Sing, Adsorption, Surface Area and Porosity, Academia Press, New York, 1982.

[28] L.H. Cohan, J. Am. Chem. Soc., 60 (1938) 433.

[29] M. Giona and M. Giustiniani, Langmuir, 13 (1997) 1138.

[30] M. Polanyi, Verk. Deutsch. Physik. Gas, 16 (1914) 1012.

[31] M. Polanyi, Z. Elecktrochem., 26 (1920) 371.

[32] M. Polanyi, Z. Elecktrochem., 35 (1929) 431.

[33] J.H. deBoer and C. Zwikker, Z. Physik. Chem., B3 (1929) 407.

[34] R. Badmann, N Stockhausen and M.J. Setzer, J. Colloid. Interf. Sci., 82 (1981) 534.

[35] M.R. Bhambhani, P.A. Cutting, K.S.W. Sing and D.H. Turk, J. Colloid Interf. Sci., 38, 109 (1972).

[36] D.H. Everett, G.D. Parfitt, K.S.W. Sing and R. Wilson, J. Appl. Biochem. Technol., 24 (1974) 199.

[37] D.A. Payne, K.S.W. Sing and D.H. Turk, J. Collid. Interf. Sci., 43 (1973) 287.

[38] S.J. Gregg and K.S.W. Sing, Surface Area and Porosity, Academic Press, New York, (1982).

[39] B.C. Lippens, G.G. Linsen and J. H. deBoer, J. Catal., 3 (1964) 32.

[40] D.H. Everett, G.D. Parfitt, K.S.W. Sing and R. Wilson, J. Appl. Chem. Biotechnol., 24 (1974) 199.

[41] F. Rodriguez-Reinoso, J.M. Martin-Martinez, C. Prado-Burguete and B. McEnaney J. Phys. Chem., 91 (1987) 515.

[42] F. Rodriguez-Reinoso, J.M. Martin-Martinez, M. Molina-Sabio, R. Torregrosa and J. Garrido-Segovia, J. Collid. Interf. Sci., 106 (1985) 315.

[43] K.J. Masters and B. McEnaney, Carbon, 22 (1984) 595.

[44] R.W. Cranston and F.A. Inkley, Adv. Catal., 9 (1957) 143.

[45] R.B. Gammage, E.L. Fuller, Jr. and H.F. Holmes, J. Colloid. Interf. Sci., 34 (1970) 428.

[46] R.B. Gammage, H.F. Holmes, E.L. Fuller, Jr. and D.R. Glasson, J. Colloid. Interf. Sci., 47 (1974) 350

[47] E.L. Fuller, Jr. and P.A. Agron, The reactions of Atmospheric vapors with Lunar Soil, U.S. Government Report ORNL-5129 (UC-34B), March, 1976.

[48] E.L. Fuller, Jr., J. Colloid. Interf. Sci., 55 (1976) 358.

Chapter 4

Theories Behind the Chi Plot

INTRODUCTION: HISTORICAL BACKGROUND

In this chapter, the theory behind the use of the chi (χ) plots is presented. As early as 1929, deBoer [1] recognized that what is being referred to here as the χ plot was an excellent fit to adsorption data. The accuracy of the χ plot has been known for many years, starting with the deBoer–Zwikker [2] equation. Adamson [3] described it as being the best description for the entire isotherm ever devised. The deBoer–Zwikker theory depended upon polarizability to explain the isotherm. In spite of its obvious advantage the theory behind it seemed, according to Brunauer, very weak. It was claimed that polarizability could not account for the high energies observed. This claim may or may not be justified. It is known that London forces are not the only forces operating for strongly adsorbed molecules. Therefore, the forces are much greater than initially calculated.

Two derivations will be presented to explain the χ plot. These include the disjoining potential theory and the quantum mechanical derivation or χ theory. The classical derivation [4] or auto-shielding physisorption theory (ASP) theory [5] is very similar to the quantum mechanical derivation

THEORY BEHIND χ PLOTS

The Disjoining Pressure Derivation

The disjoining pressure theory by Churaev et al. [6] begins with the definition of the disjoining pressure, Π. There is a quantity that is a function of the coverage, Γ, or adsorbed film "thickness"[1], t, defined by the equation (for the theory t and Γ can be used interchangeably)

$$\Pi(t) = \frac{\partial f(t)}{\partial t}\bigg|_{T} \tag{77}$$

---

[1]The meaning of film "thickness" on a nearly atomic scale in somewhat questionable. Nevertheless, it is a convenient concept from our macroscopic, continuum viewpoint.

This physical quantity is interpreted to be the pressure needed to separate two parallel plates from each other when there is an intervening liquid phase. In this case, the liquid phase is interpreted to be an adsorbed phase. Thus, the chemical potential of this intervening phase may be specified by the pressure of the gas phase. Π can be related to the difference in the chemical potential, $\Delta\mu$, between the pure liquid phase at the saturation pressure, μ_l, and the chemical potential of the adsorbate, μ_{ad}, or

$$\Delta\mu = \mu_{ad} - \mu_l \tag{78}$$

or, more simply,

$$\Delta\mu = RT\ln(P/P_s) \tag{79}$$

By the expression [7],

$$V_m\Pi(t) = -\Delta\mu \tag{80}$$

(Notice that since $\Delta\mu$ is negative then by definition Π is positive.) The excess surface energy, Φ, is obtained from the product of the surface excess, Γ, and the change in chemical potential, provided the surface is flat. Using the above equation then

$$\Phi(\Gamma) = -\Gamma V_m\Pi(\Gamma) \tag{81}$$

(Φ is negative since it is an expression of exothermicity.) Up to this point, no modeling has been introduced, merely thermodynamics and definitions. The functionality of Π becomes important to proceed. The dependence of Π upon the film thickness is known [8,9] to reliably follow an exponential equation or

$$\Pi(t) = \Pi_0\exp(-t/\lambda) \tag{82}$$

where λ has been referred to as a "characteristic length". λ seems to be about a monolayer in distance. Substituting into Eq. (81) and replacing t/λ with the an equivalent type expression in Γ, i.e. Γ/Γ_m, one obtains

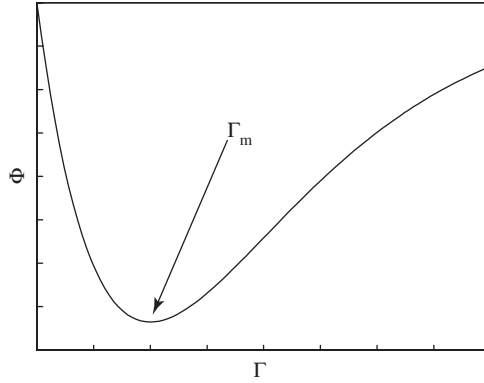$$\Phi(\Gamma) = -\Pi_0 V_m\Gamma\exp(-\Gamma/\Gamma_m) \tag{83}$$

Fig. 40. The functionality of surface excess energy, Φ, with coverage, Γ.

Fig. 40 is a sketch of how this function looks like. The function starts out at $\Phi = 0$ and goes to a minimum at $\Gamma = \Gamma_m$. This can be demonstrated by differentiating Eq. (83)

$$0 = \frac{d\Phi(\Gamma)}{d\Gamma} = -\Pi_0 V_m \left[\exp(-\Gamma/\Gamma_m) - \frac{\Gamma}{\Gamma_m} \exp(-\Gamma/\Gamma_m) \right] \tag{84}$$

from which one can obtain $\Gamma(\min \Phi) = \Gamma_m$. The question is: "What is the molecular meaning of Γ_m?" A similar question will be addressed in the χ theory formulation about the meaning of a_{ex}.

The Meaning of Γ_m in the Hard Sphere Model

Although one could argue whether the exponential assumption of Eq. (83) is or is not part of thermodynamics but rather modeling, it is clear that the meaning of Γ_m does require a model. There is no clear connection up to this point between Γ_m and the actual surface coverage. The following model should be a fairly accurate picture of what is happening on an atomic scale. It is important to realize that the modeling is based upon the hard sphere model for the adsorbate molecules and a correction should be made to this assumption. This will be performed for the χ-theory formulation in correcting the value for a_{ex} and should apply equally to Γ_m.

The maximum incremental energy released by the adsorption process should be at this minimum point. In other words, for two plates held

together by the intermolecular forces of the liquid, Γ_m is the point at which the maximum force operates. Assuming the molecules are hard spheres, this should occur when there is exactly one monolayer between the two plates. One may be able to visualize this by referring to Fig. 41. The maximum number of adsorbate–plate interactions is available in the arrangement "B", that is when there is one monolayer between the plates. This implies that below a monolayer, as illustrated by "A", the absolute value of Φ is less. When the value in a monolayer is exceeded, then the Π falls off due to the fact that there must be more than one adsorbate molecule between the two plates at some positions. Assuming that the forces between the adsorbate molecules are weaker than the forces between the adsorbate molecules and the plate molecules, then a relative easy separation can occur between adsorbate molecules that are stacked between the plates. This is the arrangement depicted as "C" in Fig. 41.

The conclusion is that there is a minimum in Φ, when there is exactly one monolayer of adsorbate between two plates. This, however is on average exactly 1/2 a monolayer for one plate. Using the symbol Γ_1 for a monolayer surface excess, then $\Gamma_m = 1/2\Gamma_1$ within the first approximation assumed with the hard sphere approximation. Using this together with Eq. (79), (80) and (82) one arrives at

$$\exp\left(-\frac{2\Gamma}{\Gamma_1}\right) = -\frac{RT}{V_m \Pi_0} \ln\left(\frac{P}{P_s}\right) \tag{85}$$

Although in this form it looks different from the χ theory equation, it is identical if $V_m \Pi_0 = E_a$ in the χ theory.

One would expect that this theory should not work for anything less than a monolayer since it depends upon the concept of a film and is therefore incorrect. It will be demonstrated in the next section that this criticism is unjustified. The quantum mechanical considerations validates the theory down to the very first adsorbed molecule.
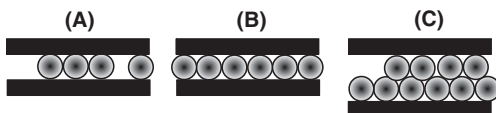

(A)   **(B)**   **(C)**

Fig. 41. Adsorbate molecules between two plates to account for the size of the force between them.

The Quantum Mechanical Derivation of the "Simple" χ Equation

The quantum mechanical derivation of the χ theory is quite simple. First a simple principle is stated. Given the solution to the wave equation, that is the energy as a function of quantum number, if one introduces a perturbation then for most wave numbers the energy is a volume (in the case of a surface an area) average of the original energy and the perturbation. Possible exceptions to this would be when the perturbation is of a size to cause significant scattering. This is the reason why the energy versus k diagrams in metal band calculations have an ideal parabolic shape near the origin for k. Therefore, if the thermal wavelength is significantly shorter then the perturbation it is very likely that this area averaging will work. Given this then the following derivation can proceed.

It is assumed that the temperature of adsorption is such that the adsorbed molecule will behave much as a liquid molecule would behave. That is, the specific potential wells on the surface are overall small compared to translational energy of the molecule. Therefore for the first adsorbate molecule to arrive at the surface one can treat it as simply a particle-in-a-potential-box. The energy of the potential of the box will be designated as E_a. For the second particle, it will arrive at the surface and it will experience one of two potentials. One of these potentials is E_a, which implies that if it were to (classically) encounter the first molecule it would "roll under" that molecule. On the other hand, if it were to "roll over" the other molecule then the energy would be an area average of E_a and the energy of interaction between the adsorbate molecules. The energy of the first molecule is also modified in the same manner due to the presence of the second molecule. In addition to this there is now the interaction energy between the molecules regardless of which one "rolls over" or "under". Thus, for the two molecules,

$$E_2 = E_a + E_a \left(\frac{A_s - a_{ex}}{A_s} \right) + 1\varepsilon \tag{86}$$

This logic is repeated for the third molecule:

$$E_3 = E_a + E_a \left(\frac{A_s - a_{ex}}{A_s} \right) + E_a \left(\frac{A_s - a_{ex}}{A_s} \right)^2 + 3\varepsilon \tag{87}$$

and for the *N*th molecule,

$$E_N = \sum_{m=0}^{N-1} E_a \left(\frac{A_s - a_{ex}}{A_s} \right)^{m-1} + (m-1)\varepsilon \tag{88}$$

The second term in Eq. (88) overestimates the number of lateral interactions possible for a molecule since it is not in contact with all other simultaneously. This is therefore modified with an average overall coordination number to be included in ε so that Eq. (88) will read as

$$E_N = \sum_{m=0}^{N-1} E_a \left(\frac{A_s - a_{ex}}{A_s} \right)^{m-1} + N\varepsilon \tag{89}$$

This takes into account all the possible interactions that could be present including lateral interactions. Typically, the thermal wavelength of the adsorbate molecules is about 1/20th of the size of the molecule itself, but the model takes into account even the long-range interactions. The wave functions for the combination of the first two molecules may be expressed as

$$\Psi = \varphi_o(1)\varphi_u(2) \pm \varphi_o(2)\varphi_u(1) \tag{90}$$

This is then extended to three and beyond by the various indistinguishable combinations. The number of these combinations is given by

$$C = \sum_{M=2}^{N} M \frac{N!}{M!(N-M)!} \Bigg/ \sum_{M=2}^{N} \frac{N!}{M!(N-M)!} \tag{91}$$

It is relatively easy to show that $C = 1/2N$ for large *N*. Rather than including this term in the ensemble that follows, it will be included in the discussion of a_{ex}. Defining a quantity,[2] $\zeta = Na_{ex}/A_s$ and recognizing that for large *N* the first part of the sum in Eq. (89) may be replaced with an integral; thus

$$E_N = E_a \int_0^N e^{-\zeta} \, dm \tag{92}$$

---

[2] The symbol θ will not be used here due to the implication that it is the number of monolayers. The symbol ζ will be used hopefully not to be confused with zeta potential. The relationship between ζ and θ will be established later.

Here the definition of the e function has been taken advantage of in taking the limit of high value of N to obtain the χ term as given. Since the energy and combinational consideration are settled, one can proceed by various paths to arrive at the isotherm. The grand canonical ensemble is convenient for this purpose. This is then given by

$$\Xi = \sum_N (\lambda Z)^N \exp$$

$$\left\{ -\left[E_a \int_0^N \exp(-\zeta)dm + N\varepsilon - 1/2NkT\left[1 - \exp(-\chi)\right] + N\mathbf{f}(T) \right] \bigg/ kT \right\} \tag{93}$$

The third and fourth terms of the exponential function are small terms which include:

1. the loss of some translational modes for the molecules near the adsorbent leading to a difference in heat capacity of $1/2kT$ for low coverages and
2. possible changes in vibrational modes, etc., for heat capacity effects in function $\mathbf{f}$.

These terms are always small but the first one has been observed with the heats of adsorption [10]. The usual method is to take the ln of Ξ and then differentiate with respect to N the maximum term obtained from the ln and setting it to 0. The canonical ensemble term λZ is replaced by the fugacity, or simply P at low pressures. Thus

$$0 = \frac{\partial \ln(\text{max term}\,\Xi)}{\partial N} = \ln(P) - \frac{\left\{ E_a e^{-\zeta} + \varepsilon + 1/2kT + \mathbf{f}(T) \right\}}{kT} \tag{94}$$

Ignoring the small terms for translation and heat capacity effect, this is rearranged and the ln function performed to yield

$$\ln[-\ln(P)] = \ln\left(-\frac{E_a}{kT}\right) - \zeta + \ln\left(-\frac{\varepsilon}{kT}\right) \tag{95}$$

(Since the adsorption is exothermic $E_a < 0$ so the ln works out well.) Knowing that as $N \to \infty$ then $P \to P_s$ this may be included along with the P term. Defining

$$\chi_c \equiv \ln\left(-\frac{E_a}{kT}\right), \quad \chi = -\ln\left[-\ln\left(\frac{P}{P_s}\right)\right] \quad \text{and} \quad \Delta\chi \equiv \chi - \chi_c \tag{96}$$

and knowing that negative values of N and therefore χ are not allowed then the simple form of the χ theory equation is obtained:

$$\zeta = \Delta\chi \mathbf{U}(\Delta\chi) \tag{97}$$

where $\mathbf{U}$ is the unit (Heaviside) step function. This equation is useful by itself. It is capable of yielding an analytical expression for standard isotherms and heats of adsorption when reported in terms of moles of material adsorbed rather than coverage. The relationship with surface area, however, is not established since the value for a_{ex} is to be determined.

The Meaning of a_{ex} – the Perfect Adsorption Equation for Hard Spheres

To relate Eq. (97), or ζ, to the surface area, a value for a_{ex}, the excluded area, needs to be determined. First, the hard sphere approximation to an adsorbed molecule will be determined. The area one would expect an average liquid molecule to cover is given by the molar area. This physical quantity, designated as a here, is given by the equation

$$a = \left(\frac{V_m}{N_A}\right)^{2/3} \tag{98}$$

Sometimes the quantity "molar area" is used, A_m, which is defined as

$$A_m = V_m^{2/3} N_A^{1/3} \tag{99}$$

However, a_{ex} cannot be a since the amount of area excluded when a test molecule travels toward another adsorbed molecule is determined by the van der Waals radius. This difference is illustrated in Fig. 42.

The van der Waal radius is twice the radius one expects from the liquid and the area that one molecule excludes another molecule is four times what one would expect from the liquid area.

This is not the entire picture, however. First, according to Eq. (91) and the approximation thereafter, half the time an adsorbate molecule will exclude another adsorbate molecule from its area and half the time it will not. Therefore, with the hard sphere approximation the excluded area is half of the van der Waal area or twice the liquid area. Second, the hard sphere approximation assumes that the energy profile as a molecule "rolls over"
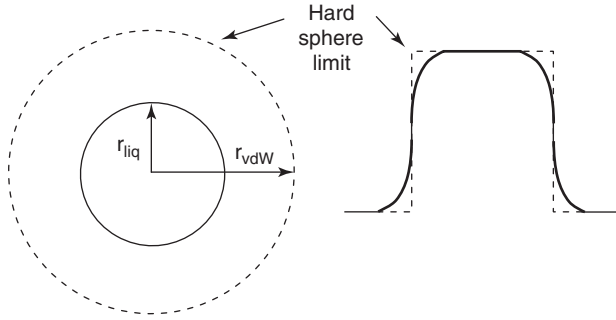
Fig. 42. The relationship between the van der Waal area and the area expected from liquid density and the difference between the energy profile expected from a hard sphere model and a more realistic energy profile.

another is like a step function. This is illustrated by the broken line on the right part of Fig. 42, whereas the solid line is more realistic. This is an additional correction, which may be dependent upon the details of the adsorbent and adsorbate.

Using only the hard sphere approximation it is possible to provide the relationship between a_{ex} and A_m. The hard sphere approximation for the χ equation becomes

$$\frac{2n_{ad}A_m}{A_s} = \Delta\chi \mathbf{U}(\Delta\chi) \tag{100}$$

From the slope of the χ plot, that is number of moles adsorbed, n_{ad}, versus χ, one may obtain the surface area for any particular coverage, i.e.

$$A_s = 2A_m \frac{\partial n_{ad}}{\partial \chi} \tag{101}$$

The Energy Correction

Fig. 42 illustrates the potential difference between the hard sphere model and a more realistic energy profile. As mentioned at the beginning of the χ theory derivation, if the quantum number is held constant and a small perturbation is made in one part of the potential energy well, then the area averaged potential energy will be observed. This principle can be applied to make a correction

to the hard sphere approximation. The exact form of this perturbation is not obvious but here a Lennard–Jones 6-12 (LJ 6-12) potential will be used.

This LJ 6-12 potential is assumed for both the adsorbate and the surface atoms. Since the adsorbate molecules are free to travel over the surface, the 6-12 potential is considered as a uniform average in the parallel plane of the surface. By referring to Fig. 43, the following geometrical arguments may be made. This is a side view corresponding to the energy diagram presented in Fig. 42. The LJ potential has a distance, r_o, designated in the 6-12 equation by

$$E_{LJ} = 4\varepsilon \left[\left(\frac{r_o}{\mathbf{r}} \right)^{12} - \left(\frac{r_o}{\mathbf{r}} \right)^6 \right] \tag{102}$$

and is related to the other r values by

$$r_o = 2^{-1/6}(r_m + 2r_t) \tag{103}$$

where r_m is the center-to-center distance between adsorbate molecules and r_t is the radius of the immobile surface atom or ion, that is, center-to-edge.

By simple geometry, (see Fig. 43), the distance between the average surface molecule or ion and the molecule that is rolling over is

$$r_s = \frac{r_m \left(\sqrt{r_m^2 - r^2} + 1/2\ r_m + r_t \right)}{r} \tag{104}$$
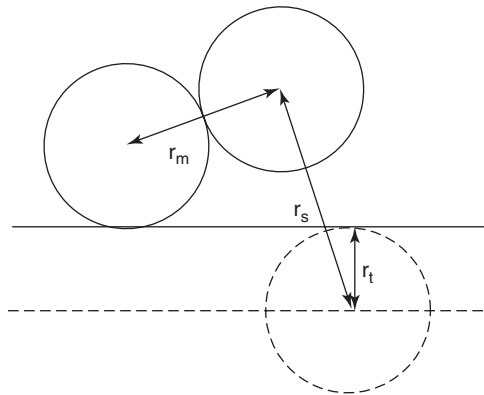

Fig. 43. The arrangement of an adsorbate molecule "rolling over" another and the distances defined for the treatment of the energy correction.

where r is the distance between centers in the plane of the surface. Using this, the effective fraction of the excluded area compared to the hard sphere ratio, s, may be calculated from the expression

$$s = \left(\int_0^{r_m} 4\varepsilon \left[\left(\frac{r_o}{r_s} \right)^{12} - \left(\frac{r_o}{r_s} \right)^6 \right] (2\pi r)\, dr \right) \bigg/ \left(\int_0^{r_m} E(2\pi r)\, dr \right) \tag{105}$$

Making the appropriate substitution for r_s and evaluating numerically, s is given as

$$s = -0.0967 \frac{r_t}{r_m} + 0.9653 \tag{106}$$

Defining a factor $f = 2s$ one may replace the factor 2 in Eq. (100) and (101) with f:

$$\frac{n_{ad} f A_m}{A_s} = \Delta\chi U(\Delta\chi) \tag{107}$$

Thus for ζ,

$$\zeta = \frac{n_{ad} f A_m}{A_s} \tag{108}$$

The ratio of r_t to r_m is always greater than 0 and is unlikely to be greater than 0.5. Therefore the reasonable range for f is from 1.83 to 1.93. This value is independent of the value for E_a or the adsorbate intermolecular force. It depends on the ratio of radii but not on the absolute values of the individual radii. The recommendation, if nothing is known about the adsorbent surface, would be to use the lower number, i.e. 1.83, for this factor

$$A_s = 1.83 A_m \frac{\partial n_{ad}}{\partial \chi} \tag{109}$$

It is unlikely that this factor will be incorrect by more than 3%.

SIMULTANEOUS PHYSISORPTION AND CHEMISORPTION

The term "localized adsorption" will be used in a rather broad sense in this section. This could refer to any type of adsorption that is site-specific including chemical bonds or chemisorption, strong localized forces, such as pi-coordinate complexing or hydrogen bonds to the surface. If the bonds are very strong then basically one has modified the surface permanently and one can revert to the normal χ plot to determine the properties of the modified surface. If these local attractions are fairly weak, then there could be reversible effects operating. One type of surface where one would expect this sort of behavior is that of graphitic carbon. In that case the exposed basal planes present the opportunity for large pi interactions. Adsorption of benzene or other aromatics on metals [11] would be another example.

For the derivation, assume that there are K sites on the surface for localized adsorption. A parameter, α, is defined as the amount of surface that is covered by localized adsorption. α can obviously vary from 0 to 1 depending upon the position in the isotherm. For the number of molecules in the first layer, M, the distribution is the familiar Langmuir form. The number of combinations is given by

$$C = \frac{K!}{M!(K-M)!} \tag{110}$$

This consideration should then be added to the grand canonical partition function. Leaving the definition of ζ in the grand canonical partition function, Eq. (93), as the same for the adsorbent except that the localized adsorbate molecules are excluded, i.e.

$$\zeta = \frac{f(n_{ad} - n_1)A_m}{A_s} \tag{111}$$

where n_1 is the number of moles adsorbed in the localized layer. The energy of adsorption for this will be designated as E_1. (There might be several E_1s as is well known in the chemisorption literature.) The energy of adsorption for subsequent layers will vary according to the amount in the localized layer; in other words by a factor of $(1-\alpha)$. Given these

considerations, Eq. (93) (for simplicity ignoring the small terms) may easily be modified to

$$\Xi = \sum_M \sum_N \frac{K!}{M!(K-M)!} \ (\lambda Z)^{N+M}$$

$$\exp\left\{-\left[ME_1 + [E_a(1-\alpha)+\alpha\varepsilon]\int_0^N\exp(-\zeta)\,dx + N\varepsilon\right]\Big/kT\right\}$$

(112)

The derivatives of the (ln max term) with respect to both M and N are now required. The results are

$$\ln P = \ln\left(\frac{\alpha}{1-\alpha}\right) + \frac{E_1}{kT}$$

(113)

(This is the expected results, the Langmuir isotherm.) and

$$kT \ln P = [E_a(1-\alpha)+\alpha\varepsilon]\exp(-\zeta) + \varepsilon$$

(114)

which is very similar to the previous equations except for the factor of $(1-\alpha)$ and the factor $\alpha\varepsilon$ being added to compensate for the loss of free surface. This latter factor may actually differ from these values if some of the adsorbate is fairly tightly bonded to the surface. This would change the interaction energy between a first layer adsorbate and subsequent adsorbate molecule to be different from that of the bulk liquid.

A few simulations of these equations in a χ plot would be useful to illustrate some of the unusual features. Fig. 44 presents a few simulations. These would be approximate for nitrogen adsorption (with an ε of about 1 kJ mol^{-1}) at 77 K with the following three cases:

Case A. $E_1=6$ kJ mol^{-1} and $E_a=12$ kJ mol^{-1}: The first part looks very much like a Langmuir isotherm followed by the onset of physisorption.

Case B. $E_1=4$ kJmol^{-1} and $E_a=12$ kJ mol^{-1}: Here one sees an interesting phenomenon. At the start of the isotherm there occurs some physisorption. However, with increased pressure the localized adsorption becomes greater, displacing some of the physisorbed material, thus producing the first step that is seen. The second step is due almost entirely to the localized adsorption. With the near completion of the first layer, this is followed by the onset of the final physisorption.
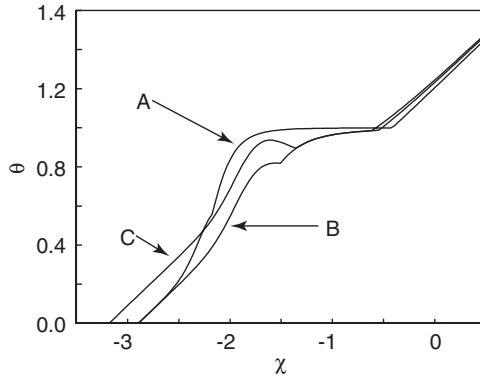
Fig. 44. Some generated χ plots for cases where there is localized adsorption. Case A, a high E_1 and a low E_a; Case B, a low E_1 and a low E_a; Case C, a low E_1 and a high E_a.

Case C. $E_1=4$ kJ mol^{-1} and $E_a=16$ kJ mol^{-1}: This is an interesting case where the displacement of the initial physisorbed material is greater than the amount of localized adsorption. This is probably not realistic.

Case B (or if it exists Case C) present some interesting implications. The heats of adsorption or isosteric heats, for example, will not be as simple as with the totally delocalized physisorption that obeys the χ plot. Multiple peaks in the heats of adsorption are to be expected.

HETEROGENEOUS SURFACES

Additivity of χ Plots
One of the nice features of the χ plots is that for several mixed surfaces the χ plots add. This is quite obvious because the dependent variable in the χ equation is amount adsorbed which, of course, must add experimentally. An important feature of the χ theory is the unit step function in Eq. (107). If there are several surface planes of different energies they would simply add

$$n_{ad} = \sum_i \frac{A_{s,i}}{fA_m} \Delta \chi_i \, U(\Delta \chi_i) \tag{115}$$

Thus, for the various slopes,

$$\frac{\partial n_{ad}}{\partial \chi} = \sum_i \frac{A_{s,i}}{fA_m} U(\Delta\chi_i) \tag{116}$$

An additional step is taken to determine the second differential

$$\frac{\partial^2 n_{ad}}{\partial \chi^2} = \sum_i \frac{A_{s,i}}{fA_m} \delta(\chi_{c,i}) \tag{117}$$

The usefulness of this last equation is that the sum of δ functions is an expression of the distribution of $\chi_c s$ and thus the distribution of the various energies of adsorption. This fact will be utilized when a distribution is detected, which is χ plot feature 1.

According to Eq. (116) when several surfaces are present with distinct energies of adsorption, the χ plot will start at low pressures with the highest energy surface. The slope then yields the surface area. After the appropriate χ_c for the next surface the slope yields the sum of the two surfaces. This addition is continued until all the χ_c values have been exceeded. Thus, at least in the early portion of the χ plot, an upward bending of the χ plot is an indication of more surfaces becoming active in the adsorption process. An upward bend can also be indicative of capillary filling in mesopores; however, this happens at the high end of the χ plot. As a rough rule, below $\Delta\chi \approx 2.5$, an upward bend may be due to additional surfaces adsorbing; above $\chi \approx -1.5$ an upward bend, especially a large upswing, is due to capillary filling. This leaves unfortunately some overlap and judgement may be required to distinguish the two.

It is not common to find pure materials with more than two distinct energies of adsorption. It may be common to find energy distributions as will be illustrated below. A couple of examples of two distinct energies of adsorption are found with carbon and with some ceramics that have distinct crystallographic planes on the surface.

Figs. 45–47 show some examples of χ plot where it appears that two or more energy surfaces are involved. These are vulcan and sterling FT carbon [12] and high-fired thoria [13]. The adsorption on thoria has an addition feature due to mesoporosity, which can be separated out from the simple surface adsorption. This separation will be used as an example in a later section.
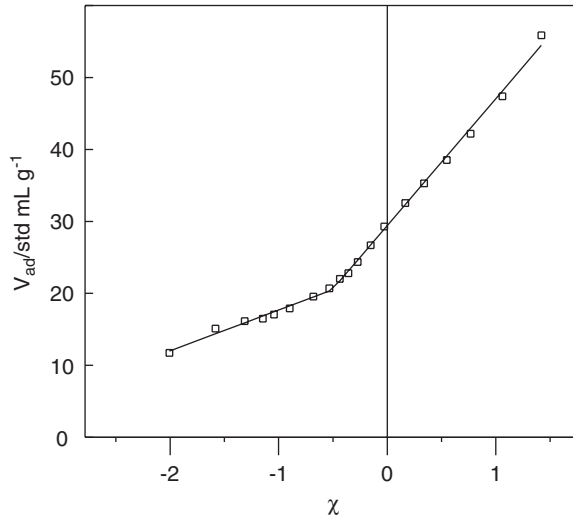
Fig. 45. χ plot of nitrogen adsorbed on vulcan carbon indicating two energies of adsorption by the two straight line fits.
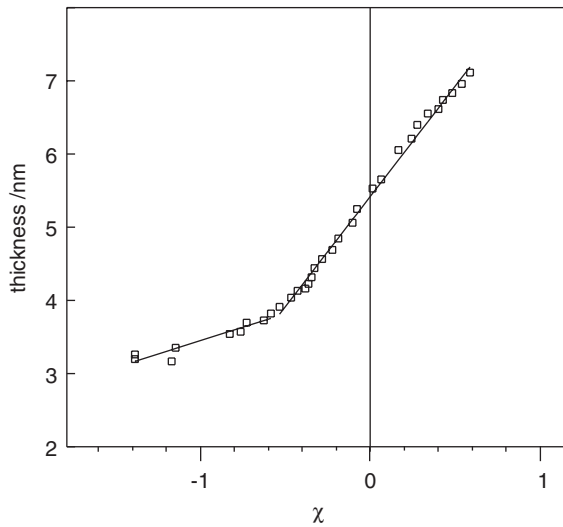

Fig. 46. χ plot of nitrogen adsorbed on sterling FT carbon indicating two energies of adsorption by the two straight line fits.
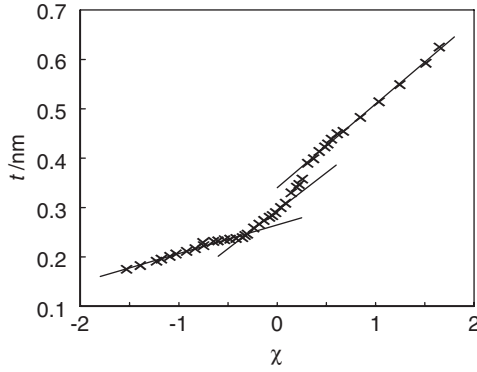
Fig. 47. χ plot of nitrogen adsorbed on high-fired thoria indicating two energies of adsorption and some other features by the multiple straight line fits.

Insensitivity for $\chi \geq \max \chi_c$

It should be obvious from Eq. (116) that after the last break in the χ plot, the slope of the line yields the total surface area. Mathematically, this can be written as

$$A_s = fA_m \left. \frac{\partial n_{ad}}{\partial \chi} \right|_{\chi > \chi_{\max i}} \tag{118}$$

Provided other complications are absent, such as capillary filling or bed porosity capillary filling, the final answer is the surface area of the total sample.

Reformulation for a Distribution of E_a Values

Eq. (117) is the starting point for treating surfaces that have a distribution of energies. In place of the sum of δ functions one may insert a distribution function. Any distribution function allows both continuous or a series of δ functions or a combination. One of the more common distributions in energy [14] is the ln normal distribution, which is the same as a normal distribution in χ_c. Therefore the modified Eq. (117) is

$$\frac{\partial^2 n_{ad}}{\partial \chi^2} = \frac{A_s}{fA_m \sigma \sqrt{2\pi}} e^{-(\chi - \langle \chi_c \rangle)^2 / 2\sigma^2} \tag{119}$$

where the symbol $\langle \chi_c \rangle$ indicates the mean of the χ_c values. σ is the standard deviation in the χ_c distribution. (When $\sigma = 0.48$ the low-pressure Freundlich isotherms are generated, whereas $\sigma = 0.23$ generates the low-pressure range for the Dubinin sets of isotherms. The demonstration of this is in a later section.) Without any additional complications, such as porosity, Eq. (119) may be integrated from $-\infty$ to χ twice to yield the shape of the isotherm as

$$n_{ad} = \frac{A_s(\chi - \langle \chi_c \rangle)}{fA_m}\left[\frac{\sigma}{2\sqrt{2\pi}}\exp\left(-\frac{(\chi - \langle \chi_c \rangle)}{2\sigma^2}\right) + \frac{1}{2}\text{erf}\left(\frac{\chi - \langle \chi_c \rangle}{\sigma\sqrt{2}}\right)\right] \qquad (120)$$

This is basically the same equation as Eq. (100) with the quantity in the square brackets replacing the step function (and indeed becomes as $\sigma \to 0$). The shape of the isotherm was given in Chapter 1 as the χ representation of type III.

HEATS OF ADSORPTION

Isosteric Heat of Adsorption, q_{st}

Dubinin [15], to derive features of the isotherm, postulated what he referred to as the "thermodynamic criterion", which is

$$\left.\frac{\partial RT\ln(P_s/P)}{\partial T}\right|_{n_{ad}} = 0 \qquad (121)$$

There does not seem to be any justification put forward for this but one can make the following interpretation. This partial derivative is the same as ΔS going from the bulk liquid phase to the adsorbed condition. Thus, the molecular arrangement in the adsorbed phase is identical to the molecular arrangement in the liquid phase. (This contradicts the Brunauer, Emmitt and Teller (BET) formulation which requires a phase transition at high coverages.) The justification for this becomes clear with the development of the χ theory [16]. If one performs this operation on the simplified χ equation, (97), an identical result is obtained. If one does not ignore only the internal modes in Eq. (94) represented by $\mathbf{f}(T)$ then one has for the partial of $\ln(P/P_s)$, with respect to $1/T$,

$$-RT\left.\frac{\partial \ln(P/P_s)}{\partial(1/T)}\right|_{n_{ad}} = (E_a - 1/2\,RT)e^{-\zeta} \qquad (122)$$

and the partial with respect to T is relatively small but finite and possibly measurable by calorimetry:

$$\frac{\partial RT \ln(P_s/P)}{\partial T}\bigg|_{n_{ad}} = 1/2R \tag{123}$$

Dubinin referred to the quantity $RT\ln(P/P_s)$ as the "adsorption potential" and represented it by the symbol "A".

One of the problems when one looks at the literature or when calorimetric quantities are reported is the variety of definitions of "heat". Hopefully the following will aid in clearing up the confusion. The quantity derived in Eq. (122) is what is often referred to as the isosteric heat of adsorption, which causes some confusion with the experimental quantity which refers a 1 atm standard state. Here it will be referred to as the heat of the liquid–adsorbate transition or q_{la}. Therefore by χ theory,

$$q_{la} = (E_a - 1/2\,RT)e^{-\zeta} \tag{124}$$

(recalling that $\varsigma = n_{ad} fA_m/A_s$). The isosteric heat should include this plus the molar enthalpy of vaporization

$$q_{st} = q_{la} + \Delta H_v \tag{125}$$

The Integral Heats of Adsorption

Experimentally, q_{st} is very difficult to measure directly. Attempts to find the partial of $\ln(P/P_s)$ with respect to $1/T$ by measuring the isotherm at two or more temperatures have not been very accurate. This is due to the uncertainty in the shape of the isotherm compared to the precision that is acceptable. Direct calorimetric measurements have been more successful. Calorimetric measurements are more precise but they measure the integral heat of adsorption, Q', and the molar heat of adsorption, $\mathbf{Q}'$, as defined by Morrison et al. [17]. Another quantity, the integral energy of adsorption, Q, was defined by Hill [18, 19] for constant volume conditions. These quantities can be obtained with more accuracy and precision than the isosteric heat. Nevertheless, the isosteric heat is often reported.

From these experimental quantities the isosteric heat is obtained by the "usual method". This "usual method" is as follows:

1. Q' is measured up to a certain amount of adsorption. The calorimetric details involve steps to calibrate the calorimeter and determine the heat capacity of the calorimeter, the adsorbent and the adsorbate and adsorptive up to the pressure corresponding to n (the subscript *ad* will be dropped here for simplicity with the understanding that n is the number of moles adsorbed) that Q' corresponds to. The isotherm must also be measured. Thus one has, after significant mathematical manipulation, a set of Q'_i, n_i and P_i.
2. It is assumed that the q_{st} for an average of two points $\langle n_i$ and $n_{i+1}\rangle$ is given by

$$q_{\langle n_i \text{ and } n_{i+1}\rangle} = \frac{Q'_{i+1} - Q'_i}{n_{i+1} - n_i} \tag{126}$$

Unfortunately, there are two problems associated with this method. The first problem is critical in terms of archiving.

1. Information is lost and cannot be recovered if the original data are not presented in some place. This is because the number of points is one less than measured. Although this may seem to be a minor problem, *none* of the original data can be recovered since this is a threaded string of calculations.
2. Problem 1 would not be so serious, if it was not for the fact that this method introduces errors due to the averaging effect. There is no guarantee that Q' is linear as implied by Eq. (126) and indeed may change suddenly. Thus, the reported Q' will be different from the actual value.
3. An additional problem is the usual introduction of scatter when one tried to digitally differentiate data as implied in Eq. (126).

Given the problems associated with this method, it would be highly advised to report Q' and not q_{st}. After all Q' is just as useful both theoretically and practically as q_{st}.

The molar integral heat, $\mathbf{Q}'$, is defined as the integral heat per mole of the adsorbate or

$$\mathbf{Q}'(n_{ad}) = Q'/n_{ad} \tag{127}$$

Both of these quantities may be referenced to the liquid state rather than to 1 atm. Using subscripts *la* to indicate this, the following may be derived by substituting into Eq. (124)

$$\mathbf{Q}'_{la} = \frac{A_s}{fA_m} \, (E_a - 1/2 \, RT)(1 - e^{-\zeta}) \tag{128}$$

and the molar integral heat is

$$\mathbf{Q}'_{la} = \frac{1}{\zeta} \, (E_a - 1/2 \, RT)(1 - e^{-\zeta}) \tag{129}$$

(One may also derive the expected heat capacity, $C_{p,ad}$, by differentiating $\mathbf{Q}'_{la}$ with respect to T.) Thus,

$$C_{p,ad}\Big|_{n_{ad}} = \frac{(1 - e^{-\zeta})}{2\zeta} R + C_{p,l} \tag{130}$$

where $C_{p,l}$ signifies the heat capacity at constant pressure for the liquid phase. Since the first term is small ($\leq 1/2\,R$), one expects the heat capacity of the adsorbed film to be about the same as the bulk liquid.

ADSORPTION OF MORE THAN ONE ADSORBATE[3]

Binary adsorption in χ theory has not been thoroughly tested due to the lack of appropriate experimental data. Here two approximations are presented. First, the approximation for the adsorption on nearly flat surfaces is discussed and, second, adsorption in pores that are filled or nearly filled is presented. For both of these cases there is some information in the literature against which the assumptions could be tested.

---

[3] The next two sections, binary adsorption and depth profiles, have not yet been published and no doubt additional research is required, both theoretically and experimentally.

Binary Adsorption on a Flat Surface

In the derivation of the χ theory, E_a was defined to derive the grand canonical ensemble. For convenience, the quantities $E_{a,1}$ for adsorbate 1 in relation to its E_a may be defined by

$$E_{a,1} \equiv E_1 + 1/2\,kT + \mathbf{f}(T) \tag{131}$$

$\mathbf{f}(T)$ for simple molecules should be zero and the $1/2kT$ is small and will be ignored to simplify matters. The E_a in Eq. (93) is given here as E_1.

Following the same prescription as before and noting that now molecules of type 2 may also form "teeth" in the particle in the box description, the energy $E_{N,1}$ for the adsorbate number 1 is

$$E_{N,1} = E_1 \sum_{M_1=1}^{N_1} \left(1 - \frac{a_{ex,1}}{A_s}\right)^{M_1-1} \left(1 - \frac{a_{ex,2}}{A_s}\right)^{N_2} \tag{132}$$

In this and subsequent equations, there are identical equations for adsorbate 2 with the indexes 1 and 2 switched. Added to this is the energy of interaction, $E_{int,1}$ between the adsorbed molecules. Since this is a "big box" approximation, the energy between the molecules will be a weighted average, or for adsorbate 1 this is

$$E_{in,1} = N_1 \frac{N_1 \varepsilon_{11} + N_2 \varepsilon_{12}}{N_1 + N_2} \tag{133}$$

This is obviously the regular solution assumption so one would expect that at high pressures the regular solution theory equation would be the result. This term could be replaced by other more complicated assumptions to yield different solution answers. In constructing the grand canonical ensemble for the χ equations for one adsorbate, no accounting was needed for the sequence in which the molecules adsorbed, since they were all indistinguishable. In the case of two adsorbates, however, this is not the case. The number of ways one can arrive at a system with N_1 molecules of adsorbate 1 and N_2 molecules of adsorbate 2 is given by the (well-known) expression

$$\text{Number of sequences} = \frac{(N_1 + N_2)!}{N_1! N_2!} \tag{134}$$

From the above considerations, the grand canonical ensemble may be written as

$$
\Xi = \sum_{N_1 N_2} \lambda_1 Z_1^{N_1} \times \lambda_2 Z_2^{N_2} \times \left[\frac{(N_1+N_2)!}{N_1! N_2!} \right]
$$

$$
\times \exp\left(-E_1 \int_0^{N_1} e^{-(x a_{ex,1} + N_2 a_{ex,2})/A_s} \, dx/kT \right) \tag{135}
$$

$$
\times \exp\left(-E_2 \int_0^{N_2} e^{-(N_1 a_{ex,1} + x a_{ex,2})/A_s} \, dx/kT \right)
$$

$$
\times \exp\left(-\left[N_1 + N_2 + \left(N_1^2 \varepsilon_{11} + N_1 N_2 \varepsilon_{21} + N_2^2 \varepsilon_{22} \right. \right. \right.
$$

$$
\left. \left. \left. + N_1 N_2 \varepsilon_{12} \right) \middle/ \left\{ \left(N_1 + N_2 \right) kT \right\} \right] \right)
$$

Following the usual procedure and taking the partial differential with respect to N_1 of the ln max term Ξ one obtains,

$$
0 = kT \frac{\partial \ln(\max \text{ term}\,\Xi)}{\partial N_1} = kT \ln(\lambda_1 Z_1) + kT - E_{a,1} e^{-(\zeta_1 + \zeta_2)}
$$

$$
-\left(a_{ex,1} / a_{ex,2} \right) \left(E_{a,2} \right) \left(e^{-(\zeta_1 + \zeta_2)} - e^{-\zeta_1} \right) + \varepsilon_{11} + X_2^2 \, \Delta \varepsilon - kT \ln X_1 \tag{136}
$$

where ζ_1 and ζ_2 have the same meaning with respect to components 1 and 2, respectively, as before ($\zeta = N a_{ex}/A_s$) and the factor f is required to relate this to moles and molar area ($\zeta = n_{ad} f A_m / A_s$). X_1 and X_2 are the mole fractions of adsorbates 1 and 2, respectively, and $\Delta\varepsilon$ is defined as

$$
\Delta\varepsilon = \varepsilon_{12} + \varepsilon_{21} - \varepsilon_{11} - \varepsilon_{22} \tag{137}
$$

Using the relationship $\ln(\lambda_1 Z_1) = \ln P_1$ and the previous definition using the subscript "s" to designate the vapor pressure of the adsorptive over its liquid with a flat surface,

$$
-kT \ln(P_{s,1}) = \varepsilon_{11} + kT \tag{138}
$$

Substituting and rearranging

$$
kT \ln\left(\frac{P_1}{P_{s,1}}\right) = \left(E_{a,1} + \frac{A_{m,1}}{A_{m,2}} E_{a,2}\right) e^{-(\zeta_1 + \zeta_2)}
$$
$$
- \frac{A_{m,1}}{A_{m,2}} E_{a,2}\, e^{-\zeta_1} - X_2^2\, \Delta\varepsilon + kT \ln X_1
\tag{139}
$$

since $a_{ex,1}/a_{ex,2} = A_{m,1}/A_{m,2}$. There are a few things to notice about Eq. (139):

1. As $n_{ad,1}$ and $n_{ad,2}$ both approach ∞, the pressure approaches the regular solution theory relationship. This fulfills one very important requirement for a valid adsorption theory, that is this limit should yield a reasonable bulk liquid answer.
2. As $n_{ad,2}$ approaches 0, the equation approaches the single χ theory equation.
3. As $n_{ad,1}$ approaches ∞, the equation yields Raoult's law for solutions.
4. If $n_{ad,1}$ is a small value and $n_{ad,2}$ approaches ∞, the equation yields Henry's law for solutions.
5. Subtraction of the #2 counterpart from Eq. (139) gives

$$
kT \ln\left(\frac{P_1 P_{s,2} X_2}{P_2 P_{s,1} X_1}\, e^{\Delta\varepsilon(X_1 - X_2)/kT}\right) = \Delta E\, e^{-(\zeta_1 + \zeta_2)}
$$
$$
+ \frac{A_{m,2}}{A_{m,1}} E_{a,1}\, e^{-\zeta_2} - \frac{A_{m,1}}{A_{m,2}} E_{a,2}\, e^{-\zeta_1}
\tag{140}
$$

where ΔE includes a group of energy terms and is zero if the two molar volumes are the same. Notice that as the coverage increases, the right-hand side of the equation tends to zero and the pressure ratios approach the regular solution of the bulk liquid. It is instructive to look at the function form of Eq. (140). As an example assume the experiment as performed with a mixture of gas whose composition is held constant, that is the ratio of P_1/P_2 is constant. At the low relative pressures there is first a tendency for the higher energy adsorbate to adsorb first with little adsorption of the lower energy adsorbate. This is followed by a region of adsorption where the relationship between the adsorbates is linear, that is

$$
n_{ad,2} = S n_{ad,1} + I
\tag{141}
$$

This is illustrated in Fig. 48 for the following values (which yields an interesting undulating curve):

$$E_1/RT = 10 \ (\chi_{c,1} = -2.303), \qquad E_2/RT = 13 \ (\chi_{c,2} = -2.565), \qquad A_1/A_2 = 0.9,$$
$$\Delta\varepsilon/RT = 1.0, \quad P_1/P_2 = 2.0$$

The extrapolated amount of adsorbate 2 is of about 0.2 monolayers on this scale and the slope is primarily determined by the energies of adsorption. At higher pressures, as can be seen in Fig. 49, the extrapolated intercept is through the origin and the slope of the fit is what is expected from the normal solution value. There appears to be only one good example of the
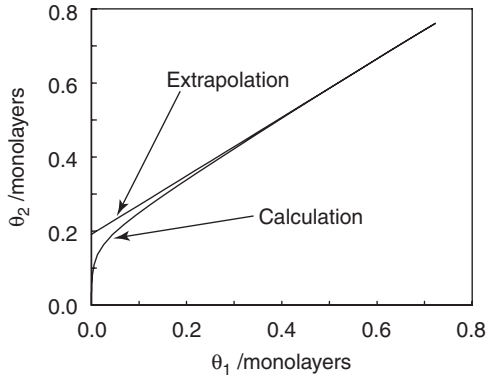

Fig. 48. The low-pressure end of the plot of $n_{ad,1}$ versus $n_{ad,2}$ in terms of monolayers.
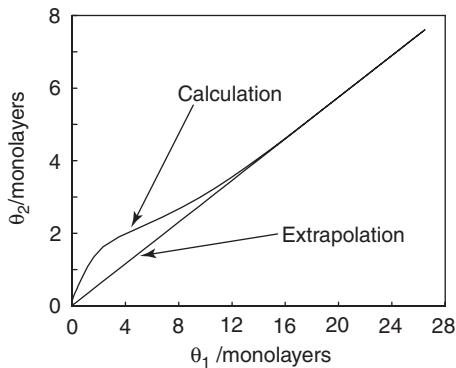

Fig. 49. The high-pressure end of the plot $n_{ad,1}$ versus $n_{ad,2}$ in terms of monolayers.

low-pressure adsorption in the literature without capillary filling. This is presented in Chapter 5.

DEPTH PROFILES AND χ THEORY

By using the χ theory, with the original postulate, one cannot calculate the depth profile. This should not be surprising since the assumptions made dealt with the two dimensional energy profile on the surface and ignored the third dimension. The overall average thickness may be calculated but the details of the profile cannot be calculated. This is in contrast to the calculations by density functional theory (DFT), where the profile is an integral part of the calculation and therefore is one of the resultant outputs. The principal disadvantage of DFT, however, is the dependence upon the specifics of the surface which is usually unknown. A secondary disadvantage is the difficulty of the calculation, which probably in the future will be no hindrance.

The situation, however, can be rectified with additional assumptions, one of which was used to determine the value for f and therefore a_{ex}. The value for f, however, could vary from 1.84 to 1.92 depending upon the specifics of the potential between the adsorbent surface atoms and the adsorbate molecules. The value of 1.84 has been used as most reasonable, but this could introduce an error of as much as 5%. It does, however, leave the theory free from the burden of needing to know the specifics of the surface composition. The assumption of the LJ 6-12 assumption for both adsorbate and adsorbent is retained. A second assumption is that within the LJ 6-12 potential only the ground quantum state of vibration is important. This is an extremely justifiable assumption since most adsorption measurements are performed at room temperature or below. Some simple calculations indicate for most cases that the second state is occupied by much less than a part per million. (Spectroscopists consistently use this assumption almost without thinking about it.) The ground state for vibration is represented by the first Hermite polynomial (H_0), which is conveniently identical to the probability mass function (PMF) or Gaussian:

$$\psi = Ne^{-(r-r_{min})^2/4\sigma^2} \tag{142}$$

Another reasonable assumption is that there is no reason to assign a different probability for the fractional occupancy of the second layer than for the

first layer,[4] nor for the third layer, etc. One may not, however, have a negative coverage. Thus for whatever amount of adsorbate that is not in the first layer is first assigned to the second layer given the same conditional probability as arrived at for the first layer. Assuming the surface is flat, the same continues for subsequent layers and this may be written mathematically as

$$\mathbf{P}(\theta_{n+1}) = \mathbf{P}\left(\theta - \sum_{i=1}^{n}\theta_i \middle| \theta_n\right) \geq 0 \tag{143}$$

The occupancy, or monolayer equivalence, of the first layer, θ_1, is the complementary function to the excluded area. Thus, by χ theory this is given as

$$\theta_1 = 1 - \exp(-\Delta\chi) \tag{144}$$

where θ is given by $n_{ad}A_m/A_s$. In the absence of porosity $\theta = \Delta\chi/f$. Substituting it for the individual θs and using the concept of Eq. (143) one obtains for the nth layer,

$$\theta_n = \max\left(0, \left[1 - \exp\left(-\frac{1}{f}\left[\theta - \sum_{n=1}^{n-1}\theta_i\right]\right)\right]\right) \tag{145}$$

The greater than zero condition is required because the function is negative before any adsorbate molecules are allowed in the nth layer. This is analogous to the threshold pressure concept. Eq. (145) provides a convenient method to calculate the number of adsorbate molecules that exists in each layer. An interesting aspect of this equation is that there is no dependence on the energy of adsorption. Fig. 50 and 51 show some results obtained from this calculation. Fig. 50 shows the buildup of the individual layers as χ increases. Fig. 51 shows the overall profile that one expects if a perfectly flat hard-wall surface is assumed. The adsorbate assumed is argon. The hard-wall assumption is, of course, unrealistic and makes the profile of the

---

[4] The definition of adsorbate layer by χ theory is not dependent upon distance from the surface but rather how many intervening adsorbate molecules there are between it and the surface. However, when the underlying layers have a value of θ approaching 1, then the correspondence to geometry is much closer.
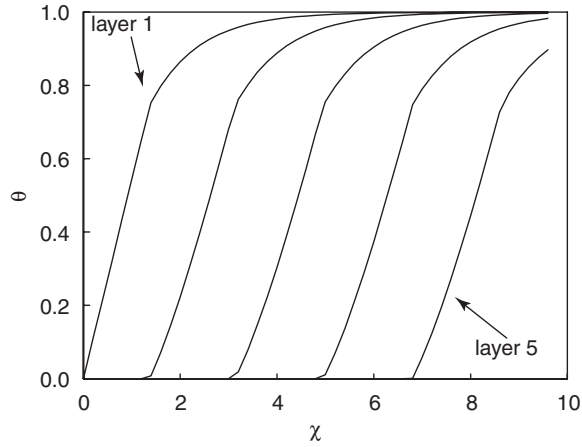
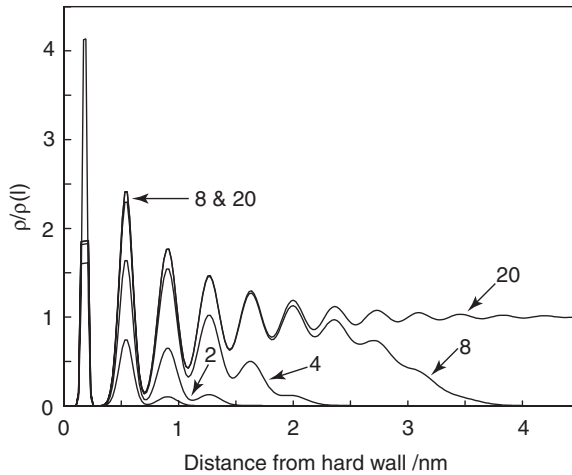Fig. 50. The individual monolayer coverages for layers 1–5.

Fig. 51. Argon depth profiles against a hard-wall for 1, 2, 4, 8 and 20 monolayer equivalent coverages.

first layer unrealistically sharp. The assumption that went into the profile calculation is that the LJ, 6-12 potential may be approximated by a parabolic potential and therefore the adatoms are perfect harmonic quantum oscillators. (Given that the surface atoms are also acting as oscillators, the

profile shown here for the second layer is probably closer to the real profile for the first layer.) The results are very similar to calculations made using DFT or grand canonical Monte Carlo calculations. (see Fig. 119).

THE THERMODYNAMICS OF THE SPREADING PRESSURE

As noted earlier in this chapter, there is definite relationship between the disjoining pressure theory of adsorption and the χ theory. In this section, some thermodynamic relationships for the spreading pressure are derived. It is questionable at this point how useful these relationships will be. They may be useful in extending the theory into the solution chemistry since these relationships are important in that area of research.

It should first be noticed that any theories that claim both the continuity to the liquid state at high pressures and the consistency with "Henry's law" violate Gibbs' phase rule. ("Henry's law" is in quotes because it is really not Henry's law as it applies to solutions. If it is assumed that the pressure and amount adsorbed approach zero simultaneously, then the relationship has the appearance of a Henry's law type behavior. The postulate that "Henry's law" must apply to any theory of adsorption can easily be disproved by finding only one system where this is not true. In Chapter 5 under "The observation of χ_c" several such examples will be presented.) One could also say that critical points violate the phase rule as well, so some researchers have made such an analogy. First, then, Gibbs' phase rule as it applies to surfaces will be reviewed.

Gibbs' Phase Rule in Systems with Surfaces

The origin of Gibbs' phase rule in thermodynamics is fairly easily deduced. It is not necessary to totally derive it here since it is available in almost any physical chemistry text (for example, see [20] p. 391). Disregarding the surface as important the phase rule reads

$$N = 2 + C - P \tag{146}$$

where N is the number of degrees of freedom, C the number of chemical components and P the number of phases present. The number 2 is a result of the terms in the free energy of "PV" and "TS". If one adds to this a surface area with a significant surface excess, an additional term similar to these two, which is "γA_s", is to be considered. Applying this to Eq. (146),

$$N = 3 + C - P \tag{147}$$

Consider, for example, the bulk case where there is only one phase and one component. For example hydrogen in a container; then the temperature and pressure may be varied arbitrarily provided, of course, the container can be made larger or smaller. This is what is meant by two degrees of freedom. If one has both a liquid and gas present, then the temperature and pressure are interdependent. This lowers N to 1.

Now consider the case where there is a surface. N now becomes 3 if only the gas phase is present. What is the third degree of freedom? In a thought process, one could say this additional degree of freedom is the surface area, which could therefore be arbitrarily varied without requiring any adjustments in either T or P. If the adsorbed gas on the surface is contiguous with the gas phase (which is the basis for Freundlich isotherm with $r_F = 1$) then the surface excess must be zero for this to be true. (Remember that this is about thermodynamics, which is related to molecular theories through statical mechanics. This requires large number of molecules and a few adsorbate molecules here and there would not be counted.) On the other hand, if a new phase forms on the surface, for simplicity call it the adsorbate, then the number of degrees decreases to 2. Now if the adsorbate phase changes, an adjustment must be made in either T or P (or both, but there is now a triplet relationship between n_{ad}, T and P). Of course, normally it is T that is held constant to produce the isotherm. Thus, the adsorbed phase is contiguous with the bulk liquid phase and not the gas phase. This requires a phase transition at some pressure which is not zero.

Most strenuous objection to the χ theory has been the prediction of a threshold pressure for adsorption. The above consideration not only allows a threshold pressure for the adsorbate phase to form, but requires it. This does not preclude the possibility of a surface gas phase, but some simple energy calculations demonstrate that if such phase existed and given reasonable energies of adsorption, the amount adsorbed would be well below today's limit of detection. (Assuming a very high energy of adsorption, 15 kJ mol^{-1}, and a very thick distance of 1 nm for this energy to operate, the number of moles that one would adsorb is about 2×10^{-8} mol m^{-2}. Even with a large surface area, this is still below most limits of detection. As an example, a realistic value for N_2 adsorption on silica at liquid N_2 temperature would be 1.5×10^{-11} mol m^{-2}.)

Derivation of the Spreading Pressure

The spreading pressure, π, is normally defined as the negative value of the surface tension. One may utilize the χ theory to obtain π in terms of

surface area and amount of adsorbate. It would be easiest to start with the simplified χ equation, that is to ignore changes in translational and internal modes. In principle, these could be added in but at this point does not seem to present any additional insight. The simplified χ equation is

$$n_{ad} = \frac{A_s}{fA_m}\left[\ln\left(-\frac{E_a}{RT}\right) - \ln\left(-\ln\left(\frac{P}{P_s}\right)\right)\right] \tag{148}$$

This may be rearranged to solve for $\ln P$:

$$\ln P = \ln P_s + \frac{E_a}{RT}e^{-n_{ad}fA_m/A_s} \tag{149}$$

Differentiating (recall that $E_a < 0$ by definition of exothermicity),

$$\frac{\partial \ln P}{\partial n_{ad}}\bigg|_T = -\frac{E_a fA_m}{RTA_s}e^{-n_{ad}fA_m/A_s} \tag{150}$$

Using the fact that $RT\mathrm{d}\ln P = d\mu$ one may substitute into the Gibbs–Duhem equation, which is

$$-A_s d\pi = n_{ad}d\mu \tag{151}$$

to arrive at

$$d\pi = \frac{E_a n_{ad} fA_m}{A_s^2}e^{-n_{ad}fA_m/A_s}dn_{ad} \tag{152}$$

At this point there are two integrations (see the article "A" [21], which is the same as here except that it is expressed in terms of χ) that can be performed. If the reference is the liquid state as is required for excess surface work then

$$\gamma_\infty - \gamma_{ad} \equiv \pi - \pi_\infty = -\frac{E_a}{A_s}e^{-n_{ad}fA_m/A_s}\left(\frac{A_s}{fA_m} + n_{ad}\right) \tag{153}$$

The other reference is $n_{ad} = 0$ (but not $P = 0$) so

$$\gamma_0 - \gamma_{ad} \equiv \pi - \pi_0 = \frac{E_a}{fA_m} - \frac{E_a}{A_s} e^{-n_{ad}fA_m/A_s} \left(\frac{A_s}{fA_m} + n_{ad} \right) \tag{154}$$

It is usually conceded that $\pi_0 = 0$ (or $\pi = 0$ when $n_{ad} = 0$ as Eq. (154) would then imply). This implies that $\pi_\infty = E_a/fA_m$.

The relationship to the disjoining pressure and excess surface work may be also derived.

The defined [22] $\Delta\mu$ ($\equiv \mu_{ad} - \mu_{liquid}$) which is consistent with the reference state for χ theory is accordingly,

$$\Delta\mu = E_a e^{-n_{ad}A_s/fA_m} \tag{155}$$

Therefore disjoining pressure is related to the partial molar spreading pressure by

$$\frac{\partial\pi}{\partial n_{ad}} = -\frac{n_{ad}fA_mV_m}{A_s^2}\Pi \tag{156}$$

or to π by

$$\pi = \frac{V_m}{A_s}\Pi\left(\frac{A_s}{fA_m} + n_{ad}\right) + \frac{E_a}{fA_m} \tag{157}$$

or another way of looking at this is through the surface excess work, Φ:

$$\pi = t_{mono}\Pi + \frac{V_m}{A_s}\Phi + \frac{E_a}{fA_m} \tag{158}$$

where t_{mono} is a monolayer thickness. Also

$$\frac{\partial\pi}{\partial n_{ad}} = -\frac{fA_mV_m}{A_s^2}\Phi \tag{159}$$

Thus, the partial molar spreading pressure is related directly to the surface excess work. Therefore, the minimum in Φ and in the χ theory plot is the maximum in the partial molar spreading pressure. The relationship with the spreading pressure itself is not very clear.

Is the χ Plot Compatible with the Freundlich and Dubinin Isotherms?

The relationship to the Freundlich isotherms is important for two reasons. First the question as to whether the χ theory can predict isotherms such as the Freundlich (of which $r_F = 1$ is a special case), Dubinin–Astakov, Dubinin–Radushkevich and Tóth isotherms? All but the Tóth isotherm will be referred to as the Dubinin–Polanyi (DP) isotherm. Second, the reason for the observation that in most cases P appears to approach 0 as n_{ad} approaches 0. Even though there are cases where P approaches a finite value, thus disproving the universal application of "Henry's law", this is not convincing without an explanation as to why it is observed in many cases.

The log-normal energy distribution has been expressed in Eq. (119), which yields the isotherm in the χ representation as expressed in Eq. (120). The DP isotherms may all be expressed as

$$n_{ad} = n_0 \exp\left(A\left[-\ln(P/P_s)\right]^k\right) \tag{160}$$

This formulation is the generalized form for all the DP isotherms. The details of each may be found in the literature [23] along with additional equivalency comparisons to χ theory. If $k=1$, this is the special case of the Freundlich isotherm. Define a quantity χ_0 as

$$\chi_0 = \frac{\ln A}{k} \tag{161}$$

Then the χ representation of the low pressure isotherm is

$$n_{ad} = n_0 \exp\left(-\exp\left(-k(\chi - \chi_0)\right)\right) \tag{162}$$

The question is then whether this is the same as Eq. (120) in the low-pressure range or not. To make a match, the second derivative of this expression should yield an expression that matches the energy distribution described by Eq. (119). The second derivative of equation (162) is

$$\frac{\partial^2 n_{ad}}{\partial \chi^2} = n_o k^2 \exp\left[-\exp\left(-k(\chi - \chi_0)\right)\right]$$
$$\left[\exp\left(-2k(\chi - \chi_0)\right) - \exp\left(-(\chi - \chi_0)\right)\right] \tag{163}$$

One of the important features to notice in this equation is that when $\chi = \chi_0$ the distribution is zero. If $\chi > \chi_0$ the distribution becomes negative. Noting

the fact that this second derivative yields the energy distribution which is not dependent upon χ theory, one must therefore conclude that the above χ_0 relationships, that is the DP, etc., cannot be literally correct. Luckily the amount of negative distribution above χ_0 is not too great. To match Eq. (163) with Eq. (119), the third and fourth derivatives (1st and 2nd of (163)) are required to match the peak position and the curvature. Performing these operations yields the following relationships:

$$\langle\chi_c\rangle = \chi_0 - \frac{2\ln\left(1 + \sqrt{5}\right) - \ln 2}{k} \approx \chi_0 - \frac{0.962}{k} \tag{164}$$

and σ is related to the DP k parameter by

$$\sigma = \frac{0.92423}{k} \tag{165}$$

In Fig. 52 some examples of generated energy distribution curves for the DP isotherms and the χ theory are given. These are normalized by dividing by the constant at the beginning of the distributions. A value of -2.0 was choosen for χ_c and χ_0 was calculated from Eq. (164). k values of 1, 1.5 and 2 were choosen and the corresponding σ calculated from Eq. (165). As may
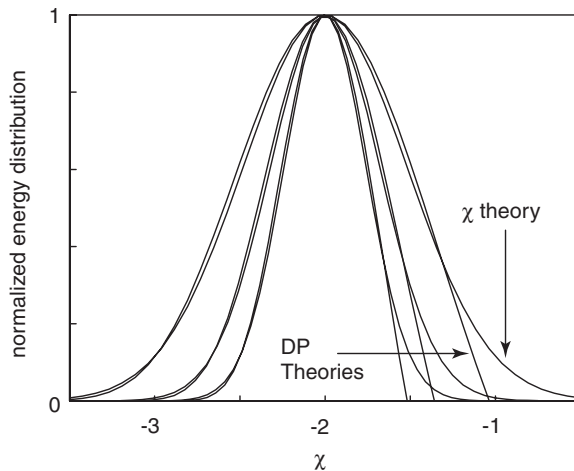

Fig. 52. A comparison of the χ theory energy distribution and DP distribution. DP k values used were, starting from the outside, 1, 1.5 and 2.

be discerned from the figure the match between the two energy distributions are almost identical except where the DP distribution drops to zero at the high-energy end.

The Freundlich isotherm is identical to the DP isotherm with $k = 1$ and $\chi_c = 0$. It is very unlikely for an adsorbate–adsorbent pair to have exactly this χ_c value. This value corresponds to an E_a at liquid nitrogen temperature of about 650 J mol^{-1}. This is a very low value. For most ceramics the value is 10–20 kJ mol^{-1}. Therefore, Freundlich isotherms with $r_F = 1$ are extremely unlikely to be observed but higher powers, $r_F > 1$ are likely.

REFERENCES

[1] J.H. deBoer, Proc. R. Acad. (Amsterdam), 31 (1928) 109.
[2] J.H. deBoer and C. Zwikker, Z. Phys. Chem., B3 (1929) 407.
[3] A.W. Adamson, Physical Chemistry of Surfaces, 2nd Ed., Wiley, New York, 1967.
[4] J.B. Condon, The Derivation of a Simple, Practical Equation for the Analysis of the Entire Surface Physical Adsorption isotherm, Y-2406, US-DOE Printing Office, National Technical Information Service, US Dept. of Commerce, Springfield, VA, USA, 1988.
[5] E.L. Fuller, Jr. and J.B. Condon, Colloid. Surface, 37 (1989) 171.
[6] N.V. Churaev, G. Starke and J. Adolphs, J. Colloid Interf. Sci., 221 (2000) 246.
[7] B.V. Derjaguin, N.V. Churaev, J. Colloid Interf. Sci., 54 (1975) 157.
[8] J. Adolphs and M.J. Setzer, J. Colloid Interf. Sci., 180 (1996) 70.
[9] J. Adolphs and M.J. Serzer, J. Colloid Interf. Sci., 207 (1998) 349.
[10] J.B. Condon, Micropor. Mesoporous Mat., 53 (2002) 21.
[11] R.B. Moyes, P.B. Wells, Adv. Catal., 23 (1973) 121.
[12] D.H. Everett, G.D. Parfitt and K.S.W. Sing, J. Chem. Biotechnol., 24 (1974) 199.
[13] R.B. Gammage, E.L. Fuller, Jr. and H.F. Holmes, J. Colloid Interf. Sci., 34 (1970) 428. (Digital data obtained directly from E.L. Fuller.)
[14] K.S.W. Sing and S.J. Gregg, Adsorption, Surface Area and Porosity, 2nd ed., p. 29, Academic Press, London, 1991.
[15] M.M. Dubinin, in "Progress in Membrane and Surface Science", (D.A. Cadenhead, J.F. Danielli, M.D. Rosenberg eds.), Vol. 9, pp. 1–70, Academic Press, New York, 1975 (ISBN 0-12-571809-8).
[16] J.B. Condon, Microporous Mesoporous Mat., 53 (2002) 21.
[17] J.A. Morrison, J.M. Los and L.E. Drain, Trans. Faraday Soc., 47 (1951) 1023.
[18] T.L. Hill, J. Chem. Phys., 17 (1949) 520.
[19] T.L. Hill, Trans. Faraday Soc., 47 (1951) 376.
[20] A.W. Adamson, A Textbook of Physical Chemistry, 2nd Ed., Academic Press, New York, ISBN 0-12-044260-4, 1979.
[21] J.B. Condon, Microporous Mesoporous Mat., 38 (2000) 359.
[22] N.V. Churaev, G. Starke, J. Adolphs, J. Colloid Interf. Sci., 221 (2000) 246.
[23] J.B. Condon, Microporous Mesoporous Mat., 38 (2000) 377.

This page intentionally left blank

Chapter 5

Comparison of the Chi Equation to Measurements

The purpose of this chapter is to first establish that the chi (χ) plot is, in most cases, an excellent analytical description of the various standard curves. Indeed, it is now questionable that those standard curves, which do not follow the χ plot are free from multiple energies of adsorption or from microporosity. Once this is established, then the χ theory (disjoining theory or standard plot application since they are all equivalent) may be used to analyze various adsorption experiments, including heat of adsorption, microporosity, mesoporosity, heterogeneity, etc. Along with this, some predictions and preliminary evidence will be presented that these predictions are correct. Additional details concerning the fit of the standard curves, regardless of these problems are given in the literature [1].

COMPARSION TO STANDARD ISOTHERMS

In Chapter 3, a variety of standard plots is presented. It is instructive to plot these as χ plots to see how well they obey the analytical expression. In the following, the χ plot fits will be performed only on original data where available. Creation of the standard plot by some fitting routine or simply using a manual spline fit is in itself a distortion of the data. Indeed, the thoria and lunar soils standard plots were created using the insights of the χ plot, so the standard plot by definition must fit the χ plot perfectly. Similar problems are encountered in analyzing heat of adsorption.

In the analysis that follows, the slope of the fit, the χ intercept (χ_c), the standard deviation of the fit and the statistical R will be presented.

The α–s Standard Plots

The most widely used standard plot is the α–s plot created by Sing et al. [2], for both N_2 and Ar adsorption. The original data [3] is presented in Fig. 53 for argon adsorption and in Fig. 54 for nitrogen adsorption. For Ar the following statistics for the fit are generated: slope$=21.1$ mL; $\chi_c=-2.23$; $\sigma = 1.1$ mL; $R = 0.998$.
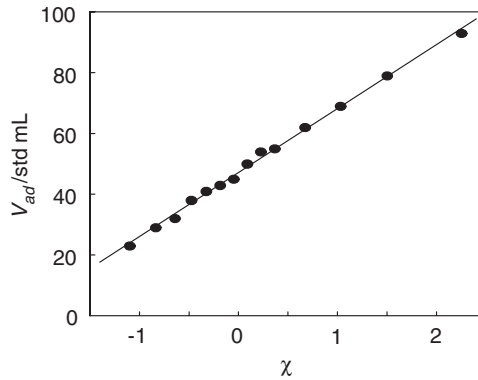
Fig. 53. Argon absorption on silica used to create the standard α–s plot as a χ plot. The line is the χ plot least-squares fit.
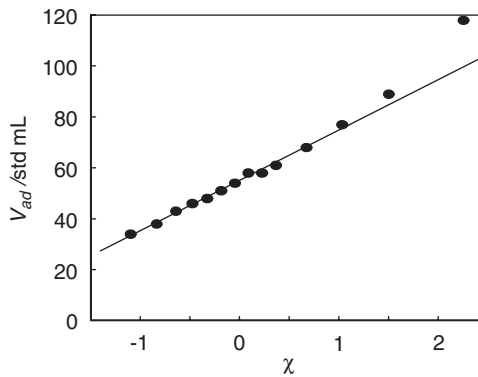
Fig. 54. Nitrogen adsorption on silica used to create the standard α–s plot as a χ plot. The line is the χ plot least-squares fit.

For the N_2 adsorption the last two points were not used in the χ plot fit. As mentioned in the first chapter, occasionally the data at high pressures, for a variety of reasons, may not be reliable. The most likely deviation is in the positive direction as seen here. Other silica data do not indicate this upswing.

The N_2 α–s plot generated the following statistics: slope$=19.8$ mL; $\chi_c=-2.78$; $\sigma = 0.99$ mL; $R=0.997$.

Cranston and Inkley Standard *t* Curve

The *t* curve by Cranston and Inkley [4] is a fairly early standard curve. The data were an average curve for a variety of ceramic materials including
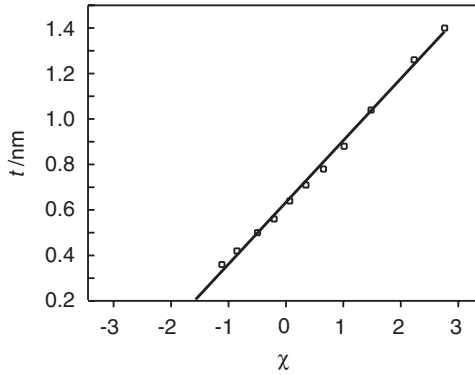
Fig. 55. Standard *t* curve constructed by Cranston and Inkley [4]. The circles are the constructed data point by the authors and the line is the χ plot least-squares fit.

alumina and silica. Given this, the statistics would seem to be meaningless, so they are not presented here. However, it is clear from Fig. 55 that the χ description is indeed a very good description of this standard plot.

deBoer's Standard *t*-Plots

deBoer et al. performed many experiments from which a standard *t*-plot could be constructed. These included most prominently the standard *t* curve on alumina by Lippens et al. [5]. (The calculation of the "thickness" value depends upon the BET calculation. Even though the actual value for the monolayer equivalence is in question, for the present discussion this does not matter.) If the standard *t* curve is plotted as a χ plot, a noticeable curvature is detected. If, however, the original data, available in the same series of papers by deBoer et al. [6], are plotted, it is not so obvious that this curvature is real. In Fig. 56 the original data used to construct the *t*-plot are given.

The earliest plot of adsorbate versus $-\ln(-\ln(P/P_s))$ was proposed by deBoer [7] which fit the adsorption of I_2 on CaF_2. Fig. 57 is the illustration of these data in χ plot representation. It was recognized by deBoer at that time that the fit to the χ plot was very good. Another example is that used by deBoer and Zwikker [8] to develop the polarization model. This example is of argon adsorption on tin II oxide as shown in Fig. 58. It appears, however, that the sample had some microporosity, however, the fit is very good up to quite a high value of χ. In addition to the well-known alumina adsorption, deBoer, Linsen and Osinga created standard plots for $BaSO_4$, TiO_2, ZrO_2, MgO, SiO_2-aerosil, Nickel antigorite, Graphon 1 carbon, Graphon 2 carbon and Sterling FT carbon. According to these authors, all but the carbon
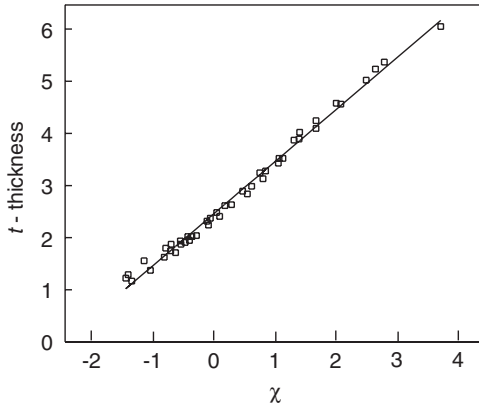
Fig. 56. Standard *t* curve data by deBoer et al. [6]. The data are the circles and the line is the χ plot least-squares fit.
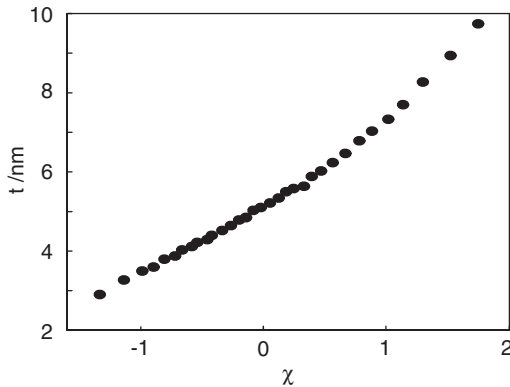

Fig. 57. N$_2$ adsorption of Ni antigorite according to deBoer et al. [6].

samples fit the standard *t* curve well. The χ plots of some of these are presented in Figs. 59 and 60. All but the carbon samples had upswings at high pressures indicating possible bed porosity.

Standard Thoria Plots

One of the advantages that thoria presents is that it is very stable with respect to high temperatures. Once a thoria produced powder is high fired to 1600°C, it is virtually physically stable. The surface chemistry is also stable with no change in stoichiometry. It is therefore an ideal powder with which to perform basic research.
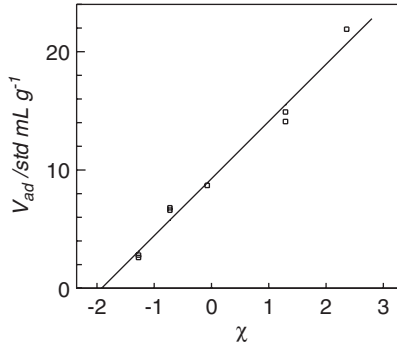
Fig. 58. Adsorption of iodine on CaF showing the χ plot relationship according to deBoer [7]. This is one of the earliest observations of the χ relationship
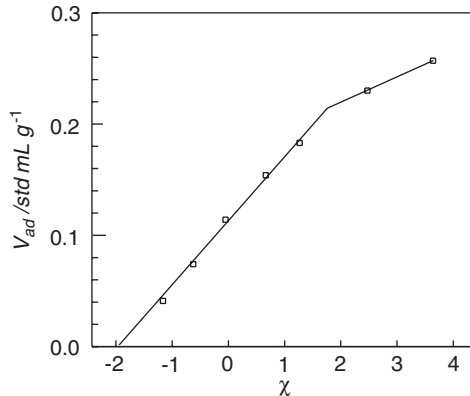

Fig. 59. Absorption of Ar on SnO according to deBoer and Zwikker [8]. The roundoff in the upper portion is probably due to microporosity.

Gammage et al. [9] have performed extensive research on this material and have determined that for powders that are out-gassed at 1000°C there are several complicating feature. Firstly, there is adsorption that is similar to chemisorption, possibly high-absorption sites in small micropores. Secondly, there is some mesoporosity and then thirdly, a normal non-porous flat surface adsorption. If the material is exposed to water and then degassed at low temperatures, one observes only the flat surface area. The isotherm for the high-temperature outgas has been presented in Chapter 4. What is of special interest is the analysis of the low-temperature out-gassed material. The thoria had previously been out-gassed at 1000°C and then exposed to water vapor. The subsequent high-vacuum degas was at 25°C. This treatment apparently covered the high-energy areas and filled the microporosity, so that
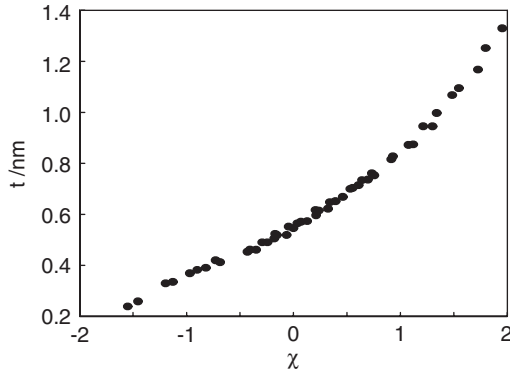
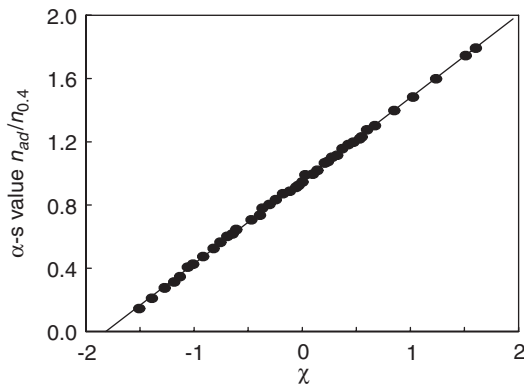Fig. 60. N_2 adsorption on MgO aerosoil according to deBoer et al. [6].

Fig. 61. Argon adsorption on thoria normalized to 0.4 *P/P*$_s$. Data by Gammage et al. [9].

only the outer surface area is in this case being measured. Figs. 61 and 62
exhibit the Ar and N_2 adsorption plots. In these figures the data have been
normalized to *P/P*$_s$ of 0.4 as one would do for an α–s plot.

    Even the water adsorption isotherm reveals a good fit to the χ plot. The
plot in Fig. 63 is for water adsorption at 25°C on a powder that had been
previously exposed to water seven times but had been out-gassed at 25°C
for an extended period of time between exposures. For each exposure there
was some additional irreversible adsorption. This would be the indication
that the high energy planes and micropores were being masked for subse-
quent adsorption cycles. The fit to the linear χ plot in Fig. 63 is quite good.

    In Table 22 the statistics for the three thoria adsorption isotherms are
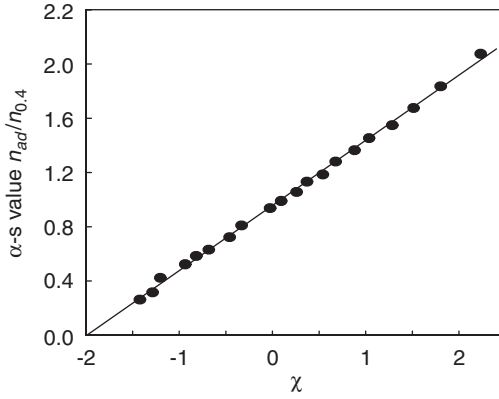given.

Fig. 62. Nitrogen adsorption on thoria normalized to 0.4 P/P_s Data by Gammage et al. [9].
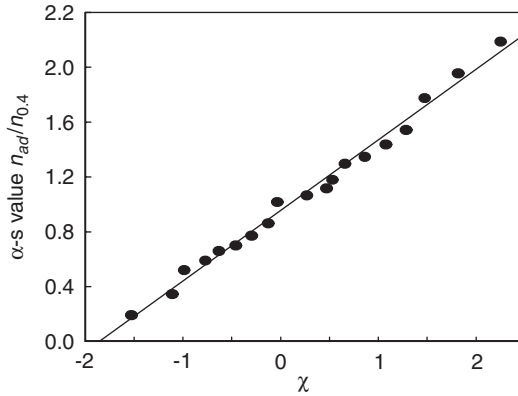
Fig. 63. Adsorption of water at 25°C after several prior adsorption cycles. Data is normalized to 0.4 P/P_s. Data by Gammage et al. [9].

Table 22
The statistics for the adsorption of gases on 25°C out-gassed thoria

	N_2 adsorption	Ar adsorption	Water adsorption
Slope	2.60	2.81	2.45
σ	0.03	0.01	0.06
χ_c	−1.993	−1.816	−1.855
R	0.9992	0.9997	0.9948

The units for the slope and σ are relative σ–s units and mol $mol_{0.4}^{-1}$.

Standard Curves for Lunar Soils

Lunar soils have an interesting property that they were well out-gassed. Soil collected from the moon was placed in a well cleaned ultrahigh vacuum aluminum alloy "moon box". The moon box was sealed on the moon with an indium seal. Upon arrival on the earth, the moon box was transferred to a pure argon box and the soils transferred to smaller well-sealed containers for distribution. It is probably true that no sample, much less soil, has been handled in such clean and uncontaminating conditions. The soils obtained were of surprisingly uniform composition.

Several different isotherms were obtained. The χ plot for these are in Fig. 64–67. One of the interesting features for the oxygen isotherm will be described in the section "The observation of χ_c".
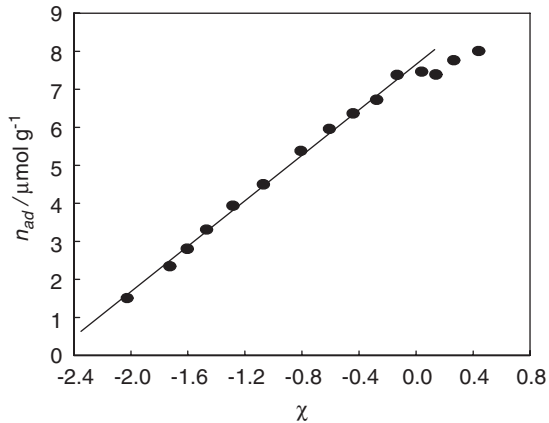

Fig. 64. N_2 adsorption on lunar soil.
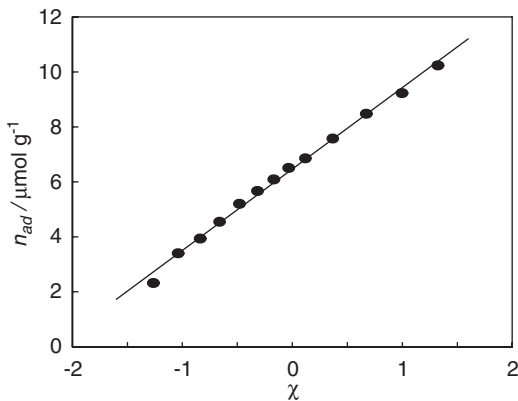
Fig. 65. Ar adsorption on lunar soil.
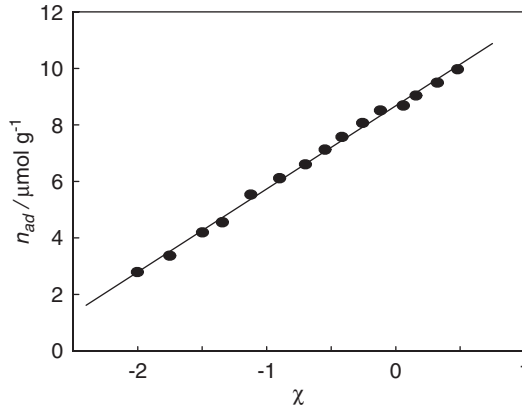
Fig. 66. CO adsorption on lunar soil.
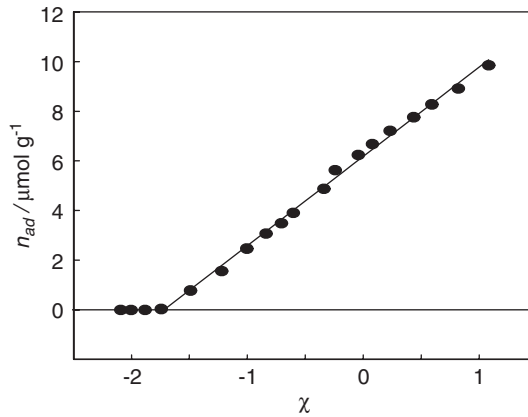
Fig. 67. O_2 adsorption on lunar soil.

Apparently, due to the very clean and uniform conditions of the surface of these soils, the χ plots are very linear. In Table 23 the statistics for the lunar soil χ plot fits are given. The following data points were ignored for these fits: the first three data points for O_2 for an obvious reason and the last three data points for N_2, which seemed to be experimentally out of line.

Either from the graphs or Table 23, it is obvious that the χ plot is an excellent description.

Table 23
The statistics for the adsorption of gases on lunar soil

	N$_2$ adsorption	Ar adsorption	CO adsorption	O$_2$ absorption
Slope	2.99	2.96	2.94	3.60
σ	0.06	0.06	0.05	0.06
χ_c	−2.564	−2.186	−2.951	−1.718
R	0.9977	0.9976	0.9984	0.9983

The unit for the slope and σ is µmol g^{-1}.

Isotherms by Nicolan and Teichner

Nicolan and Teichner [10] obtained several isotherms for various materials. They studied adsorption on non-porous silica and NiO. The χ plots of the adsorption on silica are presented in Figs. 68–69. Although, these indicate a nearly linear fit, the applicability is questionable since the lowest data point is more than a (postulated) monolayer of adsorbate. Furthermore, the range of the data is, compared to the α–s data, relatively rather short. The data for the adsorption of N$_2$ on NiO are presented in Fig. 70. Here the range of the data is better and the fit to the χ plot is also very good.

Isotherms Quoted by Bradley

In addition to his own work [11,12] of Ar adsorption on sulfate salts, Bradley cited the work of McGavack and Patrick [13] of SO$_2$ adsorption on SiO$_2$ and water adsorption on CuO by Bray and Draper [14]. Although these data are quite old, there is no reason to suspect that they are not accurate. Furthermore, they represent some rather unique isotherms which provide here a broader perspective. Figs. 71 and 72 show the isotherms of Ar on CuSO$_4$ and Al$_2$(SO$_4$)$_3$ by Bradley in the χ representation.

For the adsorption of Ar on CuSO$_4$, several measurements were made at slightly different temperatures in an attempt to extract the isosteric heat of adsorption. One can see this in Fig. 71 by groupings of data with trends at the low-adsorption end of the isotherm.

The data by Bray and Draper of water on CuO and on a mix of 38.1% MnO$_2$ and 61.9% CuO show obvious evidence of porosity. The data by McGavack and Patrick are a bit inconsistent but do not evidence porosity. Their higher data points, however, are too close to the P_s, indeed some are greater, to be seriously considered. The data may be represented quite well by either a Freundlich isotherm or a χ plot as may be discerned from Figs. 73 and 74. In these figures, three plots of adsorption of SO$_2$ are shown at 0°C, which was the only repeated temperature. It is clear that something was not
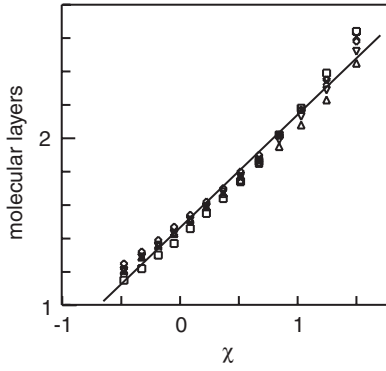
Fig. 68. N_2 adsorption on SiO_2 by Nicolan and Teichner [10].
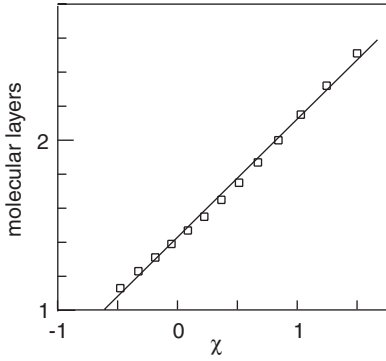
Fig. 69. Ar adsorption on SiO_2 by Nicolan and Teichner [10].
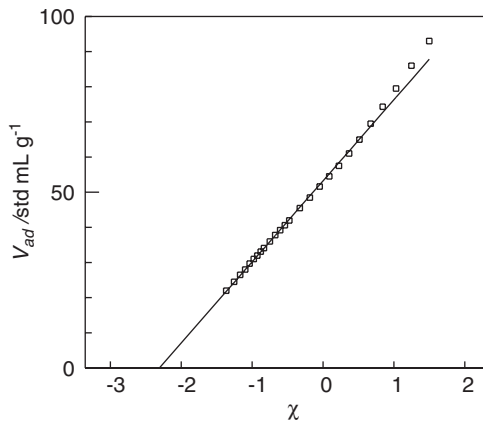
Fig. 70. N_2 adsorption on NiO by Nicolan and Teichner [10].
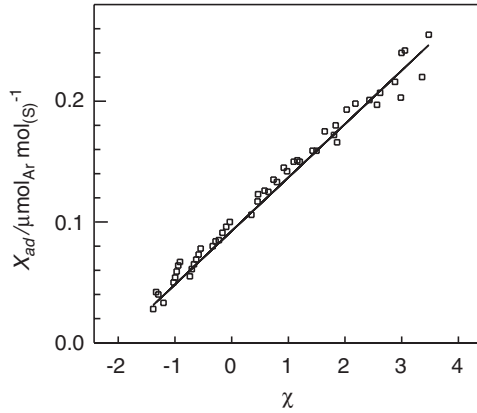
Fig. 71. Adsorption of Ar on CuSO$_4$ according to Bradley [11,12].
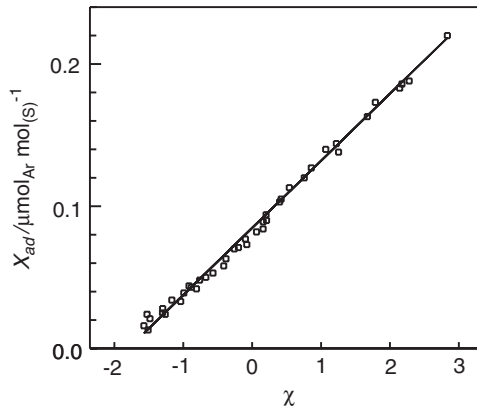
Fig. 72. Adsorption of Ar on Al$_2$(SO$_4$)$_3$ according to Bradely [11,12].

controlled satisfactorily since the slopes of the three χ plots and the magnitudes of the Freundlich isotherms are different. The χ plots indicate that these samples have different surface areas, about a factor of 2 variations, but very similar E_as of about 15.0 kJ mol^{-1}.

Conclusion and some Comments about Carbon

From the discussion above, it should be quite clear that the χ plot is at least a good empirical description for most simple isotherms. In constructing a standard isotherm, the fit to the χ plot would be the overall best choice. Numerous other examples could be cited with a variety of adsorbates–adsorbent pairs
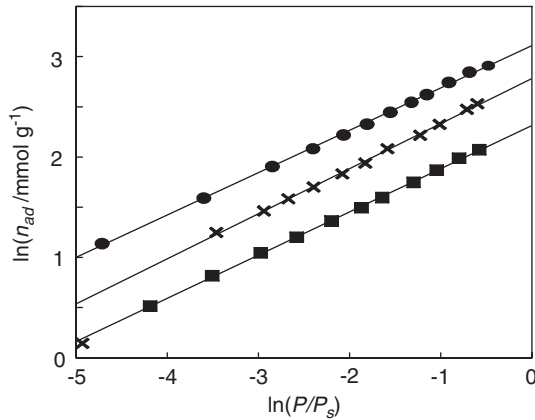
Fig. 73. The Freundlich isotherm representation of the absorption of SO_2 on SiO_2 according to McGavack and Patrick [13].
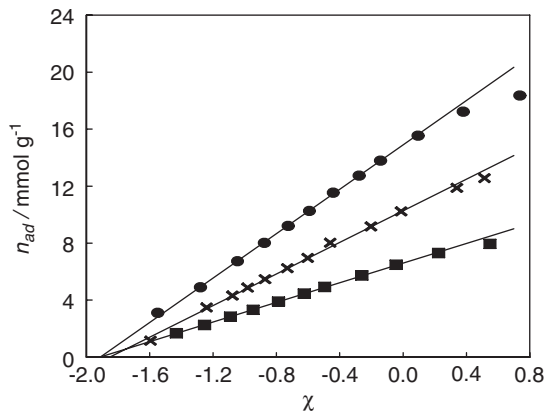
Fig. 74. The χ plot representation of the adsorption of SO_2 on SiO_2 according to McGavack and Patrick [13].

and an analytical expression for standard curves could then be constructed. It is, however, much more that just a standard curve. It frees one from the restrictions and uncertainties of the standard curve. As related in Chapter 3, it allows calculations of microporosity and mesoporosity without the use of a standard and all the uncertainties attached with this approach. Furthermore, it provides a value for the surface area that is founded upon some very sound principles and reasonable assumptions.
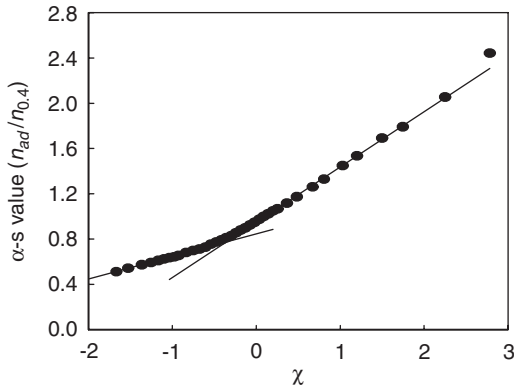
Fig. 75. The RMBM standard α–s carbon curve.

There are several cases where more than one energy of adsorption must be dealt with. One of these is carbon. Most carbon samples have the additional complicating feature of microporosity. Apparently in some carbon sample, such as the Sterling FT and Vulcan 3G do not have this complicating feature but still have more than one energy of adsorption. Indeed, one of these may be an in-register adsorption of either nitrogen or argon and has a very high adsorption energy.

Representative of such adsorption is the Rodrigues, Martin, Prado and McEnaney (RMBM), [15]) standard curve. Using the values of this standard curve and plotting them as a χ plot, as in Fig. 75, one is able to see two adsorption curves. The first one has a calculated energy of adsorption of about 45 kJ mol^{-1}, which is very high for delocalized adsorption. The second one has a reasonable physisorption energy of adsorption of about 4.5 kJ mol^{-1}. The individual carbon curves have similar double fits. In general the low-energy (higher pressure) line is about the same for all the curves, whereas the energy of the high-energy portion varies from about 30 to 100 kJ mol^{-1}. This is an obvious indication that something other than simple physisorption is present.

THE OBSERVATION OF χ_c

The implication of χ_c is one of the most controversial aspects of χ theory. The presence of this parameter, which is related to the energy of adsorption of the first adsorbed molecule, implies that below a certain pressure of adsorption there exists no adsorbate on the surface. (Again this is from thermodynamics,

i.e. large numbers, point of view.) In Chapter 4, the argument was put forth that Gibbs' phase rule requires the presence of a threshold pressure. The theory that "Henry's law", in spite of the fact that it is hardly ever observed, if one does not count the other Freundlich isotherms as "Henry's law", must be present is easily disproved by only one observation of the threshold pressure. It should be emphasized at this point that *"Henry's law" for adsorption is not derivable from nor is it required by thermodynamics.* "Henry's law" for adsorption is a postulated equation of state just as is, for example, the ideal gas law is for gases. It is a result of the Langmuir isotherm, however, the Langmuir isotherm was formulated for chemisorption in which case a new component is created in the process, which in turn changes the values in the Gibbs' phase rule. If the material on the surface is the same component as in the gas, then the Langmuir isotherm is not relevant. These arguments, however, do not seem to carry much weight so in this section some examples are presented where there is clear evidence of a threshold pressure.

There are three reasons that the threshold pressure has not been recognized in the past. Firstly, researchers knowing that "Henry's law" should be obeyed have not looked for a threshold pressure. Indeed, there are many incidences in the literature where an extrapolation is performed on the data to include 0,0 and some computer programs for instruments likewise to perform this extrapolation. Secondly, most adsorbents studied are ceramic materials which have a fairly high energy of adsorption. The threshold pressure for these materials is typically below a P/P_s of 1×10^{-6}, below the normal measurement range. An extrapolation from 0.001 of P/P_s to this value appears no different than an extrapolation through 0.0. (In other words, precisely speaking the threshold pressure is insignificant.) The third reason is that many samples have heterogeneous surfaces or are contaminated with a variety of chemisorbed species thus giving the appearance of a heterogeneous surface. With a heterogeneous surface, an energy distribution is obtained that obscures the threshold effect. The calculations in Chapter 4 demonstrated this.

Firstly, there is some indirect evidence for the presence of χ_c, which is the energy consideration.

Observations of the Energy Implications of χ_c

The value of χ_c is related to an energy, E_a, by the equation

$$E_a = -kTe^{-\chi_c} \tag{166}$$

where E_a is interpreted to be the energy that the first adsorbate molecule for any particular patch of surface releases upon adsorption. It is also related to the threshold pressure,

$$E_a = kT \ln(P_t/P_s) \tag{167}$$

A discussion of how this energy is related to the substrate and the adsorbing gas has been given elsewhere [16]. Intuitively, one would expect this energy to be a function of both the gas and the solid. The expected trends for the value of $-E_a$ would follow:

- for adsorbing gases, the expected trends should follow the values of the dipole moment, polarity, etc. Thus, one expects for $|E_a|$: $H_2O > CO_2 > N_2 > O_2 > Ar > He$ and
- for solids, one expects the trend to follow the energy of a cleaved surface of the material (also follow the trend in surface dipole moments, etc.) Thus, one expects, for example; $ThO_2 > MgO >$ polystyrene > polytetrafluoroethylene (Teflon®).

For a series of compounds, such as oxides, the trend in $|E_a|$ should follow closely the enthalpies of the compound formations. The reason for this is that the higher the $\Delta_f H^\ominus$ the more polarized are the oxide ions. Thus, for the following oxides the trends would be given as

$$UO_2 \approx U_3O_8 > Y_2O_3 > Al_2O_3 > ThO_2 > SiO_2 > BeO > H_2O > CO$$
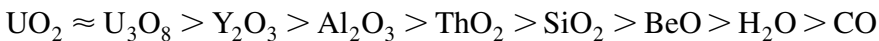
Experimental observation of such a trend in $|E_a|$ would be a strong indication that the threshold phenomenon is real. Fig. 76 shows the results of nitrogen adsorption on the above-mentioned oxides most of which were reported by Fuller and Thompson [17]. (H_2O is for water pre-covered oxides and CO is for partially oxidized carbon.) The value for E_a of oxides is plotted as a function of the enthalpy of their formation. Since the threshold pressures for some of the oxides are too low to be measured directly, χ_c values are obtained from the χ theory equation. It is apparent that the correlation does exist as predicted. Although not claimed, due to the question of stoichiometry to be used for the cleaved solid surface, this figure shows a linear relationship between the energies of the threshold and the enthalpies of formations. For the intersection at $\Delta_f H^\ominus = 0$, the value for E_a should be
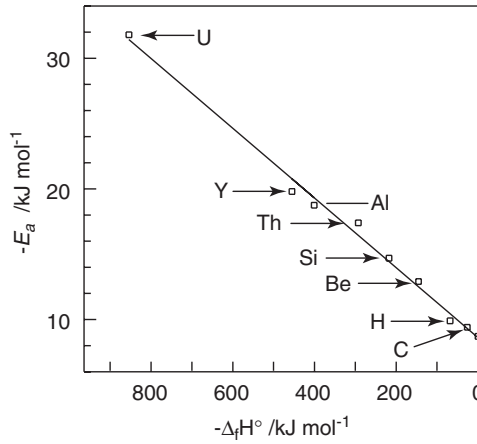
Fig. 76. E_a versus the enthalpy of formation of various oxides.

that expected for the liquefaction of N_2. The data point on this axis repre-
sents a surface whose energy is such that there is no preference for liquefy-
ing on the surface. A fit for the data yields a value of 8.6 kJ mol^{-1}, which is
somewhat high but in qualitative agreement.

Direct Observation of χ_c

In this section, to satisfy the disproof of "Henry's law" several
instances of the observed χ_c are presented. This has indeed been reported in
the literature by others. With the adsorption of water on NaCl reported by
Peters and Ewing [18,19] the threshold pressure is very clear, confirmed by
both the isotherm and by infrared. In their investigation of the microp-
orosity of Y-zeolites for which very low-pressure measurements were
needed Guo et al. [20] reveal threshold pressures along with the reported
oscillating adsorption. The oscillations are undoubtedly due to a variety of
effect but one of these could be change in E_a.

Gil et al. [21] present data which seem to evidence a threshold pres-
sure for N_2 adsorption. This observation was for nitrogen adsorption on
microporous carbon. What is important about this data is that the threshold
pressure is obvious even when looking at the data from the point of view of
Henry's law. Fig. 77 illustrates this quite well. This plot illustrates that the
threshold pressure is not an artifact of the transformation to the χ plot. In
this figure the threshold pressure appears to be at about 1.0×10^{-6} P/P_s;
whereas, a χ plot indicates it to be about 1.2×10^{-6} P/P_s.
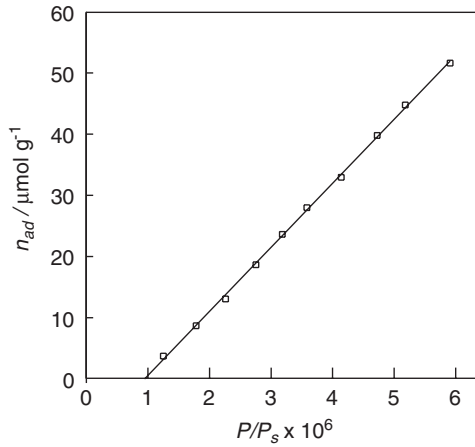
Fig. 77. The observation of a threshold pressure by Gil, de la Puente and Grange [21] with microporous carbon.

In an attempt to observe the threshold pressure, Thompson selected a material that one would believe to have a low energy of adsorption. The direct observation of the threshold pressure is possible, if the interaction energy between the surface and the adsorbed molecules is small. This can be easily illustrated with adsorption of N_2 or Ar on polytetrafluoroethylene (Teflon®) obtained by Thompson [22], which according to theory should have a very high threshold pressure. The threshold pressure may clearly be seen at a pressure of about 0.01 atm (about 8 Torr), well within (by a factor of at least 10^5) the capability of the most modern instrumentation. Direct observations of threshold pressures, which are lower, require the use of more sensitive gravimetric techniques. This was also found experimentally by Thompson with adsorption data on diamond and alumina that had an ultrahigh vacuum surface cleaning. Since the results of Thompson's polyte-trafluoroethylene experiments have not been reported in the open literature, these will be discussed in some detail.

The powder used was a Teflon® Dupont resin obtained from Aldrich Chemical Company (polytetrafluoroethylene lot #6). The measurements on this material were performed over an extended period of time in both the adsorption and desorption mode. There was *absolutely no* indication that the isotherms exhibited any type of metastable condition or that the phe-nomenon reported herein is related to kinetics. The kinetics of both adsorp-tion and desorption were indeed measured. The adsorption measurements

and the desorption measurements were in agreement after the kinetic stage. What is shown here are only the stable thermodynamically valid portions of the measurements.

The results of the adsorption Ar on Teflon® shown in Fig. 78 are in the untransformed form to illustrate the shape of the isotherm. The data for this figure are given in Table 24 to show the precision and accuracy that is obtainable with the instrumentation described. In this form, even with a high threshold pressure, the presence of a threshold pressure for most experiments, especially the volumetric type, would be missed. The zero pressure recording, however, is very obvious with the instruments described. This value is well within any conceivable error by a factor of 10^5. The flat portion of the pressure curve is more evident in the χ plot. This plot is shown
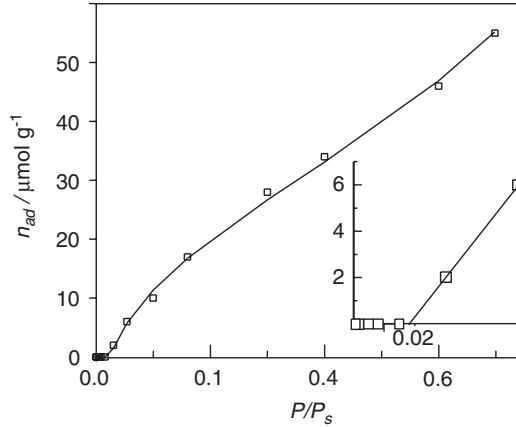
Fig. 78. Ar adsorption on polytetrafluoroethylene (Teflon®) with the normal P/P_s axis by Thompson [22].

Table 24
Data for the adsorption of Ar on polytetrafluoroethylene (Teflon®)

P/P_s	$m_{ad}(\text{g g}^{-1})$	P/P_s	$m_{ad}(\text{g g}^{-1})$
0.000003	0.0×10^{-8}	0.053560	2.40×10^{-7}
0.000023	0.0×10^{-8}	0.099731	4.00×10^{-7}
0.000129	0.0×10^{-8}	0.159684	6.80×10^{-7}
0.001273	0.0×10^{-8}	0.299779	1.12×10^{-7}
0.004805	0.0×10^{-8}	0.399902	1.36×10^{-7}
0.008105	0.0×10^{-8}	0.599674	1.84×10^{-7}
0.015051	0.0×10^{-8}	0.698356	2.20×10^{-7}

in Fig. 79. Here the presence of the threshold pressure becomes very obvious. This is very strong confirming evidence for the validity of the χ theory with respect to the threshold phenomenon.

A variety of isotherms were obtained and the experiment repeated several times. Fig. 80 shows some data for three different types of experiments. For the low coverages, a slight rounding off of the χ equation plot is apparent as seen in Fig. 80. However, the threshold pressure still exists well above the limit of detection. This rounding phenomenon may be attributed to the heterogeneous nature of the surface energy. The threshold pressure with this rounding is also seen with some other common standard isotherms.
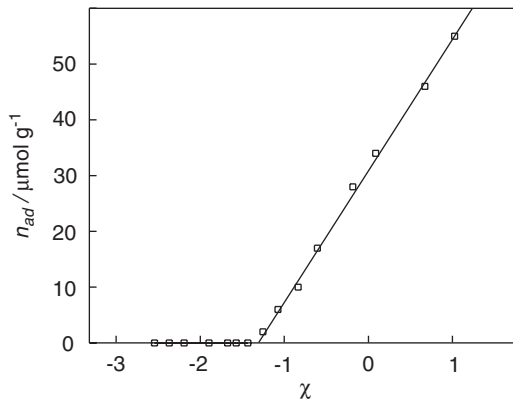
Fig. 79. The χ plot of the argon adsorption on Teflon®.
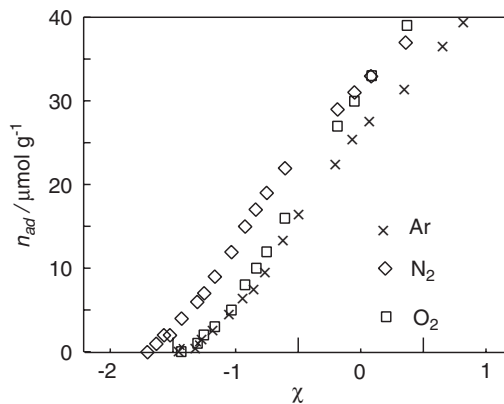
Fig. 80. Various adsorption isotherms on polytetrafluoroethylene (Teflon®).

Similar threshold behavior is also apparent for both well-cleaned diamond and alumina surfaces only at lower pressures. The results of these experiments are available in the open literature from a conference proceedings [23]. Thompson performed several experiments on these materials to test the hypothesis that a uniform surface may be created by a good ultrahigh vacuum cleaning, thus simulating the possible conditions that the lunar soils had. Heating in hydrogen at a high temperature and degassed under an ultrahigh vacuum created the right conditions to observe a threshold pressure for the argon adsorption isotherm.

Some of the details of the experiment are as follows. The diamond powder was 1 μm powder obtained from Amplex Corporation. This powder was degassed and heated in H_2 to obtain a clean surface. It is well known that heating in H_2 up to 1000°C can eliminate the graphitic carbon that often contaminates diamond surfaces, but there should also be other chemically bonded contaminates. The alumina powder was NBS 8571 which was cleaned in a similar manner. Entirely different isotherms for both materials are obtained if the outgassing step is performed in a different fashion. According to Smirnov et al. [24], such a difference in surface structure with diamond may be due to the variation of the radicals on the surface. On the other hand, alumina may become slightly sub-stoichiometric on the surface. Figs. 81 and 82 contain the results of the adsorption isotherms in the χ plot form on these materials. A very important observation was made with these materials. When the surfaces
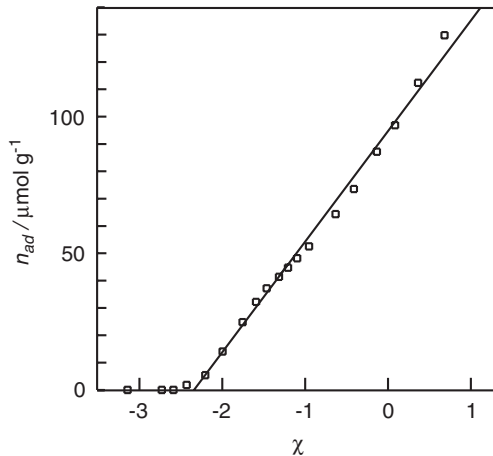
Fig. 81. χ plot of argon adsorption on diamond that has been cleaned in hydrogen data by Thompson [22].
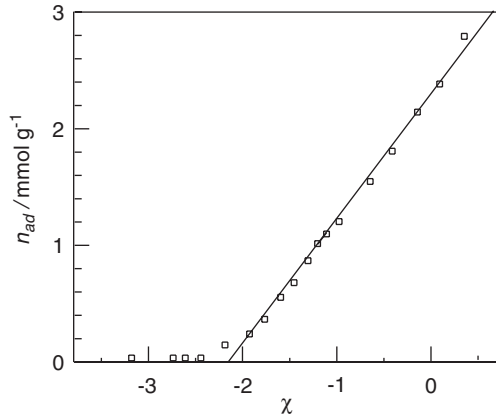
Fig. 82. Nitrogen adsorption on hydrogen-cleaned alumina. Data by Thompson [22].

were contaminated, the threshold was not as apparent. Indeed, for diamond the adsorption isotherm followed the in-register χ theory analysis. This is probably due to the contamination creating a number of high-energy adsorption sites on the surface, thus masking the threshold effect. The hydrogen treated alumina evidences a threshold pressure; whereas, normally alumina χ curves, have abundant literature some of which are presented in this book, do not go to low enough pressures to observe this. The hydrogen treatment, which could yield a sub-stoichiometric surface, apparently creates a lower energy of adsorption for nitrogen on alumina.

Fig. 67 presents the χ plot for the adsorption of oxygen on lunar soils. It should be noted that the adsorption of oxygen below a χ-value of -1.72 was non-existent. This was indeed observed for this material and was not an error in measurement. Thus, well-cleaned soil from the moon exhibits the threshold phenomenon with oxygen are at a relative high value of P/P_s, i.e. about $P/P_s = 0.0038$. Whether the other adsorbates would have exhibited such a clear threshold is unknown since the value of χ_c was below the detection limit.

Conclusion Concerning χ_c

As mentioned previously, in order to disprove the universality of "Henry's law" one needs to present only one example of a threshold pressure. Several examples have been presented above so the disproof is complete.

Along with the observation of the threshold pressure the indirect evidence of the energy implications was also presented. The prediction of both the threshold pressure and energy implications is very strong supporting

evidence for the validity of the χ theory. The predictions of the isosteric heats of adsorption, calculations of porosity, measurements of multiple plane adsorption (with its additive nature) and calculations of binary adsorbate mixture are not only supporting evidence but are quite useful. It is certainly an improvement over the BET which is theoretically weak and predicts very little.

MULTIPLANE ADSORPTION

The terminology "plane" and "multiplane" here are used in the sense that there are distinct areas with differing E_as. These may indeed be different crystallographic planes, but adsorption experiments cannot determine this. The different E_as may be due to other factor such as, for example, microporosity. In the case of a distribution, it may be due to a multiplicity of chemical species on the surface or contamination.

Examples of Two Plane Adsorption

An example of a multiplane adsorption has already been presented in Fig. 75. This, however, is a compilation of isotherms for carbon adsorbent. Examining just one isotherm for carbon, for example N_2 adsorption on Sterling FT carbon in Fig. 83, the break in the isotherm is still obvious, if not more so. In this figure, there are two lines drawn on the right axis corresponding to a monolayer of the total surface, the upper line, and a monolayer of the high-energy planes only, the lower line. It seems unlikely that
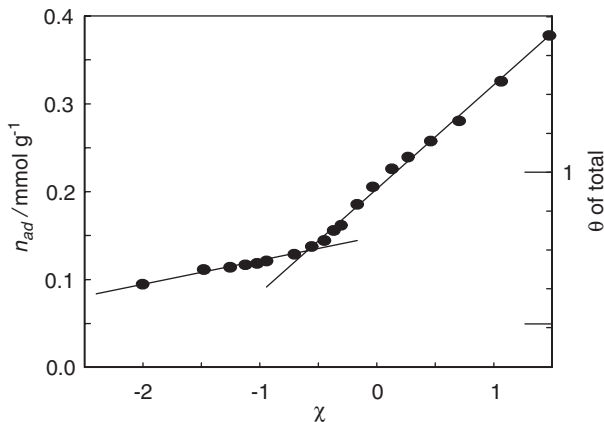
Fig. 83. Chi plot of IUPAC lab "H" adsorption of N_2 on Sterling FT carbon.

the adsorption on the high-energy planes is by physisorption only since the extrapolation to χ_c yields an energy of about 150 kJ mol^{-1}. There is probably one of two possibilities that would show up if lower, pressure measurements were available. Firstly, there could be some chemisorption or in-register adsorption taking place on about 1/5th of the surface or secondly, and more likely as observed on other carbon samples [25], there is a considerable amount of microporosity present and the observed adsorption for the first fit is only the external area of these particular portions. The filling of the microporosity would have already been accomplished before the observation of the first data point.

Another example of multiplane adsorption is the 1000°C fired thoria powder mentioned in Chapter 3. This sample, however, evidences some mesoporosity and will be a good example to analyze in the next chapter.

The Freundlich, Dubinin-Polanyi and Tóth isotherms

The comparison to isotherms, when there is a distribution, comes back to the "Henry's law" question. Why is it that sometimes one observes the Freundlich isotherm and thus at least the appearance that the pressure and adsorbate amount simultaneously approach zero. As demonstrated in Chapter 4 a log-normal distribution in E_a yields the Dubinin–Polanyi (DP) set of isotherms of which the Freundlich isotherm is a subset. The Tóth isotherm is similar but mathematically not in this class. The question becomes, are the generated isotherms, and not just the energy distributions, similar.

For these isotherms, especially the DP and Tóth isotherms, not only must the distribution in E_a be considered but also the distribution in the micropore sizes. The reason for this is that these two distributions are close enough to overlap somewhat, thus interacting to change the values of the parameters.

As a review, the general form for the Freudlich–Dubinin–Polanyi equation is

$$n_{ad} = A \exp\left(-r_F \ln\left(\frac{P_s}{P}\right)^{r_{DP}}\right) \tag{168}$$

where A, r_F and r_{DP} are the parameters. This may also be written in terms of χ

$$n_{ad} = A \exp(-r_F \exp)(-r_{DP}\chi) \tag{169}$$

With $r_{DP} = 1$, one obtains the Freundlich isotherms and if additionally $r_F = 1$ then one obtains "Henry's law". With $r_{DP} = 2$, one obtains the Dubinin–Raduchkevich [26] (-Kaganer) equation. Other values of r_{DP} yield the Dubinin–Astakhov [27] equation. The DP equations were originally used to analyze porous carbon for which the porosity is slit-like. Thus, the simple formulation of the χ theory, that is initial adsorption followed by a cutoff of adsorption with a simple normal distribution for both, is appropriate. One need not be concerned about the possibility that geometrical changes will change the effective surface area as might be the case with cylindrical pores. Thus, the energy distribution together with the cutoff of the pores will consist of two normal distributions

$$\frac{\partial^2 n_{ad}}{\partial \chi^2} = \frac{A_s}{fA_m \sigma \sqrt{2\pi}} \left[\exp\left(-\frac{(\chi - \langle \chi_c \rangle)^2}{2\sigma_c^2} \right) - F \exp\left(-\frac{(\chi - \langle \chi_p \rangle)^2}{2\sigma_p^2} \right) \right] \qquad (170)$$

where the subscripts "c" and "p" correspond to the energy distribution and the pore distribution, respectively. The parameter F is the fraction of the surface area that is inside the slit pores. For the purposes here it will be assumed that F is 1. For very porous carbon samples this could be close to 1. The problem is as stated before. To see the correspondence between Eqs. (169) and (170) one needs to double integrate (170) and set the values of each at $\chi = \infty$ to be equal. One then needs to find the maxima and minima in (170) and the maxima and minima in the second derivative of (169) (given in Chapter 4) and set the magnitude and curvature of each to be equal. This is mathematically a little messy but possible. In Chapter 4 this was performed with only the energy distribution for the χ equation and the match between these demonstrated. Here the porosity is introduced.

Examples of the matches are shown in Figs. 84–86. In these figures the dotted line is the second derivative of the DP equations and the circles are the overall DP isotherm. The solid lines are the results expected from the χ theory with a distribution for both the E_a and pore size. Fig. 84 shows the DP isotherm which is identical to "Henry's law" isotherm, $r_F = 1$, whereas Fig. 85 shows a more realistic Freundlich isotherm with $r_F = 0.5$. The only difference is a shift on the χ axis.

Fig. 86 is the case of the Dubinin-Raduchkevich (DR) equation. These figures have all been normalized to a final pore volume of 1. The second derivative match is not perfect in Fig. 86, but it is evident that it is good enough to match the overall isotherm.
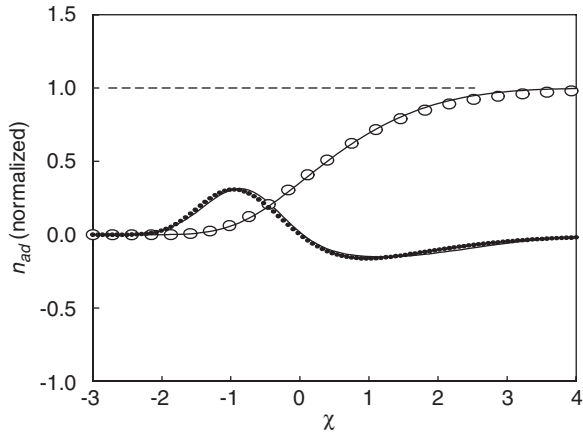
Fig. 84. Comparison of "Henry's law" isotherm to a χ theory plot with an E_a distribution and a pore distribution.
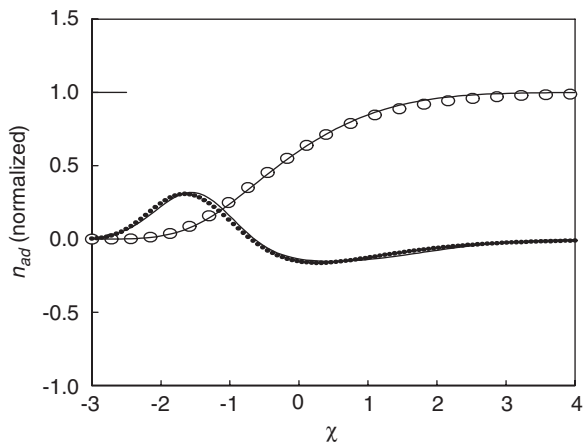
Fig. 85. Comparison of a Freundlich isotherm to a χ theory plot with an E_a distribution and a pore distribution.

The Tóth isotherms [28], referred to as the T-equation [29] were presented in Chapter 3 as a good representation for many isotherms. This should not be surprising since it includes five fitting parameters (n_m, K, m, k, and $P_{r,e}$). $P_{r,e}$ is a low relative pressure value and can be ignored with a small amount of distortion. Figs. 87 and 88 show two examples of a comparison with the T-equation fit for nitrogen and argon adsorbed on SiO_2. In these figures the second derivative for the Tóth T-equation was obtained
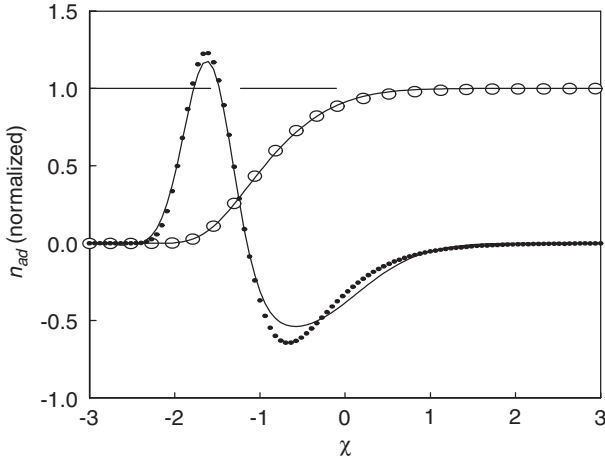
Fig. 86. Comparsion of the DR equation to the χ theory with a distribution in E_a and pore size.
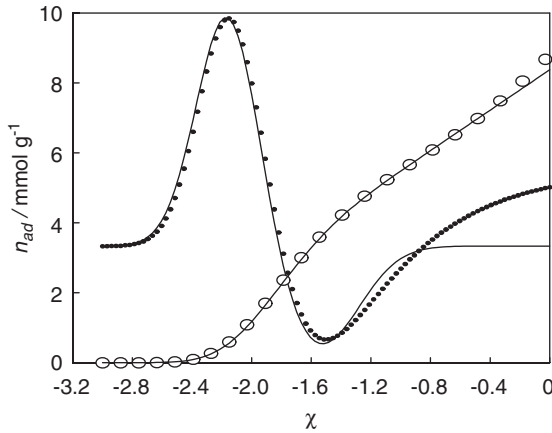
Fig. 87. Comparison of the Tóth T-equation versus χ theory fit for nitrogen adsorbed on silica.

digitally and is slightly offset due to this. It should be noticed that the T-equation second derivative has a tendency to exceed 0 at high values, which does not make sense from an energy point of view. In terms of χ theory an upward bend in the isotherm is either due to additional lower energy planes adsorbing or capillary filling has commenced. It is unlikely that SiO_2 would have these low-energy planes and capillary filling would be more rapid than shown here.
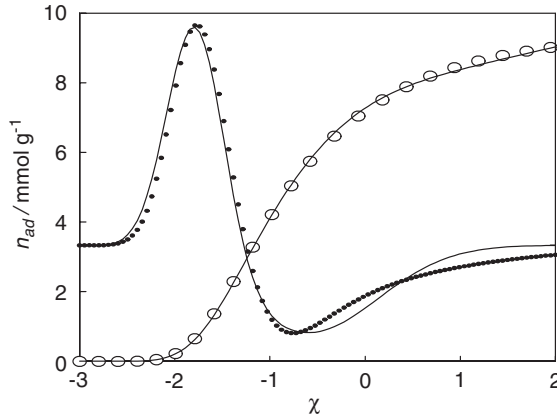
Fig. 88. Comparison of the Tóth T-equation versus χ theory fit for argon adsorbed on silica.

As was the case for the DP isotherms, Eq. (170) was used to simulate the energy and pore size distributions. For the nitrogen adsorption, about 55% of the adsorbate is in micropores whereas for argon 90% is in micropores according to the χ analysis. The Tóth analysis indicated nearly identical surface areas using either N_2 and Ar, whereas the χ analysis indicates the surface area with the N_2 was less than with Ar. These conclusions from the χ analysis are quite possible since the N_2 molecule is about 10% larger than the Ar atom. In addition to fewer molecules be packed into the micropores, some of the micropores available for Ar adsorption may not be available to N_2.

The above comparison to some well-known isotherms is not strong support for χ theory since porosity must be assumed without any other indicators. It does, however, demonstrate that the theory is consistent with the literature.

Conclusion Concerning Multiple Energies

χ theory is capable of very simply explaining the results obtained from isotherms that do not seem to follow the standard isotherm model. It is straightforward and consistent with the entire theoretical framework of the χ theory.

HEAT OF ADSORPTION

Heat of adsorption is an area where the χ theory is clearly superior to other theories of adsorption. The Dubinin concept of adsorption potential and the

postulated "thermodynamic criterion" imply that the adsorption potential does not vary with temperature. This can easily be derived from χ theory. The adsorption potential is simply the Gibbs' free energy going from the bulk liquid state to the physisorbed state and the χ theory predicts that this value should be $1/2RT$. This is very small compared to most heat of adsorption thus yielding the "thermodynamic criterion".

A few examples of the predictions of χ theory to yield the various defined heat of adsorption are presented here. Other examples and more detail can be found in an article on the subject [30]. In order to make a parameterless prediction of the isosteric or integral heat of adsorption, an adsorption isotherm is first obtained. If there are no complicating features, such as simultaneous chemisorption or microporosity, then these heat of adsorptions can be predicted without any further information. (This is what is referred to as a parameterless prediction or fit. That is, all the constants needed to make a calculation are available from some other measurements.)

One of the problems encountered in the literature is that the data have been transformed and presented in such a way that it is difficult, if not impossible, to unscramble the presentation to obtain the original data. Luckily, some can be obtained directly, as is the case with data by Pace et al. [31,32], from original sources, such as PhD dissertations [33,34], or mathematically unwinding it as is the case with information supplied by Harkins and Jura [35]. Fig. 89 shows the molar integral heat of adsorption of water on anatase as obtained
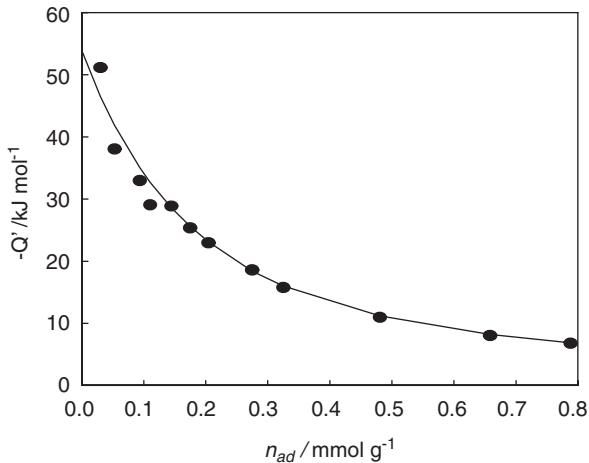
Fig. 89. The dependence of the molar integral heat of adsorption with amount adsorbed from the data by Harkins and Jura [35]. The line is the zero parameter calculation.
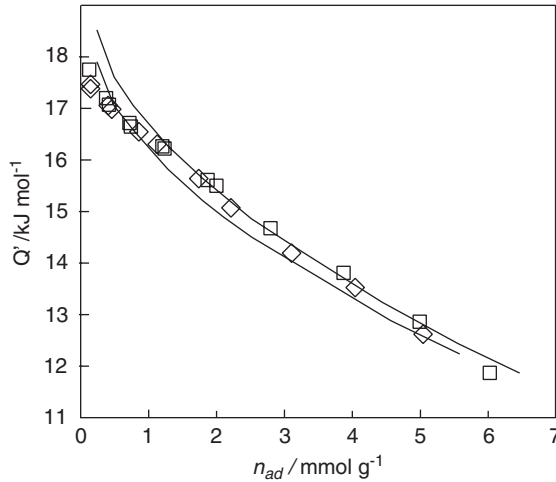
Fig. 90. The dependence of the molar integral heat of adsorption with amount adsorbed from the data by Berg [34]. The upper and lower lines are the calculation $+1\sigma$ and $-\sigma$.

from the data by Harkins and Jura. It is interesting to note that and alternative one parameter fit can be performed on these data but yields very little improvement. The adsorption of Kr on anatase was performed by Berg [34]. In this case, the isotherm is used to obtain the entire dependence of the molar heat of adsorption as a function of the amount adsorbed. Fig. 90 shows a representation of the calculation obtained for this along with the data by Berg. The upper and lower lines are the calculation $\pm 1\sigma$ with the χ-theory predict $1/2\,RT$ included. At 140 K there is a significant difference, about 0.6 kJ mol^{-1}. The uncertainty lines drawn are for one standard deviation as determined in the χ plot. One point to notice is that even with this treatment, the calculated uncertainty increases from the adsorption isotherm to the heat of adsorption.

For more examples, one should consult the cited article.

ADSORPTION OF MORE THAN ONE ADSORBATE

The theoretical foundation for the interpretation of binary adsorption by χ theory was presented in Chapter 4. A few examples illustrate these predictions.

Adsorption on Non-Porous Surface

The only experiment of binary adsorption on non-porous materials, at least to this author's knowledge, where the adsorbates are different enough to have differing E_as and differing A_ss is that by Arnold [36]. Arnold studied

the co-adsorption of N_2 and O_2 on anatase. (Luckily, counter to intuition, anatase was a good choice with only one E_a as was later seen from the data by Berg.) Fig. 91 shows the χ plots for the adsorption of the pure N_2 and O_2 with an extrapolated χ_cs of –2.665 and –2.477, respectively. There is considerable uncertainty in these numbers as one would gather from the scatter and higher pressure deviation as seen in Fig. 91.

The resultant binary plot with the ratios of the pressures staying constant at 50.2% O_2 and 49.8% N_2 is shown in Fig. 92 along with the calculation. The overall picture is fairly close with the offset in the
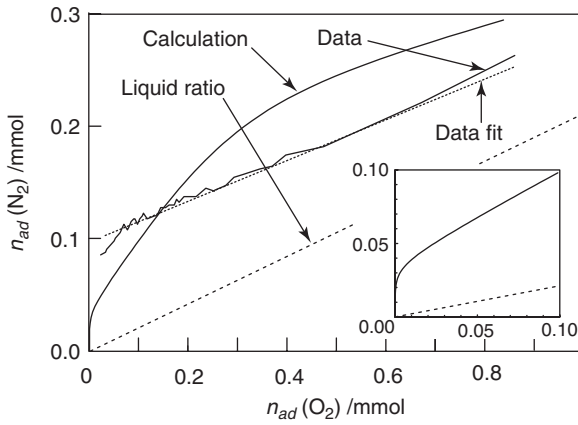
Fig. 91. The moles of nitrogen adsorbed versus moles of oxygen adsorbed for 50% mix of gases. The calculation yields about the same intercept as the data.
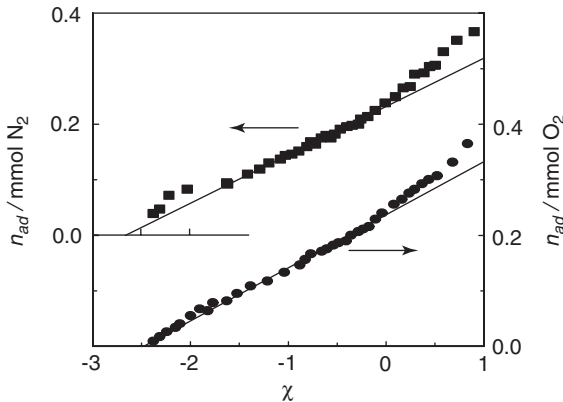
Fig. 92. Chi plot of the pure nitrogen and pure oxyen adsorption on anatase by Arnold [36].

calculation being about 0.17 mmol, whereas the experimental value is about 0.10 mmol. The value for $\Delta\varepsilon/kT$, the regular solution correction, for this system is about 0.22 and makes very little difference in the calculation. It is interesting to note that the offset actually due to the energy difference is only about 0.04 by calculation. This is evident in the inset of the figure. (It is easy to test this by setting both E_as to be equal in the simulation and seeing what difference results.) The rest of the offset is due to a multiplicity of factors and is not intuitively obvious.

The data by Arnold, which after all was performed with instrumentation that today would be considered rudimentary, reveal a fair agreement between experiment and the χ theory. Surely, more experiments along this line with modern instruments would be very useful.

Binary Adsorption in Micropores

For the following simplified case of binary adsorption one could expect that Lewis-Randall [37] rule should apply:

1. the pores are filled or nearly full,
2. the adsorbate molecules are approximately the same size,
3. the adsorbate molecules have simple geometry and
4. the intermolecular forces are simple van der Waal forces.

Lewis Rule Assumption

Lewis' rule assumes that (1) the densities of the adsorbates are the same as the densities of the liquid-phase adsorptive and (2) the volumes of the adsorbates add to yield the pore volume. Both assumptions could be incorrect, but for mixing liquid phases, assumption (2) is usually fairly good. These assumptions yield

$$n_{ad,1} V_{m,1} + n_{ad,2} V_{m,2} = V_p \tag{171}$$

or

$$\frac{n_{ad,1}}{n_{p,1}} + \frac{n_{ad,2}}{n_{p,2}} = 1 \tag{172}$$

where the n_ps are the determined number of moles adsorbed to fill the pores for each adsorbate alone.

Assumption (1) could be incorrect as observed by Dubinin et al. [38] and calculated by χ theory [39]. An intuitive explanation for this phenomenon is that the first "layer" is not fully dense, therefore the subsequent layers also cannot be fully dense. Since the areal density is not the same as the liquid density, then the molar volumes also cannot be the same as the molar volume of the liquid. (The Brunaver, Deming, Deming and Teller (BDDT) equation also predicts this.) Fig. 93 shows a calculation of the molar volume as a function of monolayer equivalent coverage as calculated from χ theory. In this calculation, it is assumed that the density in the normal direction from the surface is not affected, but only the areal density. From the figure it is apparent that by a surface coverage of 2 monolayers the molar volume of the adsorbate is nearly the same as the liquid. Even at 1 monolayer equivalence the correction is not large. In any case, micropores with a radius or width less than a monolayer thickness would not allow adsorption within the pore. Therefore, the minimum measurement possible for a filled pore is at 1 monolayer and it is more likely to be greater than this amount. Therefore, the correction for the change in molar volume would not seem to be an issue for adsorption in pores.

The analysis of binary adsorption in micropores depends somewhat upon the analysis of adsorption of the pure adsorptives. The ideal situation would be to analyze the adsorption of the pure adsorptives and from this information predict the adsorption of the binary adsorptives. The analysis of the pure adsorbates is given in Chapter 6. Some of the results of the analysis will be used here to demonstrate a few points.
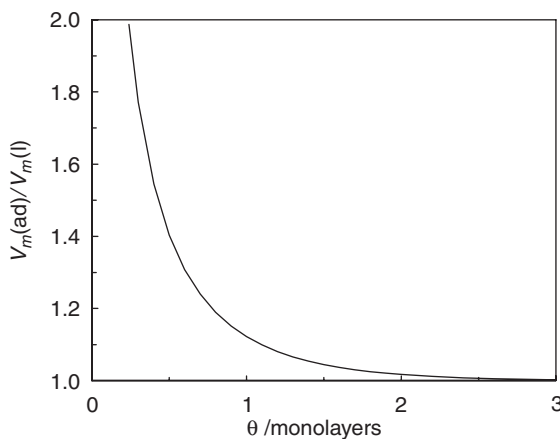
Fig. 93. Relative molar volume as a function of coverage in terms of monolayer equivalence.

It is not completely necessary to do a thorough investigation of the pure adsorbates, if one is willing to make a few measurements for the binary system. The following analysis will demonstrate this.

Binary Adsorption at a Constant Pressure

Assuming that Lewis' rule applies regardless of the pressure and that the value for $n_{p,1}$ and $n_{p,2}$ are specified only by the value one expects for the pure adsorbate (1 or 2) at the specified pressure then Eq. (172) could be symbolized as.

$$\frac{n_{ad,1}}{\mathbf{n}_{p,1}(P)} + \frac{n_{ad,2}}{\mathbf{n}_{p,2}(P)} = 1 \tag{173}$$

where P designates the total pressure. Here, the external amount adsorbed may be included in $\mathbf{n}_{p,1}$ and $\mathbf{n}_{p,2}$ so that even at pressures where the pores are completely filled there might be a slight pressure dependence. Obviously, the simplest case, both theoretical and experimental, is to hold P constant and just vary the composition. For such a case, $\mathbf{n}_{p,1}$ and $\mathbf{n}_{p,2}$ revert to being constants which, if required, are relatively easy to obtain from the pure adsorbate isotherms.

It is clear that within the space of the pores that it is not possible for both adsorbates 1 and 2 to follow the χ equation or the standard curve. If adsorbate 1 has a much higher $|E_a|$ than adsorbate 2 then the adsorption of 1 will predominate and adsorbate 2 will fill out the remaining space according to Lewis' rule. Therefore, the value of χ_c for adsorbate 1 will remain unchanged, whereas χ_c for adsorbate 2 will change due to the pre-adsorption of 1. For whatever total pressure is used, then $n_{p,1}$ will equal $n_{ad,1}$ at that pressure. Picking a particular pressure for a standard (in many cases 1 atm at which the experiment is performed) and since n_{ad} is linear with χ, this yields two equations

$$n_{ad,1}^* = m\chi_1^* + b$$
$$0 = m\chi_{c,1} + b \tag{174}$$

where the symbol "*" indicates at the pressure picked for the experiment. From these equations, m and b may be obtained. Thus,

$$n_{ad,1} = \frac{n_{ad,1}^*(\chi_1 - \chi_{c,1})}{\chi_1^* - \chi_{c,1}} \tag{175}$$

The quantities $n_{ad,1}^*$ and $\chi_{c,1}$ may be obtained from the isotherm of the pure adsorbate 1. $n_{ad,2}$ is therefore,

$$n_{ad,2} = n_{ad,2}^* \left(1 - \frac{n_{ad,1}^*(\chi_1 - \chi_{c,1})}{\chi_1^* - \chi_{c,1}} \right) \tag{176}$$

where $n_{ad,2}^*$ may be obtained from the isotherm of pure adsorbate 2. Notice that $n_{ad,2}$ is not linear with χ_2 but rather linear with χ_1. One need not have the information from the pure adsorbates to obtain the parameters for Eqs. (175) and (176). One may instead use some data from the binary adsorption isotherm at the pressure of interest. This is particularly advantageous for obtaining $n_{ad,1}^*$ and $n_{ad,2}^*$, since these quantities would normally be obtained in such a measurement. A few additional data points are needed to obtain $\chi_{c,1}$.

Comparison to Experiments

An example of some data where both the pure adsorption isotherms were obtained over a broad pressure range and the binary phase diagrams at 1 atm pressure were also measured are given by Danner and Wenzel [40]. The measurements were made for the various combinations of CO, N_2 and O_2 on 5A and 10X zeolites.

A summary of the obtained parameters is given in Table 25. The analyses of the adsorption isotherms for the pure adsorbate is given in Chapter 6. The simple, flat-surface χ theory is not appropriate for analysis in micropores and the expansion on the theory is present in Chapter 6. The order of the $|E_a|$s are
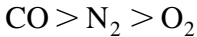
$$CO > N_2 > O_2$$

Thus for the combination CO–N_2 and CO–O_2 the χ_c for CO should be used and for N_2–O_2 combination the χ_c for N_2 is proper (as italicized in the second column). Thus, the χ_c for O_2 is not relevant.

The $\chi_{c,1}$ values from the pure adsorbate experiments and the binary experiments are in fair agreement except for two cases. The adsorption of CO–O_2 on 5A zeolite is particularly a variant and the adsorption of N_2–CO

Table 25
Analysis of the parameters for binary adsorption versus the pure adsorbates. Italics indicate the high energy absorbate

	Absorbate	$\chi_c{}^a$	$n_{ad,760}$
Binary 5A	$N_2 - O_2$	-2.399	4.52
	$N_2 - CO$	-2.620	4.99
	$CO - O_2$	-3.195	5.00
Pure 5A	CO	-2.751	5.02
	N_2	-2.446	4.59
	O_2	-2.071	4.94
Binary 10X	$N_2 - O_2$	-2.225	4.52
	$N_2 - CO$	-2.238	5.71
	$CO - O_2$	-2.554	5.57
Pure 10X	CO	-2.559	4.72
	N_2	-2.323	5.59
	O_2	-1.873	5.08

$^a\chi_c$ for the pure adsorbates is the mean $\langle\chi_c\rangle$ calculated in Chapter 6.
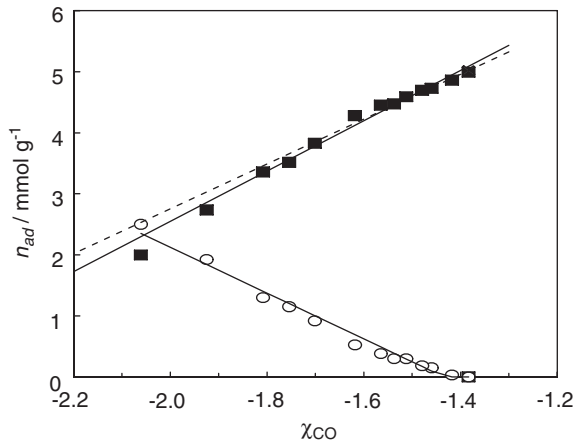
Fig. 94. Adsorption of CO–N_2 mix on 5A zeolite at 1 atm.

on 10X zeolite is nearly as bad a fit. Figs. 94 and 95 present two cases of the plots of the n_{ad}s versus the appropriate χ_1. In these figures:

- the solid lines are the χ fits from the binary experiment and
- the dotted line is the prediction from the measurements with the pure adsorbates.
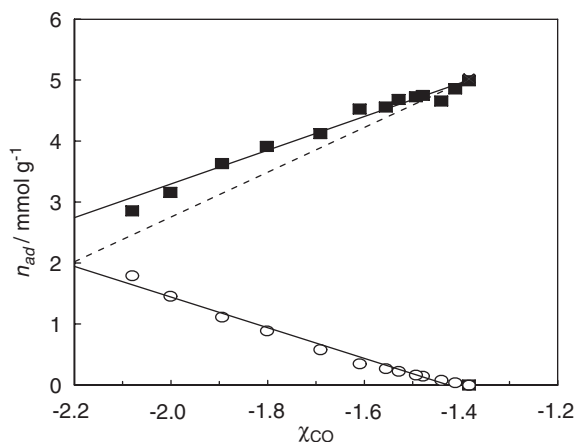
Fig. 95. Adsorption of CO–O$_2$ mix on 5A zeolite at 1 atm.

Fig. 94 is for the 5A with the binary mix of N$_2$–CO, which according to Table 25 was fairly well predicted by the pure adsorption isotherms. The difference between the $\chi_{c,1}$ from the pure to binary measurement was 0.13. Fig. 95 is for the adsorption of CO and O$_2$ on 5A, which according to the data of Table 25 was the set with the worst agreement between the binary adsorption and that expected from the pure adsorbate isotherms. The difference in $\chi_{c,1}$ for this latter set was 0.44. The reason for the difference for this latter data set could be experimental. The calculated value for E_a for the binary adsorption is about 29 kJ mol^{-1}, which seems to be quite high. One normally does not observe E_as for these adsorbates on silica materials greater than 20 kJ mol^{-1}.

A common method of presenting the adsorption data for binary mixes is the gas-adsorbate phase diagram. This is a plot of partial pressure versus amount adsorbed at constant total pressure. The data and fits shown in Figs. 94 and 95 may be redrawn to form such phase diagrams, these are shown in Figs. 96 and 97. In these figures:

- The solid lines are the χ fits to binary measurements.
- The dashed lines are predictions from the pure adsorption.
- The lines with arrows are Henry's law for liquid–gas.

An additional piece of information is provided in these figures, that is, the expected phase diagram from Henry's law (liquid–gas). The arrows are intended to indicate that the Henry's law line is on the opposite side of the diagram from the data. The difference between a liquid–gas diagram and adsorbate–gas diagram is very obvious in these cases.
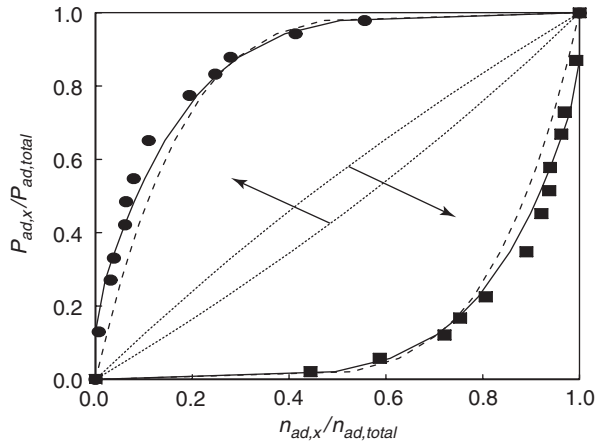
Fig. 96. Phase diagram of N_2–CO in 5A zeolite. ■ CO, ● N_2.
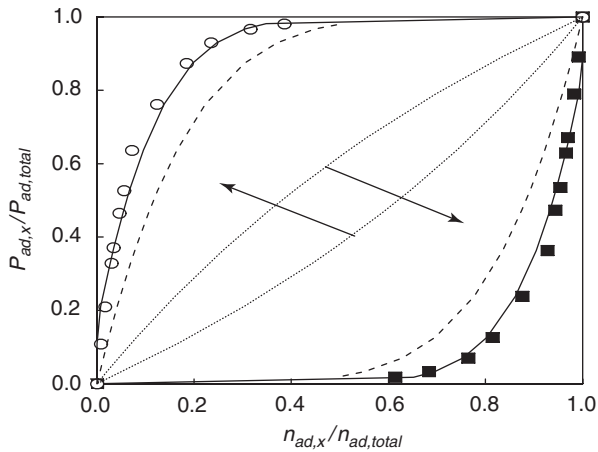
Fig. 97. Phase diagram of CO–O_2 in 5A zeolite. ■ CO, ○ O_2.

Except for the two cases mentioned, the predictions from the pure adsorbate isotherms would be, for most practical purposes acceptable. The advantage of being able to predict the phase diagrams from the pure isotherms is that if one wishes to do a screening study the number of isotherms for n adsorbents is n, whereas for the various combinations it is $n(n-1)$ which for a large number of adsorbents could be considerably more work. There are several other sets of experimental data available in the literature. For most, the χ formulation works quite well.

Conclusions Regarding Binary Adsorption

With the possible exception of density functional theory (DFT), χ theory is the only theory which is capable of making some predictions regarding binary adsorption. DFT, in principle, should be able to calculate the binary adsorption for all types of pores given all the atomic details. The latter proviso is the principal problem with DFT, that is it is presently not capable of dealing with unknown surfaces and unknown geometries. χ theory determines some of the properties from the experimental data and then goes on to make predictions.

There is no doubt that much more research is needed in the area of binary adsorption, both theoretical and experimental. The binary adsorption in micropores depends upon the development of the theory of adsorption in micropores which, as noted in Chapter 6, itself could benefit from further development.

STATISTICAL COMPARISONS OF OTHER ISOTHERMS TO THE χ PLOT

A statistical comparison of χ theory with the BET or the DP isotherm fits is not completely possible due to the fact that for the latter two a best-fit range is required in order obtain the parameters. This requires some judgement as to what this range is. The normal recommendation for the BET is to select the range in P/P_s from 0.05 to 0.35. However, this can also vary as noted previously depending upon the energetics of the adsorption. For ceramic materials, this range is usually OK. The DP range, however, is best determined by an examination of the transformed plot, i.e. $\ln(n_{ad})$ versus $\ln(P/P_s)$. Fig. 98 shows a typical example of the three fits to the data used for the construction of the α–s plot. It should be noted that the DP isotherms were originally not intended for non-porous materials although the extension by Kagener would indicate this. The DP formulations are best for fitting the data at the high coverage end of the isotherm for microporous adsorbates. In Fig. 98 it is obvious that the deviation is very great for the BET equation at the higher pressures. The DP formulation deviates somewhat in the low direction for these high pressures.

Table 26 presents statistics for the fit to the data used to construct the α–s curves. Not surprisingly, the F-test for the full range of the isotherms for the BET and DP isotherms are very poor. Even over the range that was judged best for these fits, the F-test would indicate a slightly better fit for the χ theory. (As noted before, the last data point for the N_2 adsorption is probably too high and is ignored in this analysis.)
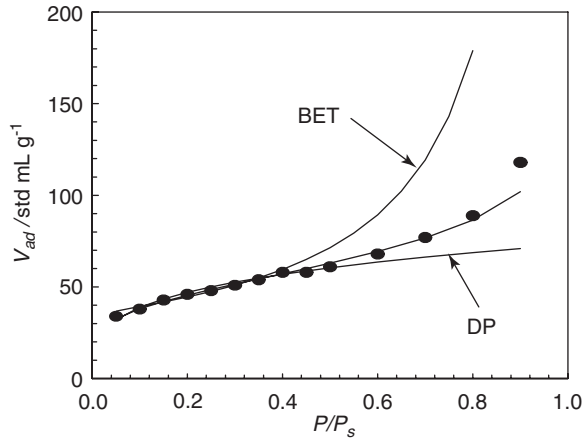
Fig. 98. Agraphical comparison of the BET, DP and χ theories.

Table 26
Statistics comparing the BET, DP and χ theories. Adsorption on silica used for the α–s plot

	χ	BET	DP
N$_2$ adsorption			
Range	0.05–0.80[a]	0.05–0.35	0.05–0.60
Sigma	1.31	1.53	1.86
F-test full	0.6088	0.0024	0.0221
F-test in range	0.9903	0.8339	0.8511
Ar adsorption			
Range	0.05–0.90	0.05–0.35	0.05–0.70
Sigma	1.21	1.31	1.66
F-test full	0.9953	0.0087	0.4785
F-test in range	0.9953	0.9136	0.7120

[a]Full range was 0.05–0.90.

For another example, the adsorption of N$_2$ and Ar on the 25°C outgassed thoria are presented in Table 27. The advantages for these data are presented under the "Standard Thoria Plots" in Chapter 5, which are the stability and uniformity of this powder with this treatment, but in addition to these, the advantage is that the measurements could be performed in a very accurate and controlled gravimetric system and many data points were collected. There is still, however, the question of range selection. The fewer the data points selected for the BET and DP fit, the better the statistics should be. (After all, if one were to select two data points one would obtain a perfect fit.) A best

Table 27
Statistics comparing the BET, DP and χ theories. Adsorption on 25°C outgassed thoria

	χ	BET	DP
N$_2$ adsorption			
Range	0.016–0.90	0.05–0.35	0.016–0.42
Sigma	0.0213	0.0180	0.0209
F-test full	0.9971	2.3×10^{-5}	0.105
F-test in range	0.9971	0.9938	0.9939
Ar adsorption			
Range	0.011–0.82	0.05–0.35	0.011–0.35
Sigma	0.00998	0.01249	0.00781
F-test full	0.9985	2.5×10^{-4}	0.130
F-test in range	0.9985	0.9835	0.9835

effort for selecting the DP range was used and the BET range was selected as the normal recommended range. Even so, the fit for the χ theory is still better.

These statistics are so close, at least in the selected ranges, that a definitive distinction is not possible. It is, however, possible to create a large number of equations that would fit the data very well. There are at least over a 100 isotherms listed in the literature from which one could choose.

GENERAL CONCLUSIONS

In this section, the terminology χ theory has been used, but one must remember that many of the applications could use a good standard curve. Furthermore, as previously demonstrated, χ theory and disjoining pressure theory are basically the same with the modification specified to calculate the surface area. The advantage of χ theory over other standard curve methods, is that the standard is internal, that is the energy of adsorption is calculated directly from the specific adsorbent sample being investigated rather than from a simulated sample. Using a simulated sample could be a source of considerable error.

If one prefers to reject the theoretical basis of χ theory, then the formulation as a standard curve is still very useful. As noted in the comparison to standard curves, the χ function is a very good analytical form for most standard curves. Having an analytical form for the standard curve is extremely handy for both practical measurements and theoretical development.

The prediction of the heats of adsorption from the adsorption isotherm without the introduction of any parameters is very difficult to explain. This

provides an explanation for the Dubinin "thermodynamic criterion", which was an assumption for which previously there was little theoretical basis.

REFERENCES

[1] J.B. Condon, Langmuir, 17 (2001) 3423.

[2] K.S.W. Sing, in "Surace Area Determination" D.H. Everett and R.H. Ottewill (eds.), p .25, Butterworths, London, 1970.

[3] M.R. Bhanbhani, R.A. Cutting, K.S.W. Sing and D.H. Turk, J. Colloid Interf. Sci., 82 (1981) 534.

[4] R.W. Carnston and F.A. Inkley, Adv. Catal., 9 (1957) 143.

[5] B.C. Lippens, B.G. Linsen and J.H. deBoer, J. Catal., 3 (1964) 32.

[6] J.H. deBoer B.G. Linsen and Th.J. Osinga, J. Catal., 4 (1965) 643.

[7] J.H. deBoer, Proc. R. Acad. (Amsterdam), 31 (1928) 109.

[8] J.H. deBoer and C.Z. Zwikker, Z. Phy. Chem., 28 (1929) 407.

[9] R.B. Gammage, E.L. Fuller and H.F. Holmes, J. Colloid Inerf. Sci., 34 (1970) 428.

[10] G.A. Nicolan and S.J. Teichner, J. Colloid Surf. Sci., 34 (1972) 172.

[11] R.S. Bradley, J. Chem. Soc., (1936) 1467.

[12] R.S. Bradley, J. Chem. Soc., (1936) 1799.

[13] J. McGavack, Jr. and W.A. Patrick, J. Am. Chem. Soc., 42 (1920) 946.

[14] W.C. Bray and H.D. Draper, Proc. Natl. Acad. Sci. USA, 12 (1926) 297.

[15] F. Rodrigues-Reinoso, J.M. Martin-Martin, C. Prado-Burguete and B. McEnaney, J. Phys. Chem., 91 (1987) 515.

[16] E.L. Fuller, Jr., J.B. Condon, M.H. Eager and L.L. Jones, Sorption Analysis in Material Science: Selected Oxides, DOE Report Y-DK-264, US Government Printing Office, Washington, DC, 1981.

[17] E.L. Fuller, Jr. and K.A. Thompson, Langmuir, 3 (1987) 713.

[18] S.J. Peters and G.E. Ewing, J. Phys. Chem. B, 101 (1997) 10880.

[19] S.J. Peters and G.E. Ewing, Langmuir, 13 (1997) 6345.

[20] X. Guo, Y. Han, Y. Zou, D. Li, J. Yu, S. Qiu and F.-S. Xiao, Micropor. Mesopor. Mat., 42 (2001) 325.

[21] A. Gil, B. de la Puente and P Grange, Micropor. Mat., 12 (1997) 51.

[22] K.A. Thompson, personal communication unpublished work.

[23] K.A. Thompson, E.L. Fuller, Jr. and J.B. Condon, Further Evidence Supporting the Autoshielding Physisorption Equation, 17th DOE Surface Studies Confernce, US Government Printing Office, Washington, DC, 1989.

[24] E.P. Smirnov, O.K. Semchinova, A.M. Abyzov and D. Uffmann, Carbon, 35 (1947) 1351.

[25] J.D. Lopez-Gonzalez, F.G. Carpenter and V.R. Deitz, J. Res. Nat. Bur. Stand., 55 (1955) 11.

[26] M.M. Dubinin, E.D. Zaverina and L.V. Radushkevich, Zhur. Fiz. Khim., 21 (1947) 1351.

[27] M.M. Dubinin and V.A. Astakhov, Izv. Akad. Nauk SSSR, Ser. Khim., 1971 (1971) 11.

[28] J. Tóth, Adv. Colloid. Interf. Sci., 55 (1955) 1.

[29] J. Tóth, Colloid. Surface., 49 (1990) 57.

[30] J.B. Condon, Micropor. Mesopor. Mat., 33 (2002) 21.

[31] E.I. Pace, K.S. Dennis and W.T. Berg, J. Chem. Phys., 23 (1955) 2166.

[32] E.I. Pace, W.T. Berg and A.R. Siebert, J. Am. Chem. Soc., 78 (1956) 1531

[33] K.S. Dennis, "Heat Capacities from 15–125K and Entropies of Keypton Adsorbed on Rutile" PhD thesis, Western Reserve University (now Case Western Reserve University) Cleveland, OH, USA, 1954.

[34] W.T. Berg. "Heat Capacities from 15–140 K and Entropies of Keypton Adsorbed on Anatase", PhD thesis, Western Reserve University (now Case Western Reserve University) Cleveland, OH, USA, 1955.

[35] W.D. Harkins and G.J. Jura, J. Am. Chem. Soc., 66 (1944) 919.

[36] J.R. Arnold, J. Am. Chem. Soc., 71 (1949) 104.

[37] K. Denbigh, The Principles of Chemical Equilibrium, 3rd ed., p. 152, Cambridge at the University Press, 1971.

[38] M.M. Dubinin, E.G. Zhukovskaya and K.O. Murdmaa, Ivza, Acad. Nauk SSSR, Ser. Khim., 1966 (1966) 620.

[39] J.B. Condon, Micropor. Mesopor. Mat., 38 (2000) 359.

[40] R.P. Danner and L.A. Wenzel, AIChE J., 15 (1969) 515.

This page intentionally left blank

Porosity Calculations

INTRODUCTION

In Chapter 3, two methods based upon the concept of the standard curve were presented for calculating the porosity. One method was presented for micropore calculations and another for mesopore calculations. Although the definition of micropore and mesopore is a bit arbitrary, the boundary being 1 nm radius by the IUPAC convention [1], it is of some practical use. It has been speculated that there is actually no difference for these cases, merely a matter of what appears obvious in the isotherm. Later on in this chapter a few calculations will be presented to illustrate this point.

In this chapter, several alternative methods will be presented. This area of investigation is still ongoing but appears to be nearing a resolution. The most useful formulations are those which are not dependent upon the specifics of the adsorbent. As mentioned previously, the reason for this is often the details of the surface of the adsorbent are unknown regardless of expectations.

A philosophical problem exists for the definition of the physical quantities "surface area", "pore volume" and "pore radius". What is meant by these terms? At first this seems to be simple, but when one considers that the physical quantity being measured and the measuring device, namely the adsorbate molecules, have approximately the same size the answer to this question becomes a little more difficult to answer. Add to this the possible molecular-sized roughness and the problem becomes more complex. This problem is the well-known fractal problem–the measurement made depends upon the ruler being used. One should not expect to get the same answer for these physical quantities using different adsorbate. Furthermore, it should not be surprising that techniques other than physisorption, such as X-ray analysis or NMR, might also yield different results. The theoretical problem is to correlate these measurements and possibly bring them into agreement. The practical consequence is that given a certain set of physical quantities,

all obtained by measuring with the same adsorptive, one should be able to reproduce the same correlated physical behavior from sample to sample based upon these physical quantities. Thus, the effort to pursue reproducible, reliable and possibly accurate measurement of the basic physical quantities is not a waste. One could argue that such agreement is not important and that the correlations between the extracted parameters and the physical–chemical behavior, for example catalytic activity, is all that is important. This, of course, can be and is done, but this then becomes an art rather than science and one is unlikely to be able to make the predictions that the scientific use of physical quantities and theories is capable of.

One of the biggest problems in the area of mesopore analysis is the hysteresis effect, that is the adsorption isotherm is different from the desorption isotherm. The hysteresis loop formed in the isotherm covers only a portion of the isotherm. The desorption branch of the isotherm always has a higher amount of material adsorbed than does the adsorption branch, which from any semi-thermodynamic point of view makes sense. Several complications have been postulated for the phenomenon. Complicating the subject is a specific case that leads to what appears to be hysteresis, for example partial chemisorption and plastic deformation of the adsorbent. The solution to non-specific hysteresis may be found in density function theory (DFT) calculations of which several have been quite insightful.

MICROPORE ANALYSIS

Microporosity is defined by IUPAC as pore sizes (diameter or slit width) of 2 nm or less. Although this is the official definition, the practical definition would be in terms of the isotherm produced. The type of isotherm that is produced is usually a type I isotherm, although this could be misleading. The chi (χ) feature associated with microporosity is feature 2 in the absence of feature 3, that is a negative curvature in the χ plot without any preceding high-pressure positive curvature.

All micropore analyses make the simple assumption that the adsorption is limited by the size of the pores, specifically the pore volume. Indeed, for the Dubinin–Radushdkevich (DR) and Dubinin–Astakhov (DA) equations the pore volume is the only practical physical quantity obtainable.

The BDDT Equation

One attempt to account for the adsorption in micropores was to modify the Brunauer, Emmett and Teller (BET) equation by limiting the number of

adsorbed layers. The resultant equation is the Brunauer, Deming, Deming and Teller [2] (BDDT) equation. With N being the number of layers allowed, this is given as

$$\frac{n_{ad}}{n_m} = \frac{C(P/P_s)\left[1-(N+1)(P/P_s)^N+N(P/P_s)^{N+1}\right]}{1-(P/P_s)\left[1+(C-1)(P/P_s)-C(P/P_s)^{N+1}\right]} \tag{177}$$

The form of this equation fits many systems well. Fig. 99 illustrates the shape of this isotherm for several values of N. An obvious question is, "If only integer values of N can exist, how could one obtain a fit to the isotherm that is not an integer?" There are two possible answers to this. First, there is no reason to assume that the adsorbate molecules stack exactly in a row and, secondly, there may be a distribution of pores and N becomes a weighted average of the various sizes. For example if $N = 2.5$, this could mean that half of the pores accommodate two layers and the other half accommodate three layers.

Notice that regardless of the value for N the value for n_m, which is interpreted to be the monolayer coverage, is extractable. This is a physical quantity that most other theories are unable to extract without the BET equation.
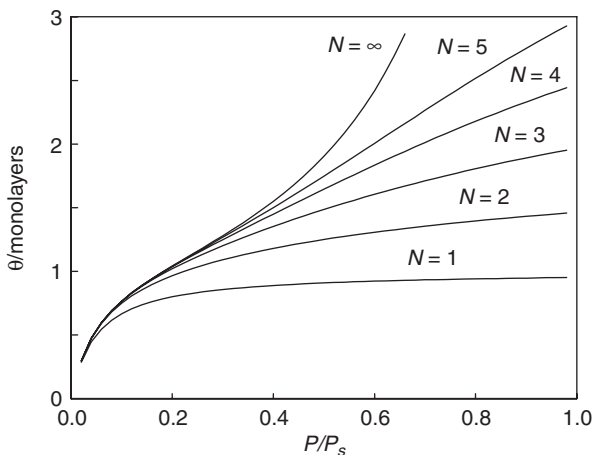
Fig. 99. The BDDT equation for various values of N. The c constant used for this was 20.

The DR and DA Equations

The DR [3] and the DA [4] equations may be expressed as

$$\ln\left(\frac{n_{ad}}{n_p}\right) = B\left(\frac{T}{\beta}\right)^k \ln^k\left(\frac{P_s}{P}\right) \tag{178}$$

where n_p are the number of moles that fill the pore volume. The constant β is interpreted to be an energy term. The interpretation of the parameters in equation other than n_p is of little practical importance. Eq. (178) may be derived using the following assumptions:

- The quantity $\partial(RT\ln(P/P_s)/\partial T = 0$ at constant n_{ad}. This is called the Dubinin "thermodynamic criterion".
- The energy of adsorption follows a distribution function, specifically the Weibull distribution curve. Thus, the parameters of Eq. (178) are related to this distribution function.

The parameter k may be any value with $k = 2$ being the special case of the DR equation.

One of the advantages of Eq. (178) is that one can plot $\ln(n_{ad})$ as a function of $\ln^k(P_s/P)$ and adjust k to obtain a straight line in the plot. With today's computers, adjusting k to obtain the best straight line is a trivial task. The intercept on the n_{ad} axis yields the value for n_p. For a wide range of micropore sizes and energies, one is able to find a fairly long range in the transformed isotherm where a straight-line fit is appropriate [5]. If the external surface area is negligible compared to pore volume such an analysis is not necessary since it is simple to extrapolate the untransformed isotherm to $P/P_s = 1$. The DR−DA extrapolation, however, works well even in the presence of significant external surface area. Fig. 100 shows an example of a DA fit to some real data. These data are for N_2 adsorption on 5A zeolite by Danner and Wenzel [6] (chosen at random from many sets of data) and are quite typical. Often there is a slight upswing or curvature in the plot near the n_{ad} axis, which indicates significant external surface area. In this case the external surface area was too small to cause this problem. Table 28 gives a summary of the DA analysis of the data by Danner and Wenzel. Notice that to obtain a straight-line fit, k has to have a considerable range.
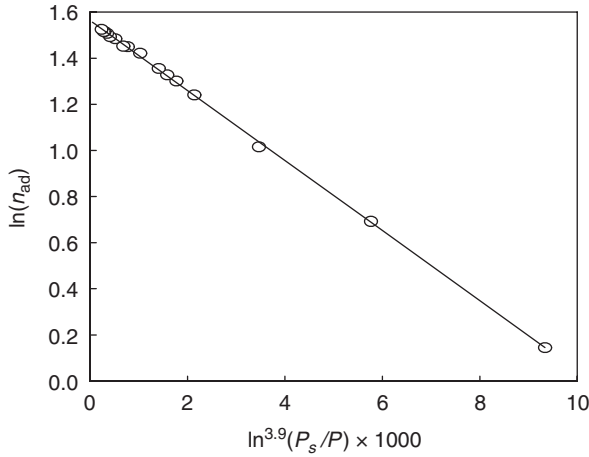
Fig. 100. An example of a DA plot illustrating the straight-line fit. The data are for N_2 adsorption in 5A zeolite by Danner and Wenzel [6].

Table 28
DA analysis of adsorption on 5A and 10X zeolites

Adsorbent	Adsorbate	V_p/mL g^{-1}	k
10X	O_2	0.46	4.2
	N_2	0.54	2.4
	CO	0.62	2.3
5A	O_2	0.40	3.8
	N_2	0.42	4.3
	CO	0.48	2.1

Data by Danner and Wenzel [6].

Standard Curve Analysis Using Distributions – Uninterpreted

In Chapter 3, the micropore analysis using a standard curve was presented. It was assumed that the system of pores was very simple in this analysis. The simplification was that there is one energy of adsorption and one pore size. This is very unlikely to be the case, so in this section additional parameters will be introduced into the standard curve analysis.

In principle, any standard curve may be used in this analysis provided the standard curve is descriptive of a homogeneous, non-porous material of identical surface composition. This is quite an order and there are only a few materials for which one could with some confidence say the standard curve

use is appropriate. Such materials could include silica, alumina and thoria. The χ theory formulation, however, does not need a separate standard. This is the main advantage it has over a calibrated standard curve. In the following analysis, the χ curve will be used due to its simplicity, but one should keep in mind that a good standard curve would work just as well.

The following analysis need not be interpreted in terms of physical quantities. Thus it yields an analytical form which one could use more easily with more traditional pore size analysis systems as well as χ theory or DFT. Included in the traditional digital methods is the pore length method originated by Wheeler [7] and developed by Shull [8], the Barrett Joyner and Halenda (BJH) [9] and the Cranston and Inkley [10]. It is, however, easier to visualize and it may be possible that once the parameters for a particular isotherm are obtained one could attach different meanings to them. Indeed, the χ plot representation has been presented [11] as a method to empirically construct an analytical expression for the standard curves.

For the curve fitting, it will be assumed that there is a distribution of energies, E_as, and a distribution of pore sizes. Furthermore, some of the surface area is not inside the pores and is referred to as external. The pore radius is reflected in a cutoff in the standard curve or in terms of χ there is a mean value $\langle \chi_p \rangle$ for which the standard curve in the pores is terminated. The probability mass function (PMF) distribution will be used with the standard deviations for energy and pore size. Any reasonable distribution could be used and the parameters expanded, for example to include skewness, etc., but usually the experimental data would not justify this. Thus there are six parameters:

1. $\langle \chi_c \rangle$ = the mean value of the start of the standard curve corresponding to the mean value of E_a.
2. σ_c = the standard deviation of χ_c in a distribution function. If one had extensive low-pressure data, it would be possible to formulate any energy distribution based on the second derivative of the χ plot.
3. $\langle \chi_p \rangle$ = the mean value of the shutdown of adsorption due to the restriction of the pores.
4. σ_2 = the standard deviation of χ_p
5. A_s = total surface area (including pore surface area).
6. V_p = the volume inside the pores.

At this point, no geometry will be assumed. With the assumption of geometry, other quantities such as pore radius may be calculated.

The distribution for the energies implies

$$\frac{\partial^2 n_{s+}}{\partial \chi^2} = \frac{A_s}{f A_m \sigma_p \sqrt{2\pi}} \exp\left(-\frac{(\chi - \langle \chi_c \rangle)^2}{2\sigma_c^2}\right) \tag{179}$$

where the symbol n_{s+} is indicating the amount adsorbed on all the surfaces and would continue to adsorb with increasing pressure if there were no porosity restriction. Likewise, the distribution in the pore size implies

$$\frac{\partial^2 n_{s-}}{\partial \chi^2} = \frac{V_p}{V_m \sigma_2 \sqrt{2\pi}} \exp\left(-\frac{(\chi - \langle \chi_p \rangle)^2}{2\sigma_2^2}\right) \tag{180}$$

where the symbol n_{s-} indicates the amount of material that is not adsorbed due to the pore restriction. σ_2 reflects the cumulative distribution for both the energy and the pore sizes and is related to these through the well-known statistical relationship for non-correlated distributions:

$$\sigma_2^2 = \sigma_c^2 + \sigma_p^2 \tag{181}$$

The problem with Eq. (181) is that it could be possible that there exists a correlation between the energies of adsorption and the pore sizes. For example, χ theory predicts that the smaller a cylindrical pore the higher is its energy of adsorption. Thus, there is really no restriction on σ_c versus σ_2. It is possible for σ_2 to be less than σ_c for which an explanation would certainly be in order for such a cross-correlation.

Obviously to get the entire isotherm Eq. (180) must be subtracted from Eq. (179) and the results doubly integrated form $\chi = -\infty$ (which is $P/P_s = 0$) to whatever χ is of interest. (A similar equation is given in Chapter 5 in the discussion of the Freundlich and Dubinin-Polanyi isotherms. There the match to the second derivatives was used as being a more sensitive test.) This yields a rather messy but quite useable and easily calculated equation:

$$n_{ad} = G\,\mathbf{Z}\big(\chi, \langle \chi_c \rangle, \sigma_c\big) - H\,\mathbf{Z}\big(\chi, \langle \chi_p \rangle, \sigma_2\big) \tag{182}$$

where

$$\mathbf{Z}(x,y,s) = \frac{s}{\sqrt{2\pi}}\mathbf{exp}\left(\frac{-(x-y)^2}{2s^2}\right)$$
$$+\frac{x-y}{2}\left(1+\mathbf{erf}\left(\frac{x-y}{s\sqrt{2}}\right)\right)$$

(183)

The parameters G and H are introduced to replace A_s/fA_m and V_p/V_m, respectively. The six parameters are then G, H, $\langle\chi_c\rangle$, $\langle\chi_p\rangle$, σ_c and σ_2. With six parameters one should be able to fit almost any isotherm that resembles a type I isotherm. Indeed, in many cases there are too many parameters so the following could be attempted to yield five parameters. (1) If the very low-pressure data are unavailable, set σ_c to zero (or for practical purpose to use the same program to a very low number such as 1×10^{-5}). (2) If σ_2 drifts in the calculation to a smaller number than σ_c then try setting $\sigma_2=\sigma_c$ or try (1), realizing that $\sigma_2<\sigma_c$ is possible.

   The simplest method to obtain the parameters for Eq. (182) is to run a minimum search routine. This is easily accomplished with a simple spread sheet. Some reasonable starting parameter would be 0.01 for both σs, -2.8 for χ_c and -1.5 for χ_p. G and H could be set equal to each other but the absolute size depends upon the sample, the measurement method and units. It would be advised to have a graphical representation of the data and the fit to have a visual guide for the initial estimates. If the starting parameters are very far from correct the calculation can drift off to a very incorrect false minimum. The criterion for minimization should be the minimization of the sum of squares of the difference between the calculated values and the experimental values.

   For illustration, the data by Danner and Wenzel for adsorption of CO, N_2 and O_2 on 10X and 5A zeolite at 144.3 K are plotted in Figs. 101 and 102, with the calculation from Eq. (182) shown as solid lines. One of these data sets, CO adsorption on 5A zeolite, illustrates the provisos listed above and the number of parameters is 5 instead of 6. The data for this particular isotherm do not extend low enough to determine the parameter σ_c. Table 29 lists the parameters extracted for Eq. (182). The CO adsorption on 5A zeolite has only five parameters, σ_c being the parameter that was forced to be 0. An attempt at determining this parameter is given in parenthesis in Table 29.
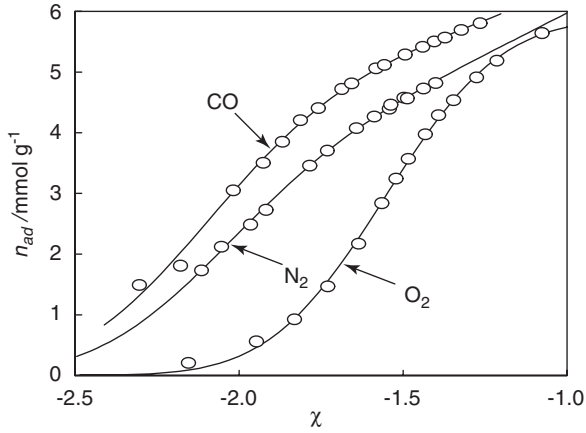
Fig. 101. Adsorption of CO, N_2 and O_2 on 10X zeolite by Danner and Wenzel [6].
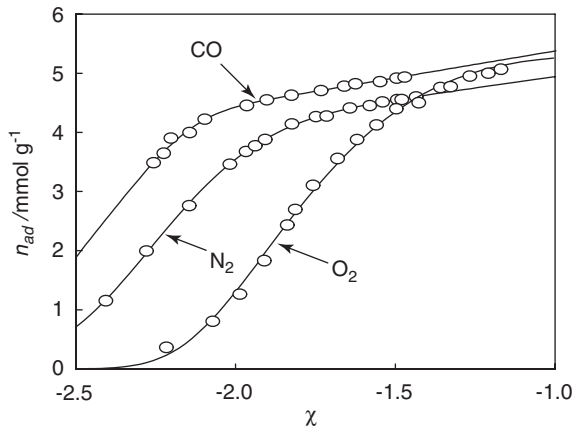
Fig. 102. Adsorption of CO, N_2 and O_2 on 5A zeolite by Danner and Wenzel [6].

Table 29
Fit to Eq. (182) for the data by Danner and Wenzel [6]

	G	H	$\langle \chi_c \rangle$	$\langle \chi_p \rangle$	σ_c	σ_2
10X-O_2	9.13	9.13	-1.873	-1.242	0.208	0.173
10X-N_2	6.93	6.93	-2.323	-1.563	0.330	0.330
10X-CO	6.05	4.25	-2.559	-1.738	0.280	0.176
5A-O_2	10.95	9.20	-2.071	-1.690	0.189	0.189
5A-N_2	10.79	10.05	-2.446	-2.063	0.241	0.238
5A-CO	7.31	6.40	-2.751	-2.161	(0.027)	0.127

Although the parameters are given symbols that would imply some interpretation, one may at this point assign whatever interpretation one wishes to these parameters. In the next section, these parameters will be interpreted in terms of the χ theory (or equally so, the disjoining pressure theory).

Chi Theory Interpretation of the Distribution Fit

Surface Areas and Pore Volume Calculations
According the χ theory, the parameter G is indicative of the total surface area, inside and outside the pores, whereas H indicates the pore volume. The difference between G and H yields the external surface area, that is the surface area excluding the pore surface area. Thus, the total surface area is given by

$$A_s = GfA_m \tag{184}$$

where $f = 1.84$ and $A_m = V_m^{2/3} N_A^{1/3}$ is the molar area, with V_m being the molar volume and N_A the Avogadro's number. The molar volume is assumed to be that of the liquid. The problem with this assumption is the question of selection of the temperature for the liquid, since the density of the liquid varies with temperature. Between the normal boiling point of a liquid and its critical point, a factor of 2 or 3 is likely. The liquid density at the boiling point is selected here, which is an acknowledgment that this assumption is an open question for χ theory. The pore volume is obtained by extrapolating to $\chi = \chi_c$ the linear asymptote for high values of χ. The slope of this asymptote is $G - H$ and the line passes through the point $\chi = \chi_p$ and $n_{ad} = G(\chi_p - \chi_c)$. Thus,

$$V_p = HV_m \Delta \chi_p \tag{185}$$

The external surface area, A_{ex}, is therefore

$$A_{ex} = (G - H)fA_m \tag{186}$$

The external surface area includes at least two types of surfaces, the surface of the adsorbent that is not in the pores, which will be referred to as the "wall" area, A_w, and the surface area of the filled pore openings, A_o. Thus,

$$A_{ex} = A_w + A_o \tag{187}$$

This can cause problems in the analysis of porosity unless the external surface area is very small compared to the surface area within the pores. If one subtracts the wall surface area from the total surface area one may obtain the surface area inside the pores, A_p. Unfortunately, the quantity A_o is unknown, therefore

$$A_s > A_p > A_s - A_{ex} \tag{188}$$

Calculation of Pore Size Assuming a Geometry

There are two ways of calculating the pore size. For the first one, one needs to assume a pore geometry. For cylindrical pores, the pore radius is given by the simply derived geometrical relationship

$$r_p = \frac{2V_p}{A_p} \tag{189}$$

If slit-like pores were assumed then r_p would become the distance between the slit walls. These are the primary types of pores; other types would require other relationships. Making the appropriate substitutions into Eq. (189) and taking into account Eq. (188) the following results:

$$\frac{2V_m \Delta \chi_p}{fA_m} \geq r_p \geq \frac{2HV_m \Delta \chi_p}{GfA_m} \tag{190}$$

Calculating r_p from $\Delta\chi_p$

An alternate derivation for Eq. (190) is to calculate r_p from the value of $\Delta\chi_p$ ($\Delta\chi_p = \langle\chi_p\rangle - \langle\chi_c\rangle$). The amount adsorbed up to any $\Delta\chi$ is given by

$$n_{ad} = \frac{A_s \Delta \chi}{fA_m} \tag{191}$$

The classical thickness if obtained from the molar volume and area covered is

$$t = \frac{V_m n_{ad}}{A_s} \tag{192}$$

Substituting one obtains

$$t = \frac{\Delta \chi_p V_m}{f A_m} \tag{193}$$

This works for a flat surface; however for a restricted geometry the amount adsorbed remains the same and the thickness will vary. In a cylindrical pore with a radius r_p, the amount adsorbed from the pore wall to a distance t from the wall is

$$n_{ad} = \frac{A_s}{V_m} \left(t - \frac{t^2}{2r_p} \right) \tag{194}$$

or t is obtained from the equation

$$\frac{\Delta \chi}{f A_m} = \left(t - \frac{t^2}{2r_p} \right) \tag{195}$$

Obviously for micropores at $\Delta \chi_p$ $t = r_p$ the upper limit of Eq. (190) is obtained.

Examples of Results

Using the same data as was used in Table 29, the calculation for the appropriate physical quantities is given in Table 30. The experiments by Danner and Wenzel were performed above the critical point and a microporous analysis would seem appropriate since the gas–liquid surface tension should be zero. In Table 30 both values for r_p from Eq. (190) are listed (which of course includes

Table 30
Interpretation of the parameters of Table 29

	A_p (m² kg⁻¹)	A_s (m² kg⁻¹)	V_p (mL g⁻¹)	r_p (nm)	A_{access} (m² kg⁻¹)
10X-O$_2$	2.49	2.49	0.42	0.34–0.34	2.24
10X-N$_2$	2.15	2.15	0.47	0.44–0.44	1.61
10X-CO	1.36	1.93	0.32	0.34–0.48	1.81
5A-O$_2$	2.51	2.98	0.26	0.17–0.21	2.13
5A-N$_2$	3.12	3.35	0.34	0.21–0.22	1.99
5A-CO	2.04	2.33	0.35	0.30–0.34	1.88

Eq. (195)). The two values for A_p are the range as designated in Eq. (188). If one were to follow the usual procedure for calculating the surface area one would not obtain the values listed in the first column of this table. However, the slope at any point on the isotherm is *not* directly reflective of the surface area. The reason for this is that as the pores fill, there is less surface area available for adsorption. Normally, it is the slope of the standard curve that determines the value of the surface area. Therefore due to the pore filling, either micropore or mesopore filling but especially micropore, the actual surface area would be underestimated. In other words, the *accessible* surface area for porous material *should be less* than the actual surface area. In the last column of Table 30, labeled A_{access}, the surface area as calculated from the maximum slope of the chi plot is listed. (A closed analytic solution is messy but possible.) As demonstrated in the table, in all cases $A_{access} < A_s$. It is also obvious from these values that the use of A_{access} in place of A_s could occasionally yield a very large error in the answer. For example, the data for CO or N_2 on $10\times$ zeolite would yield an answer that is much lower than the actual surface area.

For another example, Table 31 a re-interpretation of the classic data by Goldmann and Polanyi [12] for various adsorbates on activated charcoal is

Table 31
Analysis of the data for adsorption on activated charcoal by Goldman and Polanyi [12] using the micropore analysis and χ theory interpretation

Adsorbate	T (K)	σ_c^1	σ_2	A_p (m^2 mg^{-1})	V_p (mL g^{-1})	r_p (nm)
Ethylene	257.85	0.279*	0.373	1.05–1.08	0.46	0.86–0.88
Chloride	273.15	0.316*	0.420	1.06–1.10	0.46	0.83–0.87
	293.15	0.373*	0.934	1.10–1.11	0.48	0.87–0.88
Diethylether	257.85	0.152	0.236	1.12–1.24	0.44	0.71–0.79
	273.15	0.443*	0.581	1.19–1.21	0.50	0.82–0.84
	293.15	0.340	0.617	1.20–1.25	0.49	0.78–0.81
n-Propane	257.85	0.618	0.596	1.23–1.25	0.47	0.76–0.77
	273.15	0.455	0.665	1.23–1.28	0.46	0.71–0.74
See note 2	273.15	0.627	0.559	1.26–1.29	0.48	0.74–0.76
	293.65	0.429	0.679	1.31–1.33	0.51	0.76–0.77
See note 2	209.5	0.758	0.492	1.81–1.86	0.46	0.50–0.51
CS$_2$	257.85	0.310	0.279	1.28–1.34	0.50	0.75–0.79
	273	0.415	0.299	1.25–1.32	0.47	0.71–0.76
	293.65	0.391	0.352	1.22–1.28	0.48	0.76–0.80

Note: (1) Owing to lack of sufficient low-pressure data, most values for σ_c are extremely questionable. Possible exceptions are those labeled with an "*".
(2) The analysis of these data are questionable since eight or less data points were available.

given. In this table the range for r_p from Eq. (190) is presented. None of the samples tested well for mesoporosity. This is not surprising since the radii are below 1 nm and, furthermore, the adsorbate molecules were considerably larger than the normal nitrogen or argon adsorbate molecule.

Except for one of the data sets marked as having too few data points, there seems to be very good agreement at least within the adsorbate set and fair agreement across adsorbate sets. There are several cases where the calculated $\sigma_c > \sigma_2$, which should normally be a combination of σ_c and σ_p. However, the data for the low-pressure ranges for these data sets are lacking. The only data sets that had more than two data points within 1 standard deviation of $\langle \chi_c \rangle$ in this table are marked with an "*". The contrast between the sets that one can obtain σ_c and where one cannot is obvious from the examples in Figs. 103 and 104. In Fig. 103 there seems to be enough data at the low-pressure end to determine the value of σ_c, In contrast, the low-pressure data are absent in Fig. 104.

In spite of the perceived problem with the estimatation of σ_c there is an agreement between data sets for r_p, Thus it appears that a good estimate of σ_c is not necessary to obtain the other physical quantities.

An example of a data series where the value for σ_c was in most cases not possible to obtain is from the data by Wisniewski and Wojsz [13]. The analysis of these data is given in Table 32. The reason that σ_c is unspecified (and therefore set to 0) in this table is clear from the plots of the data.
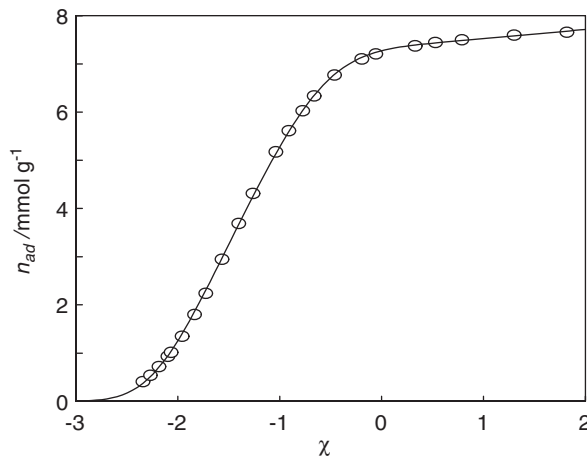

Fig. 103. Adsorption of ethylene chloride on charcoal at 273 K by Goldmann and Polanyi [12], illustrating the low-pressure data needed for the calculation of σ_c.
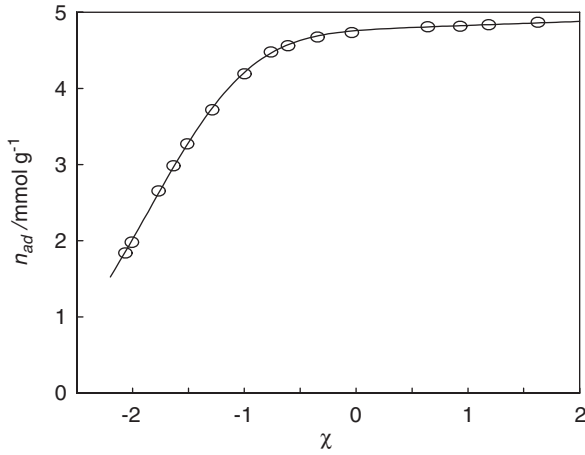
Fig. 104. Adsorption of *n*-pentane on charcoal at 257 K by Goldmann and Polanyi [12], illustrating the absence of the low-pressure data needed for the calculation of σ_c.

Table 32
Analysis of the microporosity from water adsorbed on Y- type zeolites

Type	σ_2	A_p/m^2 mg^{-1}	V_p/mL g^{-1}	r_p/nm
NH$_4$Y	0.236	1.53–1.64	0.28	0.34–0.36
CaY	0.492	1.59–1.64	0.30	0.37–0.38
HY	0.437	0.65–0.72	0.18	0.45–0.55
MgY	0.249	1.51–1.59	0.29	0.36–0.38
NaY	0.068	1.45–1.67	0.26	0.31–0.35

Data are by Wisniewski and Wojsz [13].

Fig. 105 shows the χ plot of the HY, CaY and MgY isotherms. The other isotherms are similar and are between the CaY and MgY isotherms. They are not presented here for clarity.

The negative curvatures for the cutoff in adsorption due to the microporosity are quite clear, but the positive curvatures for the energy distribution at the beginning of the plots are missing. This is due simply to the fact that the low-pressure data were not obtained, a very common situation. (In this case the χ value of-2 is a pressure of about 0.02 Torr, which could have been their limit of detection.) To perform the calculation the value of σ_c was set to be equal to σ_2, although it made little difference if it were set to zero.

These examples are presented here to illustrate some problems that one might encounter both in the fitting of the standard curve in general and in
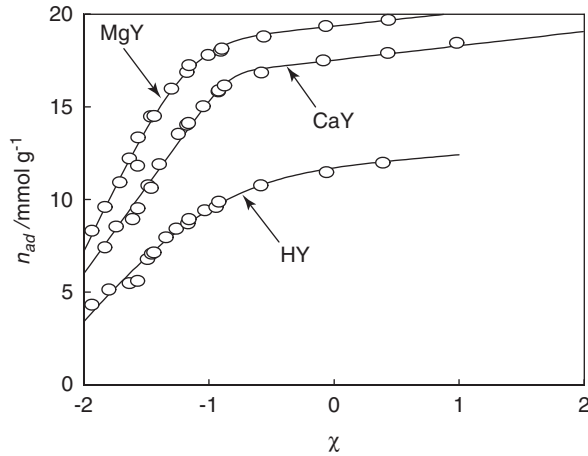
Fig. 105. Chi plot of the adsorption of water on Ca, H and Mg substituted Y-zeolites at 298 K according to Wisniewcki and Wojsz [13]. There was no data below $\chi = -2$.

the interpretation by χ theory. One cannot blindly analyze the data but rather pay particular attention to the low-pressure data. If not enough data are available, there are two tactics which work. One tactic is to set the value of σ_c to a very low number and not let it vary and the another is to set σ_c to always be equal to σ_2.

In all three cases, the use of the mesoporosity calculation is deemed unsuitable. For the Danner and Wenzel data, it was clearly inappropriate since γ is theoretically zero. For the Goldmann–Polanyi data, the criterion to check if mesoporosity is consistent, as presented in the next section, failed by a large margin. For the Wisniewski and Wojsz data, when the mesoporosity calculation was turned on, the amount of capillary filling was extremely small and made an insignificant difference in the answer. Again, it is advised not to make these calculations blindly, but to examine the results, both numerically and graphically, to check for appropriateness of the calculation.

ANALYSIS OF MESOPOROSITY

The signals in the isotherm that indicate mesoporosity are the type IV and V isotherm or feature 3 in the standard plot designation, that is a positive curvature at pressure well above the threshold in the standard or χ plot. This would be a practical definition for purposes of analysis. The IUPAC definition is

pore sizes greater than 2 nm but less than 10 nm. This high value might be extended in the future due to better control and measurements for the high-pressure region.

Nearly all of the analysis of mesoporosity starts with the Kelvin–Cohan [14] formulation. Foster [15] proposed the Kelvin equation for the effect of vapor pressure on capillary rise but did not anticipate its use for very small capillaries where the adsorbate "thickness" is a significant geometrical perturbation. Cohan formulation subtracts the adsorbate "film thickness" from the radius of the pore to yield the modified Kelvin equation

$$-RT\ln\left(\frac{P}{P_s}\right) = \frac{b\gamma_{gl}V_m}{(r_p - t)} \tag{196}$$

where γ_{gl} is the gas–liquid surface tension and m a constant which depends upon the geometry of the interface. The most common values of m are:

- $m=1$ for a cylindrical interface, herein referred to as the 2-dimensional (2D) case
- $m=2$ for a spherical interface, herein referred to as the 3-dimensional (3D) case

Whether one is referring to a 2D or 3D case is not necessarily the same as the pore geometry and is embedded in whatever theory is being used. This could be a confusing point and herein it will be clearly stated as whether a 2D or 3D *interface* is being referred to. There could be intermediate cases between strictly a cylindrical interface and a spherical interface and there could be, in principle at least, cases where m is > 2. Obviously for flat surfaces $m=0$ and $P=P_s$. Therefore "P_s" will always be used for the flat surface vapor pressure. (The notation "P_o" has been used occasionally in the literature for the vapor pressure over a pure liquid with possibly a curved interface. Therefore it will be avoided here.)

Some Comments about the Standard Plot of Determining Mesoporosity

The most common method for determining the mesoporosity from a standard plot was presented in Chapter 3 in some detail. This will not be repeated here.

It should be noted that the derivation in Chapter 3 assumed a 3D form for the Kelvin–Cohan equation. In other words, the meniscus that is causing

the prefilling is a spherical meniscus with the assumption that it is very difficult to have a perfectly cylindrical pore that is open at both ends. This would seem to be the equilibrium situation and the situation upon desorption. If the metastable 2D situation should arise upon adsorption this would lead to a hysteresis. This hysteresis would yield the pressure dependance of approximately a square root proportionality. That is, given t for adsorption is approximately the same as t for desorption then:

$$\frac{P_{adsorption}}{P_s} \approx \sqrt{\frac{P_{desorption}}{P_s}} \tag{197}$$

This is only approximate since the two ts are not equal. The relationship between the two pressures may be determined using Eq. (27) in Chapter 3 since r_p is the only parameter in common between adsorption and desorption. Even χ_c can change from adsorption to desorption for a variety of reasons. This latter fact is usually ignored.

The use of the Kelvin–Cohan equation does not necessarily imply that a liquid film, with a sharp gas–liquid interface exists before commencement of capillary filling. It only implies, that given other alternatives, that the lowest Gibbs' free energy situation is for the sudden appearance of a 2D or 3D interface. Thus, a continuous correction for the surface tension before capillary filling may not be justified if the theory does not depend upon an interface before the transition. This is the case for most conventional calculations of capillary filling and χ theory is in this respect conventional.

One of the subtleties of the χ theory was ignored in Chapter 3 and that was the density variation and the change in V_m upon adsorption. The question is, "Is this correction important in the mesopore calculation?" It certainly was important for micropore analysis. The calculation for Fig. 93 yields the answer. For example, assuming $\Delta\chi_p = 3$ changes the molar volume by a little more than 3% and corresponds to the adsorption of about 1.6 monolayer equivalences. From the other perspective, a 2 nm cylindrical pore, or a 1 nm radius, for Ar adsorption would have a cutoff of 2.8 monolayer equivalences. The molar volume for this amount adsorbed would be 99.6% that of the pure liquid. Thus for most practical purposes, this correction is not necessary.

The most widely used theory for calculating the mesoporosity other than the Kelvin—Cohan method is the Broekhoff—deBoer (BdB) method. This is presented next.

The Broekhoff—deBoer Theory

The BdB theory [16] relates to the capillary filling of cylindrical pores. It makes the following assumptions:

1. The adsorbed layer is continuous with the density of the liquid phase, thus with a sharp outer boundary.
2. The chemical potential of the adsorbed layer is what determines the thickness of the film using the same functional dependence as with a flat adsorbed layer.
3. The Kelvin–Cohen equation determines the chemical potential for a curved adsorbate layer. For cylindrical pores, this is the 2D use of the equation.
4. The surface tension, γ_{gl}, of the gas–liquid (or -adsorbent) is a constant.

Given these assumptions and some rather fundamental thermodynamic relationships some equations are derived for a generalized isotherm. The isotherm function is written in terms of the gas pressure, P, and the vapor pressure over a flat surface, P_s, as

$$-RT \, \mathbf{ln}\left(\frac{P}{P_s}\right) = \mathbf{F}(t) \tag{198}$$

where $\mathbf{F}(t)$ is an arbitrary function of the layer thickness, t, that may be found either theoretically or experimentally. One need not know the theory behind $\mathbf{F}(t)$ so long as one can write a reasonably good analytical form for it. Alternately, one may write this in terms of the chemical potentials of the liquid, μ_{liq} (again over a flat surface) and the adsorbed layer μ_{ad}:

$$\mu_{liq} - \mu_{ad} = \mathbf{F}(t) \tag{199}$$

Using the following thermodynamic relationship one can obtain the equilibrium condition

$$dG\big|_{P,T} = \mu_c dn_{ad} - \mu_g dn_{ad} + \gamma_{gl} dA_{gl} \tag{200}$$

where μ_c is the chemical potential of the condensed phase flat or otherwise, μ_g the chemical potential of the adsorbent and A_{gl} the area of the adsorbate

layer–gas interface. The equilibrium condition may be obtained knowing dA_{gl}/dn_{ad}. Since what is being addressed here are cylindrical pores, the inside area of the adsorbed layer in the pore of radius r_p is given by

$$A_{gl} = 2\pi(r_p - t)l \tag{201}$$

where l is the total length of all the pores. The number of moles adsorbed is given by

$$n_{ad} = \frac{2\pi}{V_m}\left(r_p^2 - [r_p - t]^2\right)l \tag{202}$$

Differentiating both of these equations and combining one obtains

$$\frac{dA_{gl}}{dn_{ad}} = \frac{-\gamma_{gl}V_m}{r_p - t} \tag{203}$$

This is the 2D assumption since what is being considered here is the adsorbed film with a cylindrical shape. Since for equilibrium $dG|_{P,T}/dn_{ad} = 0$, then

$$\mu_c - \mu_g = \frac{\gamma_{gl}V_m}{r_p - t} \tag{204}$$

Utilizing assumption 2, that is that $\mu_{ad} = \mu_c$ and adding Eq. (199) to Eq. (204)

$$\mu_{liq} - \mu_g = \mathbf{F}(t) + \frac{\gamma_{gl}V_m}{r_p - t} \tag{205}$$

or the modified isotherm is

$$-RT\ln\left(\frac{P}{P_s}\right) = \mathbf{F}(t) + \frac{\gamma_{gl}V_m}{r_p - t} \tag{206}$$

One way of viewing this equation is to think of the chemical potential inside the adsorbed film as being the sum of the chemical potential of the gas

adsorbent plus the change in the chemical potential due to the hydrostatic pressure produced by the gas–liquid interface. This is very similar to the effect of osmotic pressure with the gas–liquid interface acting as a semipermeable membrane. Fig. 106 illustrates this schematically. The second term on the right side of Eqs. (204)–(206) is the hydrostatic correction term.

For thermodynamic stability, the condition (a minimum and not a maximum in the Gibbs' free energy change)

$$\frac{d^2G\big|_{P,T}}{dn_{ad}^2} \geq 0 \tag{207}$$

must be met. In this case the condition is stable provided

$$\frac{d\mathbf{F}(t)}{dt} + \frac{\gamma_{gl}V_m}{(r_p - t)^2} \leq 0 \tag{208}$$

Thus there could be some value of t for which the right-hand side of this equation becomes 0. This is referred to as the critical thickness, t_{cr}, and a corresponding pressure, P_{cr}, for which the layer becomes unstable. Above
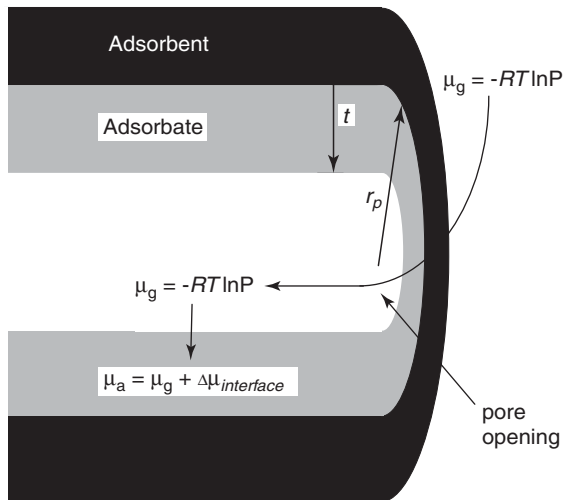

Fig. 106. The BdB model for adsorption in a cylindrical pore. The adsorbate–gas interface creates a hydrostatic pressure which changes the chemical potential of the adsorptive.

P_{cr} the condition of the 2D, i.e. a cylindrical coordinate, adsorbed layer may no longer exist and the capillary filling commences to convert to the 3D, i.e. spherical coordinate, condition. Notice that the second term of the equation must always be positive therefore the slope of $F(t)$ must be negative, that is F is a decreasing function with P. Upon examination of the definition (198) this must be the case. The question then is whether the value for $|dF/dt|$ is large enough to satisfy Eq. (208).

   If given that t_{cr} exists then one can determine the free-energy change from this value to other values by substituting into Eq. (199) and integrating:

$$\int_{t_{cr}}^{t} dG\,|_{P,T} = \int_{t_{cr}}^{t} \left[-RT \ln\left(\frac{P}{P_s}\right) - F(t) - \frac{\gamma V_m}{r_p - t} \right] dn_{ad}, \quad t \le r_p \tag{209}$$

where $\mu_c - \mu_g$ has been replaced. Converting dn_{ad} into terms of t using the pore length, l_p,

$$\Delta G =$$
$$\frac{\pi l_p}{V_m} \left\{ -RT \ln\left(\frac{P}{P_s}\right)(t - t_{cr})(2r_p - t - t_{cr}) - 2\int_{t_{cr}}^{t} F(t)(r_p - x)\,dx - 2\gamma V_m(t - t_{cr}) \right\} \tag{210}$$

For equilibrium this value of ΔG is set to 0 to obtain the desorption pressure at which the filled capillary will spontaneously revert to an adsorbed layer. Since for the filled pore $t = r_p$ this value should be different from the spontaneous capillary filling value t_c. Thus Eq. (210) becomes

$$-RT \ln\left(\frac{P}{P_s}\right) = +\frac{2\int_{t_{cr}}^{r_p} F(x)(r_p - x)\,dx}{(r_p - t_{cr})^2} + \frac{2\gamma V_m}{(r_p - t_{cr})} \tag{211}$$

This then should, according the BdB theory, yield the desorption branch. There is a very close resemblance between Eqs. (206) and (211) with the former containing the 2D form of the Kelvin–Cohan equation and the latter the 3D form. Notice that by L'Hospital's rule as $t_{cr} \to r_p$ the first term on the right-hand side will approach $F(t_{cr})$ thus yielding the 3D form.

Fig. 107 is an illustration of the capillary filling and capillary empty-ing as envisioned by the BdB theory. The difference in the filling and emp-tying geometry is the postulated reason for hysteresis. The sequence from left to right:

- just before core collapse,
- just after collapse,
- at fully filled,
- desorption at same geometry as 2,
- just before capillary emptying and
- just after emptying.

It would be instructive to show some plots of the isotherm predicted by Eq. (206) to see what this equation means. Fig. 108 shows some plots in terms of moles adsorbed for a 2, 5 and 10 nm pore radius. This calcula-tion uses the α–s plot for the function $F(t)$. At the points marked with a "✖" the critical thickness is reached and the isotherm follows the dotted lines. The point of capillary filling as predicted by Eq. (208) and the amount of capillary filling are indicated by the dashed lines. Fig. 109 shows the dependance of t and P/P_s on the pore radius. A comparison of the BdB the-ory with the Kelvin–Cohan equation, both the 2D and 3D form, is shown in Fig. 110.
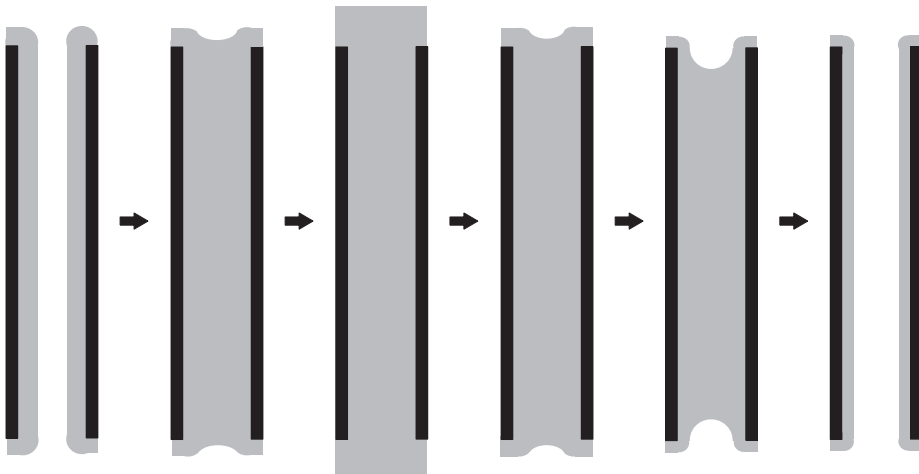
Fig. 107. The BdB model of pore filling and pore emptying.
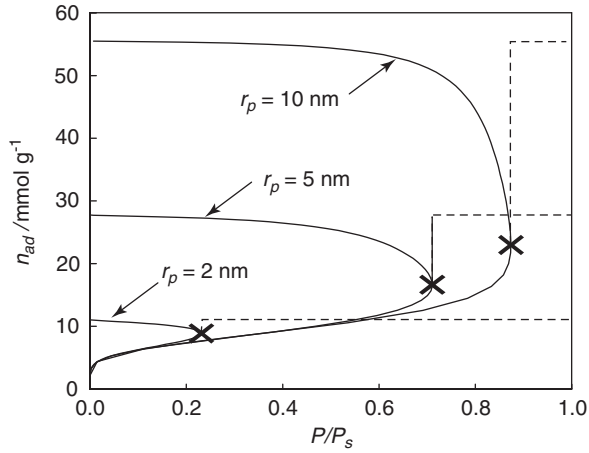
Fig. 108. The isotherms for adsorption on porous SiO_2 according to the BdB theory.
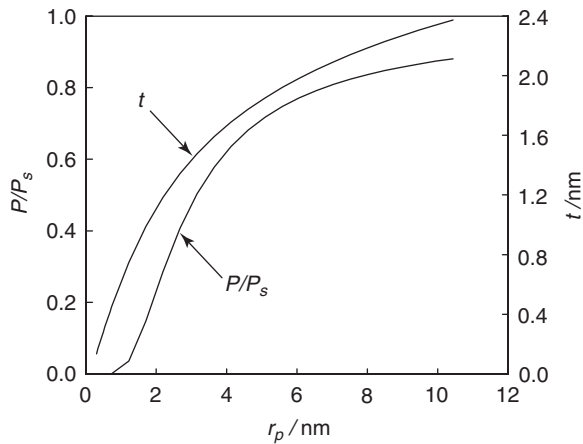
Fig. 109. The relationship between the pore radius in SiO_2 as the critical thickness and the critical relative pressure according to the BdB theory. The lines correspond to the ✖s in Fig. 108.

Several modifications have been made to the theory including proposals for the function $F(t)$ and making γ a function of t (or $r_p - t$) as well. For example, Kowalczyk et al. [17] proposed a double χ form for $F(t)$: i.e.

$$F(t) = \Pi_1 \exp(-t/\lambda_1) + \Pi_2 \exp(-t/\lambda_2) \tag{212}$$
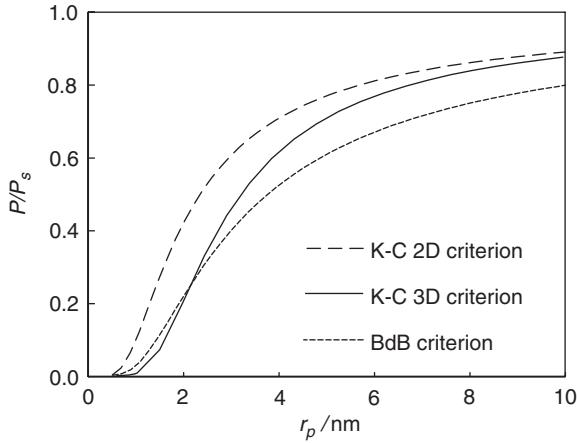
Fig. 110. Comparison of the BdB theory with the Kelvin–Cohan calculation for the switch to capillary filling. $F(t)$ uses the α–s for nitrogen on SiO_2 as the model isotherm.

where the subscripted quantities are basically parameters which are interpreted in terms of the disjoining pressure theory (see Chapter 4). Along with this equation a dependence of γ_{gl} on the core radius as proposed by Miyahara et al. [18,19] was used. This relationship was given as

$$\gamma(r_c) = \gamma_\infty \left(1 + \frac{\delta}{r_c}\right) \tag{213}$$

where $r_c = r_p - t$ and the value of δ is about the same value as the van der Waal radius. (For consistency and practical purposes, r_c and r_p are positive throughout this book.) At the low end of the mesopore range this could yield about a 40% correction for nitrogen adsorption. This is about a 10% correction for a pore radius of 3 nm.

A similar correction to γ has been calculated by Ahn et al. [20]. The calculations are rather complex but yield results similar to that derived by Tolman [21]:

$$\frac{\gamma(r)}{\gamma_\infty} = \left[1 + \frac{2\delta}{r}\right]^{-1} \tag{214}$$

which is more convenient. The values for the parameter δ are approximately the same as the diameter of the liquid molecule, i.e. the van der Waal radius.

Table 33
δ values for the Tolman equation to correct γ
for surface curvature

Liquid	δ/nm
Argon	0.314
Nitrogen	0.330
Cyclohexane	0.503
Benzene	0.461
Water	0.274

In Table 33 some values for this parameter are given. Clearly the two cor-
rections for γ_{gl} are not the same, with the latter being more complex than the
former. For liquid N_2 the first correction is about 16% for a 2 nm pore,
whereas the second one is about 50%. Whether this correction is required or
not is still a question.

The original BdB theory, due to assumption 1, cannot be applied to slit-
like pores. Indeed, the BdB theory predicts that slit-like mesopores should
behave the same as micropores with no capillary filling upon adsorption.

IS IT MICROPOROUS OR MESOPOROUS AND DOES IT MATTER?

This is an obvious question. What if one were to treat a microporous sam-
ple as a mesoporous sample or vice versa? Furthermore, how can one really
tell if the sample is microporous or mesoporous? What is precisely the
boundary between the two?

Combined Mesopore/Micropore Equation

To answer these questions, a few calculations are in order. The following
simulations are based upon the ideas presented previously for the analysis of
microporosity and mesoporosity. These two methods can be combined into one
formulation with a special interpretation for mesoporosity. Using the χ dona-
tion (again, any standard curve notation would work as well) the following has
been postulated. For a single energy of adsorption and a single pore size,

$$n_{ad} = \frac{A_s}{fA_m}\left(\Delta\chi\,\mathbf{U}(\Delta\chi) - p\,\Delta\chi_p\,\mathbf{U}(\Delta\chi_p)\right)$$
$$+ \frac{V_p}{V_m(\Delta\chi)}\mathbf{U}(\Delta\chi_p) \qquad (215)$$

where $\Delta\chi$ has the usual meaning, i.e. $\chi - \chi_c$, $\Delta\chi_p$ is the difference between the zero adsorption point and the pore-filling, i.e. $\Delta\chi_p = \chi_p - \chi_c$ and p the fractional amount that is in the pores, so that $(1-p)$ is the amount external. The molar volume of the adsorbate, V_m, could be a function of $\Delta\chi$ as shown. This possibility will be ignored. If instead of a single energy and a single pore size there is a distribution of energy, $\mathbf{D}_1$, and a distribution of pore sizes, $\mathbf{D}_2$ then the delta function that created the step function expression is replaced with the appropriate integral expressions

$$
\begin{aligned}
n_{ad} = & \int_{-\infty}^{\chi} dx \int_{-\infty}^{x} G\,\mathbf{D}_1\big(y,\langle\chi_c\rangle,\sigma_c,...\big) - H\,\mathbf{D}_2\big(y,\langle\chi_p\rangle,\sigma_2,...\big)\,dy \\
& + J \int_{-\infty}^{\chi} \mathbf{D}_2\big(y,\langle\chi_p\rangle,\sigma_2,...\big)\,dy
\end{aligned}
\tag{216}
$$

where the parameters G $(= A_s/fA_m)$, H $(= pG)$ and J (V_p/V_m) have been introduced to remove the equation from interpretation. The distributions could be any arbitrary distribution. An obvious requirement for the $\mathbf{D}$ is that the values approach 0 when the value of y approaches either $+\infty$ or $-\infty$. The question is whether anything more complicated than a PMF is justified by the precision of the data. The number of parameters in the distribution, other than position on the standard (or χ) axis, mean value and the standard deviation, is also arbitrary. Again beyond these three distribution parameters, the data usually do not justify more. All together then Eq. (216) has seven parameters. If the forms of both $\mathbf{D}$s are PMFs, then Eq. (216) on integration becomes

$$
\begin{aligned}
n_{ad} = & G\,\mathbf{Z}\big(\chi,\langle\chi_c\rangle,\sigma_c\big) - H\,\mathbf{Z}\big(\chi,\langle\chi_p\rangle,\sigma_2\big) \\
& + \frac{J}{2}\left(1 + \mathbf{erf}\left(\frac{\chi - \langle\chi_p\rangle}{s\sqrt{2}}\right)\right)
\end{aligned}
\tag{217}
$$

which is simply Eq. (182) with an added term. The function $\mathbf{Z}$ is the same as before, that is, Eq. (183). Eq. (217) could be used as a non-interpreted fit to the isotherm. Again, as with Eq. (182), the simplest method of determining the parameters is a minimum search routine.

The Interpretation of Mesopore Equation Using Standard Curve

The interpretation of Eq. (217) presented here is classical in its approach and should work for any standard curve. The χ interpretation of the standard curve is used here.

First – a practical matter. χ theory can provide some guidance for the initial estimates of the parameters. The estimates are the same as for Eq. (182) but the same advice concerning a graphical guidance apply. This latter method is the best way to get an initial estimate of J.

The interpretation of the parameters is basically the same for the mesopore analysis as it is for the micropore analysis with additional relationship with respect to the presence of the parameter J. Thus, Eq. (190) is a test for the validity of the calculation of the pore radius. Eqs. (184) and (186) yield the total surface area and the final external surface area (wall plus pore openings), respectively. Eq. (185) is modified by the addition of the parameter J:

$$V_p = V_m(H \Delta \chi_p + J)\tag{218}$$

In addition, r_p may be calculated from $\langle \chi_p \rangle$ and $\Delta\chi_p$ using the Kelvin–Cohan Eq. (196) and Eq. (194). In this case $t \neq r_p$ and is specified by Eq. (195). Converting in to χ notation,

$$r_p = \frac{2\gamma_{gl}V_m}{RT}\mathbf{e}^{\chi_p} + t\tag{219}$$

(One could solve for t in Eq. (195) and substitute into this equation and solve for r_p or as a practical matter simply leave it as is and make a circular calculation to solve for r_p).

The above analysis, which includes the last term of Eq. (217), will be referred to as the "mesopore analysis". An analysis without this last term, which is identical to the analysis for microporous materials described previously will be referred to as "micropore analysis". Essentially, the non-interpreted micropore analysis uses Eq. (217) without the last term and sets the pore radius, in place of Eq. (196) equal to t obtained from Eq. (194). (Simply doing this does *not* yield the same value for t as obtained from the mesopore analysis due to the interactions between the parameters in the fitting routine.)

It would be instructive to first examine and compare by modeling, the micropore and mesopore regions. This will answer some of the questions posed above.

The Boundary Between Mesopores and Micropores
Using the above equations, one could model how isotherm should look like as a function of pore size. The most sensitive representation is the standard
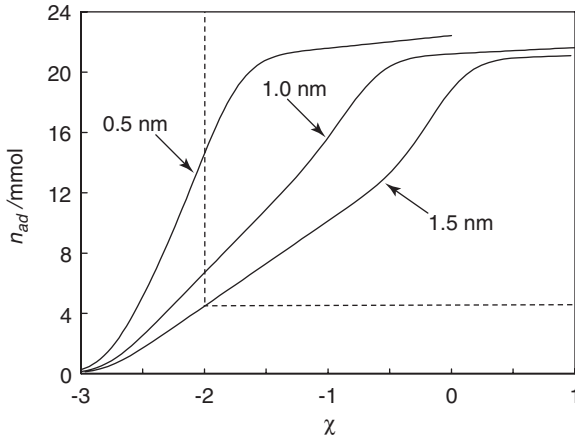
Fig. 111. Standard plot using the modeling that includes mesopores to illustrate the transition from "micropores" to "mesopores".

plot representation, whereas with the use of P/P_s some details in the low-pressure portion become obscured. In Fig. 111 are the standard plots for modeled adsorption of N_2 at 77 K on porous silica for the pore radii of 0.5, 1.0 and 1.5 nm (pore sizes 1, 2 and 3 nm). (The other input quantities are $\chi_c = -2.8$. $\sigma_c = 0.20$, $\sigma_2 = 0.25$ thus $\sigma_p = 0.15$, percent in pores = 95%, $\gamma = 8.8$ mJ m^{-2}. The surface area and χ_p were adjusted to yield the desired r_p with the pore volume held constant for scaling purposes). The sample with pore radius of 1.5 nm is from the diagram obviously mesoporous and the sample with a pore radius of 0.5 nm would obviously be declared microporous. For the 1.0 nm pore radius the answer is not so obvious even over the full range.

A common range for measurement is indicated by the dotted box in the figure which would make the 1.0 nm sample appear very much as if no mesoporosity were present.

From this one would conclude that there is a continuous transition from "mesopore" to "micropore"–the quotes indicating that this is a rather artificial definition based upon judgement. The next question is: "Does it matter in the answer?"

Does it Matter Whether to Use a Micropore or a Mesopore Analysis?

There are some complications in answering this question. First, is the question of the precision of the data. If Eq. (217) is to be fitted to the data,

the simplest method is to run a minimum search routine comparing the equation to the data. Unfortunately, such a method can get stuck in the many false minima that even very precise data provide. Graphically adjusting the input parameters to get an approximate fit before running such a routine helps. Second, if the low-pressure data are not present, leaving σ_c as a parameter is very likely to create an error. Therefore, in such cases σ_c should be set to a very low value (0 is not tolerated in the PMF) and not allow it to change. Third, data that lack the low-pressure points will make it difficult to separate the various parameters and large uncertainty arises in the final answer.

Nevertheless, it is instructive to attempt analysis on some modeled data to see what happens. In the following, the data generated for Fig. 111 are analyzed in four different ways:

1. All the data are used and the capillary filling part of the equation is used.
2. All the data are used but the capillary filling is ignored and r_p is determined as for the micropore case.
3. The higher pressure data (above $\chi = -2$) are used and the capillary filling part retained
4. The higher pressure data (above $\chi = -2$) are used and the micropore analysis is performed.

The results of this exercise for the 1.0 and 1.5 nm were very far from correct as expected. Table 34 contains the results for 0.5 nm model. Several attempts were made with differing starting approximations, which led to a large spread in the calculations for the microporous analysis assumption. Unfortunately, in the microporous analysis the fit looked graphically very good for all the fits obtained, so there does not appear to be a way to discern that between the numbers. Keeping in mind that this is with "perfect data" then for experimental data the problem must surely be worse. The mesoporous analyses works very well with the values rebounding nicely to about the same value.

Table 34

Analysis to yield r_p from modeled data (starting with $r_p = 0.50$ nm) by the two techniques and by availability of data

"Micro" (all data used)	"Meso" (all data used)	"Micro"(only $\chi \geq -2$ used)	"Meso"(only $\chi \geq -2$ used)
0.39 → 0.48 nm	0.50 nm	039 nm	0.49 nm

The answer seems to be that it does indeed make a difference whether the mesoporous portion of the analysis is used. For "microporous" samples it should be noted that the collapsing core is small compared to the amount already adsorbed in the pore; thus an error in the value for γ_{gl} does not lead to a large error in the answer. Of course, γ_{gl} needs to be approximately correct. With the more mesoporous samples the value of γ becomes more critical, but the possible dependance of γ_{gl} on t would not be a problem. An analysis of the effect of changing γ_{gl} on the answer for the pore radius obtained is given in Table 35.

The trend makes sense since the proportion of the amount in the adsorbed layer before capillary filling versus the amount of core that is filled is relatively greater for the smaller pores. This is consistent with the conclusions made above concerning the qualitative appearance of the isotherm.

Real Data Examples

So far questions have been answered using simulated data, which is fine if comparisons are made. The question remains: "How well does the method work on real data?" Not much work has been performed to answer this question. Some analysis of data by Qiao et al. [22] for adsorption of N_2 on MCM-41 porous materials has been successfully performed [23]. MCM-41 material has been described extensively in the literature since its discovery and development [24, 25]. It is a regular uniform mesoporous material for which the pore size may be varied depending upon preparation. The advantage of the specific data used is that X-ray analysis of the material was performed that yielded the packing distances between pores. With an assumption about the wall thickness between the pores, the pore radius is easily calculated.

Table 35

The effect of changing γ_{gl} on the answer for the pore radius, r_p. The answer is the answer for r_p as a percent of the original

Pore size	Percentage change in γ	
	150 (%)	75 (%)
0.50 nm	111	95
1.00 nm	111	93
1.50 nm	125	88

Table 36
Mesopore analysis of the data by Qiao et al. [22]

Sample designator	X-ray d_{100} (nm)	r_p Adsorption (nm)	Wall thickness (nm)	r_p Desorption (nm)	Wall thickness (nm)
C-10	2.87	1.00	0.87	1.03	0.81
C-12	3.25	1.23	0.78	1.26	0.73
C-14	3.56	1.40	0.77	1.41	0.75
C-16	3.87	1.58	0.71	1.58	0.70
C-18	4.24	1.82	0.60	1.78	0.68
C-22	4.88	2.10	0.69	1.95	0.97

Table 36 gives the summary of the mesopore analysis using the above method. From the mesopore analysis and the X-ray data, the wall thickness is calculated. With the exception of the desorption data for the last data set, which is designated C-22, the wall thickness is calculated to be between 0.60 and 0.87 nm, which is fairly reasonable according to the criterion of Eq. (190).

What Does Chi Theory Say about Hysteresis?
Hysteresis is undoubtedly a real phenomenon. It has been widely reported and reproducibly observed. The BdB theory and the theories that propose a switch from 2D to 3D meniscus are capable of explaining it, although whether they calculate it properly is open to question. It is unclear whether this is an experimental problem, that is a matter of kinetics, or not. χ theory does not explain hysteresis except for the following caveat. This caveat should be taken into account for any calculation that may be attempted.

Referring to the data by Qiao et al., in the untransformed isotherm there appears to be hysteresis for nearly all the samples. However in the analysis it should be noticed that the r_p for adsorption is nearly the same as that for desorption, indicating no hysteresis. Thus in the plots of n_{ad} versus $\Delta\chi$, instead of χ, the adsorption data and the desorption data coincide. This is true for all the samples except the largest pore size sample, C-22 (which interestingly enough has a pore size just exceeding the value specified by the BdB theory where one should observe hysteresis). Even for sample C-22 in the plot n_{ad} versus $\Delta\chi$ instead of χ, the hysteresis is considerably less – about half. The absence of hysteresis on a $\Delta\chi$ plot for all samples except C-22 and the decrease in the hysteresis for C-22 would indicate that the value of E_a increases from the adsorption branch to the desorption branch.
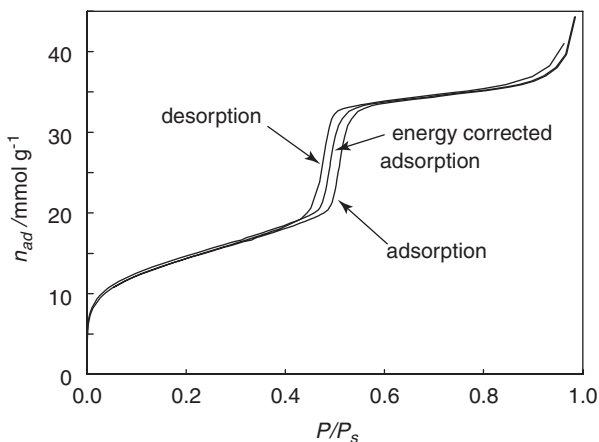
Fig. 112. The hysteresis loop for the data Qiao et al. showing the original data and the postulated energy correction for the adsorption data.

There are several explanations for this phenomenon, one of which is that the adsorption process eliminates pre-adsorbed gases which would artificially lower the adsorption energy. Adsorbed gases such as CO or H_2 are very difficult to avoid even in very good ultrahigh vacuums.

To illustrate the decreased amount of hysteresis, the data of sample C-22 for adsorption are modified by shifting the P/P_s value by an energy amount required by the difference in χ_c of the adsorption versus desorption. Thus an untransformed plot of "energy corrected adsorption" may be obtained to compare with the desorption branch. The plot so obtained along with the original adsorption and desorption data is illustrated in Fig. 112. Although this explains some of the hysteresis, it does not explain all of the hysteresis. The use of the nearly half-power relationship mentioned with respect to Eq. (197), or using 1 in place of 2 in Eq. (196), overestimates the hysteresis by a considerable amount and does not explain the total absence of hysteresis for the other samples. The BdB theory also considerably overestimates the magnitude of the hysteresis.

CONCLUSIONS

All theories of porosity require the following:
- A reliable measurement of the surface area
- A reliable standard curve against which to compare the porous materials

- A mechanism for the cutoff of adsorption for micropores
- A mechanism for the enhanced adsorption for mesopores
- An explanation for the switch-over from microporous behavior to mesoporous behavior

The first requirement is normally fulfilled using the BET equation for the low-pressure adsorption. The usual procedure is to determine the standard curve and the BET surface area associated with it and to use this standard curve to analyze the porous material. There are several problems with this:

- The linear range, deemed to yield the "correct" surface area, varies widely from adsorbate–adsorbent pairs. For some, it is not possible to find a linear range. The range of 0.05–0.35 P/P_s is appropriate for SiO_2 materials.
- For microporous materials, the actual surface area may be much larger than the surface area determined from a BET-based standard plot. This is due to the difference between the accessible surface, i.e. that not covered by filled pores, and the real surface area under the adsorbate.
- There is much controversy about the validity of the BET equation as it relates to adsorption within the liquid "film" temperature range. There are a large number of references [26] that have pointed out the weakness of the theory.
- Even if the BET yielded the correct surface area for a standard, it is very difficult to create standards that exactly mimic the surface properties of the porous material.

An alternative to the BET approach is to use the χ theory approach. The disjoining pressure approach is identical if one takes into account the factors presented in Chapter 3. χ theory is basically a sample-determined standard curve approach and as such could be reinterpreted in terms of any theory, for example with the BdB theory. With the χ theory approach, one does not need a separate standard curve; it is incorporated directly in the theory. The principal problem with χ theory is that it has not been sufficiently tested and several aspects are still in question.

For the cutoff in adsorption for microporous materials, all theories assume the same postulate, that is, the adsorption stops when the pores are fully filled. An exception to this is the problem associated with the change in density of the adsorbate with the amount adsorbed. This problem was first discovered by Dubinin et al. [27] and seems to be predicted by χ theory [28]. If this were the case, then the values for the microporosity listed in tables of micropore radii would be quite low.

The enhanced filling associated with mesoporosity is dependent on all cases upon the Kelvin equation in some way. Some of the theories, such as the original Cohan formulation or the BdB theory, assume a fully formed liquid film with a sharp liquid–gas interface.

REFERENCES

[1] IUPAC Manual of Symbols and Terminology, Appendix 2, part 1, Colloid and Surface Science, Pure Appl. Chem., 31 (1972) 578.

[2] S. Brunauer, L.S. Deming, W.E. Deming and E. Teller, J. Am. Chem. Soc., 60, (1938) 309.

[3] M.M. Dubinin, E.D. Zaverina and L.V. Radushkevich, Zhur. Fiz. Khim., 12 (1947) 1351.

[4] M.M. Dubinin and V.A. Astakhov, Izv. Adad. Nauk SSSR, Ser. Khim., 1971 (1) (1971) 5–17.

[5] J.B. Condon, Micropor. Mesopor. Mater., 38 (2000) 359.

[6] R.P. Danner and L.A. Wenzel, AlChE J., 32 (1986) 1263.

[7] A. Wheeler, Catalysis, Vol II, p. 118, Reinhold, NY, 1955.

[8] C.G. Shull, J. Am. Chem. Soc., 79 (1948) 1410.

[9] E.P. Barrett, L.G. Joyner and P.H. Halenda, J. Am. Chem. Soc., 73 (1951) 373.

[10] R.W. Cranston and F.A. Inkley, Adv. Catal. 9 (1957) 143.

[11] J.B. Condon, Langmuir, 17 (2001) 3423.

[12] F. Goldmann and M. Polanyi, Physikal. Chem., 132 (1928) 321.

[13] K.E. Wisneiwski and R. Wojsz, Zeolites, 12 (1992) 37.

[14] L.H. Cohan, J. Am. Chem. Soc., 60 (1938) 433.

[15] A.G. Foster, Trans. Faraday Soc., 28 (1932) 645.

[16] J.C.P. Broekhoff and J.H. deBoer, J. Catal., 9 (1967) 8.

[17] P. Kowalczyk, M. Jaroniec, A.P. Terzyk, K. Kaneka and D.D. Do, Langmuir, 21 (2005) 1827.

[18] M. Miyahara, H. Kanda, T. Yoshioka and M. Okazaki, Langmuir, 16, (2000) 4293.

[19] H. Kanda, M. Miyahara, T. Yoshioka and M. Okazaki, Langmuir, 16 (2000) 6622.

[20] W.S. Ahn, M.S. Jhon, H. Pak and S. Chang, J. Coll. Interf. Sci., 33 (1972) 605.

[21] R.C. Tolman, J. Chem. Phys., 17 (1949) 333.

[22] S.Z. Qiao, S.K. Bhatia and X.S. Zhao, Micropor. Mesopor. Mater., 65 (2003) 287.

[23] J.B. Condon, Micropor. Mesopor. Mater., 84 (2005) 105.

[24] J.S. Beck, J.C. Vartuli, W.J. Roth, M.E. Leonowicz, C.T. Krege, K.D. Schmitt, C.T. -W. chu, D.H. Olson, E.W. Sheppard, S.B. McCullen, J.B. Higgins and J.L. Schlenker, J. Am. Chem. Soc., 114 (1992) 10834.

[25] D. Zhao, Q. Huo, J. Feng, B.F. Chmelka and G.D. Stucky, J. Am. Chem. Soc., 120 (1998) 6024.

[26] G. Halsey, J. Chem. Phys., 16 (1948) 931.

[27] M.M. Dubinin, E.G. Zhukovskaya and K.O. Murdmaa, Ivza. Acad. Nuak USSR, Ser. Khim 1966 (1966) 620.

[28] J.B. Condon, Micropor. Mesopor. Mater., 38 (2000) 359.

This page intentionally left blank

Chapter 7

Density Functional Theory

INTRODUCTION

Density functional theory (DFT) as applied to adsorption is a classical statistical mechanic technique. For a discussion of DFT and classical statistical mechanics, with specific applications to surface problems, the text book by Davis [1] is highly recommended. (Here the more commonly used symbol for number density $\rho(r)$ is used. Davis uses $n(r)$ so one will have to make an adjustment for this text.) The calculations at the moment may be useful for modeling but are questionable for analysis with unknown surfaces. The reason for this is that the specific forces, or input parameters, required for a calculation are dependent upon the atoms assumed to be present on the surface. For unknown surfaces, a reversion to the use of the Brunaver, Emmett and Teller (BET) equation is often employed.

DFT and for that matter the Monte Carlo techniques are methods for calculating the modeling of adsorption given certain assumptions. These assumptions usually include site-wise attractions between the surface atoms and the adsorbate molecules and attractions between the adsorbate molecules. Interaction potentials and surface spacings are assumed. The configuration of the adsorbate molecules are adjusted to yield a minimum in the overall free energy of the system. In DFT this adjustment in configuration is performed by adjusting the number density as a function of distance from the surface, primarily.

It is difficult to find a complete explanation of how DFT works in the literature, so in the following an attempt is made to explain the technique. There are several parts that need to put together in DFT calculations, so it may seem that the sections reviewed here are not related until they are finally compiled.

WHAT IS A FUNCTIONAL?

First the question is: "What is a functional?" One may think of a functional as a function of a function. Thus, one writes $F(\mathbf{y}(r))$ where y is a

function of the vector r and F depends upon y. One might ask what is the difference then between a function and a functional since the mapping of r to the final values of F is like a function? Indeed, if the function $\mathbf{y}$ remained constant, then F would be simply a function but this is not necessarily the case with functionals. Consider an example from quantum mechanics. The expectation value for a particular physical quantity is given by a functional which contains the wave functions in the functional. For example, using 1 dimension for purposes of illustration, the energy is given by

$$E_n = \frac{\int \psi_n^*(x)\mathbf{H}\psi_n(x)\,dx}{\int \psi_n^*(x)\psi_n(x)\,dx} \tag{220}$$

The subscripts n are more than just numbers; they change the function ψ and not simply its argument x. For another example, examine the functional

$$F = \int_0^1 (\mathbf{y}(x)+x)\,dx \tag{221}$$

Clearly, F has a definite value and can be determined provided $\mathbf{y}$ is known. One would not, however, expect to get the same value for F for different functions of $\mathbf{y}$. Consider the series $\mathbf{y} = x^n$ as an example. The values obtained for F for some of the functions $\mathbf{y}$ are given in Table 37.

   The function inside the functional need not be an analytic function. For example, what approximately is the average age for all Iowans given the

Table 37
The values of the functional, F, from Eq. (221) given the function $\mathbf{y}$

$\mathbf{y}=x$, $F=1$
$\mathbf{y}=x^2$, $F=5/6$
$\mathbf{y}=x^3$, $F=3/4$
$\mathbf{y}=x^4$, $F=7/8$
$\mathbf{y}=x^5$, $F=2/3$

number of people who have had their first, second, third, etc. birthday? This could be approximated by

$$F = \sum_i i n_i \Big/ \sum_i n_i$$

(222)

where i is the last birthday passed and n_i are the number of people who have obtained that ith birthday status. Obviously, this functional will vary with time as the distribution in n changes. Thus a functional may be dependent upon an arbitrary function, even a digitally specified function as is normally the case for the density distribution for adsorbate molecules. Notice that for the birthday functional the size of the population is not relevant in the answer, which has led to the idea of statistical sampling, i.e. given a sufficiently large random sample one can get a good estimate of F without sampling the entire population.

The challenge in modeling adsorption is to first construct a functional of number density of the adsorbed molecule that is capable of calculating the free energy of the system. The density, which is a function of position, is then adjusted to minimize this free energy.

THE FUNCTIONAL DERIVATIVE

One of the steps in DFT will be to find the most probable arrangement, i.e. the most probable physical distribution of the adsorbate molecules. Assuming one is able to write the free energy as a function of the distribution then minimizing this energy by rearranging the distribution will solve the entire adsorption problem. Between the distribution of where the molecules are, referred to as the density distribution, the free energy is the construction of a model to relate the two. Irrespective of the model proposed, the free energy will be a functional of the density and the minimization will require a type of derivative. This derivative is referred to as a functional derivative.

How does one minimize or, for that matter, finds other extrema, of a functional? Referring to the functional as $F(\mathbf{y}(x))$ the question is how are total changes of $\mathbf{y}$ for the entire range of x (from a to b) going to change F. Thus the entire range of x is to be considered and if one were to select probe values of x for this, one would add these up so that

$$F(\mathbf{y}(x) + \varepsilon(x)) = \sum_{i \ni a < x < b} \frac{\partial F(\mathbf{y}(x_i))}{\partial y_i} \varepsilon(x_i)$$

(223)

with ε being a small incremental change in the function $\mathbf{y}$. To make this a continuous expression in place of a sum we can make the increments between the x_i to be of constant size and change the sum to an integral. (Note the following may not be rigorous but should give a "feel" for what the functional derivative is.) Define another functional $G(\mathbf{y}, x)$ such that

$$F = \int_a^b G(\mathbf{y}, x)\, dx \tag{224}$$

Then,

$$F(\mathbf{y}(x) + \varepsilon(x)) = \int_a^b G(\mathbf{y}(x) + \varepsilon(x), x)\, dx \tag{225}$$

Expanding G

$$F(\mathbf{y}(x) + \varepsilon(x)) = \int_a^b \left[G(\mathbf{y}(x), x) + \frac{\delta G}{\delta \mathbf{y}}\delta \mathbf{y} + \cdots \right] dx \tag{226}$$

where the $\delta \mathbf{y}$ is related to ε. Evaluating the first term of the integral, which is simply $F(\mathbf{y}(x))$, and subtracting this from the left-hand side, thus making this dF :

$$dF = \int_a^b \frac{\delta G}{\delta \mathbf{y}}\delta \mathbf{y}\, dx \tag{227}$$

Since a limit is taken to obtain dF $(\lim \varepsilon \to 0)$ the higher terms of G may be ignored. The functional $\delta G/\delta \mathbf{y}$ is referred to as the *functional derivative* of F and is simply represented by the notation $\delta F/\delta \mathbf{y}$ rather than using a new letter. One important property of a functional derivative is obtained from the mathematics involved with Euler–LaGrange relationships. If F is of the form

$$F(\mathbf{y}(x)) = \int G(\mathbf{y}(x), x)\, dx \tag{228}$$

that is with G being a function of only x and $\mathbf{y}$, then the functional derivative of F is readily obtained by

$$\frac{\delta F}{\delta \mathbf{y}(x)} = \frac{\partial G(\mathbf{y}(x), x)}{\partial \mathbf{y}} \tag{229}$$

By setting $\delta F/\delta \mathbf{y} = 0$ one should obtain the extrema for the variation of F as a function of $\mathbf{y}$ as evaluated for the entire range from a to b. As with functions, whether a particular extremum is a local minimum, maximum or a (vertical) inflection point may be determined by the second and third derivatives.

The extension of the functional to higher dimensions follows the same principles. For n classical particles, one can construct a functional describing the positions and velocities of all the particles, in which case there would be $6n$ dimensions.

CORRELATION FUNCTIONS

A well-known relationship in statistics is if two sets of observations are independent of each other then the variances are additive. However, if they are not, then there is what is referred to as a correlation between the observations. In terms of probability this can be expressed as follows.

Given a probability that particle #1's position is at the coordinate position $\mathbf{r}_1$, i.e., $P\{\mathbf{r}_1\}$ regardless of the position of all the other particles and likewise for particle #2 at position $\mathbf{r}_2$, i.e. $P\{\mathbf{r}_2\}$, if they are independent of each other then the combined probabilities, $P\{\mathbf{r}_1, \mathbf{r}_1\}$, is equal to

$$P\{\mathbf{r}_1, \mathbf{r}_2\} = P\{\mathbf{r}_1\} \, P\{\mathbf{r}_2\} \tag{230}$$

If this is not true, then there is a correlation between the two probabilities designated by $g(\mathbf{r}_1, \mathbf{r}_2)$ defined as

$$P\{\mathbf{r}_1, \mathbf{r}_2\} = P\{\mathbf{r}_1\} \, P\{\mathbf{r}_2\} \, g(\mathbf{r}_1, \mathbf{r}_2) \tag{231}$$

The function g is referred to as the (two-body) *correlation function*. It is convenient to define a number density by the following. The number density, $\rho\{\mathbf{r}_1\cdots\mathbf{r}_M\}$, for M particles in a system of N total particles is

$$\rho\{\mathbf{r}_1\cdots\mathbf{r}_M\} = \frac{N!}{(N-M)!} P\{\mathbf{r}_1\cdots\mathbf{r}_M \mid N\} \tag{232}$$

Obviously, the number density inspecting just one particle is $NP\{\mathbf{r}_1\}$. Since N is normally very large,

$$\rho\{\mathbf{r}_1,\mathbf{r}_2\} = \rho\{\mathbf{r}_1\}\,\rho\{\mathbf{r}_2\}\,g(\mathbf{r}_1,\mathbf{r}_2) \tag{233}$$

The velocity components of P have no cross-terms where the velocity of one component depends directly on another particle (i.e. $\frac{1}{2}\,m_1 v_1^2$, for example has no sub 2, etc., term and the kinetic energies are additive in the exponent of P) and therefore cancel.

Determining of g is very important. Given the function g and the interparticle and external potentials for the entire system in question, one may calculate all of the thermodynamic functions and $\rho(\mathbf{r})$.

If one were to know g for the entire system in question (including its dependence as a function of position) and the distribution of molecular velocities or kinetic energies (using the Maxwell distribution since what is referred to here is classical), then all thermodynamic functions can be determined.

A QUICK TRIP THROUGH SOME PARTITION FUNCTIONS

In calculations of statistical mechanics, it is only the two-body correlations which are important, although there may be many particles that have an influence upon a particular particle. The reason for this is simply that the forces acting upon a body from multiple directions are additive in a vector sense. Since the force is the divergence of potential energy, the calculated potential energies generated from the particles are also additive at each point in space. Or for forces, $\mathbf{F}$, and potential energies, u,

$$\begin{aligned} \mathbf{F}_j &= \sum_i \mathbf{F}_{i,j}, \ \text{ thus, } \ \nabla u_j = \sum_i \nabla u_{i,j} \\ &\text{and therefore } \ u_j = \sum_i u_{i,j} + c \end{aligned} \tag{234}$$

where c is the inevitable arbitrary offset for potential energies. Here the index i,j indicates the quantity expected with only particles i and j are present, and

the index j indicates the total force or potential on the particle labeled "j". Thus, only pair-wise interactions and correlations are of importance. (The vectors $\mathbf{F}$ above all have the same coordinate system. The most convenient, of course, would be with the origin at the center of particle j.)

Using very simple arguments (for most this is simply a review for orientation purposes. For a more thorough and rigorous explanation see, for example, Denbigh [2]), one can relate probabilities to energy states. In the following the probability is in a general fashion related to the energy state, that is, $P\{E_i\} = f(E_i)$, where $P\{E_i\}$ is the probability of a particle being in designated state which has the energy E_i. For two isothermal bodies of constant volume that are in contact the probabilities are multiplicative. Furthermore, the first law of thermodynamic dictates that the total energy for the overall probability $P\{E_i + E_j\}$ is simply the sum of individual energies, $E_i + E_j$. Thus,

$$P\{E_i + E_j\} = P\{E_i\}\, P\{E_j\} \tag{235}$$

Therefore, since Ps are real they must be of the form

$$P\{E_i\} = C_i \mathrm{e}^{\beta E_i}, \;\; P\{E_j\} = C_j \mathrm{e}^{\beta E_j}$$
$$\text{and } \; P\{E_i + E_j\} = C_{ij}\mathrm{e}^{\beta(E_i + E_j)} \tag{236}$$

β and the Cs are arbitrary constants. Since the sum of all probabilities is 1, i.e. $\sum P_i = 1$, the values for the Cs are given by

$$C = \frac{1}{\sum\limits_i \mathrm{e}^{\beta E_i}} \equiv \frac{1}{Q} \tag{237}$$

The normalizing factor Q is referred to as the *partition function*. Further arguments relating these relationships to thermodynamics by analogy reveals that $\beta = -kT$ (or RT on a per mole basis).

Partition functions in general can usually be separated into separate multiplicative parts, such as rotational, vibrational, electronic and translational. For the following discussions, the internal portions, that is vibrational and electronic, are being ignored and the molecules in question are assumed to be spherically symmetrical, or nearly so, so the rotational portion is also ignored.

Examining the classical notation, the probability that N particles will have the positions $\mathbf{r}_1$ for particle #1, $\mathbf{r}_2$ for particle #2,$\cdots$ $\mathbf{r}_N$ for particle #N and velocities $\mathbf{v}_1$ for particle #1, $\mathbf{v}_2$ for particle #2,$\cdots$$\mathbf{v}_N$ for particle #N (or more precisely #1 between $\mathbf{r}_1$ and $d^3\mathbf{r}_1$, etc.) is designated by

$$P\{\mathbf{r}_1\cdots\mathbf{r}_N, \mathbf{v}_1\cdots\mathbf{v}_N\} = \frac{e^{-H(\mathbf{r}_1\cdots\mathbf{r}_N,\mathbf{v}_1\cdots\mathbf{v}_N)/kT}}{\int\cdots\int e^{-H(\mathbf{r}_1\cdots\mathbf{r}_N,\mathbf{v}_1\cdots\mathbf{v}_N)/kT}\prod_{i=1}^{N}d^3\mathbf{r}_i d^3\mathbf{v}_i} \tag{238}$$

where H is the total of the classical potential and kinetic energies (Hamiltonian) and the $\mathbf{r}$s and $\mathbf{v}$s inside the integrals are dummy variables that are integrated over all space and velocity, versus the specific $\mathbf{r}$s and $\mathbf{v}$s in the numerator. The denominator of this expression is a normalizing factor so that all the singular probabilities or combinations of probabilities that would include all the particles add up to 1, the certainty probability. For the classical system, i.e. which uses continuous variation in $\mathbf{r}$ and $\mathbf{v}$ versus states, the summation for the partition function is replaced by an integral

$$Q = \int\cdots\int e^{-H/kT}\,d^3 r^N \quad \left(\text{defining }\ d^3 r^N \equiv \prod_{i=1}^{N}d^3\mathbf{r}_i\right) \tag{239}$$

In general, the total energy may be separated into velocity-(kinetic) and position-dependent (potential) portions yielding a product in the integrals in equation. Thus,

$$\int\cdots\int e^{-(1/kT)\left(1/2\sum_{i=1}^{N}m_i v_i^2 + \sum_{i=1,j=i+1}^{N}u_{ij}\right)}d^3 r^N d^3 v^N$$
$$\equiv \int\cdots\int e^{-(1/kT)\left(1/2\sum_{i=1}^{N}m_i v_i^2\right)}d^3 v^N \int\cdots\int e^{-(1/kT)\left(\sum_{i=1,j=i+1}^{N}u_{ij}\right)}d^3 r^N \tag{240}$$

The second term of this equation is defined as the *configuration partition function* for N particles, Z_N:

$$Z_N \equiv \int\cdots\int e^{-(1/kT)\left(\sum_{i=1,j=i+1}^{N}u_{ij}\right)}d^3 r^N \tag{241}$$

In similar fashion, one may define a configuration probability distribution function for particles 1 through S in a total population of N particles:

$$P\{\mathbf{r}_1\cdots\mathbf{r}_S \mid N\} = \frac{\int_{S+1}\cdots\int_N \exp\left(-\frac{1}{kT}\sum_{i=S+1, j=i+1}^{N} u_{ij}\right) d^3 r^{N-S}}{Z_N} \tag{242}$$

(In Eqs. (240) and (242) the factors which are obtained from the kinetic energy cancel since

$$\int \exp\left(-\frac{m v_i^2}{2kT}\right) d^3 v_i = \left(\frac{2\pi kT}{m}\right)^{3/2} .) \tag{243}$$

Of interest in adsorption are systems that are open, that is where particles are able to move with a certain over-pressure. To take this into account, one could imagine that energy is brought in an out of the system by pig-backing on particles. (Again this is not rigorous. Most readers are probably already familiar with the grand canonical partition function anyway.) With this in mind, one modifies Eqs. (238) and (239) to add a term $N\mu/kT$ to the exponents. A similar normalizing factor to Eq. (240) is obtained :

$$\Xi = \int\cdots\int e^{-1/2\sum_i m\mathbf{v}_i^2 + \sum_{i,j>i} u_{in}(\mathbf{r}_i-\mathbf{r}_j) + \sum_i u_{ex}(\mathbf{r}_i) + \frac{N\mu}{kT}} d^3 r^N d^3 v^N \tag{244}$$

which is the grand partition function. In this function the potential energy due to external force has been added by using the symbol u_{ex} to distinguish it from the potential energy due to inter-particle forces which is designated by u_{in}. The density distribution for m particles from a population of N particles in an open system if thus given by

$$\rho\{\mathbf{r}_1\cdots\mathbf{r}_m\} = \sum_{N=m}^{\infty} \frac{1}{(N-m)!\,\Xi}$$
$$\int\cdots\int e^{-1/2\sum_i m\mathbf{v}_i^2 + \sum_{i,j>i} u_{in}(\mathbf{r}_i-\mathbf{r}_j) + \sum_i u_{ex}(\mathbf{r}_i) + \frac{N\mu}{kT}} d^3 r_{m+1}\cdots d^3 r_N \tag{245}$$

DIRECT CORRELATION FUNCTIONS

The equation for a non-ideal gas could be written as the ideal gas equation plus additional terms. The chemical potential could likewise be written as

$$\mu = -kT \ln\left[Q_{\text{int}} \left(\frac{2\pi MRT}{h^2} \right)^{3/2} \right] + u_{ex}(\mathbf{r}) - kT \ln(\rho(\mathbf{r})) + C^{(1)}(\mathbf{r}) \qquad (246)$$

where $C^{(1)}(\mathbf{r})$ is the correction factor to the ideal gas chemical potential and is referred to as the singlet direct correlation function. $C^{(1)}(\mathbf{r})$ is related to Eq. (245) which yields the direct correlation function by functional derivatives as demonstrated below. A functional φ is defined as

$$\varphi(\mathbf{r}) = u_{ex}(\mathbf{r}) - \mu \qquad (247)$$

Using Eq. (245) one can demonstrate that

$$\rho\{\mathbf{r}\} = -kT \frac{\delta \ln \Xi}{\delta \varphi(\mathbf{r})} \qquad (248)$$

and

$$-kT \frac{\delta \rho\{\mathbf{r}\}}{\delta \varphi(\mathbf{r}')} = (kT)^2 \frac{\delta^2 \ln \Xi}{\delta \varphi(\mathbf{r}')\delta \varphi(\mathbf{r})} = \rho\{\mathbf{r},\mathbf{r}''\} - \rho\{\mathbf{r}\}\rho\{\mathbf{r}'\} + \rho\{\mathbf{r}\}\delta(\mathbf{r}'-\mathbf{r}) \qquad (249)$$

where the notation $\delta()$ represents the Dirac delta function. Using the functional derivative chain rules and rearranging one ends up with the following equation:

$$\frac{\delta \varphi(\mathbf{r})}{\delta \rho\{\mathbf{r}'\}} = -kT \left[\frac{\delta(\mathbf{r}-\mathbf{r}')}{\rho\{\mathbf{r}\}} + C^{(2)}(\mathbf{r},\mathbf{r}') \right] \qquad (250)$$

where $C^{(2)}$ includes several ρ terms and is referred to as the *direct correlation function*. On the other hand, by taking the functional derivative of (245) with respect to $\rho(\mathbf{r})$ one obtains

$$\frac{\delta\varphi(\mathbf{r})}{\delta\rho\{\mathbf{r}'\}} = -kT\left[\frac{\delta(\mathbf{r}-\mathbf{r}')}{\rho\{\mathbf{r}\}} + \frac{\delta C^{(1)}(\mathbf{r})}{\delta\rho\{\mathbf{r}'\}}\right] \tag{251}$$

so it is obvious that

$$C^{(2)}(\mathbf{r},\mathbf{r}') = \frac{\delta C^{(1)}(\mathbf{r})}{\delta\varphi(\mathbf{r}')} \tag{252}$$

With a few mathematical manipulations and the definition of g given in Eq. (233), one can obtain the equation

$$g(\mathbf{r},\mathbf{r}')-1 = C^{(2)}(\mathbf{r},\mathbf{r}') + \int C^{(2)}(\mathbf{r},\mathbf{r}'')\rho(\mathbf{r}'')\left[g(\mathbf{r}',\mathbf{r}'')-1\right]d^3\mathbf{r}'' \tag{253}$$

This equation is known as the Ornstein–Zernicke equation and if one were able to solve it, all the thermodynamic quantities, along with the density profiles, etc., would be known. To do so, $C^{(2)}$, or alternatively $C^{(1)}$, is required at least as a function of the other functions in Eq. (253).

The Percus–Yevick approximation uses $C^{(2)}=g[1\text{-}\exp(u_{in}/kT)]$ to obtain the physical quantities of a homogeneous fluid. Before examining this and the Carnahan–Starling (CS) approximation for hard spheres, some manipulations for one-dimensional (1D) rods is presented to get a feel for the methods.

THE HARD-ROD APPROXIMATIONS

The reason for studying the hard-rod approximations is to obtain some qualitative intuition of the consequences of various assumptions. By simplifying to one dimension, rather than three dimensions, the mathematics is simpler, albeit still messy in some places. More than one type of particle can also be included. To make the following discussion simple, only two molecular diameters will be assumed, a_1 and a_2 for species 1 and 2, respectively.

The canonical partition function is given as

$$Q_N = \frac{\int_{x=0}^{L} \cdots \int_{x=0}^{L} e^{-\frac{u(x_1 \cdots x_2)}{kT}} dx_1 \cdots dx_N}{N_1! N_2! \Lambda_1 \Lambda_2}$$

$$\text{where } \Lambda_{1\,or\,2} = \left(\frac{h^2}{2\pi m_{1\,or\,2} kT}\right)^{1/2} \text{ and } u(x) = \begin{cases} \infty, & |x| < d \\ \infty, & |x| > d \end{cases} \tag{254}$$

where d is the distance $(a_1+a_2)/2$, $(a_1+a_1)/2$ of $(a_2+a_2)/2$, depending upon which is appropriate and L the length of the 1D box which contains these particles. The integral in the numerator of this equation is the configuration partition function, Z_N. Given the conditions with respect to u, i.e. the hard-rod conditions, this can be simplified to

$$Z_N = (L - N_1 a_1 - N_2 a_2)^N \tag{255}$$

For the open system, one needs the grand canonical partition function or

$$\Xi = \sum_{N_1=0}^{\infty} \sum_{N_2=0}^{\infty} e^{-(N_1\mu_1 + N_2\mu_2)/kT} Q_N \tag{256}$$

or, using the above considerations

$$\Xi = \sum_{N_1=0}^{\infty} \sum_{N_2=0}^{\infty} \frac{e^{-(N_1\mu_1 + N_2\mu_2)/kT}}{N_1! N_2! \Lambda_1^{N_1} \Lambda_2^{N_2}} (L - N_1 a_1 - N_2 a_2)^N \, \mathrm{U}(L - N_1 a_1 - N_2 a_2) \tag{257}$$

The unit step function, **U**, is inserted to account for the obvious fact that the total length of the rod cannot exceed the length of the box. For each individual N_1 and N_2 the probability, $P\{N_1, N_2\}$ is

$$P\{N_1, N_2\} = \frac{1}{\Xi} \frac{e^{-(N_1\mu_1 + N_2\mu_2)/kT}}{N_1! N_2! \Lambda_1^{N_1} \Lambda_2^{N_2}} (L - N_1 a_1 - N_2 a_2)^N \, \mathrm{U}(L - N_1 a_1 - N_2 a_2) \tag{258}$$

The 1D pressure, P,[1] is obtained from Ξ by analogy to the 3D case, that is the length, L, replaces the volume; so

$$P = kT \left(\frac{\partial \ln \Xi}{\partial L} \right)_{T,\mu_1,\mu_2} \tag{259}$$

or,

$$P = \frac{NkT}{L - N_1 a_1 - N_2 a_2} \quad \text{provided } L > N_1 a_1 + N_2 a_2 \tag{260}$$

The extension to more than two molecular species should be clear from the above by simply adding additional terms for species 3, 4, etc. It is easy to model the above on a spread sheet. To obtain an idea of what this would look like, consider the case of only one species. For the probabilities as a function of the distance, L, Eq. (258) becomes

$$P\{N\} = \frac{1}{\Xi} \frac{e^{-N\mu/kT}}{N! \Lambda^N} (L - Na)^N \, U(L - Na) \tag{261}$$

The number density is

$$\rho = \sum_{N=0}^{\infty} \frac{NP\{N\}}{L} \tag{262}$$

and the total 1D pressure would be

$$P = \sum_{N=0}^{\infty} \frac{NkT}{L - Na} \tag{263}$$

From these equations one can easily calculate the profiles of these quantities. The results of these calculations are shown in Figs. 113–115. The values for

---

[1] The IUPAC rule for italicing pressure is being broken here to distinguish between probalility P{ } and pressure P.
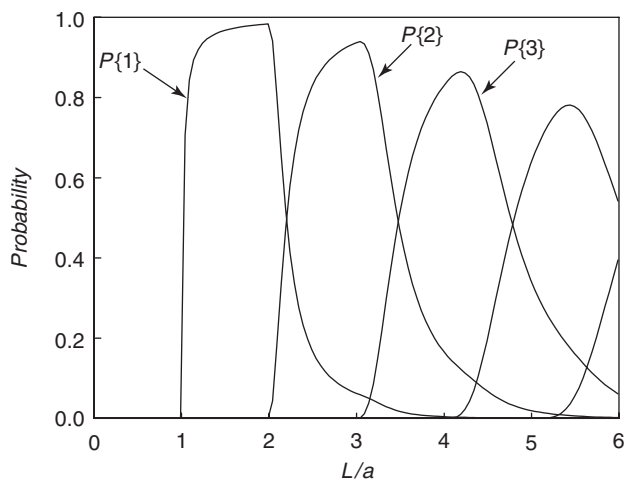
Fig. 113. Probabilities for the number of layers to be 1, 2, 3, etc. for the hard-rod calculation as a function of layer thickness.
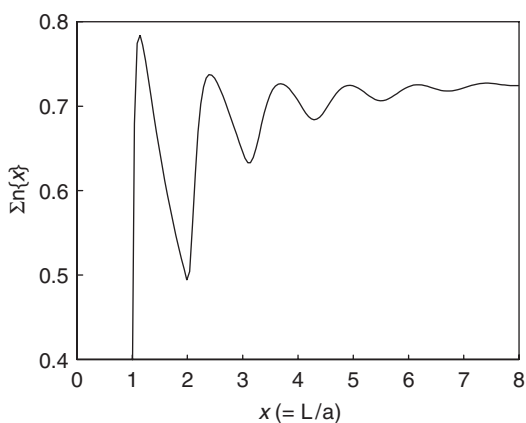

Fig. 114. Number density (total) for the hard-rod case as a function of thickness.

Λ and kT are arbitrary and scaled for clarity. These figures represent the various quantities as a function of layer thickness and not a distance between confining walls. The extension to multiple adsorbates is obvious from the above equations but requires some little more calculation since for a total of N particles there may be several combinations for N_1 and N_2.
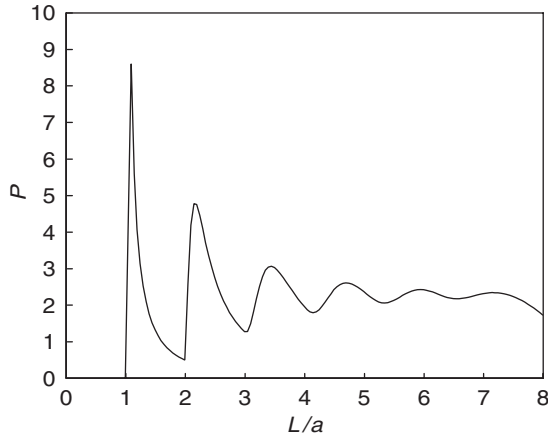
Fig. 115. 1D pressure for the hard-rod model as a function of thickness.

HARD RODS BETWEEN TWO WALLS

Another relatively easy modeling is for hard rods confined between two walls. The mathematics is a little messier and will not be completely given here (see Davis [1] or other statistical mechanic books). The modeling can also include an external field, which is also instructive. Using y and z for the position of the walls, Q, the canonical partition function for this case is

$$Q_N = \frac{\int_y^z \cdots \int_y^z \exp\left(-\sum_{i>j=1}^N \frac{u_{ij}(x_1 \cdots x_2)}{kT} - \sum_{i=1}^N \frac{v_i(x_i)}{kT}\right) dx_1 \cdots dx_N}{N_1! N_2! \Lambda_1 \Lambda_2} \tag{264}$$

With a considerable amount of reworking, a reformulation of this is obtained in what is referred to as the p formulation. The p formulation separates the solution into two solutions, one from each wall. The solutions are

$$p_\pm(x) = \sum_i \mathbf{w}_i(x \pm a_i/2)\, e^{\mp \int_x^{x \pm a_i} p_\pm(z)\,dz} \tag{265}$$

with the function $\mathbf{w}_i$ for the ith size rod given by

$$\mathbf{w}_i(x) = \frac{e^{\mu_i + v_i(x)/kT}}{\Lambda_i} \tag{266}$$

The number density for the ith size rod is obtained from

$$\rho_i(x) = \mathbf{w}_i(x)\exp\left(-\int_{-\infty}^{x}[p_+(z + a_i/2) - p_-(z - a_i/2)]dz\right) \tag{267}$$

The solution to these equations is rather messy because of the shifts in x that are required. Notice that in Eq. (265) there is a shift from $x \pm a_i/2$ to x. Numerical techniques are obviously called for to perform this calculation. Restricting the calculation to one-sized rod is relatively simple for a spreadsheet calculation. Fig. 116 shows a series of calculations for various slit widths (varying distance between the walls) with the chemical potential, temperature held constant and the externally imposed potential, $v(x)$, set to zero. For this calculation, one wall was held as $x=0$ and the other wall was allowed to move. Since the center of the rod cannot approach any closer to the fixed wall than the distance $a/2$, n is zero up to this point. A similar comment is in order for the wall that is allowed to move.
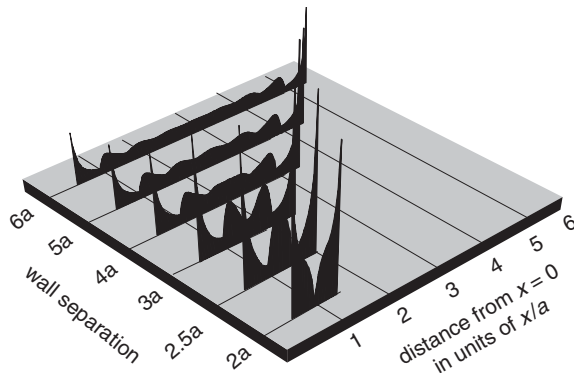

Fig. 116. Number density as a function of slit width for one type of rod with a length of a.
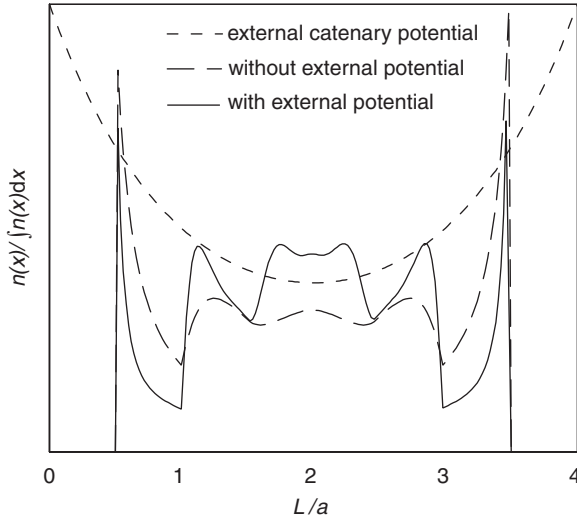
Fig. 117. The effect of an external field on the number distribution.

With the above equations it is simple to add in an external potential to see how the adsorption is affected. In Fig. 117 a catenary potential has been added, that is

$$u_{ex}(x) = c\left(e^{-bx} - e^{-b(L-x)}\right) \tag{268}$$

As one would expect, the density is suppressed at the walls and enhanced in the middle with such a field present.

The hard-rod modeling should not be taken too seriously as reflecting the situation in adsorption other than in a qualitative sense. One could start adding such features as a Leanard–Jones 6-12 potential for the walls as an external potential and add in interparticle potentials. Such modeling does not seem to be justified for the 1D case. First, molecules are not hard spheres and, second, the 1D picture is not very accurate since even the hard spheres would not line up exactly like a string of beads. It does, however, indicate that the density functional approach is at least qualitatively reasonable.

PERCUS–YEVICK SOLUTION EXPANSION FOR HARD SPHERES

Almost all of the DFT calculations require a hard-sphere equation of state as part of the calculation. The van der Waal and other approximations have

been used but the most widely used approximation is the CS. The following sequence utilizes the Ornstein–Zernicke equation and makes some assumption to solve the equation. The first of these assumption yields a solution by Percus and Yevick [3]

$$\exp\left(\frac{u(\mathbf{r})}{kT}\right)g(\mathbf{r}) = 1 + \langle\rho\rangle\int\left(\exp\left(\frac{u(\mathbf{r}')}{kT}\right) - 1\right)g(\mathbf{r}')(1 - g(\mathbf{r} - \mathbf{r}'))d^3r' \quad (269)$$

(with u here being u_{in}). This equation was rewritten in a form easier to solve with

$$\tau(\mathbf{r}) := \exp\left(\frac{u(\mathbf{r})}{kT}\right)g(\mathbf{r}) \tag{270}$$

to give

$$\tau(\mathbf{r}) = 1 + \langle\rho\rangle\int\tau(\mathbf{r}')\left(\exp\left(-\frac{u(\mathbf{r}')}{kT}\right) - 1\right)\left(\exp\left(-\frac{u(\mathbf{r} - \mathbf{r}')}{kT}\right)\tau(\mathbf{r} - \mathbf{r}') - 1\right)d^3\mathbf{r}'$$

$$(271)$$

With this equation Percus and Yevick were able to extract various thermodynamic quantities and the virial coefficients. The virial coefficients agreed very well with the results of Monte Carlo calculations lending credibility to the approach.

THIELE ANALYTICAL APPROXIMATION

Thiele [4], having noticed the precision of the Percus–Yevick equation, postulated that an exact analytical solution could be found. Starting with this equation and after *considerable* mathematical manipulations he arrived at the equation for pressure as

$$P = nkT\left[\frac{1 + 2z + 3z^2}{(1 - z)^2}\right] \quad \text{where} \quad z = \frac{\pi a^3\rho}{6} \tag{272}$$

and a is the diameter of the hard sphere.

THE CARNAHAN–STARLING APPROXIMATION

An accurate reduced equation of state for the hard-sphere approximation using the virial expression was determined by Ree and Hoover [5]. The first six virial coefficients[2] are given by

$$\frac{PV}{nRT} = 1 + 4z + 10z^2 + 18.36z^3 + 28.2z^4 + 39.5z^5 \tag{273}$$

where z has the same meaning as above. It was noticed by Carnahan and Starling [6] that the expression

$$\frac{PV}{nRT} = 1 + 4z + 10z^2 + 18z^3 + 28z^4 + 40z^5 + \cdots \tag{274}$$

is very close to the virial equation shown above, and may be (Padé) approximated by

$$\frac{PV}{nRT} = 1 + \frac{4z - 2z^2}{(1-z)^3} \tag{275}$$

Eq. (275) has been written here in the form of two terms. The first term on the right-hand side is the same as the ideal gas. One may think of the second term as a correction to the ideal gas. In Fig. 118 is a comparison of Eq. (275) with the virial equation derived by Ree and Hoover. It is apparent that this is a good approximation above a value of $V/V_m(\mathrm{l}) \approx 2$. Comparison to experimental data is difficult since, firstly, there is no such gas represented by hard spheres and, secondly, experimental virial coefficients even for gases such as argon are not readily available to the fifth term. This, however, seems to be a reasonable staring point for modeling.

Notice that this does not include any attractive potential as one would add in, for example, the van der Waal equation. Some authors have added in

---

[2] The units for the coefficients are not given but they are such that each term of the virial equation on the right-hand side is dimensionless. Likewise, the second term of Eq. (275) is dimensionless overall.
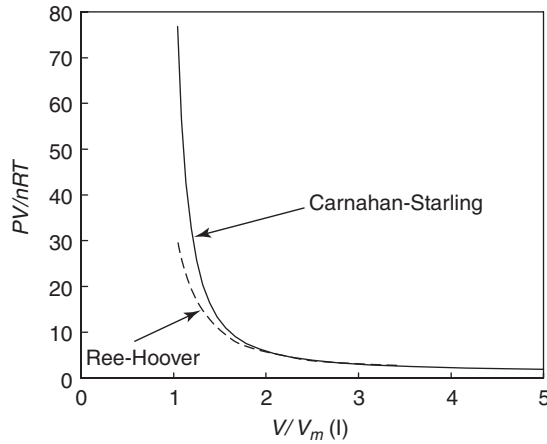
Fig. 118. A comparison of the Carnahan-Starling approximation with the Ree and Hoover hard sphere calculation.

an attractive term dependent upon the square of the molecular density to give what is referred to as Carnahan–Starling–van der Waal approximation, i.e.

$$P = \rho kT \left(1 + \frac{4z - 2z^2}{(1-z)^3} - \frac{a_{vdW}\rho}{N_A} \right) \tag{276}$$

where a_{vdW} is the usual van der Waal constant associated with pressure.

HELMHOLTZ FREE ENERGY FROM THE CS APPROXIMATION

There are several forms similar to Eq. (275) which could be used to arrive at a Helmholtz free energy. The CS form, however, is presently the most widely used. In the following the internal contributions, vibrational electronic, etc., are not considered. The molar Helmholtz free energy, A, is related to the pressure of the fluid at constant temperature whether ideal or not by

$$dA \big|_T = -PdV \tag{277}$$

where V is the molar volume. Thus for an ideal gas,

$$dA_I \big|_T = -\frac{RT}{V} dV \tag{278}$$

Integration of Eq. (278) yields the Helmholtz free energy of the ideal gas with the question of what the integration constant is. This, however, is known from quantum statistical thermodynamics, i.e.

$$A_I = -RT\left[\ln\left(\frac{V}{N}\right) + \frac{3}{2}\ln\left(\frac{mkT}{2\pi\hbar^2}\right) + 1\right] \tag{279}$$

The second term of Eq. (275) may be integrated keeping in mind that the ideal gas is applicable as the volume approaches infinity and so the total CS Helmholtz free energy, A_{CS} is

$$A_{CS} = RT\left[\ln\left(\frac{\rho(r)}{n_Q}\right) - 1 + \frac{4z^2 - 3z}{(z-1)^2}\right] \tag{280}$$

where n_Q is referred to as the "quantum density" (or $n_Q = 1/\Lambda^3$, where Λ is the deBrolie wavelength).

NON-LOCAL DENSITY FUNCTIONAL THEORY

The distinction between the local and the non-local density functional theory (NLDFT) is the assumption for the local that the fluid is structureless for calculating the long-range interactions between fluid particles. This assumption works when there are no strongly interacting boundaries but breaks down for surface adsorption. Intuitively, this seems obvious from the calculation made for the 1D hard-rod case above. As seen in the figures, the walls have a considerable influence upon the number density as does the strong catenary potential. In adsorption it is not usual for the adsorption potential to be 5 to 10 times greater than the interparticle potential, so the non-local assumption is called for.

To compensate, Nordholm et al. [7] introduced a non-local calculation based upon the van der Waal model. Percus [3] provided a general framework for the NLDFT that follows these lines:

A reference Helmholtz free energy[3] and a perturbation energy are assumed to compose of the overall Helmholtz free energy; so

$$A = A_{ref} + \lambda A_p \tag{281}$$

A_{ref} consists of the following parts: (1) the external field contribution, $A_{external}$, (2) the ideal gas contribution, A_I and (3) an excess free energy functional term, A_{excess}. $A_{external}$ is given by

$$A_{external} = \int \rho(r) u_{external}(\mathbf{r}) d^3\mathbf{r} \tag{282}$$

and A_I is given by Eq. (279) above. The free-energy approach developed by Tarazona [8] and Evans [9] has been the most successful modeling approach so far. In this modeling, the excess free-energy term is obtained by using a smoothed density functional. This is given by

$$A_{excess} = \int \rho(\mathbf{r}) \Delta \psi(\overline{\rho}(\mathbf{r})) d^3\mathbf{r} \tag{283}$$

where $\overline{\rho}$ is a smoothed density function. From the derivative of pressure with respect to volume from the CS equation ((275) above) one has for $\Delta\psi$,

$$\Delta\psi(\rho) = \frac{kT(4z - 3z^2)}{(1-z)^2} \qquad \left(z = \frac{\pi a^3 \rho}{6} \right) \tag{284}$$

The smoothed density functional, $\overline{\rho}$, is expanded to a quadratic series to make the homogeneous fluid match the Percus–Yevick using the expression

$$\overline{\rho}(\mathbf{r}) = \sum_{i=0}^{2} (\overline{\rho})^i \int \mathbf{w}_i(\mathbf{r} - \mathbf{r}') \rho(\mathbf{r}') \, d^3\mathbf{r}' \tag{285}$$

---

[3] The standard IUPAC Helmholtz free-energy symbol used here is A. Many physics paper use the symbol "$\mathcal{F}$" for this. I have also expanded the subscripts to be more descriptive.

where the **w** functions are referred to as weighting functions. The conditions for a homogeneous fluid also require

$$\int \mathbf{w}_0(\mathbf{r} - \mathbf{r}') \, d^3 r = 1$$
$$\int \mathbf{w}_{1 \text{ or } 2}(\mathbf{r} - \mathbf{r}') \, d^3 r = 0$$

(286)

The functions $\mathbf{w}_0$ through $\mathbf{w}_2$ are evaluated as a function of $\mathbf{r}/a$. The weighting function $\mathbf{w}_0$ for the homogeneous fluid is given simply as

$$\mathbf{w}_0 = \begin{cases} \dfrac{3}{4\pi a^3}, & |\mathbf{r}| < a \\ 0, & |\mathbf{r}| > a \end{cases}$$

(287)

which fulfills the first integral of Eq. (286) (reflecting that the volume of a hard sphere is simply $4\pi a^3/3$). Using only this weighting function yields a generalized van der Waal modeling. Thus, the higher powers in the smoothed density are the more subtle (but important) corrections to the vdW approach.

To obtain $\mathbf{w}_1$ and $\mathbf{w}_2$ the following strategy is used:

1. The direct correlation, defined in Eq. (252), is related to the excess free energy, Eq. (283), by

$$C(\mathbf{r}, \mathbf{r}') = -\frac{1}{kT} \frac{\delta\delta \int \rho(\mathbf{r}) \Delta\psi(\overline{\rho}(\mathbf{r})) \, d^3\mathbf{r}}{\delta\rho(\mathbf{r})\delta\rho(\mathbf{r}')}$$

(288)

so that evaluating the functional derivatives for the homogenous fluid with a density of ρ_0

$$-kTC(\mathbf{r} - \mathbf{r}') = \frac{\partial \Delta\psi(\rho_0)}{\partial \rho(\mathbf{r})} \left[\left. \frac{\delta\overline{\rho}(\mathbf{r})}{\delta\rho(\mathbf{r}')} \right|_{\rho_0} + \rho_0 \int \frac{\delta^2 \delta\overline{\rho}(\mathbf{r}'')}{\delta\rho(\mathbf{r})\delta\rho(\mathbf{r}')} \, d^3\mathbf{r}'' \right]$$
$$- \frac{\partial^2 \Delta\psi(\rho_0)\rho_0}{\partial\rho\partial\rho} \int \left. \frac{\delta\overline{\rho}(\mathbf{r}'')}{\delta\rho(\mathbf{r})} \right|_{\rho_0} \left. \frac{\delta\overline{\rho}(\mathbf{r}'')}{\delta\rho(\mathbf{r}')} \right|_{\rho_0} \, d^3\mathbf{r}$$

(289)

2. The function $\Delta\psi$ is obtained from the CS approximation or, as recommended by Tarazona, from the original virial expansion expression for the hard sphere. The derivatives are then easily obtained.

3. The derivatives of $\bar{\rho}$ are obtained from Eq. (285) with $\mathbf{w}$ being expanded into a power series in ρ :

$$\mathbf{w}(\mathbf{r},\rho) = \mathbf{w}_0(\mathbf{r}) + \mathbf{w}_1(\mathbf{r})\rho + \mathbf{w}_2(\mathbf{r})\rho^2 + \cdots \tag{290}$$

The terms beyond ρ^2 are assumed to be small.

4. This information is substituted back into $\bar{\rho}$, Eq. (285), and into the derivatives of $\bar{\rho}$.

5. $\bar{\rho}$, $\Delta\psi$ and their derivatives are then substituted into the direct correlation function thus getting a power series for C.

6. The power series for C must agree with the direct correlation function results from the Percus–Yevick calculation for the homogeneous fluid over a large range. Thus a match is made to obtain the appropriate functions for the $\mathbf{w}_i$s for Eq. (290). These functions are available in either Davis' book or in the original article by Tarazona.

MODELING WITH THE PRESENCE OF A SURFACE

The presence of a surface is modeled with an external potential simulating the solid surface. The external field portion is typically modeled as an infinitely high-potential hard wall or, with more sophistication, a LJ potential. The former model, used by Tarazona, can be used for a slit pore with the conditions

$$u_{ex}(x) = \begin{cases} \infty, & x < \dfrac{a}{2} \text{ and } x > L - \dfrac{a}{2} \\ 0, & \dfrac{a}{2} < x < L - \dfrac{a}{2} \end{cases} \tag{291}$$

Using only the x direction the weighing function coefficients are appropriately adjusted. This condition is equivalent to making $\rho = 0$ when $x \leq 0$ or $x \geq L$. (Thus the integrals may end with a 0 or L.)

     The results of the calculation are in excellent agreement with Monte Carlo calculations, which require considerably more computer computations. Fig. 119 shows the results of this calculation from one side of a hard-wall slit with a comparison with the expected results from χ theory. The χ theory calculation used a harmonic oscillator approximation to the LJ 6-12 potential to calculate the normal direction profile. The χ theory calculation is broader and deeper than the Monte Carlo calculation, whereas the DFT calculation is almost indistinguishable from the Monte Carlo calculation.

     It is desirable to replace the hard-wall assumption, Eq. (291), with a wall potential. This potential could be a detailed LJ 6-12 potential (see Eq. (102)) or possibly an average-type potential such as the Steele [10] 10-4-3 potential. This modifies A_{external} accordingly.

     The part left for inclusion is A_p in Eq. (281). For this perturbation, the interparticle forces are normally chosen to be a LJ 6-12 potential. With the perturbation fully in force, that is $\lambda = 1$,

$$A_p = \frac{1}{2} \int \rho(\mathbf{r}) \rho(\mathbf{r}') g(\mathbf{r}, \mathbf{r}') E_{LJ} \left(\left\| \mathbf{r} - \mathbf{r}' \right\| \right) d\mathbf{r} \, d\mathbf{r}' \tag{292}$$

where $|\mathbf{r} - \mathbf{r}'|$ in the LJ potential, E_{LJ}, is the distance between the centers of the molecules, that is $\mathbf{r}$ of Eq. (102).
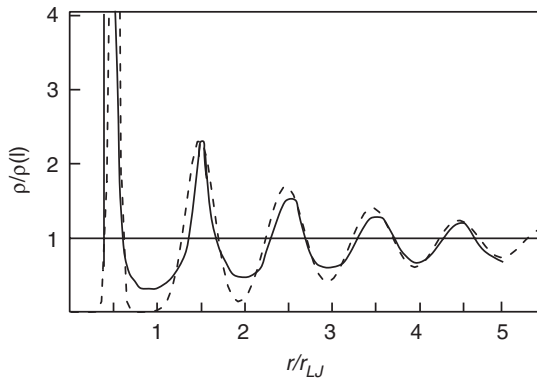

Fig. 119. Results of the NLDFT calculation by Tarazona (solid line) and results of harmonic oscillator approximation from χ theory (dashed).

The chemical potential of the adsorbent/adsorbate is give by the derivative of the Helmholtz free energy with respect to the number density:

$$\mu = \frac{\delta A}{\delta \rho(\mathbf{r})} \tag{293}$$

Combining the parts of *A* together (substituting (102) into (292), substituting (284) into (283) and adding these to (279) and (282)) and differentiating with respect to $\rho(\mathbf{r})$ one obtains the relationship between the density profile and μ (on a number basis):

$$\mu = kT \ln(\Lambda^3 \rho(\mathbf{r})) + \Delta\bar{\psi}(\rho(\mathbf{r})) + \int \rho(\mathbf{r}) \frac{\delta \Delta \psi(\bar{\rho}(\mathbf{r}))}{\delta \bar{\rho}} \, \delta\bar{\rho} \, \delta\rho \, d\mathbf{r}'$$
$$+ \int \rho(\mathbf{r}') E_{LJ} \left(\|\mathbf{r} - \mathbf{r}'\| \right) d\mathbf{r}' + u_{ex}(\mathbf{r}) \tag{294}$$

The smoothing and *g* are those obtained by using Tarazona's weighting functions. Since the CS formulation is used for $\Delta\psi$ one obtains two roots for each value of μ, one corresponding to the adsorbate and one for the adsorbent. Needless to say solving this equation requires successive approximations for ρ for each μ specified. The amount adsorbed is then obtained by integrating the profile from the surface to a large value.

Advances on this technique for use in analyzing adsorption isotherms and porosity measurements are being pursued with some encouraging results. For example, Olivier [11] has made calculations for the adsorption of argon and nitrogen on carbon materials. The initial results indicated a somewhat stepped isotherm, which followed the experimental isotherm reasonably. The initial assumption, however, was that the correlation function, *g*, was the same as the homogeneous liquid regardless of the location with respect to the surface. This assumption intuitively would seem to be an oversimplification. Although one is not normally interested in the depth profiles in adsorption experiments, the calculation requires the accurate accounting of the profile due to the integration of the profile. To correct the profile, Olivier introduced an additional weighting function which depends upon distance from the surface. This weighting function compensates for the postulated variation of *g* with respect to distance. This weighting function varies with distance from the surface and should be characteristic of the adsorbate. Therefore, once one has this standard weighting curve for a

particular adsorbate, it should apply to all isotherms. Excellent fits to the isotherms are obtained using this technique. This technique has been incorporated in some of the instruments that measure the isotherm.

There are a large number of calculations, modifications and explanations for NLDFT as applied to physisorption and porosity measurements. Some are mentioned here for a starting reference. Sokolowski and Fischer [12] calculated adsorption on capillary filling for generic pores, which gave insight into the observed isotherms. More specifically, adsorption on real mesoporous materials and comparison to the experimental isotherms are available. Many MCM-41 porous materials were calculated and the pore size distributions determined using NLDFT by Ravikovitch et al. [13] with fair agreement to experiment. Ravikovitch and Neimark [14], [15] have used NLDFT to calculate the surface area and porosity of the zeolite materials designated as SBA, which have larger pores. The explanation of hysteresis appears to be within reach [14,16,17] with the calculation of the metastable and equilibrium branches of adsorption in mesopores.

It is anticipated that NLDFT will in the future be very useful especially if it were combined with QM considerations.

REFERENCES

[1] H.T. Davis, "Stastical Mechanics of Phases, Interfaces, and Thin Films", VCH Publishers, New York, 1955, ISBN 1-56081-513-2.
[2] K. Denbeig, The Principles of Chemical Equilibrium, 3rd ed., Cambridge University Press, Cambridge, U.K., 1971, chapter 11.
[3] J.K. Percus and G.J. Yevick, Phys. Rev., 110 (1958) 1.
[4] E. Thicle, J. Chem. Phys., 39 (1963) 474.
[5] F.H. Ree and W.G. Hoover, J. Chem. Phys., 40 (1964) 939.
[6] N.F. Carnahan and K.E. Starling, J. Chem. Phys., 51 (1969) 635.
[7] S. Nordholm, M. Johnson and B.C. Fraesier, Aust. J. Chem., 33 (1980) 2139.
[8] P. Tarazona, Phys. Rev. A, 31 (1985) 2672.
[9] P. Tarazona and R. Evans, Mol. Phy., 52 (1984) 847.
[10] W.A. Steele, Surf. Sci., 36 (1973) 317.
[11] J.P. Oliver, J. Porous Mat., 2 (1995) 9.
[12] S. Sokolowski and J. Fischer, J. Chem. Soc. Farady Trans., 89 (1993) 789.
[13] P.I. Ravikovitch, G.L. Haller and A.V. Neimark, Adv. Coll. Inter. Sci., 76–77 (1998) 203.
[14] P.I. Ravikovitch and A.V. Neimark, Langmuir, 18 (2002) 1550.
[15] P.I. Ravikovitch and A.V. Neimark, J. Phys. Chem. B, 105 (2001) 6817.
[16] A.V. Neimark and P.I. Ravikovitch, Micropor. Mesopor. Mat., 44–45 (2001) 697.
[17] P.I. Ravikovitch, A. Vishayakov and A.V. Neimark, Phy. Rev. E, 64 (2001) 011602.

This page intentionally left blank

Appendix

EQUIPMENT SPECIFICATIONS

The following list of equipment and the specifications were obtained from the manufacturers. The author was able to identify 19 equipment manufacturers to measure the physical adsorption isotherm. Prices are not included since they can vary considerably. The author does not have personal experience with any of the equipment since he has constructed all of his own equipment in the past with the exception of a large number of Cahn microbalances (some models are still available) used for long-term studies.

The following list and information contained is *not guaranteed* and the individual should contact the manufacturers or representatives for information. Information was obtained from a variety of sources – directly from manufactures, from representatives at conferences, from information on the internet and personal contact. Corrections, additions and contact information for future reference would be appreciated.

Manufacturer	Beckman Coulter
Model	SA 3100
Measurement method	Volumetric
Maximum sample size	Limited by tube size
Sensitivity	0.01 m^2 g^{-1}
Number of simultaneous sampling	1 3 sample prep ports
Pressure range	0–1000 Torr
Pressure sensitivity	Minimum relative pressure 6×10^{-5}
Temperature control – sample	degas: 30–350°C
Temperature control – manifold	degas: ± 1°C
Vacuum capability	1×10^{-3} Torr
Method of data collection	Collected and analyzed with a variety of choices
Computer control	Fully automated
Auxiliary equipment	
Special features	
Contact	Multiple contacts worldwide. See: www.beckmancoulter.com

Manufacturer	Bel Japan, Inc.
Model	Belsorp-mini
Measurement method	Volumetric
Maximum sample size	2 mL (5 mL option)
Sensitivity	0.01 m^2 g^{-1}
Number of simultaneous sampling	3 high precision 1
Pressure range	0–1000 Torr, four ranges
Pressure sensitivity	$\pm 0.25\%$ of full range of sensor
Temperature control – sample	Cryogenic
Temperature control – manifold	
Vacuum capability	
Method of data collection	Computer collected and analyzed with a variety of programs
Computer control	
Auxiliary equipment	Optional pretreament system available with three ports
Special features	Compensating gas balance gas bulb to eliminate dead volume error due to change in liquid N_2 level or dilution with O_2
Contact	Bel Japan, Inc. 11-27, 2-Chome, ShinKitano, Yodogawa-ku, Osaka 532-0025 Japan www.nippon-bel.co.jp Colloidal Dynamics 11 Knight st. Building E18 Warwick, RI 02886, USA Tel.: 1-402-738-5515

Manufacturer	Hiden Analytical, Inc.
Model	HTP1-S
Measurement method	Volumetric gas sorption and TPD-MS
Maximum sample size	10 g
Sensitivity	1 μg
Number of simultaneous sampling	1
Pressure range	0–1000 Torr with selection of four different ranges down to 1 Torr
Pressure sensitivity	0.02% full scale and 0.1% full scale depending upon range
Temperature control – sample	−196–500°C Electrical heating as standard and optional refrigrerated recirculating water bath or cryo-cooling pump
Manifold T control	
Vacuum capability	Ultrahigh vacuum, leak rate $<10^{-12}$ atm Ls^{-1}
Method of data collection	Data collected by digital and analogue interface direct with imbedded PC. Sorption data analyzed in real time by applications PC using trend analysis of the approach to equilibrium
Computer control	Pressure control separate from data collection
Auxiliary equipment	Minimum of vacuum pumps and PC
Special features	The HTP1-S is most commonly used as a hydrogen storage analyzer and provides two methods for measuring the sorption capacity, both by volumetric (Sievert's) sorption and by quantitative thermal desorption
Contact	Hiden Analytical, Inc. 75 Hancock Road Suite H Peterborugh, NH 03458-1100 www.hiden.co.uk

Manufacturer	Hiden Analytical, Inc.
Model	HTP1-V
Measurement method	Volumetric gas sorption
Maximum sample size	10 g
Sensitivity	1 μg
Number of simultaneous sampling	1
Pressure range	0–1000 Torr with selection of four different ranges down to 1 Torr
Pressure sensitivity	0.02% full scale and 0.1% full scale depending upon range
Temperature control – sample	−196–500°C. Electrical heating as standard and optional refrigrerated recirculating water bath or cryo-cooling pump
Manifold T control	
Vacuum capability	Ultrahigh vacuum, leak rate $<10^{-12}$ atm Ls^{-1}
Method of data collection	Data collected by digital and analogue interface direct with imbedded PC. Sorption data analyzed in real time by applications PC using trend analysis of the approach to equilibrium
Computer control	Pressure control separate from data collection
Auxiliary equipment	Minimum of vacuum pumps and PC
Special features	The HTP1-V is most commonly used when the requirement is for both ideal and non-ideal gases and is therefore complementary with the Hiden IGA-001. A typical application is the measurement of isothermal uptake of hydrogen in storage media combined with in situ surface area and porosity analysis
Contact	Hiden Analytical, Inc. 75 Hancock Road Suite H Peterborugh, NH 03458-1100 www.hiden.co.uk

Manufacturer	Hiden
Model	IAG-001
Measurement method	Gravimetric dynamic gas sorption
Maximum sample size	5 g
Sensitivity	0.1 μg
Number of simultaneous sampling	1
Pressure range	0–1000 Torr with selection of four different ranges down to 1 Torr
Pressure sensitivity	0.02% full scale and 0.1% full scale depending upon range
Temperature control – sample	−196–1000°C – liquid N_2, cryofurnace, refrigerated recirulating water bath, infra-red or conventional furnaces
Manifold T control	DNA
Vacuum capability	Ultrahigh vacuum, leak rate $<10^{-12}$ atm Ls^{-1}
Method of data collection	Data collected by digital and analogue interface direct with imbedded PC. Sorption data analysed in real time by applications PC using trend analysis of the approach to equilibrium
Computer control	Pressure control separate from data collection
Special features	The IGA-001 is suited to a wide range of single component gas sorption analyses and is most commonly used when the requirement is for both ideal and non-ideal gases. A typical application is the measurement of isothermal uptake of hydrogen in storage media and this can be combined with in situ surface area and porosity analysis
Auxiliary equipment	Minimum of vacuum pumps, PC and one thermostat option to suit application
Contact	Hiden Analytical, Inc. 75 Hancock Road Suite H Peterborugh, NH 03458-1100 www.hiden.co.uk

Manufacturer	Hiden Analytical, Inc.
Model	IGA-002
Measurement method	Gravimetric gas and vapor sorption
Maximum sample size	5 g
Sensitivity	0.1 µg
Number of simultaneous sampling	1
Pressure range	0–1000 Torr with four different ranges down to 1 Torr
Pressure sensitivity	0.02%–0.1% full range depending on range selection
Temperature control – sample	-196–1000°C – Liquid N_2, cryofurnace, refrigerated recirculating water bath, infra-red or conventional furnaces
Manifold T control	DNA
Vacuum capability	Ultrahigh vacuum, leak rate $< 10^{-12}$ atm Ls^{-1}
Method of data collection	Data collected by digital and analogue interface direct with imbedded PC. Sorption data analyzed in real time by applications PC using trend analysis of the approach to equilibrium
Computer control	Pressure control separate
Auxiliary equipment	Minimum of vacuum pumps, PC and one thermostat option to suit application
Special features	The IGA-002 is suited to a wide range of single-component gas and vapor sorption analyses and is most commonly used for the characterization of equilibria and diffusivity in porous media using diverse non-ideal probe molecules
Contact	Hiden Analytical, Inc. 75 Hancock Road Suite H Peterborugh, NH 03458-1100 www.hiden.co.uk

Manufacturer	Hiden
Model	IAG-003
Measurement method	Gravimetric dynamic gas sorption and (optional) TGA-MS
Maximum sample size	5 g
Sensitivity	0.1 μg
Number of simultaneous sampling	1
Pressure range	0–1000 Torr with selection of four different ranges down to 1 Torr
Pressure sensitivity	0.02% full scale and 0.1% full scale depending upon range
Measurement sensitivity	0.2 μg
Temperature control – sample	-196–$1000°C$ – liquid N_2, cryofurnace, refrigerated recirulating water bath, infra-red or conventional furnaces
Manifold T control	DNA
Vacuum capability	Ultrahigh vacuum, leak rate $<10^{-12}$ atm Ls^{-1}
Method of data collection	Data collected by digital and analogue interface direct with imbedded PC. Sorption data analysed in real time by applications PC using trend analysis of the approach to equilibrium
Computer control	Pressure control separate from data collection
Special features	The IGA-003 is suited to a wide range of single- and multicomponent gas sorption analyses and is most commonly used for the characterization of heterogeneous catalysts. The IGA-003 is supplied with between two and six flow controllers to generate gas mixtures for dynamic experiments. The system operates with a combination of upstream flow control and down stream pressure control
Auxiliary equipment	Minimum of vacuum pumps, PC and one thermostat option to suit application. Dynamic Sampling Mass Spectrometer (DSMS) is required for optional TGA-MS mode

Contact   Hiden Analytical, Inc.
                                           75 Hancock Road
                                           Suite H
                                           Peterborugh, NH 03458-1100
                                           www.hiden.co.uk

Manufacturer	Hiden Analytical, Inc.
Model	IGA-100
Measurement method	Gravimetric dynamic gas and vapor sorption and (optional) TGA-MS
Maximum sample size	5 g
Sensitivity	0.1 μg
Number of simultaneous sampling	1
Pressure range	0–1000 Torr with four different ranges down to 1 Torr
Pressure sensitivity	0.02–0.1% full range depending on range selection
Temperature control – sample	-196–1000°C – Liquid N_2, cryofurnace, refrigerated recirculating water bath, infra-red or conventional furnaces
Manifold T control	DNA
Vacuum capability	Ultrahigh vacuum leak rate $<10^{-12}$ atm Ls^{-1}
Method of data collection	Data collected by digital and analogue interface direct with imbedded PC. Sorption data analyzed in real time by applications PC using trend analysis of the approach to equilibrium
Computer control	Pressure control separate from data collection
Auxiliary equipment	Minimum of vacuum pumps, PC and one thermostat option to suit application
Special features	The IGA-100 is supplied with between two and six flow controllers to generate gas mixtures for dynamic experiments. The system operates with a combination of upstream flow control and down stream pressure control. The IGA-100 is suited to the widest possible range of single and multi-component gas/vapor sorption analyses
Contact	Hiden Analytical, Inc. 75 Hancock Road, Suite H Peterborugh, NH 03458-1100 www.hiden.co.uk

Manufacturer	Hiden Analytical, Inc.
Model	IGA-Sorp
Measurement method	Gravimetric dynamic water sorption
Maximum sample size	5 g
Sensitivity	0.1 µg
Number of simultaneous sampling	1
Pressure range	N/A. Uses humidification at ambient pressure
Pressure sensitivity	DNA
Temperature control – sample	5–350°C
Manifold T control	DNA
Vacuum capability	DNA
Method of data collection	Data collected by digital and analogue interface direct with imbedded PC. Sorption data analyzed in real time by applications PC using trend analysis of the approach to equilibrium
Computer control	Pressure control separate from data collection
Auxiliary equipment	PC
Special features	The IGAsorp is most commonly used in the characterization of pharmaceuticals, e.g. for the measurement of hydrates and amorphicity
Contact	Hiden Analytical, Inc. 75 Hancock Road Suite H Peterborugh, NH 03458-1100 www.hiden.co.uk

Manufacturer	Insurface Adsorption Instruments
Model	Kelvin 1040
Measurement method	Flow method
Maximum sample size	20 mL
Sensitivity	$0.01 \ m^2 \ g^{-1}$ Pore sizes: 2–50 nm $\leq 3\%$ Precision
Number of simultaneous sampling	6
Pressure range	0.02–0.93 P_0
Pressure sensitivity	
Temperature control – sample	Degassing: 35–350°C Ambient: 15–35°C
Temperature control – manifold	
Vacuum capability	DNA
Method of data collection	A variety of data analyses equations used
Computer control	
Auxiliary Equipment	
Special Features	Six Single-point analyses in 15 min
Contact	Rubotherm Präzisionsmesstechnik, GmbH Universität St. 142 44799 Bochum, Germany http://www.rubotherm.de

Manufacturer	Insurface Adsorption Instruments
Model	Kelvin 1040
Measurement method	Flow method
Maximum sample size	20 mL
Sensitivity	$0.01 \text{ m}^2 \text{ g}^{-1}$ Pore sizes: 0.2–200 nm $\leq 3\%$ precision
Number of simultaneous sampling	6
Pressure range	5×10^{-4}, -0.995 of P_0
Pressure sensitivity	
Temperature control – sample	Degassing: 35–350°C Ambient: 15–35°C
Temperature control – manifold	
Vacuum capability	DNA
Method of data collection	A variety of data analyses equations used
Computer control	
Auxiliary equipment	
Special features	Six single-point analyses in 15 min
Contact	Rubotherm Präzisionsmesstechnik, GmbH Universität St. 142 44799 Bochum, Germany http://www.rubotherm.de

Manufacturer	Micromeritics
Model	ASAP 2020
Measurement method	Volumetric
Maximum sample size	9 mL – depends upon specific application bulb – 3000 m^2g^{-1}
Sensitivity	0.001 $m^2\ g^{-1}$
Number of simultaneous sampling	1
Pressure range	0–950 Torr
Pressure sensitivity	1000 Torr transducer = 1×10^{-3} Torr 10 Torr transducer = 1×10^{-5} Torr 1 Torr transducer = 1×10^{-6} Torr
Temperature control – sample	Cryogenic up to 72 h
Temperature control – manifold	Accuracy 5°C, precision and stability 1°C
Vacuum capability	High-vacuum capable with pumps installed, $<1 \times 10^{-8}$atm
Method of data collection	Computer-controlled data collection recommended
Computer control	
Auxiliary equipment	
Special features	Capable of sample temperatures up to 1100°C
Contact	Micromeritics One Mircomeritics Drive Norcross, GA 30093-1877 Phones: US 770-662-3633, International (001)-770-662-3660 www.micromeritics.com

Manufacturer	Micromeritics
Model	Autochem II 2920
Measurement method	Volumetric – flow through
Maximum sample size	
Sensitivity	
Number of simultaneous sampling	Quick turnaround for successive sample with a special cooler
Pressure range	
Pressure sensitivity	
Temperature control – sample	-100–$1100°C$ Programable for temperature-programed (TP) cycles
Temperature control – manifold	Four internal independent zones that may be heated to 150°C
Vacuum capability	
Method of data collection	Computer collected and analyzed for graphical display. Programs for analyzing MS data included
Computer control	Computer controlled included
Auxiliary equipment	Vapor generator, cryocooler
Special features	Includes a large array of temperature-programed cycles. Main use is to study chemisorption and catalysis. Analyses include TPR (reduction), TPD (desorption), TPO (oxidation), TPRx (reaction) as well as surface area measurements. Includes MS port
Contact	Micromeritics One Mircomeritics Drive Norcross, GA 30093-1877 Phones: US 770-662-3633, International (001)-770-662-3660 www.micromeritics.com

Manufacturer	Micromeritics
Model	FlowSorb III Series
Measurement method	Flowing gas method
Maximum sample size	9 mL – depends upon specific application bulb – 280 m^{2}g^{-1}
Sensitivity	0.01 m^2 g^{-1}
Number of simultaneous sampling	1
Pressure range	DNA
Pressure sensitivity	
Temperature control – sample	Cryogenic
Temperature control – manifold	DNA
Vacuum capability	DNA
Method of data collection	Computer data collection
Computer control	
Auxiliary equipment	
Special features	Automated operation – designed for rapid sample throughput
Contact	Micromeritics One Mircomeritics Drive Norcross, GA 30093-1877 Phones: US 770-662-3633, International (001)-770-662-3660 www.micromeritics.com

Manufacturer	Micromeritics
Model	Gemini V Series
Measurement method	Volumetric
Maximum sample size	Up to 12 mL
Sensitivity	$0.01\ m^2\ g^{-1}$ for specific surface area 4×10^{-8} for pore volume
Number of simultaneous sampling	1
Pressure range	0–950 Torr
Pressure sensitivity	0.01%
Temperature control – sample	Cryogenic
Temperature control – manifold	
Vacuum capability	20 µTorr
Method of data collection	Computer supplied optional – two versions of embedded software
Computer control	
Auxiliary equipment	
Special features	Has a "balance tube" to eliminate dead-space correction errors as cryogenic fluid evaporates
Contact	Micromeritics One Mircomeritics Drive Norcross, GA 30093-1877 Phones: US 770-662-3633, International (001)-770-662-3660 www.micromeritics.com

Manufacturer	Micromeritics
Model	TriStar 3000
Measurement method	Volumetric
Maximum sample size	10 mL
Sensitivity	As low as 0.01 $m^2\ g^{-1}$
Number of simultaneous sampling	3
Pressure range	0–1000 Torr
Pressure sensitivity	0.05 Torr
Temperature control – sample	Cryogenic
Temperature control – manifold	0.25°C
Vacuum capability	20 µTorr
Method of data collection	Computer control is versatile with many built-in analyses programs
Computer control	
Auxiliary equipment	
Special features	
Contact	Micromeritics One Mircomeritics Drive Norcross, GA 30093-1877 Phones: US 770-662-3633, International (001)-770-662-3660 www.micromeritics.com

Manufacturer	Porotec, GmbH
Model	QSurf M1
Measurement method	Volumetric – surface area and pore volume
Maximum sample size	50 m^2 g^{-1}
Sensitivity	0.05 m^2 g^{-1}
0.005 m^3 g^{-1}	
Number of simultaneous sampling	1 2 sample prep ports
Pressure range	0–2 atm
Pressure sensitivity	0.25% of reading (0.15% optional)
Temperature control – sample	Sample preparation up to 300°C liquid N$_2$ adsorption
Temperature control – manifold	Sample prep: ±1°C
Vacuum capability	DNA
Method of data collection	Output to printer. Output ports for computer data collection
Computer control	
Auxiliary equipment	
Special features	N$_2$ in He as adsorbate varied for control Five single-point BETs per hour or 1 multipoint per hour
Contact	Porotec Vertrib von Wissenshaftlichen Geräten, GmbH Niederhofheimer Str. 55a 65719 Hofheim/Ts. Germany www.porotec.de Also available from Thermo Electron Corporation, www.thermo.com

Manufacturer	Porotec, GmbH
Model	QSurf M3
Measurement method	Volumetric – surface area and pore volume
Maximum sample size	50 m^2 g^{-1}
Sensitivity	0.05 m^2 g^{-1} 0.005 m^3 g^{-1}
Number of simultaneous sampling	3 3 sample prep ports
Pressure range	0–2 atm
Pressure sensitivity	0.25% of reading (0.15% optional)
Temperature control – sample	Sample preparation up to 300°C Liquid N$_2$ adsorption
Temperature control – manifold	Sample prep: ±1°C
Vacuum capability	DNA
Method of data collection	Output to printer. Output ports for computer data collection
Computer control	
Auxiliary equipment	
Special features	N$_2$ in He as adsorbate varied for control 15 single-point BETs per hour or three multipoint per hour
Contact	Porotec Vertrib von Wissenshaftlichen Geräten, GmbH Niederhofheimer Str. 55a 65719 Hofheim/Ts. Germany www.porotec.de Also available from Thermo Electron Corporation, www.thermo.com

Manufacturer	Porotec, GmbH
Model	QSurf S1
Measurement method	Volumetric – surface area only
Maximum sample size	50 m^2 g^{-1}
Sensitivity	0.05 m^2 g^{-1}
Number of simultaneous sampling	1 2 sample prep ports
Pressure range	0–2 atm
Pressure sensitivity	0.25% of reading (0.15% optional)
Temperature control – sample	Sample preparation up to 300°C Liquid N$_2$ adsorption
Temperature control – manifold	Sample prep: $\pm$1°C
Vacuum capability	DNA
Method of data collection	Output to printer. Output ports for computer data collection
Computer control	
Auxiliary equipment	
Special features	30% N$_2$ in He as adsorbate rotameter control Five single-point BETs per hour
Contact	Porotec Vertrib von Wissenshaftlichen Geräten, GmbH Niederhofheimer Str. 55a 65719 Hofheim/Ts. Germany www.porotec.de Also available from Thermo Electron Corporation, www.thermo.com

Manufacturer	Porotec, GmbH
Model	QSurf S1
Measurement method	Volumetric – surface area only
Maximum sample size	50 m^2 g^{-1}
Sensitivity	0.05 m^2 g^{-1}
Number of simultaneous sampling	3 3 sample prep ports
Pressure range	0–2 atm
Pressure sensitivity	0.25% of reading (0.15% optional)
Temperature control – sample	Sample preparation up to 300°C Liquid N_2 adsorption
Temperature control – manifold	Sample prep: $\pm$1°C
Vacuum capability	DNA
Method of data collection	Output to printer. Output ports for computer data collection
Computer control	
Auxiliary equipment	
Special features	30% N_2 in He as adsorbate rotameter control 15 single-point BETs per hour
Contact	Porotec Vertrib von Wissenshaftlichen Geräten, GmbH Niederhofheimer Str. 55a 65719 Hofheim/Ts. Germany www.porotec.de Also available from Thermo Electron Corporation, www.thermo.com

Manufacturer	Porotec, GmbH
Model	Sorptomatic 1990
Measurement method	Volumetric
Maximum sample size	Only limited by sample bulb
Sensitivity	0.2 m^2 g^{-1} surface area (0.005 m^2 g^{-1} with Kr) 0.0001 mL g^{-1} pore volume
Number of simultaneous sampling	1
Pressure range	0–1000 Torr standard 0–10 Torr for micropore option 0–100 Torr for chemisorption option
Pressure sensitivity	0.25% of reading (0.15% optional)
Temperature control – sample	sample preparation up to 450°C
Temperature control – manifold	Sample prep: ± 1°C
Vacuum capability	5×10^{-3} Torr standard, 1×10^{-6} Torr optional turbopump
Method of data collection	Computer collected and displayed
Computer control	Fully automatic
Auxiliary equipment	
Special features	Special gas burette arrangement for chemisorption option Automatic pressure sensor calibrations and leaktests. Automatic gas introduction
Contact	Porotec Vertrib von Wissenshaftlichen Geräten, GmbH Niederhofheimer Str. 55a 65719 Hofheim/Ts. Germany www.porotec.de Also available from Thermo Electron Corporation, www.thermo.com

Manufacturer	Porous Material, Inc.
Model	BET Liquisorb Sorptometer
Measurement method	Volumetric
Maximum sample size	Limited by tube size
Sensitivity	0.01 $m^2\,g^{-1}$ surface area 1.0–50 nm pore sizes
Number of simultaneous sampling	1 Multiple sample chamber available as option
Pressure range	100 – 10,000 Torr
Pressure sensitivity	Accuracy: 0.15%, precision: 5×10^{-5}
Temperature control – sample	Elevated temperatures possible
Temperature control – manifold	
Vacuum capability	
Method of data collection	Computer data collection and analysis
Computer control	Can handle all controls, data collection and analysis
Auxiliary equipment	
Special features	
Contact	Porous Materials, Inc. 20 Dutch Mill Rd. Ithaca, NY 14850 USA info@pmiapp.com www.pmiapp.com PMI Europe Koningin Fabiolapark 45 BE 9820 Merelbeke Belgium

Manufacturer	Porous Material, Inc.
Model	BET Sorptometer
Measurement method	Volumetric
Maximum sample size	Limited by sample bulb size
Sensitivity	0.01 $m^2\,g^{-1}$ surface area 3.5 to 2000 μm pore size
Number of simultaneous sampling	1 Multiple sample chambers available as option
Pressure range	10–1000 Torr
Pressure sensitivity	Accuracy: 0.15%, precision: 1×10^{-5}
Temperature control – sample	Sample prep. from sub-freezing to elevated cryogenic adsorption
Temperature control – manifold	
Vacuum capability	
Method of data collection	Computer data collection and analysis
Computer control	Can handle all controls, data collection and analysis
Auxiliary equipment	
Special features	Chemisorption over a wide range of pressures and temperature
Contact	Porous Materials, Inc. 20 Dutch Mill Rd. Ithaca, NY 14850 USA info@pmiapp.com www.pmiapp.com PMI Europe Koningin Fabiolapark 45 BE 9820 Merelbeke Belgium

Manufacturer	Porous Material, Inc.
Model	Envelope Surface Area Analyzer
Measurement method	Flow method
Maximum sample size	10 m^2 g^{-1}
Sensitivity	0.1 m^2 g^{-1} surface area
Number of simultaneous sampling	1 Multiple sampe chamber available as option
Pressure range	0–250,000 Torr flow from 10 to 100 mL min^{-1}
Pressure sensitivity	
Temperature control – sample	
Temperature control – manifold	
Vacuum capability	
Method of data collection	Computer data collection and analysis
Computer control	Can handle all controls, data collection and analysis
Auxiliary equipment	
Special features	Test time approximately 5 min for fast throughput
Contact	Porous Materials, Inc. 20 Dutch Mill Rd. Ithaca, NY 14850 USA info@pmiapp.com www.pmiapp.com PMI Europe Koningin Fabiolapark 45 BE 9820 Merelbeke Belgium

Manufacturer	Quantachrome Instruments
Model	Autosorb-1-C
Measurement method	Volumetric designed to include chemisorption
Maximum sample size	Depends upon sample tube
Sensitivity	$< 3.8 \times 10^{-10}$ mol either adsorbed or desorbed 0.0005 m^2 surface area, 0.0001 mL porosity
Number of simultaneous sampling	5 automatically switched
Pressure range	0–1000 Torr, 3 detectors 1, 10 and 1000 Torr
Pressure sensitivity	0.000025% of full range of detectors
Temperature control – sample	Chemisorption up to 1100°C Crogenic adsorption control to 450°C – coolant control to ± 0.5 mm
Temperature control – manifold	
Vacuum capability	1×10^{-3} Torr
Method of data collection	Computer collected with a large array of programs for analysis including standard plots, DR, NLDFT, etc.Calculated active metal at the surface
Computer control	Fully automatic
Auxiliary equipment	Most features standard with a few options
Special features	Automated Chemisorption/Physisorption Surface Area and Pore Size Analyzer, P/N 02019-C-1LP, is a fully automated, vacuum volumetric, gas sorption system. The Autosorb ® -1-C is a high-throughput, cost-effective system that tests one sample while simultaneously and independently degassing a further two samples
Contact	Quantachrome Instruments 1900 Corporate Drive Boynton Beach, Florida 33426 USA www.quantachrome.com Don Weirick Don.Weirick@quantachrome.com 800-989-2476 Office 561-945-3136 Cellular

Manufacturer	Quantachrome Instruments
Model	Autosorb-1-MP/LP
Measurement method	Volumetric
Maximum sample size	Depends upon sample tube
Sensitivity	$< 2 \times 10^{-8}$ mol either adsorbed or desorbed 0.0005 m^2 surface area, 0.0001 mL porosity
Number of simultaneous sampling	1 2 Degassing stations
Pressure range	0–1000 Torr, 3 detectors 1, 10 and 1000 Torr
Pressure sensitivity	0.05% full scale for 1000 Torr, 0.15% of reading for 1 and 10 Torr 0.000025% of full range of detectors
Temperature control – sample	Degassing up to 450°C – thermister controlled $\pm$ 1% of set-point Automatic coolant control to 0.5 mm
Temperature control – manifold	
Vacuum capability	Ultrahigh (3.8×10^{-10} Torr)
Method of data collection	Computer collected with a large array of programs for analysis including standard plots and NLDFT for some systems
Computer control	Included
Auxiliary equipment	Most features standard with a few options
Special features	
Contact	Quantachrome Instruments 1900 Corporate Drive Boynton Beach, Florida 33426 USA www.quantachrome.com Don Weirick Don.Weirick@quantachrome.com 800-989-2476 Office 561-945-3136 Cellular

Manufacturer	Quantachrome Instruments
Model	Autosorb-1-"Multi Gas"
Measurement method	Volumetric
Maximum sample size	Depends upon sample tube
Sensitivity	$< 2 \times 10^{-9}$ mol either adsorbed or desorbed 0.05 m^2 surface area, 0.0001 mL porosity
Number of simultaneous sampling	1
Pressure range	0–1000 Torr, 3 detectors 1, 10 and 1000 Torr
Pressure sensitivity	0.000025% of full range of detectors
Temperature control – sample	Degassing up to 450°C – thermister controlled $\pm$ 1% of set point Automatic coolant control to 0.5 mm
Temperature control – manifold	
Vacuum capability	1×10^{-3} Torr
Method of data collection	Computer collected with a large array of programs for analysis including standard plots, DR, NLDFT, etc.
Computer control	Included
Auxiliary equipment	Most features standard with a few options
Special features	Fully automated for rapid throughput
Contact	Quantachrome Instruments 1900 Corporate Drive Boynton Beach, Florida 33426 USA www.quantachrome.com Don Weirick Don.Weirick@quantachrome.com 800-989-2476 Office 561-945-3136 Cellular

Manufacturer	Quantachrome Instruments
Model	Monosorb
Measurement method	Volumetric
Maximum sample size	> 0.01 m^2 g^{-1}
Sensitivity	0.1 m^2 surface area, 0.001 mL porosity
Number of simultaneous sampling	1 1 built in preparation stations
Pressure range	$0-1000$ Torr
Pressure sensitivity	0.0015%
Temperature control – sample	Preparation: 450°C Adsorption: liquid N$_2$
Temperature control – manifold	Preparation control by TC bridge
Vacuum capability	1×10^{-3} Torr
Method of data collection	Direct readout for single-point BET
Computer control	
Auxiliary equipment	Most features standard with a few options
Special features	The Monosorb ® Automated Surface Area Analyzer, P/N 02027-2, is a dynamic flow, single-point BET surface area analyzer with direct front panel readout of results, complete with built-in automatic dewar elevator and sample preparation station Single-point analysis typically 2–5 min
Contact	Quantachrome Instruments 1900 Corporate Drive Boynton Beach, Florida 33426 USA www.quantachrome.com Don Weirick Don.Weirick@quantachrome.com 800-989-2476 Office 561-945-3136 Cellular

Manufacturer	Quantachrome Instruments
Model	Nova 1200e
Measurement method	Volumetric
Maximum sample size	> 0.01 m^2 g^{-1}
Sensitivity	$< 1\times10^{-7}$ mol 0.01 m^2 surface area, 0.0001 mL porosity
Number of simultaneous sampling	1 2 Built-in preparation stations
Pressure range	0–1000 Torr
Pressure sensitivity	0.0015%
Temperature control – sample	Preparation: 450°C (with quartz option) Adsorption: liquid N$_2$
Temperature control – manifold	Preparation ± 1%
Vacuum capability	1×10^{-3} Torr
Method of data collection	Computer collected with a large array of programs for analysis including standard plots, DR, NLDFT, etc.
Computer control	Fully automatic
Auxiliary equipment	Most features standard with a few options
Special features	High-Speed, Automated Surface Area and Pore Size Analyzer, P/N 02090-1AG-1, is a fully automated, vacuum volumetric, gas sorption system. High throughput, cost effective system tests one sample while degassing a further two samples
Contact	Quantachrome Instruments 1900 Corporate Drive Boynton Beach, Florida 33426 USA www.quantachrome.com Don Weirick Don.Weirick@quantachrome.com 800-989-2476 Office 561-945-3136 Cellular

Manufacturer	Rubotherm
Model	DNA
Measurement method	Gravimetric
Maximum sample size	80 or 10 g
Sensitivity	About 1 µg max Precision = 0.002% of measured value
Number of simultaneous sampling	1 Special attachment allows up to 10
Pressure range	Ultrahigh vacuum to 500 atm for metal system Low vacuum to 1.3 atm for glass system
Pressure sensitivity	0.25%
Temperature control – sample (coupled to balance)	−196 – 350°C in metal system −60 – 250°C in glass system Up to 2000°C in metal system Up to 900°C in glass system
Temperature control – manifold	DNA
Vacuum capability	Ultrahigh for metal, low vacuum for glass
Method of data collection	Computer data collection recommended
Computer control	
Auxiliary equipment	
Special features	Has a magnetic separation between the balance and the sample chamber May also be used in flow system A very versatile system for variety of measurements Capable of being linked with a volumetric method
Contact	Rubotherm Präzisionsmesstechnik, GmbH Universität St. 142 44799 Bochum, Germany http://www.rubotherm.de Donald Lupfer 92 Glen St. Natick, MA 01760 USA

Manufacturer	Sartorius
Model	ME5 and SE2 Ultra-Micro balances
Measurement method	Gravimetric
Maximum sample size	ME5: 5.1 g, SE2: 2.1 g
Sensitivity	ME5: 1µg, SE2: 0.1µg
Number of simultaneous sampling	1
Pressure range	DNA
Pressure sensitivity	DNA
Temperature control – sample	DNA
Temperature control – manifold	DNA
Vacuum capability	DNA
Method of data collection	Digital (RS232C) output
Computer control	Only for balance control
Auxiliary equipment	Consists only of the balance – all the rest of the equipment must be supplied
Special features	Fully automatic calibration and adjustment
Contact	Sartorius AG Weender Landstrasse 94-108 37075 Goettingen, Germany www.sartorius.com Tel.: (0)49.551.308.0

Manufacturer	Thermo Electron Corporation
Model	Cahn C-34 and C-35
Measurement method	Gravimetric
Maximum sample size	loop A: 1.5 g, loop B: 3.5 g
Sensitivity	loop A: 0.1 mg, loop B: 10 mg
Number of simultaneous sampling	1
Pressure range	DNA
Pressure sensitivity	DNA
Temperature control – sample	DNA
Temperature control – manifold	DNA
Vacuum capability	DNA
Method of data collection	Digital (RS232) output
Computer control	Only for balance control
Auxiliary equipment	All vacuum, pressure, etc. must be supplied
Special features	
Contact	Thermo Electron Corporation 81 Wyman Street Waltham, MA 02454 Tel.: 781-622-1000 Fax: 781-622-1207 www.thermo.com

Author Index

This page intentionally left blank

Subject Index